Genetic Optimisation of Bacteria-Induced Calcite Precipitation

Hoffmann, Timothy

Award date:
2021

Awarding institution:
University of Bath

Genetic Optimisation of Bacteria-Induced Calcite Precipitation

---

Timothy Dennis Hoffmann

A thesis submitted for the degree of Doctor of Philosophy

University of Bath

Department of Biology and Biochemistry

September 2020

Declaration of authorship

I am the author of this thesis, and the work described therein was carried out by myself personally, with the exception of Chapter 1 which is presented as a literature review manuscript where Figure 3 was prepared by Bianca J. Reeksting and sections 1.5 and 1.6 were written together between the two of us.

Signed

Timothy D. Hoffmann

Table of Contents

Table of Figures

Table of Tables

Table of Equations

List of Abbreviations

BHI	brain heart infusion
BICP	bacteria-induced calcite precipitation
bla^r	resistance to beta lactamase (ampicillin)
ble^r	resistance to bleomycin/phleomycin
cat^r	resistance to chloramphenicol
D-Ala	D-alanine
dH_2O	deionised water
DNA	deoxyribonucleic acid
dNTP	deoxyribonucleotide triphosphate
GC	guanine-cytosine
GFP	green fluorescent protein
kan^r	resistance to kanamycin
LB	lysogeny broth
LBC	lysogeny broth calcite precipitation
LBU	lysogeny broth urea
LBGM	lysogeny broth glycerol manganese
LBGMC	lysogeny broth glycerol manganese calcite precipitation
LB Alk	lysogeny broth alkaline
LFH	long flanking homology
MLS	resistance to macrolides (erythromycin), lincosamides (lincomycin), streptogramins
OD_{600}	optical density at 600 nm
PCR	polymerase chain reaction
qPCR	quantitative polymerase chain reaction
RNA	ribonucleic acid
SOB	super optimal broth
SOC	super optimal broth catabolite repression
spc^r	resistance to spectinomycin
zeo^r	resistance to Zeocin (phleomycin D1)

Acknowledgments

First of all I would like to thank my supervisor Susanne Gebhard and my second supervisor Kevin Paine for entrusting me with the opportunity to undertake this project. My greatest gratitude goes to my supervisor Susanne who has supported and guided me over that last 5 years through my BSc, MRes and PhD. Her positivity, enthusiasm, and encouragement especially when things do not work out is truly inspiring, I am so grateful to have had you as my supervisor and to have had the opportunity to learn from you. Next, I would like to thank all my lab colleagues and everyone else in the lab 3S1.09 for their support and with whom the experience was a lot more fun. A particular thank you goes to the post-doc Bianca Reeksting for all her discussions and advice throughout this project. Thank you also to Kevin's research team for their discussions and insights, with whom we closely collaborated as well as everyone else on the RM4L team. Thank you to David Leak and Matthew Styles for their guidance and inspiration. A special thank you goes to Dragana Catici who was there for me through all the good and hard times, thank you for all your support and encouragement along the way. A big thank you goes to my family who always supported me and without whom I would not be where I am today. Finally I would like to thank the University of Bath, the EPSRC RM4L project, the Microbiology Society, and the Biochemical Society for funding and making this project possible.

Abstract

Bacteria in our environment contribute to Earth's landscapes through mineral deposits via a process known as bacteria-induced calcite precipitation (BICP). Over recent years, such bacteria have been at the basis of innovative biotechnologies arising within civil engineering sectors, finding application for example in self-healing concrete where encapsulated bacteria (such as those of the genus *Bacillus*) facilitate the repair of cracks that appear during aging of built structures. BICP occurs as a product of bacterial metabolism, which creates a microenvironment that favours the precipitation of calcium cations and carbonate anions in the form of mineral calcite. This process is dependent on changes in pH, availability of cell surface nucleation sites, and ion concentrations. Current approaches using this technology in industrial applications require bacteria that are both capable of BICP, as well as possessing specific growth characteristics required for the respective application (e.g. pH/salt tolerance). This project explored the genetic optimisation of BICP using *Bacillus subtilis* as a model Gram-positive and industrially relevant organism. Genetic engineering was coupled with functional characterisation of the resulting strains, quantitative and qualitative assessment of BICP under laboratory conditions and electron microscopy imaging of resulting crystals. This work identified key molecular components needed for BICP to occur and a way to mobilise these into better-suited chassis organisms for application predominantly in the context of improving self-healing concrete. Results showed that heterologous expression of the ureolytic pathway and modulation of biofilm production offer mechanisms whereby BICP can be engineered into a non-precipitating strain. In contrast modulation of bacterial surface charge was found to be ineffective in improving BICP. A plasmid suitable for mobilisation to a broad host range of Gram-positive bacteria was also developed to facilitate the future shuttling of BICP-promoting genes to application relevant bacteria. The results presented here provide a systematic exploration of the genetic components that drive BICP and will help pave the way for the rational design or selection of better precipitators for application. The ultimate goal is for these fundamental findings to contribute to the formulation of bio-concrete that increases the lifespan of cementitious structures and consequently decreases the maintenance costs and carbon dioxide release associated with concrete production and building.

Chapter 1

Manuscript:

Bacteria-Induced Mineral Precipitation: a mechanistic review

Timothy D. Hoffmann, Bianca J. Reeksting, Susanne Gebhard

ABSTRACT *Microorganisms contribute to Earth's mineral deposits through a process known as bacteria-induced mineral precipitation (BIMP). It is a complex process which is still not fully understood as it cannot be attributed to a singular pathway. Rather, it is a by-product of the activity of a breadth of bacteria, each with individual surface structure compositions and metabolisms. These all directly or indirectly influence precipitation parameters of saturation state and nucleation catalysis, which leads to biomineralisation. BIMP has formed the basis of many new innovative biotechnologies, such as soil consolidation, heavy metal remediation, restoration of historic buildings and even self-healing concrete. However, these applications to date have primarily incorporated BIMP-capable bacteria sampled from the environment without detailed investigations of the underlying bacterial mechanisms. This review covers our current mechanistic understanding and highlights the complexity and connectivity between the different cellular and metabolic processes involved. Ultimately, such detailed insights will facilitate the rational design of application-specific, custom BIMP technologies and deepen our understanding of how bacteria are shaping our world.*

1.1 Bacteria-induced mineral precipitation.

Bacterial activity is evident in our landscapes and throughout the geological record, where it has helped shape Earth's mineral deposits (Zavarzin, 2002). This has occurred, amongst other contributors, via a process known as bacteria-induced mineral precipitation (BIMP). These deposits can take on the form of stalactites and stalagmites (Banks *et al.*, 2010), microbialites, stromatolites and thrombolites (Riding, 2000; Kaźmierczak *et al.*, 2015) as well as large scale sedimentation (Riding, 2000). Precipitation of mineral species in an aqueous system occurs when the ion concentration exceeds solubility and reaches a degree of super-saturation. Once the activation energy barrier is overcome, initial crystal nucleation occurs, in which metastable critical nuclei form that may dissolve back into the bulk phase. Subsequent aggregation of individual nuclei describes the process of crystal growth and precipitation (Fortin *et al.*, 1997; Benning and Waychunas, 2008; Cubillas and Anderson, 2010). Nucleation can take place either homogeneously, whereby nucleation occurs when critical nuclei form in absence of foreign particles (via random collisions of ions or atoms in solution), or heterogeneously, whereby nucleation takes place when critical nuclei form on surfaces of foreign particles (Fortin *et al.*, 1997; Benning and Waychunas, 2008; Cubillas and Anderson, 2010). Such particles lower the activation energy by providing templates with spacing that enhance nucleation and thus, precipitation (Fortin *et al.*, 1997; Benning and Waychunas, 2008; Cubillas and Anderson, 2010). Furthermore, during the nucleation process foreign particles may aggregate leading to mixed precipitates forming (Reeder *et al.*, 1999). Bacteria can induce the process of precipitation by indirectly and involuntarily modulating these parameters through changes in local ion concentrations and/or by providing nucleation sites. In generalised terms, the bacterial process involves the attraction of cations to cell surfaces, while metabolism provides the appropriate counter anions and microenvironment so that these cations may precipitate as minerals (Schultze-Lam *et al.*, 1996). The BIMP trait is common amongst bacteria across environments (Boquet *et al.*, 1973; Anbu *et al.*, 2016; Krajewska, 2017; Seifan and Berenjian, 2019; Reeksting *et al.*, 2020), and, depending on bacterial species and environment, it can lead to a range of minerals precipitated through bacterial activity (Table 1). The bacterial precipitation of some of these minerals can further lead to co-precipitation of additional divalent metal cations and anions (Basnakova *et al.*, 1998; Podda *et al.*, 2000; Lauchnor *et al.*, 2013). Bacterial influence on precipitation parameters of saturation state and nucleation catalysis can be broadly separated into two contributing areas: cell surface and cell metabolism, the mechanisms of which will be reviewed here.

Table 1. Minerals precipitated in association with bacterial activity[a].

Mineral	Chemical formula	Reference
Carbonates		
Calcite	$CaCO_3$	(Boquet *et al.*, 1973)
Dolomite	$CaMg(CO_3)_2$	(Wright and Wacey, 2005; Deng *et al.*, 2010)
Kutnahorite	$CaMn(CO_3)_2$	(González-Muñoz *et al.*, 2008)
Siderite	$FeCO_3$	(Kooli *et al.*, 2018)
Magnesite	$MgCO_3$	(Thompson and Ferris, 1992; González-Muñoz and Chekroun, 2000)
Otavite	$CdCO_3$	(Li *et al.*, 2010)
Strontianite	$SrCO_3$	(Schultze-Lam and Beveridge, 1994)
Rhodochrosite	$MnCO_3$	(Naik-Samant and Furtado, 2019)
Cerussite	$PbCO_3$	(Kang *et al.*, 2015)
Hydrozincite	$Zn_5(CO_3)_2(OH)_6$	(Podda *et al.*, 2000; Ngwenya *et al.*, 2014)
Dypingite	$Mg_5(CO_3)(OH)_2{\cdot}5H_2O$	(Power *et al.*, 2007)
Witherite	$BaCO_3$	(Sanchez-Moral *et al.*, 2004)
Phosphates		
Tricalcium phosphate	$Ca_3(PO_4)_2$	(Benzerara *et al.*, 2004)
Struvite	$NH_4MgPO_4{\cdot}6H_2O$	(González-Muñoz *et al.*, 2008; Rivadeneyra *et al.*, 2014)
Bobierrite	$Mg_3(PO_4)_2{\cdot}8H_2O$	(Rivadeneyra *et al.*, 1987; Rivadeneyra *et al.*, 2014)
Baricite	$(MgFe)_3(PO_4)_2{\cdot}8H_2O$	(Rivadeneyra *et al.*, 2014)
Vivianite	$Fe_3(PO_4){\cdot}2H_2O$	(Kooli *et al.*, 2018)
Autunite	$Ca(UO_2)_2(PO_4)_2{\cdot}10\text{-}12H_2O$	(Merroun *et al.*, 2011)
Uramphite	$NH_4UO_2PO_4$	(Macaskie *et al.*, 1992; Newsome *et al.*, 2014)
Apatite	$Ca_{10}(PO_4)_6(OH)_2$	(Crosby and Bailey, 2012)
Pb-hydroxyapatite	$Ca_{2.5}Pb_{7.5}(OH)_2(PO_4)_6$	(Chen *et al.*, 2016)
Strengite	$FePO_4{\cdot}2H_2O$	(Konhauser *et al.*, 1994; Konhauser, 1997)
Variscite	$AlPO_4{\cdot}2H_2O$	(Ehrlich, 1999)
Silicates		
Gehlenite	$Ca_2Al(AlSiO_7)$	(Biswas *et al.*, 2010)
Silica	SiO_2	(Yee *et al.*, 2003)
Nontronite	$Na_{0.3}Fe^{3+}{}_2(Si,Al)_4O_{10}(OH)_2{\cdot}nH_2O$	(Ta *et al.*, 2017)
Chamosite	$(Fe_5Al)(Si_3Al)_{10}(OH)_8$	(Konhauser, 1997)
Kaolinite	$Al_4(Si_4O_{10})(OH)_4$	(Konhauser, 1997)
Sulphides		
Mackinawite	FeS	(Picard *et al.*, 2018)
Greigite	Fe_3S_4	(Lefèvre *et al.*, 2011; Picard *et al.*, 2018)
Pyrite	FeS_2	(Baas Becking and Moore, 1961)
Covellite	CuS	(Baas Becking and Moore, 1961)
Sphalerite	ZnS	(Baas Becking and Moore, 1961)
Galena	PbS	(Baas Becking and Moore, 1961)
Digenite	Cu_9S_5	(Baas Becking and Moore, 1961)
Argenite	Ag_2S	(Baas Becking and Moore, 1961)
Sulphates		
Gypsum	$CaSO_4{\cdot}2H_2O$	(Schultzelam *et al.*, 1992; Thompson and Ferris, 1992)
Celestite	$SrSO_4$	(Schultze-Lam and Beveridge, 1994)
Barite	$BaSO_4$	(Sanchez-Moral *et al.*, 2004; Keren *et al.*, 2017)
Oxides		
Magnetite	Fe_3O_4	(Frankel *et al.*, 1983; Kooli *et al.*, 2018)
Hematite	Fe_2O_3	(Konhauser, 2007; Polgári *et al.*, 2019)
Ferrihydrite	$Fe_2O_3{\cdot}0.5H_2O$	(Polgári *et al.*, 2019)

Geothite	α-FeO(OH)	(Polgári *et al.*, 2019)
Manganite	MnOOH	(Greene and Madgwick, 1991)
Vernadite	MnO_2	(Villalobos *et al.*, 2003; Jürgensen *et al.*, 2004; Webb *et al.*, 2005)
Hausmannite	Mn_3O_4	(Mann *et al.*, 1988)
Todorokite	$(Ca,Na,K)_x(Mn^{4+},Mn^{3+})_6O_{10}\cdot 3.5H_2O$	(Polgári *et al.*, 2019)
Birnessite	$(NaCa,K)_x(Mn^{4+},Mn^{3+})_2O_4\cdot 1.5H_2O$	(Polgári *et al.*, 2019)
Uranite	UO_2	(Lovley and Phillips, 1992; Suzuki *et al.*, 2003)
Calcium Arsenate	$CaHAsO_3$	(Achal *et al.*, 2012)

[a] Overview of the types of minerals that have been shown to be precipitated in association with bacterial activity. The minerals listed and accompanying sources are non-exhaustive of the examples available in literature.

1.2 Cell surface: nucleation catalysis, saturation state, and nucleation template.

The large surface area to volume ratio of bacteria make them ideal nucleation sites. Covered by functional groups with a net negative charge, their surface acts as a metal cation scavenger concentrating dilute cations attracted from the environment. (Beveridge and Fyfe, 1985; Schultze-Lam *et al.*, 1996; Douglas and Beveridge, 1998). Net negative surface charge is imparted by carboxyl ($R\text{-}CO_2H$) and phosphate groups ($R\text{-}PO_4H_2$) of teichoic acids in Gram-positive bacteria, and phospholipids and lipopolysaccharides in Gram-negative bacteria (Madigan *et al.*, 2018). Bacterial S-layers further influence net surface charge depending on the presence or absence of S-layer glycol proteins with glycosylated long carbohydrate chains, and depending on the structural groups exposed within their lattice pores (Schultzelam *et al.*, 1992; Sleytr *et al.*, 2014; Merroun *et al.*, 2005). These bacterial surface structures are illustrated in Figure 1. Extracellular polymeric substances (EPS), capsules, sheaths, slimes and, biofilm matrices may further surround Gram-positive or Gram-negative bacteria. These are also usually associated with a net negative charge imparted by carboxyl and phosphate groups, which are free to interact with soluble cations (Southam, 2000). The extent of the surface negative charge is governed by the deprotonation of functional groups with an increase in pH: carboxyl, phosphate, hydroxyl (R-OH), and sulphate ($R\text{-}SO_4$) groups increase their negative charge, while amine ($R\text{-}NH_2$) groups decrease their positive charge. For bacteria living in natural environments with neutral pH ranges, this means that surfaces tend to be negatively charged and have a high affinity for cationic species (Warren and Haack, 2001; Merroun *et al.*, 2011). Carboxyl groups in particular have been found to contribute strongly to the metal binding capability. Studies on *Bacillus subtilis* used chemical modification of phosphate and carboxyl functional groups to demonstrate their importance in and relative contribution to metal ion binding (Beveridge and Murray, 1980; Doyle *et al.*, 1980). More recent studies of Gram-positive cell walls support this role, with half the binding of calcium and magnesium coming from polyphosphate groups of teichoic acids and half from carboxyl groups of peptidoglycan (Thomas and Rice, 2014).

Teichoic and teichuronic acids, as well as LPS are natively stabilised by the presence of divalent cations, providing starting nucleation sites for mineral formation (Southam, 2000). Surface cation binding sites are assumed to form the centre of crystal growth. Mineral precipitation occurs from nucleation of cations to previously adsorbed surface cations. The formation of these critical nuclei is stabilised by the surface functional groups through a reduction of tension between the bulk water phase and mineral nucleus (Southam, 2000). Once bound, supersaturation is achieved by lowering the free energy necessary for precipitation, often with the help of metabolic changes in pH. Consequently precipitation can then occur faster than in systems without bacteria (Bäuerlein, 2003) For example, in the precipitation of the calcium-magnesium mineral dolomite, the dehydration of the magnesium ion and subsequent carbonation are the rate limiting step of nucleation. In the presence of carboxyl groups, $[Mg(H_2O)_6]^{2+}$ binds and dehydrates to $[Mg(H_2O)_5(R\text{-}COO)]^{+}$. This lowers the activation energy for subsequent carbonation and attachment of Ca^{2+} to form dolomite ($CaMg(CO_3)_2$) (Katz *et al.*, 1998; Kluge and Weston, 2005; Roberts *et al.*, 2013). Thus, bacteria provide a mechanism of heterogeneous precipitation, with their surfaces acting as a nucleation catalyst and template, as well as increasing the saturation state through local attraction of cations.

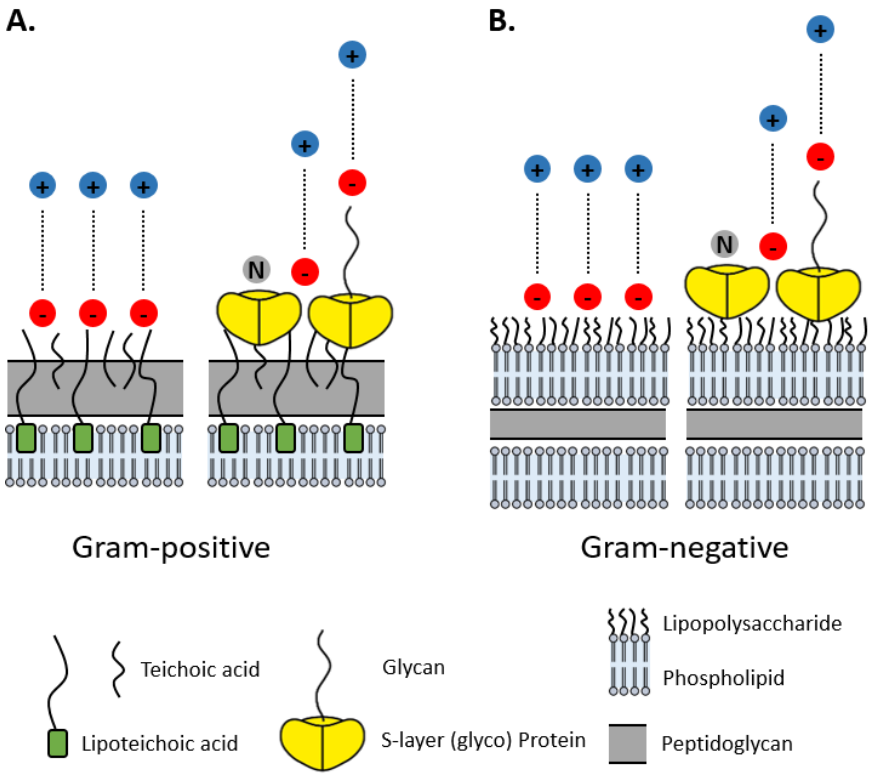

Figure 1. Schematic of the major supramolecular structures on the surface architecture of (A) Gram-positive and (B) Gram-negative bacteria, which provide sites for metal cation interaction. The red circles represent sites of negative charge, the grey circle represent sites of neutral charge, the blue circles represent positively charged cations, and dotted lines illustrate the attraction

between negative and positive charges. Adapted from (Sleytr et al., 2014; Seifan and Berenjian, 2018).

Beyond the direct influence of bacterial surfaces, the microenvironment they create also plays a very important role in influencing ion saturation state. All submerged surfaces, such as those of microorganisms, are surrounded by a thin-filmed water envelope called the hydrodynamic boundary layer. Bacteria live at an extremely low Reynolds number, that is, the viscous forces of the environment dominate over their ability to move. As a consequence, these bacteria experience greater viscous drag and so struggle to escape their thin water envelope (Purcell, 1977). Within this surrounding water envelope, concentration gradients of ions can form where local concentrations are higher than in the bulk aqueous environment. Supersaturation will vary with ion concentration and so precipitation will be favoured within the cell surface vicinity where the concentration is highest. The concentration gradient is the combined result of cell surfaces lowering thermodynamic activation energies, sequestering cations, as well as cell metabolism reactions providing anions, all of which occurs within the surrounding water layer (Thompson and Ferris, 1992; Schultze-Lam *et al.*, 1996). This principle can be extended further to other layers surrounding microbial surfaces such as biofilm matrices, slimes, sheaths, filaments, capsules, and EPS secretions. These layers can create a microenvironment that favours supersaturation and thus precipitation via local changes in ion mobility, viscosity and nucleation kinetics (Buczynski and Chafetz, 1991). For example, mineralization has been seen on bacterial sheaths and filaments (Jürgensen *et al.*, 2004; Gilbert *et al.*, 2005), slimes (Braissant *et al.*, 2003; Frankel and Bazylinski, 2003), biofilms and EPS (Braissant *et al.*, 2007). Some findings even showed that purified EPS alone could contribute to mineral precipitation, while other studies found that EPS production was not always associated with mineral precipitation (Ercole *et al.*, 2007; Kim *et al.*, 2017; Fishman *et al.*, 2018). This emphasises the complexity of the process dependent on the bacterium, environment, mineral formed, and underlying mechanism. In cyanobacterial systems, EPS has been shown to inhibit the precipitation in the bulk phase of the environment by trapping large amounts of divalent cations in its sugars, acidic residues, and negatively charged functional groups. Only upon degradation of EPS and liberation of the cations does the saturation index increase, allowing for the precipitation of minerals (Dupraz and Visscher, 2005; Kremer *et al.*, 2008; Dupraz *et al.*, 2009). Further to creating favourable conditions, the microenvironment is not subject to the same kinetics as the bulk environment and therefore also protects against inhibiting factors such as ion complexing and cation hydration (Wright and Oren, 2005). Thus, bacterial surfaces and their microenvironments allow precipitation to occur in even unfavourable conditions such as acidic environments (Fernández-Remolar *et al.*, 2012). Over the course of precipitation and with the eventual

degradation of some extracellular organic components, the microenvironment is broken down and leaves behind a mineral organic phase encasing the cell, illustrated in Figure 2.

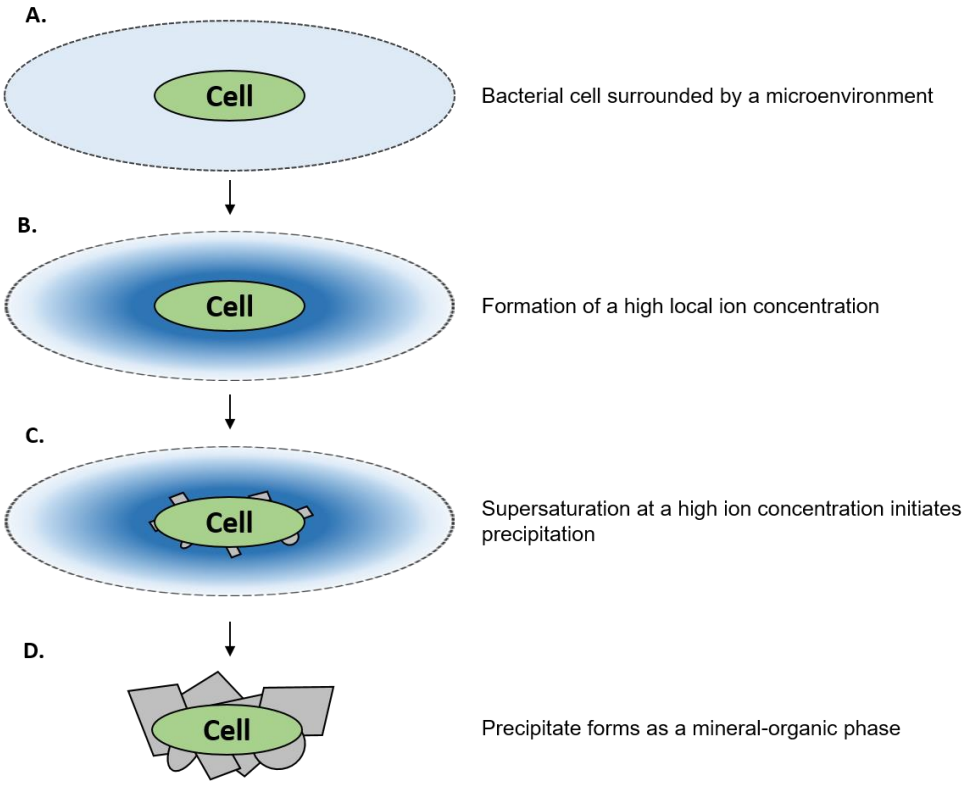

Figure 2. Mineral encasement of a bacterial cell. A. Bacterial cell (green) surrounded by a microenvironment (light blue) created by an extremely low Reynolds number and/or sheaths, capsules, slimes, biofilm matrices or extracellular polymeric substances. B. Accumulation, stabilisation and slow diffusion of ions within the microenvironment close to the cell occurs from metabolism and cell surface interactions creating a high local ion concentration (dark blue). C. Within the cell surface vicinity, at a high ion concentration, the equilibrium is shifted in favour of supersaturation and thus precipitation (grey shapes). D. Onset of precipitation can lead to the breakdown of the microenvironment and, along with the degradation of some extracellular organic components, leaves behind a mineral-organic phase encasing the cell (grey shapes).

1.3 Cell surface: polymorph ratio, crystal morphology, mineral type, and crystal size.

In addition to providing nucleation sites and concentrating ions, surface structures can influence mineral polymorph ratio, crystal morphology, and the type of minerals precipitated. Polymorphs have the same chemical structure but differ in their crystal structure (Tegethoff, 2001). Calcium carbonate encompasses the polymorphs calcite, vaterite and aragonite, and their ratios can be affected by cell surface chemistry. For example, the presence of carboxylic groups, phosphonates,

sulfonates, and amino acids has been found to promote formation of vaterite (Rodriguez-Navarro *et al.*, 2007). The morphology of calcium carbonate crystals was also found to be influenced by an increase in acidity of L-amino acids and xanthan content, where calcite crystals transitioned from rhombohedra to fibro-radial spherulites, and vaterite crystal spheres evolved from clustered short needles to clustered large hexagons (Braissant *et al.*, 2003). The type of minerals precipitated is in part determined by the selective adsorption of metals to certain functional groups. Different metals were found to bind cell surface components with different affinities. For example, it was reported that Mg^{2+} bound with a higher affinity than Ca^{2+} to cell walls of the Gram-positive *B. subtilis* (Beveridge and Murray, 1976; Beveridge and Murray, 1980; Doyle *et al.*, 1980) as well as to cell envelopes of the Gram-negative *Escherichia coli* (Beveridge and Koval, 1981). The selective adsorption of calcium and strontium cations versus that of magnesium to pores within S-layers of *Synechococcus sp.* governed the preferred precipitation of the sulphate minerals gypsum and celestite (Schultze-Lam and Beveridge, 1994).

When investigating the role of bacterial organics on crystal precipitation, it may also be useful to look beyond microbiology and into other organisms capable of mineral formation. Life on Earth shares the same fundamental building blocks and so one may be able to transfer some understanding of crystal formation from other biological systems into that of microbiology. For example in molluscs, studies found that amino acid charge, size, rigidity, and pK_a of carboxyl and amino functional groups were important in governing mineral phase interaction and crystalline lattice inclusions (Borukhin *et al.*, 2012). The formation of mollusc biominerals occurs through a complex chemical interaction between the organic and inorganic matrix where one provides a template for the other, guiding crystallization plane and crystal size. Steric arrangements of the functional groups, their folding, and sequence will govern ion binding and positioning and thus, ultimately the specifics of mineralization, mineral type and polymorph (Gilbert *et al.*, 2005). Material science studies have also explored the use of functional groups, including carboxyl, amine, hydroxyl, phosphate, sulfonic ($R\text{-}SO_3H$), methyl ($R\text{-}CH_3$), and thiol (R-SH) groups, in calcium carbonate precipitation to control size and physical properties (Deng *et al.*, 2013). These studies found that chemical group composition, properties (e.g. hydrophobicity, charge and geometry) and environment (e.g. temperature and ion concentrations) greatly influenced crystallization, such that some variability was always observed even when conditions were kept similar (Deng *et al.*, 2013; Deng *et al.*, 2015). Therefore, when considering the diverse range of microbes and their surface compositions, individual species will influence the specifics of the mineral formed. The complexity and variety of bacterial surfaces thus is an important contributor to the complexity and variety of minerals in the environment.

1.4 Cell surface or metabolism: are precipitating bacteria dead or alive?

There is some debate as to whether the mechanism of BIMP is dependent on bacterial activity, i.e. dead or live cells. This leads to different interpretations of how important cell surface structures are for the process of mineral precipitation. While material science studies showed that precipitation can occur on functional group monolayers (Deng *et al.*, 2013), absence of precipitation on dead cells suggests that the organic material is not simply a nucleation seed, but that metabolism also plays a key role (Yates and Robbins, 1998; Rivadeneyra *et al.*, 2014). In contrast, other work found that minerals do form on dead cells and their debris (Ercole *et al.*, 2007; Velásquez and Dussan, 2009; Picard *et al.*, 2018). This discrepancy may be simply a result of the differences between bacterial species, environmental conditions or methodologies used to prepare the dead cells, as this may have structural consequences (Banks *et al.*, 2010). An active point of discussion is that, if only living cells precipitated minerals, the whole bacterial community/population could run the risk of complete entombment and death. The argument here is that precipitation with the risk of entombment would not be favoured in evolution unless there is an associated benefit, such as detoxifying the environment of metal cations and thereby making it a more favourable environment for further generations before complete community collapse (Banks *et al.*, 2010). To allow for the continued growth of a population, precipitation would therefore be assumed to occur on dead cells and/or a restricted number of live cells (Benzerara *et al.*, 2004). There have been observations of microbes seeming to actively evade entombment by shedding encrusted S-layers (Schultzelam *et al.*, 1992), forming mineral sheaths/capsules (Gilbert *et al.*, 2005), forming nanoglobules to act as decoy precipitation targets (Aloisi *et al.*, 2006; Bontognali *et al.*, 2008), or even controlling surface functional group distribution to control precipitation occurrence (Asada and Tazaki, 2001). Another observation has been that induction of a proton motif force by metabolic activity of live cells reduced the cell wall metal binding ability (Urrutia Mera *et al.*, 1992). Metabolism as an active mechanism against entombment has been proposed in cyanobacteria and suggested that dead cells could potentially be better at mineral precipitation because they retained more of their negative surface charge (Martinez *et al.*, 2010). Zeta potential analysis was used to approximate the net surface charge of the bacteria by measuring the potential differences between the cell and fluid interface (Martinez *et al.*, 2008). In these studies, metabolic activity was found to contribute to a more positive surface charge, likely regulated to attract anions for metabolism. On the other hand, dead cells retained a constant negative charge on their surface structures (Martinez *et al.*, 2008). At a community level i.e. a mixture of live and dead bacteria, one explanation for the ability of these bacteria to precipitate minerals on their surface may be as a result of cations binding to negatively charged surfaces of dead or inactive cells. Alternatively, a somewhat counterintuitive explanation might be the attraction of carbonate anions to metabolically active cells and letting

these act as the seed for nucleation rather than the typical cations (Martinez *et al.*, 2008). Evidence of changes in cell surface charge between dead and live cells is still limited, and there is likely to be variability among bacterial species depending on their surface structures. Taking into account these observations, the more likely explanation is that most often both surface structure and bacterial metabolism are required as catalysts to modulate precipitation parameters by influencing saturation state and nucleation ability. Precipitation should occur under conditions of supersaturation, when cations attracted to the bacterial surface react with counter anions in the environment. Anion concentration is in turn environment dependent or may be supplemented by metabolism, suggesting both live and dead bacteria may be needed.

1.5 Cell metabolism: pH, dissolved inorganic carbon (DIC) and inorganic anions.

Cell metabolism has an integral role in influencing conditions such as pH and anion concentrations, which along with the cell surface is a key contributor to mineral precipitation. For reasons of brevity, only the key contributing factors to mineral precipitation created by different metabolic pathways are discussed here. The details of individual metabolic pathways in mineral precipitation have been reviewed elsewhere (Castro-Alonso *et al.*, 2019; Seifan and Berenjian, 2019). Metabolic activity is accompanied by changes in pH due to the production of various metabolic by-products. This in turn affects precipitation potential, with higher pH directly contributing to the availability of anions through deprotonation and supersaturation. For example, in the case of carbonates, the precipitation potential is dependent on both the pH and the total dissolved inorganic carbon (DIC), which is the sum of the dissolved forms of CO_2, HCO_3^-, and CO_3^{2-}. The concentration of anions is directly related to the pH through the dissociation constant as seen in the carbonate equilibrium (Equation 1) (Zeebe and Wolf-Gladrow, 2001). In addition, the carbonate alkalinity, defined as the total concentration of HCO_3^- and CO_3^{2-}, in turn drives an increase in pH. At higher pH, the carbonate equilibrium is shifted to the right and carbonate species are deprotonated. As a result, more bicarbonate and carbonate ions are available for precipitation. Similarly, phosphate groups will be subject to changes in protonation state, depending on environmental pH (Equation 2). Sulphate groups will typically be present in their deprotonated state due to their low pKa values (usually below 2.5), which will generally be exceeded by environmental pH (Braissant *et al.*, 2007). Precipitation at low pH is possible in theory, but mostly applies to phosphate-containing minerals where the anion component has a lower pKa. However, low pH in practice often leads to dissolution of minerals.

$$CO_2 + H_2O \overset{\text{pKa } 6.35}{\longleftrightarrow} HCO_3^- + H^+ \overset{\text{pKa } 10.3}{\longleftrightarrow} CO_3^{2-} + 2H^+ \quad \text{(Equation 1)}$$

$$H_3PO_4 \quad \text{(Equation 2)}$$
$$\overset{pKa\ 2.16}{\longleftrightarrow} H_2PO_4^- + H^+ \overset{pKa\ 7.21}{\longleftrightarrow} H_2PO_4^{2-} + H^+ \overset{pKa\ 12.32}{\longleftrightarrow} H_2PO_4^{3-} + H^+$$

In addition to the effects of pH on protonation of anions, the concentration of anions such as phosphates, sulphates, and carbonates are also important, because they are needed to combine with cations to precipitate as minerals. These anions are produced as by-products of bacterial metabolism, and when high concentrations of these anions occur in the bulk phase they react with cations and authigenic mineral precipitation occurs (Ehrlich, 1999). Autotrophic pathways such as non-methylotrophic methanogenesis, oxygenic and anoxygenic photosynthesis utilise CO_2 to produce organic matter (Madigan *et al.*, 2018; Dupraz and Visscher, 2005) and in so doing cause a depletion in CO_2 that alters the bicarbonate equilibrium (Equation 1) (Hammes and Verstraete, 2002). The resulting increase in bicarbonate ions as well as hydroxide ions, coupled with the increase in pH caused by the removal of H^+, favours precipitation in the presence of cations (Figure 3). Similarly, heterotrophic metabolism can cause local increases in anion concentration and pH through a range of different reactions. Aerobic heterotrophs break down organic carbon, producing CO_2 as a metabolic by-product that partially converts to carbonate and bicarbonate and increases DIC and pH in the bulk phase (Dupraz and Visscher, 2005; Krause *et al.*, 2018). Within the nitrogen cycle, ureolysis, dissimilatory reduction of nitrate, and deamination of amino acids lead to production of ammonium and hydroxide ions and consumption of H^+ ions, increasing pH and again shifting the carbonate equilibrium (Figure 3) (Krause *et al.*, 2018). In the sulphur cycle, dissimilatory reduction of sulphate, carried out in anoxic conditions by sulphate-reducing bacteria results in the production of carbonate, bicarbonate and hydrogen sulphide (H_2S) (Figure 3). Whether this leads to biomineralisation depends on the fate of the H_2S produced. Excreted sulphide can lead to authigenic precipitation in the bulk phase by directly reacting with metal cations in the environment to precipitate sulphide minerals (Ehrlich, 1999). Alternatively, loss of H_2S can occur through degassing or consumption by anoxygenic sulphide phototrophic bacteria that oxidise H_2S to elemental sulphur and form intra- or -extracellular deposits. The removal of H_2S increases the pH and thus favours precipitation (Figure 3) (Castanier *et al.*, 1999). On the other hand, autotrophic sulphide-oxidising aerobic bacteria use H_2S (and other reduced sulphur compounds, S^0 and $S_2O_3^{2-}$) to produce sulphate ions that form sulphuric acid, decreasing the pH and dissolving precipitates

(Castanier *et al.*, 1999; Dupraz and Visscher, 2005). The balance between precipitation and dissolution will be dependent on environmental conditions such as oxygen availability, light, and pH, which serve to decouple the different metabolic processes in time and space and establish local conditions where net precipitation can occur (Visscher *et al.*, 1998). Precipitation reliant on these metabolic by-products, and the changes in pH and anion concentrations that accompany them, is generally considered as a passive bacterial process.

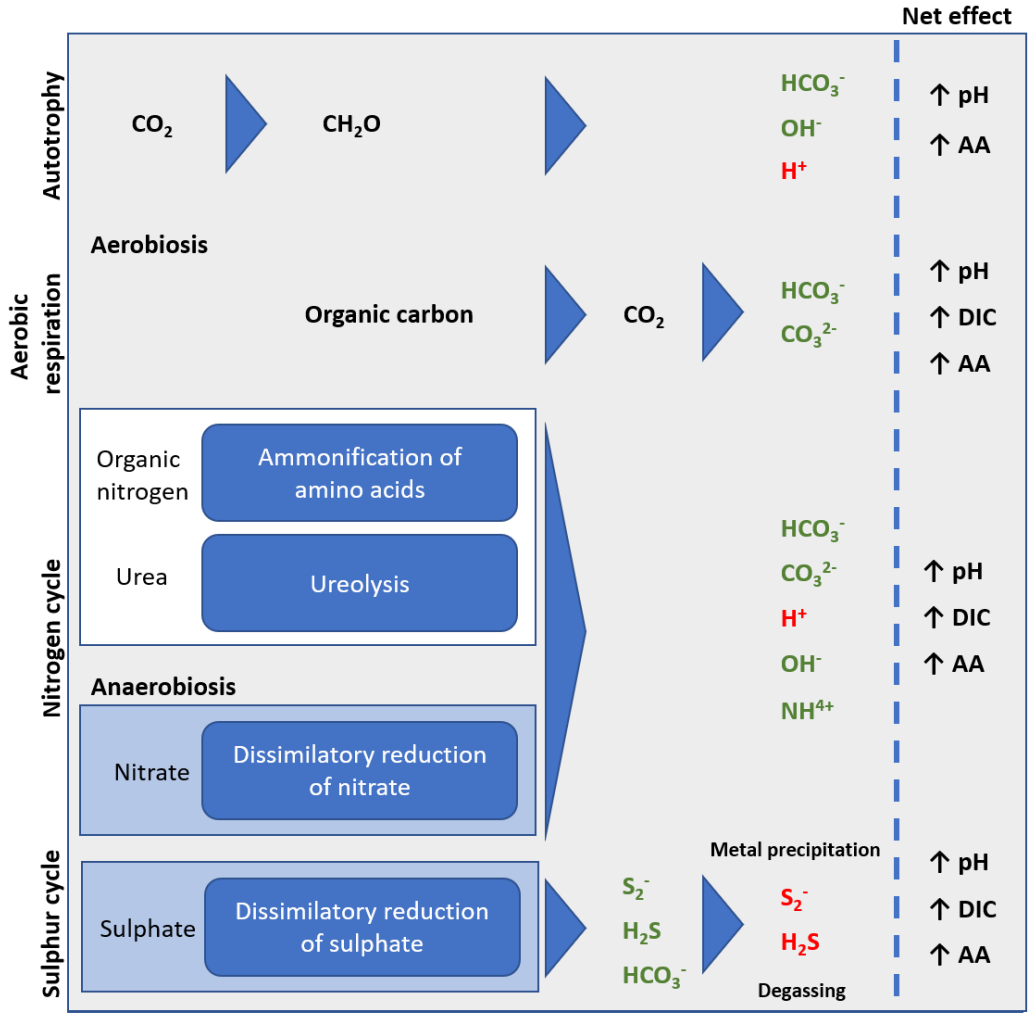

Figure 3. Metabolic pathways associated with bacteria-induced calcite precipitation. Various products of metabolism result in a net effect that primes the environment for mineral precipitation. AA refers to anion availability, typically bicarbonate and carbonate. Products in green indicate an increase and red indicate a decrease. Adapted from (Castanier *et al.*, 1999).

Aside from these metabolic processes, specific enzymes can also contribute to precipitation. Acid phosphatases liberate phosphoryl groups, accelerating formation of phosphate mineral species, and strains overproducing this enzyme were shown to precipitate uranium phosphate species

(Basnakova *et al.*, 1998; Powers *et al.*, 2002; Martinez *et al.*, 2007; Newsome *et al.*, 2014). However, not all bacteria with phosphatase activity can precipitate minerals, lending weight to the idea that specific cell surface structures are likely required to provide nucleation sites for precipitation (Macaskie *et al.*, 1994). Carbonic anhydrase, catalysing the interconversion of CO_2 to HCO_3^- and H^+, has been suggested as a key enzyme in precipitation due to its effect on local HCO_3^- concentration. The presence of extracellular carbonic anhydrase was found to govern the location of crystal precipitates in biofilms of *Alcanivorax borkumensis* (Krause *et al.*, 2018). Indeed, carbonate precipitation was restricted to areas with high extracellular concentrations of carbonic anhydrase. The increase in pH associated with increased HCO_3^- as well as other metabolic by-products lead to supersaturation of the environment with carbonate and subsequent mineral precipitation.

1.6 Cell metabolism: cation accumulation.

Apart from the generation of anion species needed for precipitation, cation availability can also be influenced through metabolic activity. This may occur when bacteria reduce a mineral compound to produce divalent cations that can then react with anions to precipitate as a different mineral (Ehrlich, 1999). Some bacteria utilise metal ions as terminal electron acceptors in microaerobic or anaerobic conditions to produce cations such as Fe^{2+} through reduction of oxidised iron (Fe^{3+}), usually from dissolution of other iron oxides (Table 1) (Lovley, 1991; Roh *et al.*, 2002). The resulting Fe^{2+} can subsequently interact with various anions to form a variety of iron minerals (Table 1). Many of these iron-reducing bacteria are also capable of reduction of manganese (Mn^{4+} to Mn^{2+}), providing Mn cations for mineral formation (Frankel and Bazylinski, 2003). Mn oxides that are reduced to Mn^{2+} can then react with anions such as CO_3^{2-} in the bulk phase to precipitate as $MnCO_3$, (Ehrlich, 1999). The precipitation of the Fe- and Mn -containing minerals described above occurs at neutral pH. Although acidophiles are more frequently associated with the dissolution and bioleaching of minerals, minerals such as metal oxides, sulphates, phosphates, and carbonates can be precipitated at acidic pH by Fe- and Mn- oxidising bacteria (Frankel and Bazylinski, 2003). Fe-oxidising bacteria gain energy through the oxidation of ferrous iron (Fe^{2+}) to the ferric state (Fe^{3+}), which forms insoluble ferric hydroxide ($Fe(OH)_3$) in water (Madigan *et al.*, 2018). Fe^{2+} oxidation can also occur under anoxic conditions through the activity of some phototrophic bacteria and some nitrate-respiring bacteria (Frankel and Bazylinski, 2003). Large deposits of ferric iron in ancients sediments are now believed to have originated from anoxygenic phototrophs oxidising Fe^{2+}(Madigan *et al.*, 2018). Similarly, Mn-oxidising bacteria mineralise Mn oxides through the oxidation of Mn^{2+} (Brouwers *et al.*, 1999).

Local cation concentration can also fluctuate due to active bacterial processes such as metal ion homeostasis via ionic pumps and channels. In high calcium environments, such as calcareous caves and limestone soils, the need to maintain a low intracellular calcium concentration is essential (Anderson *et al.*, 1992). Microbes can achieve this through active efflux of intracellular calcium by ATP-dependent antiporters, increasing the local calcium availability and pH near the cell surface and thus contributing to precipitation (Hammes and Verstraete, 2002). This has been demonstrated by radioisotope tracer studies that showed intracellular calcium being incorporated into extracellular calcium carbonate (Yates and Robbins, 1999). Supporting this, deletion of the calcium ion efflux pump ChaA in *Salmonella typhimurium* led to a loss of growth on media with high calcium concentrations (Banks *et al.*, 2010). Such active processes may precede the passive precipitation discussed previously and allow microbes to act as nuclei for subsequent crystal growth (Castanier *et al.*, 1999).

1.7 Prospects.

In exploring the underlying processes enabling BIMP, a lot of benefit has been gained from research across multiple disciplines investigating the different aspects of organic-mineral interphases. While there are mechanistic differences in the way bacteria induce mineralization dependent on their surface architecture and metabolism, understanding the contributing components is important when applying bacteria for biotechnologies. An additional layer of complexity is introduced when considering that bacteria do not occur in isolation, and that metabolic processes of one group of organisms are often interdependent with the activities of other groups. Indeed, in nature precipitation results from the activities of mixed populations, which often grow as biofilms rather than planktonic cells (Castanier *et al.*, 1999; Dupraz *et al.*, 2009). This could possibly be exploited in utilising communities and biofilm growth of microorganisms to maximise precipitation potential. BIMP has seen increased applications in civil engineering and biotechnology over recent years, as extensively reviewed elsewhere (De Muynck *et al.*, 2010; Dhami *et al.*, 2013; Phillips *et al.*, 2013; Zhu and Dittrich, 2016; Arias *et al.*, 2017). In brief, mineral precipitation mainly has two different roles in these technologies. For applications that include soil consolidation, heritage conservation and self-healing concrete, precipitated minerals and embedded cells and organic components become the ‘glue’ that binds and/or seals the surrounding matrix. For applications of bioremediation such as of toxic heavy metals or radionuclides or in carbon dioxide sequestration, the elements in question are directly precipitated or co-precipitated, rendering them bio-unavailable (Phillips *et al.*, 2013; Zhu and Dittrich, 2016). Fundamental mechanistic insight will therefore be important in making more informed decisions in choosing the appropriate bacteria for

a specific application in terms of strain characteristics and minerals precipitated. This could allow for selective mineral precipitation, dependent on preferential surface binding and metabolic anion production of the chosen bacterium. Additionally one could even modulate the speed of precipitation through the choice of metabolism, depending on application need. In the future, this may even drive more rational directed evolution or genetic engineering approaches for application-driven strain development. The complexity of BIMP dependency on precise bacterial properties may therefore even be viewed as a benefit as we gain deeper mechanistic insights. Nature may reveal a useful and versatile toolbox of different bacteria, supplemented by systematic strain engineering to meet future needs for sustainable BIMP technologies.

Chapter 2

Tiny Architects: Biotechnological Applications of Bacteria-Induced Calcite Precipitation

ABSTRACT *The biotechnological applications surrounding bacteria-induced calcite precipitation with focus on the construction industry, and more specifically self-healing concrete, are briefly introduced. Following this, the overarching thesis aim and objectives are outlined and tied together.*

2.1 BICP biotechnologies: self-healing concrete.

Microbes in our built environment are mostly associated with topics of biodegradation, biofouling, biocorrosion and bioweathering instead of positive impacts (Gadd, 2017). However, over the recent decades bacteria have been at the basis of innovative technologies arising in civil engineering, all based around the principle of bacteria-induced calcite precipitation (BICP) (De Muynck *et al.*, 2010; Dhami *et al.*, 2013; Phillips *et al.*, 2013; Anbu *et al.*, 2016; Zhu and Dittrich, 2016; Arias *et al.*, 2017). The first patented application is considered to have been by Adolphe *et al* in 1990 for the biological surface treatment of stone (Adolphe *et al.*, 1990). Since then more technologies have been developed, with the most attention surrounding that of self-healing concrete, first pioneered by Jonkers (Jonkers, 2007). This uses bacteria as a biological self-healing agent within concrete, where the calcite precipitated by bacterial activity *in situ* acts as the 'glue' to seal cracks formed within the cementitious structures (Jonkers, 2007; Jonkers and Schlangen, 2007). A schematic of this technology is given in Figure 4, and a more detailed explanation is provided below.

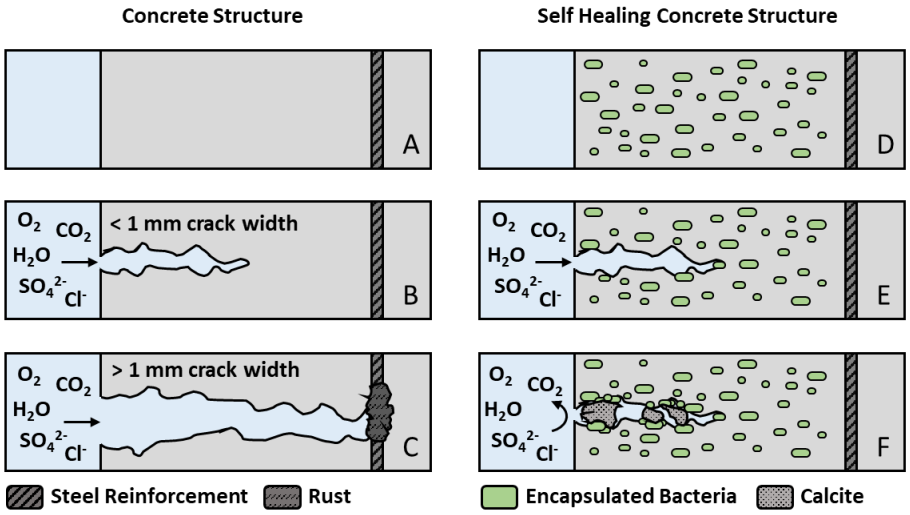

Figure 4. Schematic cross-section of conventional concrete (A) and self-healing concrete (D). Ingress of chemicals into micro cracks degrades concrete matrix and accelerates corrosion of steel reinforcements (B-C). Encapsulated bacteria released upon cracking and germinated by ingress of water leads to microbial induced calcite precipitation and sealing of crack (E-F). Diagram adapted from (Jonkers, 2007).

Concrete constructions must withstand weathering and tensile stresses that lead to their progressive decay over time, as cracks are formed and porosity increases (De Muynck *et al.*, 2010). Ingress of harmful chemicals into these cracks, such as carbon dioxide (CO_2), sulphates (SO_4^{2-}) and chlorides (Cl^-) lead to the accelerated corrosion of steel reinforcements, further decreasing

structural integrity (Jonkers, 2011). Concrete and steel make up the most commonly used materials for construction, with nearly 80 % of global infrastructure built from steel-reinforced concrete (Joshi *et al.*, 2017). Consequently, anywhere between 30 and 50 % of the annual money spent in the construction industry is for repair and maintenance of these structures. This equates to an annual repair budget of 68 million euros in the Netherlands and 4 billion dollars in the United States (Wiktor and Jonkers, 2016; Jonkers *et al.*, 2010). These values are compounded when taking into account the economic loss arising from disruptions and delays (Al-Tabbaa *et al.*, 2018). Apart from the high costs, the production of cement needed for concrete also contributes to approximately 5 – 8 % of anthropogenic carbon dioxide emissions, making it the third largest single source of anthropogenic carbon dioxide emission (Worrell *et al.*, 2001; Andrew, 2019). It has been estimated that to be able to align with the Paris Agreement on climate change at least a 24 % cut in cement production associated emissions is required (IEA, 2017). This challenge is further multiplied by the forecasted rise in demand for concrete production, which is set to increase by 12-13 % by 2050 as rapid development and urbanisation in developing countries occurs (IEA, 2017). There is a clear need in the construction industry to address economic and environmental impacts of cement production, the solution to which will be most definitely multifaceted. Consequently there has been great interest and resources spent by industries and governments alike to develop smart materials, like self-healing concrete, that can auto-repair when damaged to thus prolong the life span of built structures and lower their maintenance costs (EPSRC, 2012; van der Zwaag and Brinkman, 2015; EPSRC, 2017; CORDIS, 2013; COST, 2016). This in turn will reduce some of the need for new concrete, minimising some production and emission related issues. BICP based self-healing concrete technology offers to be part of one of these solutions.

Designing BICP-based self-healing concrete starts with the selection of bacteria suited for the application. Traditionally, these have ideally been alkali-tolerant spore-forming bacteria such as those of the *Bacillus* and *Sporosarcina* genera (Jonkers *et al.*, 2010; De Belie *et al.*, 2018). These bacteria suit the harsh environment concrete poses with an alkalinity anywhere between pH 9 and 14. Additionally, self-healing is desired to activate only upon crack formation, and until then the bacteria must remain viable and dormant (Lee and Park, 2018). The formation of spores allows the bacteria to withstand mechanical and chemical stress, remaining dormant and viable for many years (Jonkers, 2011). To further increase their lifespan and protect them against cement hydration, which can compress the surrounding matrix to pore diameter bellow 1 µm, they can be encapsulated. Encapsulation technologies vary and can encompass numerous types of light weight aggregates (De Belie *et al.*, 2018) such as porous expanded clay particles (Jonkers, 2011) and perlite (Alazhari *et al.*, 2018), polymer based microcapsules (Wang *et al.*, 2014; Liu *et al.*, 2016; Pungrasmi

et al., 2019), and hydrogels/super absorbent polymers (SAPs) (Wang *et al.*, 2015; Nielsen *et al.*, 2020). The bacterial spores are encapsulated so as to survive the mixing phase but the encapsulating agent is brittle enough to break to expose the bacteria after crack formation. Nutrients can be encapsulated along with the bacteria or be directly added to the cementitious mix. Further advantages to the encapsulation is that it not only acts as the healing agent reservoir but can also provide a structural element (Wiktor and Jonkers, 2016). Encapsulation methods such as SAP also increase water retention, making it more readily available to the bacteria, as well as provide a scaffold in which the bacteria can precipitate calcite (Wang *et al.*, 2015). Once cracked open and upon ingress of water and oxygen, spores are triggered to germinate and grow inducing BICP and thus healing cracks by breaking down nutrients to dissolved inorganic carbon, which together with the calcium in the surrounding concrete leads to calcite precipitation (Chapter 1), an optimal crack filler (Breugel, 2012; Jonkers, 2011).

The self-healing concrete market, which encompasses BICP approaches, is expected to grow at a compound annual growth rate of 26.4 % over the forecasted period between 2018-2025 to a market size of 1.3 billion dollars (Banik, 2019). This illustrates the large potential of such technology to reform our current practices and is evident by the emergence of start-up companies founded on BICP technologies over recent years, such as Green Basilisk and bioMASON® Inc in the construction sector and Bind-X GmbH (previously Dust BioSolutions GmbH) to encompass other applications. There is a readiness and willingness to reform technologies to encompasses environmentally friendly solutions.

2.2 Challenges to BICP application.

There are many aspects to consider when choosing bacteria for self-healing concrete. One consensus has been to select for bacteria that are the quickest at precipitating calcite, as this would speed up crack closure and reduce the exposure time towards harmful elements. Ureolytic bacteria such as *Sporosarcina pasteurii* are therefore commonly chosen as they are rapidly able to precipitate calcite (De Muynck *et al.*, 2010). A range of different non-ureolytic bacteria still find application in self-healing concrete and while they may be slower at precipitation they still heal cracks (Sharma *et al.*, 2017). In a recent publication, precipitation morphology was shown to vary between fast ureolytic induced precipitation and slower non-ureolytic precipitation. The ureolytic pathway produced fine homogenous crystals, while non-ureolytic pathways caused the incorporation of organic material into the precipitate, while still precipitating the same quantity over the long run (Reeksting *et al.*, 2020). The application setting therefore needs to be thoroughly

considered in context with the chosen bacterium's metabolism and characteristics. In the instance of self-healing concrete, precipitation by the slower non-ureolytic pathway may give more robust results as it forms a stronger 'glue' that is not as readily displaced (Reeksting *et al.*, 2020). Contrarily, fast precipitation may be of benefit to spray-on applications, e.g. for the restoration of historic buildings (Reeksting *et al.*, 2020). The ability of a bacterium to be able to switch between a fast ureolytic and slow non-ureolytic induced precipitation in response to nutrients in the environment adds another layer of complexity that may however provide solutions to other applications. For example, in soil consolidation technologies premature clogging at injection sites minimises the depth in which bio-cementation can occur (Cheng and Cord-Ruwisch, 2014). Overcoming this could exploit bacteria with slow non-ureolytic pathways that can then switch to fast ureolytic pathways under nitrogen limitation (Reeksting *et al.*, 2020). This illustrates the need for fundamental mechanistic understandings of BICP and bacteria-induced mineral precipitation in general, so future technologies may take advantage of a toolbox of microbes with different metabolic properties capable of calcite precipitation. This is especially the case as metabolism pathways are not straightforward, they often exhibit secondary effects that may or may not be advantageous in their respective application. For example, nitrogen loading of the environment from the addition of urea and subsequent degradation by ureolytic bacteria in cementitious mixes is considered a drawback to the fast ureolytic precipitation pathway (Jonkers *et al.*, 2010). On the other hand, BICP driven by nitrate reducers produces nitrates that act as steel corrosion inhibitors in steel reinforced concrete and so exert the additional effect of acting as an intrinsic corrosion inhibitor (Erşan *et al.*, 2016; Ersan *et al.*, 2015). When developing self-healing concrete it is therefore important to consider the factors that make up the environment the bacteria will inhabit. This in turn benefits from the close collaboration between microbiologists and civil engineers.

Apart from the alkaline conditions within concrete, the built structures themselves are also exposed to different environments from cold to hot, dry and marine. These environments pose new challenges and selected bacteria may need to cover psychrophilic, thermophilic, and halophilic natures on top of alkaliphilic (Palin *et al.*, 2016). A lot of current research is done on mesophilic organisms, with some applied studies in alkaliphiles. It will become important to translate our understanding of the process and requirements to a range of extremophilic bacteria to cover the range of needed applications. Only more recent studies are now focusing on marine concrete applications which incorporate halotolerant bacteria (Bansal *et al.*, 2016; Palin *et al.*, 2017). BICP is a widespread phenomenon amongst microbes (Boquet *et al.*, 1973), covering even harsh conditions like thermophiles (Yoshida *et al.*, 2010; Murai and Yoshida, 2013), halophiles (Stabnikov *et al.*, 2013; Arias *et al.*, 2019; Kunal *et al.*, 2016) and psychrophiles (Mykytczuk *et al.*, 2016; Yan *et al.*, 2016),

indicating there are bacteria and metabolisms to be found which suite the different technological requirements. Another approach to the problem is to take advantage of genetic engineering approaches whereby favourable genetic elements may be shuttled to more suitable extremophile chassis organisms. Understanding of fundamentals of BICP from model organisms will therefore be important when applied to such extremophiles.

A search through the literature reveals a lack in systematic approaches taken in understanding the fundamentals of calcite precipitation for ultimate biotechnological application. Rather, the environment is frequently sampled in a top-down approach, characterising the strains and testing them in application. Little research has taken a bottom-up approach, engineering strains for BICP. This requires an understanding of the genetics of the metabolic pathways and surface structures that are involved in influencing precipitation. Identifying these genetic elements would allow for modulation of precipitation and the potential to mobilise such into better suited chassis organisms for application. In the instances where BICP has been investigated through genetic and metabolic engineering approaches, it has predominantly been focused on individual enzymes such as carbonic anhydrase and urease. Carbonic anhydrase have seem some metabolic engineering approaches for calcite precipitation investigating extracellular secretion (Chen *et al.*, 2012), surface bound (Fan *et al.*, 2011; Del Prete *et al.*, 2017) or periplasmic localisation to reduce cytosolic toxicity (Jo *et al.*, 2013). In *Bacillus subtilis* NCIB 3610 carbonic anhydrase has also been shown to influence calcite distribution in complex colony surface architecture (Oppenheimer-Shaanana *et al.*, 2016). The majority of metabolic engineering work has however been done on Gram-negative bacteria which in a concrete setting do not reflect the best strain choice due to their lack of spore formation which would ensure their long term survival. Ureases have also seen metabolic engineering approaches and are considered a more promising target as they account for one of the fastest metabolic routes of calcite precipitation (De Muynck *et al.*, 2010). Directed evolutionary approaches have screened for increased ureolytic activity, calcite precipitation and pH tolerance, through random mutagenesis experiments in *S. pasteurii* (Achal, Mukherjee, Basu and Sudhakara Reddy, 2009). Rational mutagenesis approaches have been used to increase ureolytic activity by increasing the solubility of the recombinantly expressed *S. ureae* urease in *Escherichia coli* to reduce toxic inclusion bodies (Whitaker, 2016). Urease genes from *S. pasteurii* have also been moved into *Pseudomonas aeruginosa* and *E. coli* for studying precipitation potential (Connolly *et al.*, 2013; Bachmeier *et al.*, 2002). More recently, engineering of *E. coli* strains with urease activity has explored precipitation morphology and size characteristics (Liang *et al.*, 2018; Heveran *et al.*, 2019). *S. pasteurii* urease genes expressed in *P. aeruginosa* a biofilm producer has been evaluated for the potential in producing inorganic-organic based precipitates. This strain however does not reflect an application

appropriate host due to it being a pathogen (Bergdale *et al.*, 2012). Gram-negative bacteria are also difficult to incorporate into concrete for long-term viability to be available for crack formation in the late life-span of a concrete structure. Spore forming bacteria are much more practical, and so there is limited use of studies in Gram-negative non-spore formers like *E. coli* and *Pseudomonas* species.

Another aspect of bacteria-induced calcite precipitation considers the role of surface charge and biofilm formation (Chapter 1). Surface charge has been linked with the potential of bacteria to precipitate calcite but to our knowledge no genetic engineering approaches have investigated the process or its modulation. Biofilm has seen a lot of study on its role of biomineralisation but there has been limited research on the effect of its modulation on BICP from a genetic engineering perspective. A recent study does however show a link between biofilm genes and their role in complex colony architecture of *Bacillus subtilis* NCIB 3610 using gene deletion strains (Oppenheimer-Shaanana *et al.*, 2016). The relative lack of systematic genetic engineering in the field of BICP still leaves many approaches and questions unanswered. For example what is the simplest metabolic unit that can induce calcite precipitation in a non-precipitator? Are there any accessory genes needed? Which specific surface structure genes induce precipitation? Can surface charge be modulated for calcite precipitation? What is the interplay between metabolism and surface structures in triggering biomineralisation? Can we create synthetic plugin modules of gene clusters for the introduction of BICP into bacteria that are optimally adapted to specific application conditions for the rational design of precipitators? These are the questions that have been addressed in this PhD project. This information will allow a more targeted development of BICP technologies that are tailored to the respective applications.

2.3 PhD aims and objectives.

The aim of this thesis was to explore the genetic optimisation of bacteria-induced calcite precipitation, as a bottom-up approach to understanding the fundamental mechanistic components needed for calcite precipitation. To eventually be able to move genetic building blocks for BICP into optimal chassis organisms for application, a second aim was to develop a genetic methodology to facilitate manipulation of environmental *Bacillus* isolates. The ultimate goal for this is to contribute understanding to the development of new generations of bio-concrete, which would increase the lifespan of cementitious structures and thus decrease the high maintenance costs and high carbon dioxide release associated with concrete production and building.

Objective 1: Assembly, introduction and characterisation of orthogonal urease gene clusters in the intrinsically low calcite precipitator *Bacillus subtilis* W168. Urease genes and their associated accessory genes where chosen from *Bacillus paralicheniformis* and characterised in their ability to induce calcite precipitation in W168. This provided insight into identifying the smallest metabolic unit of the ureolytic pathway needed to drive calcite precipitation and the interplay between its accessory genes.

Objective 2: Characterise the role of surface charge and biofilm formation on calcite precipitation in the intrinsically low calcite precipitator *Bacillus subtilis* W168. Modulating surface charge by upregulating the *dltABCDE* operon, which adds positively charged D-alanine groups to teichoic acids of the cell surface, was evaluated for its ability to induce calcite precipitation. To evaluate the contribution of biofilm components on calcite precipitation, the genes *tasA* (encoding the proteinaceous component) and *epsH* (encoding exopolysaccharide) were deleted. This provided insight into identifying the relationship between metabolism and biofilm in the ability to precipitate calcite and whether one could occur without the other.

Objective 3: Assemble and characterise a plasmid shuttle system to manipulate environmental or extremophilic relatives of *Bacillus subtilis*, which may be better suited to application conditions. A conjugation method was developed to shuttle a broad host range mobilisable Gram-positive plasmid with a promoter and green fluorescent reporter protein to a range of meso- and alkaliphilic *Bacillus* species. This supplied the parts to a genetic toolbox namely plasmid, promoter, reporter, and conjugational helper strain that could be used to shuttle favourable genetic elements that promote calcite precipitation to better suited environmental isolates.

Chapter 3

Scientific Methods

ABSTRACT *Collection of methods, plasmids, primers and strains used throughout this PhD work.*

3.1 Chemicals and growth media.

All chemicals were obtained from Merck, Sigma-Aldrich or Thermo Fischer unless stated otherwise. Lysogeny Broth (LB) contained 10 g/L tryptone, 5 g/L yeast extract and 10 g/L NaCl. For LB urea (LBU), for obligate ureolytic stains, LB was supplemented with urea to a final concentration of 20 g/L. For LB alkaline (LB Alk) for alkaliphilic strains, LB was supplemented with 100 ml/L Na-sesquicarbonate ($NaHCO_3$ 24 g/L , and Na_2CO_3 53 g/L) to achieve pH 9.5. Biofilm promoting medium LBGM contained LB supplemented with 1 % (w/v) glycerol and 0.1 mM $MnSO_4$ (Shemesh and Chaia, 2013). Brain Heart Infusion (BHI) contained 5 g/L beef heart infusion, 12.5 g/L calf brain infusion, 2.5 g/L disodium phosphate, 2 g/L dextrose, 10 g/L peptone and 5 g/L NaCl. Super Optimal Broth with Catabolite repression (SOC) contained 20 g/L tryptone, 5 g/L yeast extract, 4 g/L glucose, 0.58 g/l NaCl, 0.19 g/L KCl, 2.03 g/L $MgCl_2$ and 1.20 g/L $MgSO_4$. Super Optimal Broth (SOB) contained 20 g/L tryptone, 5 g/L yeast extract, 0.5 g/l NaCl, 2.5 mM KCl final pH 7.0. CC buffer contained 10 mM PIPES pH 6.7, 15 mM $CaCl_2$, 250 mM KCl and 55 mM $MnCl_2$. SC buffer contained 0.15 M NaCl, 0.01 M sodium citrate and pH 7.0. MNGE composed of 88.21 mM K_2HPO_4, 203.88 mM KH_2PO_4, 255.8 mM Trisodium citrate, 1.9 % w/v Glucose, 0.19 % w/v K-Glutamate, 0.01 mg/ml Fe[III]-ammonium-citrate, 0.047 mg/ml Tryptophan, 28mM $MgSO_4$ and were necessary 0.047 mg/ml Threonine. Expression Mix contained 2.38 % w/v yeast extract, 2.38 % w/v casamino-acids and 0.24 mg/ml Tryptophan. Starch media contained 7.5 g/L Nutrient Broth and 5 g/L starch. Solid media contained an additional 15g /L Agar. Where antibiotic selection was required additions of 10 µg/ml kanamycin, 5 µg/ml chloramphenicol, 100 µg/ml spectinomycin, 20 µg/ml Zeocin or MLS (1 µg/ml erythromycin + 25 µg/ml linocomycin) for *Bacillus subtilis*, 150 µg/ml spectinomycin for *Enterococcus faecalis*, 100 µg/ml ampicillin, 50 µg/ml kanamycin, or 25 µg/ml chloramphenicol for *Escherichia coli* and 20 µg/ml Zeocin for alkaliphilic *Bacillus* were made.

3.2 Growth conditions and storage.

Escherichia coli DH5α and plasmid-harbouring derivatives were grown in LB at 37°C, 200 rpm and with respective antibiotics. Wildtype *Bacillus* strains were grown in LB at 37°C, 200 rpm and environmental strains in LB or LBU at 30°C, 150 rpm. Recombinant *Bacillus subtilis* strains producing urease were grown in LB at 30°C, 150 rpm and with respective antibiotic addition. Alkaliphilic *Bacillus* strains were grown in LB Alk at 30°C, 150 rpm with respective antibiotic. *Enterococcus faecalis* was grown in BHI at 37°C without agitation and with respective antibiotic. Cell optical densities were routinely measured in a Novaspec Pro spectrometer (Biochrom Ltd, United Kingdom) at 600 nm in cuvettes of 1 cm light path length (OD_{600}). For long-term storage, glycerol stocks were prepared by adding glycerol to overnight cultures to a final concentration of 20 % (w/v)

and storing in cryo-vials at -80°C. For *Bacillus subtilis* strains with recombinant urease genes glycerol stocks were prepared by scraping off cells from growth on solid media and re-suspending in autoclaved dH_2O before adding glycerol to a final concentration of 20 % (w/v).

3.3 Plasmid and strain construction.

3.3.1 DNA manipulation.

All molecular biology manipulation techniques (polymerase chain reactions, ligation reactions, restriction digests, electrophoresis gels) followed standard protocols (Sambrook and W Russell, 2001) and reagent manufacturer's recommendations. Restriction and DNA modifying enzymes were obtained from New England Biolabs (NEB). PCR gene amplifications were carried out with final concentrations of 0.02 U/µl Q5®High-Fidelty DNA Polymerase, 1× Q5 buffer, 0.4 µM of each primer and 200 µM dNTPs using 1 ng-1 µg genomic DNA or 1 pg-10 ng plasmid DNA. Thermocycling conditions followed 98°C initial denaturation for 30s continued by 35 cycles of 98°C denaturation for 10s, annealing at respective temperature for 30s and extension at 72°C for 30s/kb, and ending with a final extension at 72°C for 2 min. Colony PCR was carried out with final concentrations of 1× OneTaq® Master Mix with standard buffer and 0.2 µM of each primer. Thermocycling conditions followed 95°C initial denaturation for 10 min continued by 30 cycles of 95°C denaturation for 30s, annealing at respective temperature for 30s and extension at 68°C for 60s/kb, and ending with a final extension at 68°C for 5 min. Primer annealing temperatures were determined using the OligoCalc web tool 'Salt Adjusted' output (Kibbe, 2007). Site-direct mutagenesis was carried out with QuiKChange PCR according to Agilent Technologies. Gibbson assemblies were carried out using Gibbson Assembly® Master mix with 50 ng of vector and 3× excess inserts (0.02-0.5 pmol total DNA fragments) incubated at 50°C for 30 min. PCR clean-ups were carried out using OMEGA E.Z.N.A Cycle pureKit (VWR) or Monarch®PCR & DNA Cleanup (NEB), DNA gel extraction using GeneJet Gel Extraction Kit (ThermoScientific) or Monarch® DNA Gel Extraction Kit (NEB), and genomic DNA isolation using GeneJet Genomic DNA Purification Kit (ThermoScientific), all following manufacturer's instructions. Plasmids were routinely isolated from *E. coli* DH5α using Monarch® Plasmid Miniprep kit following manufacturer's instructions (NEB). Plasmids were sequenced using the Mix2Seq (NEB) kit with volumes of ≤ 10 ng/µl DNA template and 20 pmol primer. Plasmids used in this study are listed in Table 2, strains in Table 3, and primers in Table 4. Crude-prep genomic DNA for *B. subtilis* W168 transformations were done through SC lysis. Volumes of 800 µl overnight cultures were added to 800 µl SC buffer. Cells were centrifugation at 16,000 ×*g* for 1 min, the pellet suspended in 1 ml SC buffer and 20 µl lysozyme added. The mixture was incubated at 37°C for

15 min after which 800 µl 5M NaCL and 200 µl were added. The DNA solution was filtered through a 0.45 µm filter ready to be used for transformation.

3.3.2 Transformations, deletion strains, and phage transduction.

E. coli.

Chemically competent *E. coli* DH5α, *E. coli* SM10 and *E. coli* S17 cells were prepared as previously described (Inoue *et al.*, 1990). *E. coli* DH5α grown in SOB while *E. coli* SM10 and *E. coli* S17 grown in LB. Volumes of 100 ml SOB/LB + 500 µl 2M $MgCl_2$ were inoculated at a ratio of 1:50 with an overnight culture. Cells were grown at 37°C and 200 rpm until OD_{600}=0.6. Cells were chilled on ice for 10 min and then centrifuged at 3,200 ×*g* for 10 min at 4°C. The cell pellet was re-suspended in 18 ml ice cold CC buffer, chilled on ice for 10 min and then centrifuged at 3,200 ×*g* for 10 min at 4°C. The cell pellet was re-suspended in 8 ml ice cold CC buffer and chilled on ice for 10 min after which 500 µl DMSO was added. Cells were then aliquoted in 200 µl volumes and flash frozen in liquid nitrogen for storage at -80°C. *E. coli* transformation reactions were prepared on ice in 50 µl volumes of competent cells with the addition of 4 µl ligation reaction or 0.5 µl purified plasmid. The reaction underwent 30 min incubation on ice and heat shock treatment at 42°C for 30 sec concluding with a 2 min incubation on ice. The reaction was then added to 750 µl SOC and incubated at 37°C, 200 rpm for 1 hour. Volumes of 100-200 µl recovered cells were spread onto LB agar with respective antibiotic and incubated overnight at 37°C.

E. faecalis.

Preparation of electrocompetent *E. faecalis* and subsequent electroporation followed the previously described method by Shepard and Gilmore (Shepard and Gilmore, 1995). In brief: electroporation was conducted in chilled electroporation cuvettes using 40 µl of electrocompetent *E. faecalis* cells and the addition of 1 µl chilled plasmid DNA (0.1-1.0 µg/µl). The cuvette was subjected to a 2.5 kV pulse, 25 µF capacitance and 200 Ω resistance using an electroporator. After pulsing, 1 ml of ice cold SGM17MC media is added and the cuvette is stored on ice for 5 min. The electroporated cells are then incubated for 2 hours at 37°C without shaking before dilutions series are plated onto growth media with appropriate antibiotic selection. The final plates are incubated at 37°C for up to 48 hours.

B. subtilis.

Transformation of *B. subtilis* W168 with plasmid DNA, PCR product or crude-prep genomic DNA followed induction of natural competence by growth in MNGE media as previously described (Harwood and Cutting, 1990). To induce natural competence, a volume of 10 ml MNGE was inoculated to $OD6_{600}$=0.1 with a *B. subtilis* overnight culture after which cells were left to grow at

37°C, 200 rpm until OD_{600}=0.6-1. *B. subtilis* transformation reactions were prepared in 400 µl volumes of natural competent cells, DNA added (1-2 µg/ linearised plasmid, 100 µl crude-prep genomic DNA or 15 µl purified long flanking homology PCR product) and incubated at 37°C for 1h. Next 100 µl expression mix was added and where necessary pre-induced with 0.0025 µg/ml Erythromycin or 0.125 µg/ml Chloramphenicol. The mixture was then incubated at 37°C for 1h after which 100-200 µl recovered cells were spread onto LB agar with respective antibiotic and incubated overnight at 37°C/30°C. Double-crossover integration of the DNA into *B. subtilis* W168 genome at the *amyE* locus was checked on starch plates. Transformants were patched onto starch media agar, grown overnight and the agar stained the following day with iodine vapour by placing a few iodine crystals in the lid. Strains with an intact copy of *amyE* had a white halo due to starch breakdown, whereas successful integration of the plasmid in *amyE* disrupted the gene and no halo was observed. Double-crossover integration of the DNA at the *lacA* locus was checked via colony PCR using primers SG0148/SG0149. Double-crossover integration into the *thrC* locus was checked via growth in MNGE media with and without threonine. Volumes of 1.5 µl overnight culture were inoculated into 150 µl MNGE on a clear flat bottom 96-well plate and incubated overnight at 37°C, 200 rpm after which the absorbance is measured at 600 nm in TECAN-Spark microplate reader (Tecan Group Ltd., Switzerland). Successful integration resulted in gene disruption which was indicated by a lack of growth in MNGE without threonine but growth in MNGE with threonine.

B. subtilis W168 gene deletions were constructed by replacing the gene of interest with an antibiotic resistance cassette using long flanking homology (LFH) mutagenesis according to the method by Wach (Wach, 1995). In brief: the resistance cassette as well as an approximately 1 kb upstream and downstream region of the gene to be knocked out were PCR amplified with overhangs for the resistance cassette. The upstream and downstream sequences were fused with the resistance cassette sequence using Q5 polymerase joining PCR, using 10 ng of each DNA fragment and a 3 × molar excess of cassette. For overlap-extension PCR the first round ran for 9 cycles without primers, followed by the addition of primers for the second round for 30 cycles. The resulting PCR product was cleaned up and transformed into *B. subtilis* W168 as described above. Successful disruption of the gene was checked via colony PCR using respective primers for outside of the upstream and downstream homology regions as indicated in Table 3.

B. subtilis NCIB 3610 strains were constructed by SPP1 mediate phage transduction from *B. subtilis* W168 strains harbouring the mutation/insertion of interest as previously described by Kearns and Losick without DNase treatment of the supernatant (Kearns and Losick, 2003).

3.3.3 Conjugations.

The protocol for conjugation of plasmids into undomesticated strains *via* an *E. coli* helper strain was adapted from (Styles *et al.*, 2020) and varied in growth media, condition and selection depending on the strains. The *E. coli* helper strain bearing the conjugative plasmid was prepared from 20 ml overnight culture to ensure sufficient cells were available. The *E. coli* cells were pelleted by centrifugation at 4,000 ×*g* for 10 min, the supernatant discarded, and the cell pellet washed once in 1 volume fresh LB to remove antibiotic traces before re suspending in 1 volume fresh LB. *Bacillus* recipient strains were prepared by subcultures, for which 20 ml fresh media was inoculated to an OD_{600}=0.1 from an overnight culture and grown until an OD_{600} of approximately 1.5 was reached. The *E. coli* and *Bacillus* cells were mixed at different ratios, with the most successful at an OD_{600} ratio of 15:1.5 (10:1). The cell mixture was pelleted at 4,000 ×*g* for 10 min and the cells spotted onto pre-warmed LB agar supplemented with 10 mM $MgCl_2$. The plates were incubated at 37°C for 24 h after which the cells were scraped off and re-suspended in 2 ml respective *Bacillus* growth media. Volumes of 20 µl cell mixture dilutions were spotted in triplicate onto selection media for recipients and transconjugants. Selection for recipients, i.e. just the bacilli, required counter-selection against *E. coli* donor cells from the mating mixture. For *Bacillus* strains grown on LB the addition of the antibiotic polymixin B at 20 µg/ml to the media was required. For alkaliphilic *Bacillus* strains, recipients were easily counter-selected from *E. coli* donor strains by simple growth on LB Alk. Transconjugants, i.e. bacilli harbouring the plasmid, required *E. coli* counter-selection and addition of the selective antibiotic, depended on plasmid used, to the media. Transformation efficiency was calculated as the number of transconjugants per recipient cell.

Table 2. Plasmids used in this study.

Plasmid	Characteristics[a.]	Source/Construction[b.]
pDG148-stu	*bla*^{r}, *ble*^{r}, *kan*^{r}, *repB*, ori ColE1	(Joseph *et al.*, 2001)
pDG2K-oriT-GFP-GG_ready	*kan*^{r}, ori ColE1, repBST1, oriT IncP, *sf-gfp*, *bgI*	Leak Lab
pUC18	lacZα, MCS, ori pMB1, *bla*^{r}	(Yanisch-Perron *et al.*, 1985)
pAT28	*spc*^{r}, ori pMB1, oriT IncP, MCS	(Trieu-Cuot *et al.*, 1990)
pSB1A3	*bla*^{r}, ori pMB1, *rfp*	Registry of Standard Biological Parts
pSB1C3-GFPmut1	*cat*^{r}, ori pMB1, GFPmut1 (*B. subtilis* codon optimised)	Mascher Lab
pSB1A3-P$_{xylA}$	*bla*^{r}, ori pMB1, P$_{xylA}$ (xylose inducible promoter)	Mascher Lab
pSB1C3-P$_{VEG}$	*cat*^{r}, ori pMB1, P$_{veg}$ (strong constitutive promoter)	Mascher Lab
pBS2E	*bla*^{r}, ori ColE1, *lacA*$'$, MLS^r, *rfp*, '*lacA*	(Radeck *et al.*, 2013)
pBS1C	*bla*^{r}, ori ColE1, *amyE*', *rfp*, cat^r, '*amyE*	(Radeck *et al.*, 2013)
pBS1Z	*bla*^{r}, ori ColE1, *amyE*', *zeo*^{r}, '*amyE*	Gebhard Lab
pXT	*bla*^{r}, ori ColE1, *thrC'*, P$_{xylA}$, spec^r, *'thrC*, mls^r	(Derre *et al.*, 2000)
pDG780	*kan*^{r}	(Guérout-Fluery *et al.*, 1995)
pBS1C-P$_{xylA}$	*bla*^{r}, ori ColE1, *amyE*', cat^r, P$_{xylA}$, '*amyE*	P$_{xylA}$ excised from pBS1A3-P$_{xylA}$ and cloned into pBS1C3 using EcoRI and SpeI. Cloned PCR checked using primers SG0424/SG0425 and sequenced with primer SG0424.
pBS2E-P$_{xylA}$	*bla*^{r}, ori ColE1, *lacA*$'$, MLS^r, P$_{xylA}$, '*lacA*	P$_{xylA}$ excised from pBS1A3-P$_{xylA}$ and cloned into pBS2E using EcoRI and SpeI. Cloned PCR checked using primers SG0245/SG0246 and sequenced with SG0245.
pBS2E-P$_{xylA}$-*ureABCEFGD*^{Sp}	*bla*^{r}, ori ColE1, *lacA*$'$, MLS^r, P$_{xylA}$, ureABCEFGD^{Sp}, '*lacA*	*ureABCEFGD* amplified from DSM 33 gDNA using primers SG0508/SG0509 and cloned into pBS2E-P$_{xylA}$ using SpeI. Cloned PCR checked with primers SG0246/SG0575 and sequenced with primers SG0245/SG0246/SG0575.
pXT-P$_{xylA}$-*ureABCEFGD*^{Bp}	*ori, bla, thrC'*, P$_{xylA}$, ureABCEFGD^{Bp}, spec^r, *'thrC*, mls^r	*ureABCEFGD* amplified from ATCC 9945a gDNA using primers SG0652/SG0653. PCR fragment cut with BsmBI and cloned into pXT cut with BamHI and EcoRI. Cloned PCR checked with primers SG0074/SG0654 and sequenced with primers SG0074/SG0075/SG0654.
pSB1A3-urt^{Bp}	*bla*^{r}, ori pMB1, *urt*^{Bp}	*urt* amplified from 9945a gDNA using primers SG0646/SG0647 and cloned into pSB1A3 using EcoRI and PstI. Cloned PCR checked and sequenced with primers SG0599/SG0600.
pSB1A3-ureH^{Bp}	*bla*^{r}, ori pMB1, *ureH*^{Bp}	*ureH* amplified from 9945a gDNA using primers SG0648/SG0649 and cloned into pSB1A3 using XbaI and PstI. The plasmid then underwent QuikChange PCR to

		remove the EcoRI site in *ureH* using primers SG0650/SG0651. Cloned PCR checked and sequenced with primers SG0599/SG0600.
pBS1C-P_{xylA}-urt^{Bp}	*bla*^{r}, ori ColE1, *amyE*', cat^{r}, P_{xylA}, urt^{Bp} '*amyE*	*urt* excised from pSB1A3-urt^{Bp} with XbaI and SpeI and cloned into pBS1C-P_{xylA} cut with SpeI and PstI. Cloned PCR checked and sequenced using primers SG0424/SG0425.
pBS1C-P_{xylA}-$ureH^{Bp}$	*bla*^{r}, ori ColE1, *amyE*', cat^{r}, P_{xylA}, $ureH^{Bp}$ '*amyE*	*ureH* excised from pSB1A3-$ureH^{Bp}$ with XbaI and SpeI and cloned into pBS1C-P_{xylA} cut with SpeI and PstI. Cloned PCR checked and sequenced using primers SG0424/SG0425.
pBS1C-P_{xylA}-urt^{Bp}-$ureH^{Bp}$	*bla*^{r}, ori ColE1, *amyE*', cat^{r}, P_{xylA}, urt^{Bp} , $ureH^{Bp}$ '*amyE*	*ureH* excised from pSB1A3-$ureH^{Bp}$ with XbaI and SpeI and cloned into pBS1C-P_{xylA}-urt^{Bp} cut with SpeI and PstI. Cloned PCR checked and sequenced using primers SG0424 and SG0425.
pSB1C3-P_{veg}-*dltABCDE*	*cat*^{r}, ori pMB1, P_{veg}, *dltABCDE*	*dltABCDE* amplified from W168 gDNA using primers SG0901/SG0902 and cloned into pSB1C3-P_{veg} using SpeI and PstI. Cloned PCR checked and sequenced using primers SG0599/SG0600.
pBS2E-P_{veg}-*dltABCDE*	*bla*^{r}, ori ColE1, *lacA*', MLS^{r}, P_{veg}, *dltABCDE*, '*lacA*	P_{veg}-*dltABCDE* amplified from pSB1C3-P_{veg}-*dltABCDE* using primers SG0929/SG0902 and cloned into pBS2E using XbaI and PstI. Cloned PCR checked and sequenced with primers SG0245/SG0246.
pUC18-P_{veg}-GFPmut1	P_{veg}, GFPmut1, ori pMB1, *bla*^{r}	P_{veg} was amplified from pSB1C3-P_{veg} using primers SG0907/SG1034. GFPmut1 was amplified from pSB1C3-GFPmut1 using primers SG1035/SG1036. pUC18 was linerarised with BamHI. The three separate DNA fragments subsequently underwent Gibson assembly. Cloned PCR checked and sequenced with primers SG0913/SG0931.
pAT28-P_{veg}-GFPmut1	*spc*^{r}, ori pMB1, *oriT* IncP, P_{veg}, GFPmut1	P_{veg}-GFPmut1 amplified from pUC18- P_{veg}-GFPmut1 using primers SG0930/SG1037. PCR fragment cut with BsmBI and EcoRI and cloned into pAT28 cut with BamHI and EcoRI. Cloned checked with diagnostic restriction digest using BamHI and EcoRI and PCR checked and sequenced with primers SG0931.
pDG148-stu-oriT	*bla*^{r}, *ble*^{r}, *kan*^{r}, *repB*, *oriT* IncP, ori ColE1	oriT amplified from pDG2K-oriT-GFP-GG_ready with primers SG1072/SG1073 and cloned into pDG148-stu with BamHI. Cloned PCR checked with primers SG1073/SG1074 and sequenced with primer SG1074.
pDG148-P_{veg}-GFPmut1-oriT	*bla*^{r}, *ble*^{r}, *kan*^{r}, *repB*, *oriT* IncP, ori ColE1, P_{veg}, GFPmut1	P_{veg}-GFPmut1 amplified from pUC18- P_{veg}-GFPmut1 using primers SG1075/SG1076 and cloned into pDG148-stu-oriT using StuI. Cloned PCR checked with primers SG1075/SG1077 and sequenced with primers SG1053/SG1054/SG1077.

a. Relevant characteristics are listed. Antibiotic resistance cassettes as follows: Bla; ampicillin resistance, Kan, kanamycin resistance; cat, chloramphenicol resistance; spc, spectinomycin resistance; MLS, erythromycin and lincomycin resistance; zeo/ble Zeocin (phleomycin D1)/bleomycin resistance.
b. Strains referred to in table 2 and primers referred to in table 3.

Table 3. Strains used in this study.

Strain	Relevant Characteristics[a.]	Source/Construction[b.]
DH5α	*Escherichia coli* DH5α	Lab stock
SM10	*Escherichia coli* SM10 λpir	(Simon *et al.*, 1983)
S17	*Escherichia coli* S17	(Simon *et al.*, 1983)
JH2-2	*Enterococcus faecalis* lab strain	Cook Lab
DSM 33	Wildtype *Sporosarcina pasteurii* DSM 33	DSM
ATCC 9945a	Wildtype *Bacillus paralicheniformis* ATCC 9945a	ATCC
DSM 8715	Wildtype *Bacillus pseudofirmus* DSM 8715	DSM
DSM 6307	Wildtype *Bacillus cohnii* DSM 6307	DSM
W168	Wildtype *Bacillus subtilis* W168	Gebhard Lab
NCIB 3610	Wildtype *Bacillus subtilis* NCIB 3610	Gebhard Lab
HB13321	W168 ytpB::MLS^{r}	(Kingston *et al.*, 2014)
SGB666	W168 *ureABC*::*kan*^{r}	LFH: *kan*^{r} amplified from pDG780 using primers SG0144/SG0145, upstream and downstream gene fragments amplified from W168 gDNA using primers SG0510/SG0511 and SG0512/SG0513. W168 transformed with PCR products joined using primers SG0510/SG0513. Double-crossover integration checked, covering outside of flanking region and cassette, with primers SG0532/SG0147 and SG0533/SG0146.
SGB739	W168 *ureABC*::*kan*^{r} , *lacA*::P$_{xylA}$-*ureABCEFGD*^{Sp}-MLS^{r}	pBS2E-P$_{xylA}$-*ureABCEFGD*^{Sp} → SGB666 Double cross over integration confirmed with colony PCR using primers SG0148/SG0149.
SGB740	W168 *lacA*::P$_{xylA}$-*ureABCEFGD*^{Sp}-MLS^{r}	pBS2E-P$_{xylA}$-*ureABCEFGD*^{Sp} → 168 Double cross over integration confirmed with colony PCR using primers SG0148/SG0149.
SGB823	W168 *ureABC*::*kan* , *amyE*::P$_{xylA}$-*urt*^{Bp}-*cat*^{r}	pBS1C-P$_{xylA}$-urt^{Bp} → SGB666
SGB824	W168 *ureABC*::*kan* , *amyE*::P$_{xylA}$-*ureH*^{Bp}-*cat*^{r}	pBS1C-P$_{xylA}$-ureH^{Bp} → SGB666
SGB825	W168 *ureABC*::*kan* , *amyE*::P$_{xylA}$-*urt*^{Bp}-*ureH*^{Bp}-*cat*^{r}	pBS1C-P$_{xylA}$-urt^{Bp}-ureH^{Bp} → SGB666

SGB826	W168 *ureABC*::*kan* , *amyE*::P_{xylA}-*urt*^{Bp}-*cat*^{r} , *thrC*:: P_{xylA}-*ureABCEFGD*^{Bp}-*spc*^{r}	pXT-P_{xylA}-*ureABCEFGD*^{Bp} → SGB823
SGB827	W168 *ureABC*::*kan* , *amyE*::P_{xylA}-*ureH*^{Bp}-*cat*^{r} , *thrC*:: P_{xylA}-*ureABCEFGD*^{Bp}-*spc*^{r}	pXT-P_{xylA}-*ureABCEFGD*^{Bp} → SGB824
SGB828	W168 *ureABC*::*kan* , *amyE*::P_{xylA}-*urt*^{Bp}-*ureH*^{Bp}-*cat*^{r} , *thrC*:: P_{xylA}-*ureABCEFGD*^{Bp}-*spc*^{r}	pXT-P_{xylA}-*ureABCEFGD*^{Bp} → SGB825
SGB844	W168 *ureABC*::*kan* , *thrC*:: P_{xylA}-*ureABCEFGD*^{Bp}-*spc*^{r}	pXT-P_{xylA}-*ureABCEFGD*^{Bp} → SGB666
SGB905	NCIB 3610 *ureABC*::*kan*	SPP1 SGB666 → 3610
SGB912	NCIB 3610 *ureABC*::*kan* , *amyE*::P_{xylA}-*urt*^{Bp}-*cat*^{r}	SPP1 SGB823 → SGB905
SGB913	NCIB 3610 *ureABC*::*kan* , *amyE*::P_{xylA}-*ureH*^{Bp}-*cat*^{r}	SPP1 SGB824 → SGB905
SGB914	NCIB 3610 *ureABC*::*kan* , *amyE*::P_{xylA}-*urt*^{Bp}-*ureH*^{Bp}-*cat*^{r}	SPP1 SGB825 → SGB905
SGB915	NCIB 3610 *ureABC*::*kan* , *thrC*:: P_{xylA}-*ureABCEFGD*^{Bp}-*spc*^{r}	SPP1 SGB844 → SGB905
SGB921	NCIB 3610 *ureABC*::*kan* , *amyE*::P_{xylA}-*urt*^{Bp}-*cat*^{r} , *thrC*:: P_{xylA}-*ureABCEFGD*^{Bp}-*spc*^{r}	SPP1 SGB844 → SGB912
SGB922	NCIB 3610 *ureABC*::*kan* , *amyE*::P_{xylA}-*ureH*^{Bp}-*cat*^{r} , *thrC*:: P_{xylA}-*ureABCEFGD*^{Bp}-*spc*^{r}	SPP1 SGB844 → SGB913
SGB923	NCIB 3610 *ureABC*::*kan* , *amyE*::P_{xylA}-*urt*^{Bp}-*ureH*^{Bp}-*cat*^{r} , *thrC*:: P_{xylA}-*ureABCEFGD*^{Bp}-*spc*^{r}	SPP1 SGB844 → SGB914
SGB926	W168 *dltABCDE*::*zeo*^{r}	LFH: *zeo*^{r} amplified from pBS1Z using primers SG0526/SG0527, upstream and downstream gene fragments amplified from W168 gDNA using primers SG0891/SG0892 and SG0893/SG0894. W168 transformed with PCR products joined using primers SG0891/SG0894. Double-crossover integration checked, covering outside of flanking region and cassette, with primers SG0895/SG0527 and SG0526/SG0896.
SGB984	W168 *dlt*::P_{veg}-*dltABCDE*-MLS	pBS2E-P_{veg}-*dltABCDE* → 168
SGB985	W168 *ureABC*::*kan*^{r} , Δ*dltABCDE*::*zeo*^{r}	gDNA SGB926 → SGB666
SGB987	W168 *ureABC*::*kan* , *amyE*::P_{xylA}-*ureH*^{Bp}-*cat*^{r} , *dltABCDE*::*zeo*^{r}	gDNA SGB926 → SGB824
SGB988	W168 *ureABC*::*kan* , *amyE*::P_{xylA}-*ureH*^{Bp}-*cat*^{r} , *dltABCDE*::*zeo*^{r} , *thrC*:: P_{xylA}-*ureABCEFGD*^{Bp}-*spc*^{r}	pXT-P_{xylA}-*ureABCEFGD*^{Bp} → SGB987
SGB989	W168 *ureABC*::*kan*^{r} , Δ*dltABCDE*::*zeo*^{r} , *thrC*:: P_{xylA}-*ureABCEFGD*^{Bp}-*spc*^{r}	pXT-P_{xylA}-*ureABCEFGD*^{Bp} → SGB985
SGB992	W168 *ureABC*::*kan*^{r} , *amyE*::P_{xylA}-*ureH*^{Bp}-*cat*^{r} , *epsH*::MLS^{r}	LFH: MLS amplified from HB13321 using primers SG0634/SG0635, upstream and downstream gene fragments amplified from W168 gDNA using primers SG1009/SG1010 and SG1011/SG1012. SGB824 transformed with PCR products joined using primers SG1009/SG1012. Double-crossover integration checked, covering outside of flanking region and cassette, with primers SG1021/SG0635 and SG0634/SG1024.

SGB993	W168 *ureABC*::*kan*^{r} , *amyE*::P_{xylA}-*ureH*^{Bp}-*cat*^{r} , *tasA*::MLS^{r}	LFH: MLS amplified from HB13321 using primers SG0634/SG0635, upstream and downstream gene fragments amplified from W168 gDNA using primers SG1013/SG1014 and SG1015/SG1016. SGB824 transformed with PCR products joined using primers SG1013/SG1016. Double-crossover integration checked, covering outside of flanking region and cassette, with primers SG1023/SG0635 and SG0634/SG1024.
SGB994	W168 *ureABC*::*kan*^{r} , *amyE*::P_{xylA}-*ureH*^{Bp}-*cat*^{r} , *spo0A*:MLS^{r}	LFH: MLS amplified from HB13321 using primers SG0634/SG0635, upstream and downstream gene fragments amplified from W168 gDNA using primers SG1017/SG1018 and SG1019/SG1020. SGB824 transformed with PCR products joined using primers SG1017/SG1020. Double-crossover integration checked, covering outside of flanking region and cassette, with primers SG1025/SG0635 and SG0634/SG1026.
SGB995	W168 *ureABC*::*kan* , *amyE*::P_{xylA}-*ureH*^{Bp}-*cat*^{r} , *epsH*::MLS , *thrC*:: P_{xylA}-*ureABCEFGD*^{Bp}-*spc*^{r}	pXT-P_{xylA}-*ureABCEFGD*^{Bp} → SGB992
SGB996	W168 *ureABC*::*kan* , *amyE*::P_{xylA}-*ureH*^{Bp}-*cat*^{r} , *tasA*::MLS , *thrC*:: P_{xylA}-*ureABCEFGD*^{Bp}-*spc*^{r}	pXT-P_{xylA}-*ureABCEFGD*^{Bp} → SGB993
SGB997	W168 *ureABC*::*kan* , *amyE*::P_{xylA}-*ureH*^{Bp}-*cat*^{r} , *spo0A*:MLS , *thrC*:: P_{xylA}-*ureABCEFGD*^{Bp}-*spc*^{r}	SPP1 SGB844 → SGB994
SGF29	JH2-2 pAT28-P_{veg}-GFPmut1	pAT28-P_{veg}-GFPmut1 → JH2-2 Presence of self-replicating plasmid confirmed with colony PCR using primers SG1053/SG1054.
SGB1000	W168 pDG148-stu-oriT	pDG148-stu-oriT → 168 Presence of self-replicating plasmid confirmed with colony PCR using primers SG1073/SG1074.
SGB1001	W168 pDG148-oriT-P_{veg}-GFPmut1	pDG148-P_{veg}-GFPmut1-oriT → 168 Presence of self-replicating plasmid confirmed with colony PCR using primers SG1075/SG1077.
SGB1002	DSM 8715 pDG148-oriT-P_{veg}-GFPmut1	S17 pDG148-P_{veg}-GFPmut1-oriT→ 8715 Presence of self-replicating plasmid confirmed with colony PCR using primers SG1075/SG1077.

a. Relevant characteristics are listed. Antibiotic resistance cassettes as follows: Kan, kanamycin resistance; cat, chloramphenicol resistance; spc, spectinomycin resistance; MLS, erythromycin and lincomycin resistance; zeo, Zeocin (phleomycin D1) resistance. b. The direction of strain construction is indicated (→) with plasmid/genomic/PCR DNA, used for transformation, phage (SPP1) transduced or *E. coli* (S17) conjugated into recipients using standard techniques. Plasmids referred to in table 1, primers referred to in table 3.

Table 4. Primers used in this study.

Name	Description	Sequence 5' → 3'[a.]
SG0074	pXT check rev	GTATTCACGAACGAAAATCG
SG0075	pXT check fwd	ACAACAAACTAATAGGTGATG
SG0144	*kan*^{r} cassette LFH fwd	CAGCGAACCATTTGAGGTGATAGG
SG0145	*kan*^{r} cassette LFH rev	CGATACAAATTCCTCGTAGGCGCTCGG
SG0146	*kan*^{r} cassette check fwd	CATCCGCAACTGTCCATACTCTG
SG0147	*kan*^{r} cassette check rev	CTGCCTCCTCATCCTCTTCATCC
SG0148	*lacA* integration check fwd	GCATACCGGTTGCCGTCATC
SG0149	*lacA* integration check rev	GAACTACATGCACTCCACAC
SG0245	pBS2E check fwd	GGCAACCGAGCGTTCTG
SG0246	pBS2E check rev	CTGACAGCGTTTCGATCC
SG0424	pBS1C check fwd	CCAGTGATTATGCCGCGATTTCCAATGAGG
SG0425	pBS1C check rev	CTTATCTTGATAATAAGGGTAACTATTGCC
SG0508	SpeI + RBS + *ureABCEFGD*^{Sp} fwd	tttaa**ACTAGTaaggaggacaaac**TTGCATTTAAATCCAGCAGAGAAAG
SG0509	SpeI + *ureABCEFGD*^{Sp} rev	tttaa**ACTAGT**TTAAACGATATAGTTAGCAAATTCATCC
SG0510	Up-fwd *ureABC* W168 LFH	TACGGAAGAGGCAGGAAAC
SG0511	Up-rev *ureABC* W168 LFH	*cctatcacctcaaatggttcgctg*CGCTGCAAAAATGAGCAATTTC

SG0512	Do-fwd *ureABC* W168 LFH	*cgagcgcctacgaggaatttgtatcg*GCCAGCCTGTCGATTATGTC
SG0513	Do-rev *ureABC* W168 LFH	GCAGTTGGCAAATATTCTTTCG
SG0526	zeo^{r} cassette LFH fwd	*cagcgaaccatttgaggtgatagg*GGCTTTTTATATGTGTTACTCTACATACAGAAAGG
SG0527	zeo^{r} cassette LFH rev	*cgatacaaattcctcgtaggcgctcgg*CAGTCGGCATTATCTCATATTATAAAAGCC
SG0532	Up-fwd *ureABC* W168 outside flank check	AGGATATCGGGAAAGCCAAG
SG0533	Do-rev *ureABC* W168 outside flank check	GAGTCTGTCTGCTGCAAATC
SG0575	*ureABCEFGD*^{Sp} check fwd	AGGTCTAGATGAGATCATTGC
SG0599	pSB1A3/pSB1C3 check fwd	TGCCACCTGACGTCTAAG
SG0600	pSB1A3/pSB1C3 check rev	ATTACCGCCTTTGAGTGA
SG0634	MLS^{r} cassette LFH fwd	*cagcgaaccatttgaggtgataggg*ATCCTTTAACTCTGGCAACCCTC
SG0635	MLS^{r} cassette LFH rev	*cgatacaaattcctcgtaggcgctcgg*GCCGACTGCGCAAAAGACATAATCG
SG0636	MLS^{r} cassette check rev	GTTTTGGTCGTAGAGCACACGG
SG0646	Biobrick prefix + RBS + *urt*^{Bp} fwd	tttaa***GAATTCGCGGCCGCTTCTAGAG*****aaggaggacaaac**ATGCGAAAAAACAAACATCATTTATTAAG
SG0647	Biobrick suffix + *urt*^{Bp} rev	tttaa***CTGCAGCGGCCGCTACTAGTA***TTATAAGTTTTGCAGAACCTTTCTTG
SG0648	XbaI + RBS + *ureH*^{Bp} fwd	tttaa**TCTAGAaaggaggacaaac**GTGGAAGGTACATTATTCTCG
SG0649	Biobrick suffix + *ureH*^{Bp} rev	tttaa***CTGCAGCGGCCGCTACTAGTA***TTAAATCCAAAGGTTAAATAAACCC
SG0650	*ureH*^{Bp} QuikChange fwd	CATTGGAATCCCCTTTGTGCTGAGTAAGAAGCGAG
SG0651	*ureH*^{Bp} QuikChange rev	GCACAAAGGGGATTCCAATGATTGTTGTAAAGAAAAGCATAC

SG0652	BsmBI w/ BamHI overhang + RBS + *ureABCEFGD*^{Bp} fwd	tttaa**CGTCTCGGATCC**<u>**aaggaggacaaac**</u>ATGCAACTATTACCGCGTGAAG
SG0653	BsmBI w/ EcoRI overhang + *ureABCEFGD*^{Bp} rev	tttaa**CGTCTCGAATTC**TTAATATTTTCTTAAAAAACTCGGGG
SG0654	*ureABCEFGD*^{Bp} check fwd	ACTGGATTAAGGAAAATGCAC
SG0891	Up-fwd *dltABCDE* W168 LFH	CTGCTGCTGGCACAAATATAG
SG0892	Up-rev *dltABCDE* W168 LFH	<u>*cctatcacctcaaatggttcgctg*</u>CGGATAAGTTTCCGCATGTG
SG0893	Do-fwd *dltABCDE* W168 LFH	<u>*cgagcgcctacgaggaatttgtatcg*</u>GATTATGACAGGTTATTCGAGC
SG0894	Do-rev *dltABCDE* W168 LFH	GATGACTGAATTGCGCGTAATG
SG0895	Up-fwd *dltABCDE* W168 outside flank check	GCTCTGCATATTGATCTTATCTG
SG0896	Do-rev *dltABCDE* W168 outside flank check	GTTACAGGTGACTATCAAACTG
SG0901	SpeI + RBS-*dltABCDE* fwd	tttaa**ACTAGT**TTGGAGAGAGAATAACTATGAAAC
SG0902	PstI + *dltABCDE* rev	tttaa**CTGCAG**TTAATTCTCCTGCGTGTTCATTTG
SG0907	Gibson pUC18/pAT28 overhang + P_{veg} fwd	<u>*gcaggtcgactctagag*</u>GGAGTTCTGAGAATTGGTATG
SG0913	pUC18/pAT28 check fwd	CTATGCGGCATCAGAGCAG
SG0929	XbaI + P_{veg} fwd	tttaa**TCTAGA**GGGAGTTCTGAGAATTGGTATGC
SG0930	BsmBI w/ BamHI overhang + P_{veg} fwd	tttaa**CGTCTCGGATCC**GGAGTTCTGAGAATTGGTATG
SG0931	pUC18/pAT28 check rev	CAATTTCACACAGGAAACAGC
SG1009	Up-fwd *epsH* W168 LFH	CACTTGTGCTCGTGTCAGG
SG1010	Up-rev *epsH* W168 LFH	<u>*cctatcacctcaaatggttcgctg*</u>CAGCGACTAACAGACTAACC

SG1011	Do-fwd *epsH* W168 LFH	*cgagcgcctacgaggaatttgtatcg*GTATCAGCGGGTGATCGAG
SG1012	Do-rev *epsH* W168 LFH	CATTGACTGCGGCTGTTACG
SG1013	Up-fwd *tasA* W168 LFH	CTCCAATCAAATCGGCGATTC
SG1014	Up-rev *tasA* W168 LFH	*cctatcacctcaaatggttcgctg*GCAGAAGCAACTCCTAAACTC
SG1015	Do-fwd *tasA* W168 LFH	*cgagcgcctacgaggaatttgtatcg*CATACTGATAAAGATGGTTACGTG
SG1016	Do-rev *tasA* W168 LFH	CGGAACAGGCGGTTAACAG
SG1017	Up-fwd *spo0A* W168 LFH	CTGGCATCGGCACTATGAC
SG1018	Up-rev *spo0A* W168 LFH	*cctatcacctcaaatggttcgctg*GCTTACCAGCTCTCGATTATC
SG1019	Do-fwd *spo0A* W168 LFH	*cgagcgcctacgaggaatttgtatcg*GGTTGCGGATAAGCTGAGG
SG1020	Do-rev *spo0A* W168 LFH	CTCGCTATTGTCGATGAAGTG
SG1021	Up-fwd *epsH* W168 outside flank check	CTCAACTTGGCTACGATGCAC
SG1022	Do-rev *epsH* W168 outside flank check	GTTCAACATTATACATCGGGAC
SG1023	Up-fwd *tasA* W168 outside flank check	GAAAGGCACTGTATGCTCAC
SG1024	Do-rev *tasA* W168 outside flank check	GAAAGCGGACTTAAGCGTATG
SG1025	Up-fwd *spo0A* W168 outside flank check	GGTGAATCTTTAGACTTACTGATC
SG1026	Do-rev *spo0A* W168 outside flank check	GACAAGACGCGCCATTGAAG
SG1034	Gibson RBS-GFPmut1 overhang + P_{veg} fwd	*gttcctcctt*ACTACATTTATTGTACAACACG
SG1035	Gibson P_{veg} overhang + RBS-GFPmut1 fwd	*taaatgtagt*AAGGAGGAACTACTATGG
SG1036	Gibson pUC18/pAt28 overhang + RBS-GFPmut1 rev	*attcgagctcggtacccggg*TTAACCGGTTTTGTAGAG

SG1037	BsmBI w/ EcorI overhang + GFPmut1 rev	tttaa**CGTCTCGAATTCT**TAACCGGTTTTGTAGAGCTC
SG1053	RBS-GFPmut1 check fwd	AAGGAGGAACTACTATGGCC
SG1054	GFPmut1 check rev	TTAACCGGTTTTGTAGAGCTC
SG1072	BamHI + oriT IncP fwd	tttaa**GGATCC**TCTTCTTGATGGAGCGCATG
SG1073	BamHI + oriT IncP rev	tttaa**GGATCC**CGCACGATATACAGGATTTTG
SG1074	oriT IncP check fwd	GCAGTGAGCGCAACGCAATTAAT
SG1075	StuI + P_{veg}-GFPmut1 fwd	tttaa**AGGCCT**GGAGTTCTGAGAATTGGTATG
SG1076	StuI + P_{veg}-GFPmut1 rev	tttaa**AGGCCT**TTAACCGGTTTTGTAGAGCTC
SG1077	P_{veg}-GFPmut1 check rev	GATGACCTCGTTTCCACCGG

a. Restriction sites are in uppercase bold; BioBrick overhangs are in uppercase bold and italicised; Added ribosome binding sites are in lowercase bold and underlined; LFH/Gibson overhangs are in lowercase underlined and italicised; QuikChange point mutation site is double underlined.

3.4 Zeta potential measurements.

The protocol was adapted from Soon *et al* (Soon *et al.*, 2011). The cells were grown at 37°C in LB with respective antibiotic either to stationary phase overnight or mid-log phase (OD_{600}=~0.5) through subcultures. For subcultures, 10 ml fresh LB was inoculated to OD_{600}=0.05 from an overnight culture and grown at 37°C with agitation until OD_{600}=0.5. Volumes of 4 ml culture were centrifuged at 4,000 ×*g* for 5 min, the supernatant discarded, and cell pellets washed once in 1 volume autoclaved dH_2O. The cell pellet was re-suspended in autoclaved dH_2O and a 2 ml volume prepared to a final OD_{600}=0.5. The zeta potential of 1 ml cell suspension was measured in DTS1061 cuvettes with a Zetasizer Nano ZS equipped with a 633 nm red laser (Malvern Instruments Ltd, Malvern, UK) using the Helmholtz-Smoluchowski theory. Measurements were performed at 25°C (120s calibration) and taken as triplicate readings (n=3) of three biological repeats.

3.5 Nisin growth inhibition assay.

This assay was adapted from concentration-dependent killing experiments (Staroń *et al.*, 2011). Overnight cultures grown at 37°C were adjusted to OD_{600}=1 with dH_20. Cell suspensions of 15 µl were used to inoculate 150 µl of LB in clear flat-bottom 96-well plates. Cells were grown in a TECAN-Spark microplate reader (Tecan Group Ltd., Switzerland) at 37°C and orbital shaking 180 rpm. When the cells reached late exponential phase (OD_{600}=0.5, corresponding to OD_{600}=1.37 in a 1 cm standard cuvettes) nisin was added to the cultures as indicated to reach final concentrations of 0-64 µg/ml. The OD_{600} reading was taken every 15 min over 5 hours. Concentration-dependent killing by nisin was deemed as a decrease in OD_{600} over time relative to the control without antibiotic addition.

3.6 Cytochrome C binding assay.

The cytochrome C binding assay was adapted from Revilla-Guarinos *et al* (Revilla-Guarinos *et al.*, 2013). Overnight cultures (approximately 2 ml of OD_{600}=2.5) were harvested by centrifugation (2 min at 16,000 ×*g*) and re-suspended in 1.8 ml 20 mM MOPS-NaOH pH 7 to an OD_{600}=2.5. Cells were suspended by thorough mixing and then incubated with 200 µl of 5 mg/ml cytochrome C (250 µg/ml final concentration) for 10 min at room temperature. The mixture was centrifuged (4 min at 16,000 ×*g*) and the concentration of unbound cytochrome c remaining in the supernatant was measured as absorbance at 530 nm wavelength in a spectrophotometer. This absorbance was compared to the absorbance of 250 µg/ml cytochrome C solution without bacterial cell (the 0 % binding bench mark) to calculate the binding percentage.

3.7 Calcite precipitation assays.

Calcite precipitation on bacterial colonies was monitored on LBC, LBGMC, and B4 solid precipitation media. LBC media contained LB supplemented with 20 g/L urea and 10 g/L calcium acetate. LBGMC contained LBGM supplemented with 20 g/L urea and 10 g/L calcium acetate. B4 precipitation media contained 0.4 g/L yeast extract, 1 g/L fructose, 0.25 g/L calcium acetate and 1.5 g/L agar, pH 8 adjusted with NaOH, was adapted from Boquet changing the sugar source (Boquet *et al.*, 1973). Xylose was added to the different media to a final concentration of 0.2 % for strains harbouring xylose-inducible genetic constructs. Cells were grown overnight on solid media with antibiotics at 30°C. Cells were scraped from growth on solid media and adjusted to an optical density of OD_{600}=0.5 using autoclaved dH_2O, from which 10 µl was spotted onto standard agar plates with either LBC, LBGMC or B4. These were subsequently incubated at 30°C for 1-2 weeks, observing and imaging the colony crystal morphology under 5× magnification with a Leica MZ7.5 stereomicroscope (Leica, United Kingdom) at regular intervals, using an Infinity 2 Lumenera microscope camera (Teledyne Technologies Inc., United States).

3.8 Whole cell urease assays.

Rapid urease test broth (RUB) containing 0.1 g/L yeast extract, 20 g/L urea, 0.67 mM monopotassium phosphate, 0.67 mM disodium phosphate, 0.01 g/L phenol red, pH 6.8*±0.2,* was used to determine urease activity. Xylose was added to RUB to a final concentration of 0.2 % w/v for strains requiring xylose induction. For the qualitative whole cell urease assay, 2 ml RUB was inoculated with either overnight culture at 1:10 – 1:1000 dilution, colonies picked directly from solid growth media or with cells scraped from solid growth media and adjusted to a 0.5 McFarland turbidity standard (McFarland, 1907). Suspensions were subsequently incubated at 30°C, 150 rpm or 37°C, 200 rpm. The semi-quantitative whole cell urease assay was based on a protocol by Okyay and Rodrigues (Okyay and Rodrigues, 2013). Cells were grown overnight on solid media with antibiotics at 30°C. Cells were scraped from growth on solid media and adjusted to an optical density of OD_{600}=0.5 using autoclaved dH_2O. Cell suspensions of 20 µl were used to inoculate 200 µl of RUB in clear flat-bottom 96-well plates. In a TECAN-Spark microplate reader (Tecan Group Ltd., Switzerland) the 96-well plates were incubated at 30°C and orbital shaking 180 rpm with readings taken at 560 nm every 15 min for 24 hours to assess the change in pink colour formation over time as a proxy for whole cell enzyme activity.

3.9 Electron microscopy.

Electron microscopy was carried out to examine the morphology of calcite precipitated by bacterial colonies. Calcite crystals were carefully scraped from the bacterial colonies that underwent the calcite precipitation assay. They were repeatedly washed in rounds of 1 ml dH_2O by gently pipetting up and down to remove any remaining cells, biofilm and agar until the water remained clear, all the while taking care not to damage to crystal. The crystals were then dried overnight at room temperature to evaporate any remaining liquid. Before imaging, samples were placed under vacuum overnight. For Scanning Electron Microscopy (SEM), samples were coated with gold for 1-3 min using an Edwards S150B sputter coater (Edwards Group Ltd., United Kingdom) and imaged on a JOEL JSM-6480LV SEM microscope (JEOL Ltd., Japan). An energy dispersive x-ray analyser (EDX) equipped on the SEM was used for elemental analysis of the calcite crystals prior to gold coating. For Field Emission Scanning Electron Microscopy (FE-SEM), samples were coated with chromium to a thickness of 20 nM using a Quorum Q150TS sputter coater (Quorum Technologies Ltd., United Kingdom) and imaged on a JOEL JSM-6301F FE-SEM microscope (JEOL Ltd., Japan).

3.10 Fluorescence measurements.

Bacterial fluorescence was measured from cells grown in subculture and overnight under their respective growth conditions. For subcultures, strains were inoculated from overnight growth to an OD_{600}=0.1 and grown until an OD_{600}=0.5. End-point fluorescence (excitation at 479 nm and emission monitored at 520 nm) and OD_{600} measurements were taken in a clear flat-bottom 96 well plate using 100 µl volumes with a SYNERGY H1 microplate reader (BioTek Instruments Inc, United Kingdom). Relative fluorescence/OD_{600} was calculated from the microplate reads.

Chapter 4

Genetic Optimisation of Bacteria-Induced Calcite Precipitation: the role of the Ureolytic Pathway, Surface Charge and Biofilm Production

ABSTRACT *To engineer* Bacillus subtilis *for calcite precipitation the* Bacillus paralicheniformis *urease gene cluster was heterologously expressed and the role of accessory genes assessed for their ability to modulate urease activity and calcite precipitation. The nickel/iron transporter* ureH *was found to contribute the most to increased urease activity and consequently calcite precipitation. Subsequently, biofilm formation and surface charge were modulated to explore their effects on* Bacillus subtilis *calcite precipitation.* Bacillus subtilis *grown on biofilm promoting precipitation medium formed crystals earlier than on standard LB-based precipitating media. EPS production was found to contribute more strongly than proteinaceous components to precipitation within biofilms.* [1]

[1] A quantitative whole cell urease assay developed in context of this work, but not included here, published in: Reeksting, B.J., **Hoffmann, T.D.**, Tan, L., Paine, K., and Gebhard, S., 2020. In-Depth Profiling of calcite Precipitation by Environmental Bacteria Reveals Fundamental Mechanistic Differences with Relevance to Application. *Applied and Environmental Microbiology*, 86(7).

4.1 Introduction.

4.1.1 The ureolytic pathway.

Sporosarcina pasteurii, previously *Bacillus pasteurii* (Yoon *et al.*, 2001), is considered the model ureolytic bacterium for application in self-healing concrete with its high urease activity. Ureolysis is the metabolic route of choice for application because it accounts for the fastest route of bacteria-induced calcite precipitation (BICP) (De Muynck *et al.*, 2010). Driven by a single enzyme, it is a straightforward model for the study of mineral precipitation in bacteria (Hammes *et al.*, 2003). The urease enzyme is capable of catalysing the intracellular hydrolysis of one mole of urea to one mole of ammonia and carbamic acid (Equation 3).

$$CO(NH_2)_2 + H_2O \xrightarrow{urease} NH_2COOH + NH_3 \qquad \text{(Equation 3)}$$

After hydrolysis of urea, the carbamic acid undergoes spontaneous hydrolysis to one mole carbonic acid and one mole of ammonia (Equation 4). Under circum-neutral pH, the overall two moles of ammonia then become protonated by water to form ammonium and hydroxide ions (Equation 5).

$$NH_2COOH + H_2O \xrightarrow{spontaneous} H_2CO_3 + NH_3 \qquad \text{(Equation 4)}$$

$$NH_3 + 2H_2O \longleftrightarrow 2NH_4^+ + 2OH^- \qquad \text{(Equation 5)}$$

The pH increases as a result of the hydroxide ions and pushes the equilibrium of carbonic acid towards the formation of bicarbonate (Equation 6) and subsequently carbonate (Equation 7).

$$H_2CO_3 \longleftrightarrow HCO_3^- + H^+ \qquad \text{(Equation 6)}$$

$$HCO_3^- + H^+ + 2OH^- \longleftrightarrow CO_3^{2-} + 2H_2O \qquad \text{(Equation 7)}$$

Given sufficient presence of calcium ions and carbonate counter ions in the micro-environment, saturation tips the equilibrium towards the precipitation of calcium carbonate (Equation 8).

$$Ca^{2+} + CO_3^{2-} \longleftrightarrow CaCO_{3(S)} \downarrow \qquad \text{(Equation 8)}$$

The rate limiting step in this BICP pathway is ureolysis, even though the enzyme increases the rate of urea hydrolysis by 10^4 relative to un-catalysed urea hydrolysis (Phillips *et al.*, 2013). This makes it a promising single enzyme process for exploiting biotechnologically.

Most microbial urease enzymes are nickel metalloenzymes, although iron-dependent ones are also found (Liu *et al.*, 2017). Ureases are multimeric, characteristically composed of three structural subunits, namely subunit γ, subunit β, and subunit α, encoded by the genes *ureA*, *ureB* and *ureC,*

respectively (Mobley *et al.*, 1995). For synthesis of the catalytically active urease, additional accessory proteins are required, typically encoded by *ureD*, *ureF*, *ureG* and *ureE* (Farrugia *et al.*, 2013). The UreD-UreF-UreG proteins form a GTP-dependent chaperone that binds the apoprotein, while UreE acts as a metallochaperone that delivers the Ni^{2+} to the active site (Soriano and Hausinger, 1999; Soriano *et al.*, 2000; Farrugia *et al.*, 2013; Fong *et al.*, 2013). Best studied in *Klebsiella aerogenes* the precise activation mechanism is still subject to ongoing investigation, a schematic and summary of our current understanding is depicted in Figure 5 (Farrugia *et al.*, 2013).

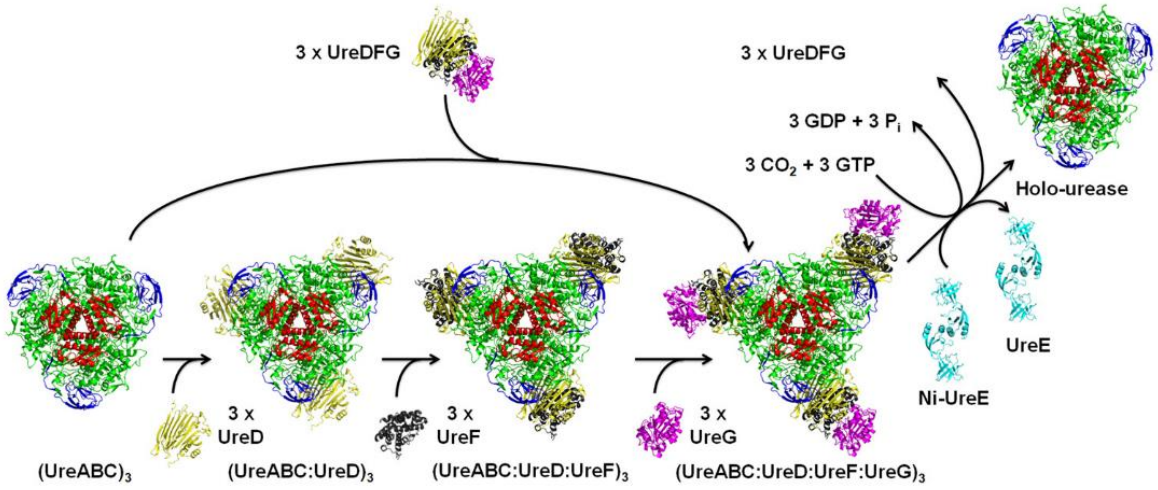

Figure 5. Schematic for urease activation in *K. aerogenes*. The urease apoprotein ($(UreABC)_3$) is a trimer of trimers composed of UreA (red), UreB (blue) and UreC (green). The apoprotein sequential binds UreD (yellow), UreF (black), UreG (purple) or the UreDFG complex directly. UreD acts as a scaffold and recruitment protein, while UreF functions to facilitate binding of the GTPase UreG, and enhances access to the apoprotein active site. Alternatively UreDFG may act as a molecular chaperone complex, binding as a unit to the urease apoprotein. The final enzyme is activated through carbamylation of Lys-217 at the active site using CO_2, GTP binding and hydrolysis by UreG, and nickel delivery by the nickel metallochaperone ureH (cyan). Diagram from (Farrugia *et al.*, 2013).

While accessory genes are necessary, bacteria such as *B. subtilis* SF10 (which lacks *ureEFGD*) may still have intrinsically low activity due to unknown activation pathways (Kim *et al.*, 2005). Variations in urease activation through other genes have also been described in *Yersinia pseudotuberculosis* and *Actibobacillus pleuropneumoniae* (Sebbane, Mandrand-Berthelot, *et al.*, 2002; Bossé *et al.*, 2001). Urease genes are typically organised into gene clusters but with varying organisation across microorganisms, an indication of evolutionary gene shuffling events (Mizuki *et al.*, 2004). In addition, less essential accessory genes may be present among the urease gene clusters (see below Figure 8); these can include nickel permeases, often denoted UreH or UreJ (Sebbane, Mandrand-

Berthelot, *et al.*, 2002). Encoded near or within the urease gene cluster, these supply nickel for the synthesis of the metalloenzyme and share homology with other nickel/cobalt transporters such as HupE (Eitinger *et al.*, 2005; Rodrigue *et al.*, 2017). Other nickel transporters are often found within urease-positive organisms, but these are not associated with the urease gene cluster, for example NixA or Ynt (Wolfram *et al.*, 2006; Sebbane, Mandrand-Berthelot, *et al.*, 2002). Another set of urease accessory genes are the acidic to neutral pH gated (H^+-gated channel) urea channel genes *ureI* and *ureI*-like encoding proteins belonging to the AmiS protein family (Bury-Moné *et al.*, 2001; Sebbane, Bury-Moné, *et al.*, 2002). Other urea transporters can be found without association to the urease gene cluster, such as the Yut protein (Sebbane, Bury-Moné, et al., 2002). Some bacteria can harbour a urea ABC-type transporter encoded by *urtABCDE* (Beckers *et al.*, 2004; Valladares *et al.*, 2002). Genes of unknown function are also found amongst the urease gene clusters (Bossé and MacInnes, 1997). In rare cases, a urea-inducible regulatory gene, *ureR*, is associated with the gene cluster (Mobley *et al.*, 1995; Dattelbaum *et al.*, 2003). This diversity in gene accessory genes gives rise to a diversity of urease gene clusters and further genes that feed into its regulation and function (see below Figure 8).

Recent studies that explored heterologous urease expression to engineer calcite precipitation have moved *S. pasteurii* urease genes into *Escherichia coli* (Liang *et al.*, 2018; Heveran *et al.*, 2019; Bachmeier *et al.*, 2002) or *Pseudomonas aeruginosa* (Bergdale *et al.*, 2012). However, these chassis organisms do not reflect the final target for biotechnological application. Of more interest are non-pathogenic category 1, spore-forming Gram-positive species, which are ideal for their safety and long term survivability as spores. Additionally, questions remain on determining the minimum set of genes of the urease cluster in terms of structural and accessory functions, required to induce precipitation in such a chassis. Therefore, the aim here was to use the Gram-positive model and industrial relevant organism *Bacillus subtilis* W168 (which has low intrinsic urease activity and calcite precipitation ability) as a chassis to determine the components of the urease gene cluster required to induce calcite precipitation. *B. subtilis* W168 is an ideal model, as with its low intrinsic BICP activity one should be able to detect small changes and get a high-resolution understanding of which genes/traits contributing to BICP.

4.1.2 Bacterial surface charge and biofilms.

Apart from metabolism as a driver for mineral precipitation, bacterial surfaces also play a role (Chapter 1). One important aspect of surfaces in mineral precipitation is thought to be the attraction of metal cations from the surrounding environment, which react with anions in the

vicinity and precipitate out as a mineral. Surface charge is governed by functional groups such as carboxyl and phosphate groups. Teichoic acids are rich in phosphate groups in their backbone, which due to their low pK_a impart an overall negative charge (Thomas and Rice, 2015). Teichoic acid composition varies between species, encompassing a range of glycopolymers containing phosphodiester-linked polyol repeat units (Brown *et al.*, 2013). A representative structure of a *B. subtilis* 168 Poly(glycerol-phosphate) wall teichoic acid is depicted in Figure 6. The phosphodiester-linked polyol repeat units contain glycosylated, hydroxyl or D-alanine side group branches which, depending on type and quantity, ultimately contribute to charge variations. Modulation of surface charge in this manner is actively controlled by bacteria through the D-alanylation of wall teichoic and lipoteichoic acids. This is a mechanisms by which bacteria decrease the net surface charge in defence against cationic antibiotics, the process of which is encoded by the proteins of the *dltABCD* operon (Revilla-Guarinos *et al.*, 2014; Brown *et al.*, 2013). The role of surface charge is considered important for BICP and there is an underlying genetic process that can be used to modulate the surface charge, as such it becomes a potential target to exploit for engineering of BICP. The interplay between surface charge and BICP raises a number of questions: (i) Does genetic manipulation of the *dlt* operon produce a sufficient change in surface charge? (ii) Does genetic manipulation of the *dlt* operon influence precipitation ability? (iii) What is the interplay between surface charge and metabolism on precipitation? While a role of surface charge in BICP has been studied in some detail, to our knowledge, artificial modulation of cell surface charge has not been explored as a means for engineering mineral precipitation. The second aim in this chapter therefore was, once BICP precipitation in the Gram-positive model organism *B. subtilis* W168 was established, to explore the effects of modulation of surface charge on calcite precipitation ability.

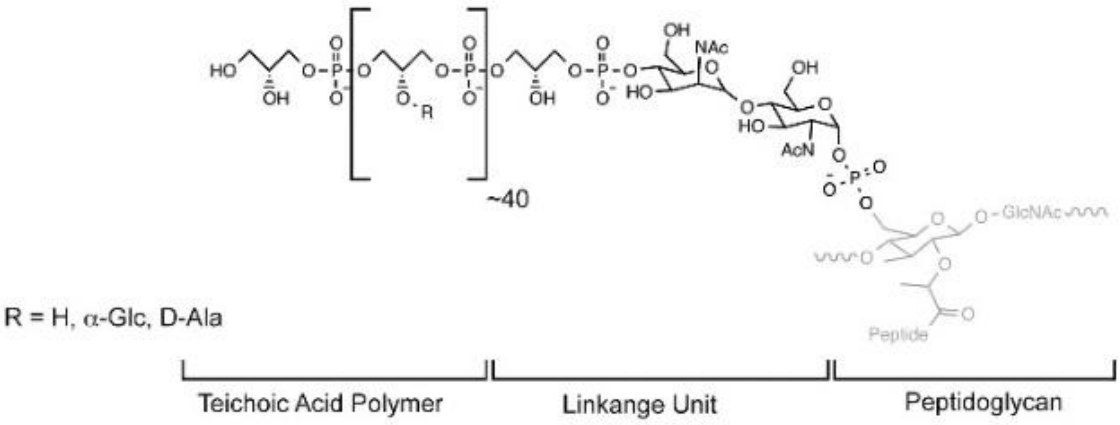

Figure 6. Representative wall teichoic acids of *Bacillus subtilis* 168. Wall teichoic acid have two main structures, a disaccharide linkage unit and teichoic acid polymer main chain. The main chain is made up of polyol repeat units with

glycosylated, hydroxyl or D-alanine side group branches. Diagram from (Sewell and Brown, 2014).

Biofilms are another factor of bacterial surfaces that influence the mineral precipitation ability of bacteria. Biofilms create a microenvironment that helps trap ions to increase local concentrations in favour of supersaturation and precipitation as well as providing favourable functional groups for precipitation (Chapter 1). *B. subtilis* biofilm compositions involve extracellular polymeric substances which are made up of polysaccharides, charged polymers, amphilic molecules and proteins, where the major components are polysaccharides and proteins (Marvasi, Visscher and Casillas Martinez, 2010; Omoike and Chorover, 2004). Exopolysaccharide production is facilitated by the 15-gene *epsA-O* operon and production of proteinaceous fibres by *tasA* of the *tapA-sipW-tasA* operon (Branda *et al.*, 2004; Kearns *et al.*, 2005; Branda *et al.*, 2006). The regulation of both these operons is intricate. Both are negatively controlled by SinR and AbrB (Chu *et al.*, 2006), while Slr additionally positively regulates the *tap* operon and is itself negatively controlled by SinR and AbrB (Chu *et al.*, 2008). All regulators of these operons ultimately fall under control of the master regulator Spo0A (Hamon and Lazazzera, 2001; Branda *et al.*, 2001). While there have been extensive investigations on the contribution of biofilm formation to biomineralisation, there has been limited investigations of genetic engineering approaches exploring the modulation of biofilm formation for calcite precipitation. Urease genes have been moved into *Pseudomonas aeruginosa*, a biofilm producer, to precipitate a mineral-organic bio-sealant better suited for application. The authors themselves, however, note that this recombinant organism is pathogenic and should not be used for application, their study instead aiding as a proof of concept (Bergdale *et al.*, 2012). Past work has looked at the role of biomineralisation in *B. subtilis* NCIB 3610*,* specifically at its stabilisation of complex biofilm morphologies. The work found that *epsH* and *tasA* deletions did impair calcite localisation within the colony architecture (Oppenheimer-Shaanana *et al.*, 2016). Due to the complexity of the biofilm morphology, this still raises the question whether the loss of the complex biofilm architecture or the loss of specific biofilm components impaired biomineralisation and to what degree. Questions also still remain on what components of biofilm are important for calcite precipitation in an application-relevant Gram-positive organisms such as *B. subtilis*. Therefore the third aim of this work was to investigate the contribution of exopolysaccharide and proteinaceous components of *B. subtilis* biofilm on its ability to precipitate calcite. Taken together, the approach taken here will elucidate how urease activity, cell surface charge and extracellular components of biofilms can be manipulated to engineer the biotechnology workhorse *Bacillus subtilis* for BICP. The outcomes are

aimed at guiding rational engineering approaches to build better precipitating strains for application.

4.2 Results.

4.2.1 The role of ureolysis in calcite precipitation by *Bacillus subtilis* W168.

4.2.1.1 Initial trials in establishing heterologous urease gene expression in *B. subtilis.*

To establish heterologous urease gene expression in *B. subtilis*, the first approach taken was to move the urease gene cluster *ureABCEFGD* from *S. pasteurii* type strain DSM33 (denoted SpU) into *B. subtilis* W168. At the time of construction the only sequence available of the SpU cluster was GenBank: KR133628.1, which lacked a ribosome binding site (RBS). Therefore, the strong *Bacillus subtilis* RBS with a 6 base pair spacer AAGGAGGACAAAC was chosen and placed directly before the *ureA* start codon (Guiziou *et al.*, 2016). The genes were placed under control of the xylose inducible promote P_{xylA} for controllable and potentially tuneable expression (Radeck *et al.*, 2013). Promoter and genes were cloned into the pBS2E plasmid which allowed for stable single copy integration into *B. subtilis* W168 genome at the *lacA* locus (Radeck *et al.*, 2013). This was aimed to reduce problems associated with replicative plasmid instability and varying copy numbers, as well as antibiotic selection for plasmid maintenance. The result was the construction of *B. subtilis* strain W-SpU (SGB740). *B. subtilis* has been shown to have some urease activity, even though it only possesses the core genes *ureABC* but lacks the accessory genes *ureEFGD,* typically required for the correct folding and assembly of the structural genes (Cruz-Ramos *et al.*, 1997; Kim *et al.*, 2005). Strain WΔ (SGB666) carrying a deletion of the native *ureABC* operon in *B. subtilis* W168 was therefore constructed to test if the intrinsic activity can be lowered further. This strain was also complimented with SpU to construct WΔ-SpU (SGB739). Together these strains were used to assess the heterologous expression of SpU in *B. subtilis* W168.

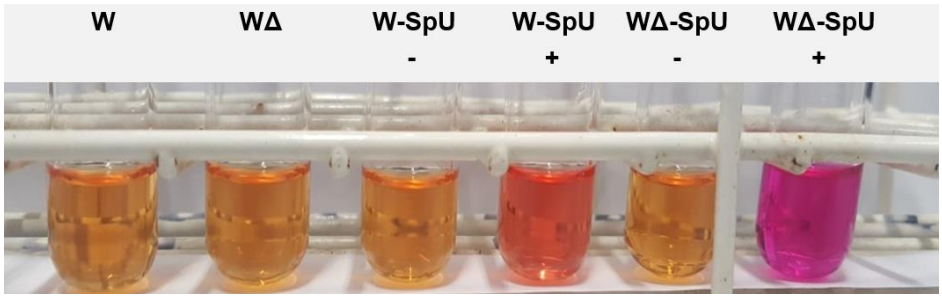

Figure 7. Qualitative rapid urease test broth assay based on changes in pH. A change of colour from yellow to pink indicates an increase in pH as a result of ammonia build-up from the cleavage of urea. Test tubes with RUB were inoculated

with cells picked straight from growth on solid media and incubated at 37°C for 2 days. Induction of heterologous gene expression with (+) and without (-) 0.2 % xylose is indicated. Wildtype *B. subtilis* (W), *B. subtilis* urease deletion strain (WΔ), *B. subtilis* with recombinant SpU (W-SpU) and *B. subtilis* urease deletion strain with recombinant SpU (WΔ-SpU) were tested.

Initial urease activity was measured qualitatively by inoculating rapid urease test broth (RUB) directly with transformants grown on solid media, as shown in Figure 7. With the qualitative urease assay, no urease activity was observed in the wildtype (W) and native urease deletion strain (WΔ), showing that as expected, *B. subtilis* W168 intrinsic urease activity was very low and thus unlikely to interfere with the assay. When the strains carrying the heterologous SpU constructs were tested without induction by xylose, no urease activity was observed indicating that any basal P_{xylA} activity did not drive production of detectable urease activity by this assay. However, when expression was induced by xylose, a colour change indicative of ureolytic activity was observed. The colour change was stronger for WΔ-SpU than for W-SpU indicating at a possible interference of the SpU with the native structural urease genes. Therefore, going forward *B. subtilis* W168 with the native urease genes deleted was chosen as the genetic background chassis for heterologous urease expression.

Repeats of this qualitative assay inoculated from growth in overnight cultures revealed problems with the reliability and reproducibility of these results. This may have been due to toxicity of the heterologous construct that led to a decrease in activity overtime. Therefore, inoculation from solid media was chosen over liquid starter cultures, and it was found that the most robust urease activity was obtained when test broth was inoculated from freshly streaked plates. Moreover, the strongest colour changes from ureolysis was observed in tubes incubated at 30°C as opposed to 37°C. From these findings it was decided that recombinant urease genes *ureABCEFGD* would consequently always be the last element introduced into a *B. subtilis* strain. Transformants would be plated out on solid media at 30°C, single colonies isolated by streaking, and glycerol stocks prepared from cell suspensions scraped from growth on solid media instead of overnight cultures. Strains would then be freshly streaked for use in subsequent assays at 30°C throughout to avoid loss of urease activity. Taken together, this initial set of experiments showed that heterologous production of urease in *B. subtilis* resulted in measurable activity and established a robust protocol for rapid testing of strains to circumvent stability problems. However, the stability issues indicated that *S. pasteurii* might not be the ideal source of urease genes. Additionally, the limited genome sequence information available at the time made it difficult to determine the exact gene composition and therefore restricted our ability to modify the construct further.

4.2.1.2 Selection of suitable urease gene cluster for heterologous expression in *Bacillus subtilis* W168.

Building on the initial trials of expressing the SpU genes in *B. subtilis* W168, the next step was to choose a urease gene cluster from a bacterium that was taxonomically more closely related to *B. subtilis* than *S. pasteurii*. The reasoning here was to provide more genetic compatibility in terms of codon usage and GC content that may occur in closer related organisms. Furthermore, urease gene clusters with additional accessory genes such as nickel/iron transporters and urea transporters were of interest to investigate how they feed into ureolysis to influence calcite precipitation. To better gauge and illustrate the variability in urease gene organisation, in terms of gene arrangement and presence/absence of accessory genes across bacteria and archaea, a range of species with different urease gene cluster organisations were chosen, grouped according to taxonomic relatedness and represented in Figure 8. The search showed that *B. subtilis* was unusual in that it only contained the core structural genes *ureABC,* while most other ureolytic organisms additionally harboured the accessory *ureEGFD* genes. Accessory nickel and/or urea transporters were not commonly observed to be associated within urease genes clusters. The figure highlights the diversity of urease gene clusters organisation and content across different microbes, while the core genes are preserved. Urease genes were subsequently chosen from *Bacillus paralicheniformis* ATCC 9945a because of its taxonomical relatedness to *Bacillus subtilis*. *B. paralicheniformis* additionally had a nickel/iron transporter *ureH* at the end of the urease gene cluster and a predicted urea transporter *urt* directly upstream, on the opposite strand, to its urease gene cluster (Figure 9-A). The urease of *B. paralicheniformis* has previously been experimentally identified as both a nickel and iron-activated urease, with the *ureH* gene encoding a transporter that supplies iron and nickel required for assembly of the active enzyme (Liu *et al.*, 2017). Codon usage in *B. paralicheniformis* was also found to be closer to *B. subtilis* than that of *S. pasteurii* (Supplementary 1). The *B. paralicheniformis ureABCEFGD* genes (denoted BpU), *ureH* (denoted H) and *urt* (denoted U) genes were all cloned with the strong RBS and spacer used previously and placed under control of P_{xylA}. BpU was cloned into the pXT plasmid for stable single-copy integration into the *thrC* locus of *B. subtilis* (Derre *et al.*, 2000). Genes *urt* and *ureH* were cloned individually and in combination into the pBS1C plasmid for stable single-copy integration into the *amyE* locus of *B. subtilis* (Radeck *et al.*, 2013). Introduction of these constructs into the *ureABC* deletion strain of *B. subtilis* W168 (WΔ) led to the construction of strains WΔ-U-BpU (SGB826), WΔ-H-BpU (SGB827), WΔ-U-H-BpU (SGB828), and WΔ-BpU (SGB844). These strains were then used for the investigation of ureolysis and calcite precipitation potential of urease genes and accessory genes in *B. subtilis* (Figure 9-B).

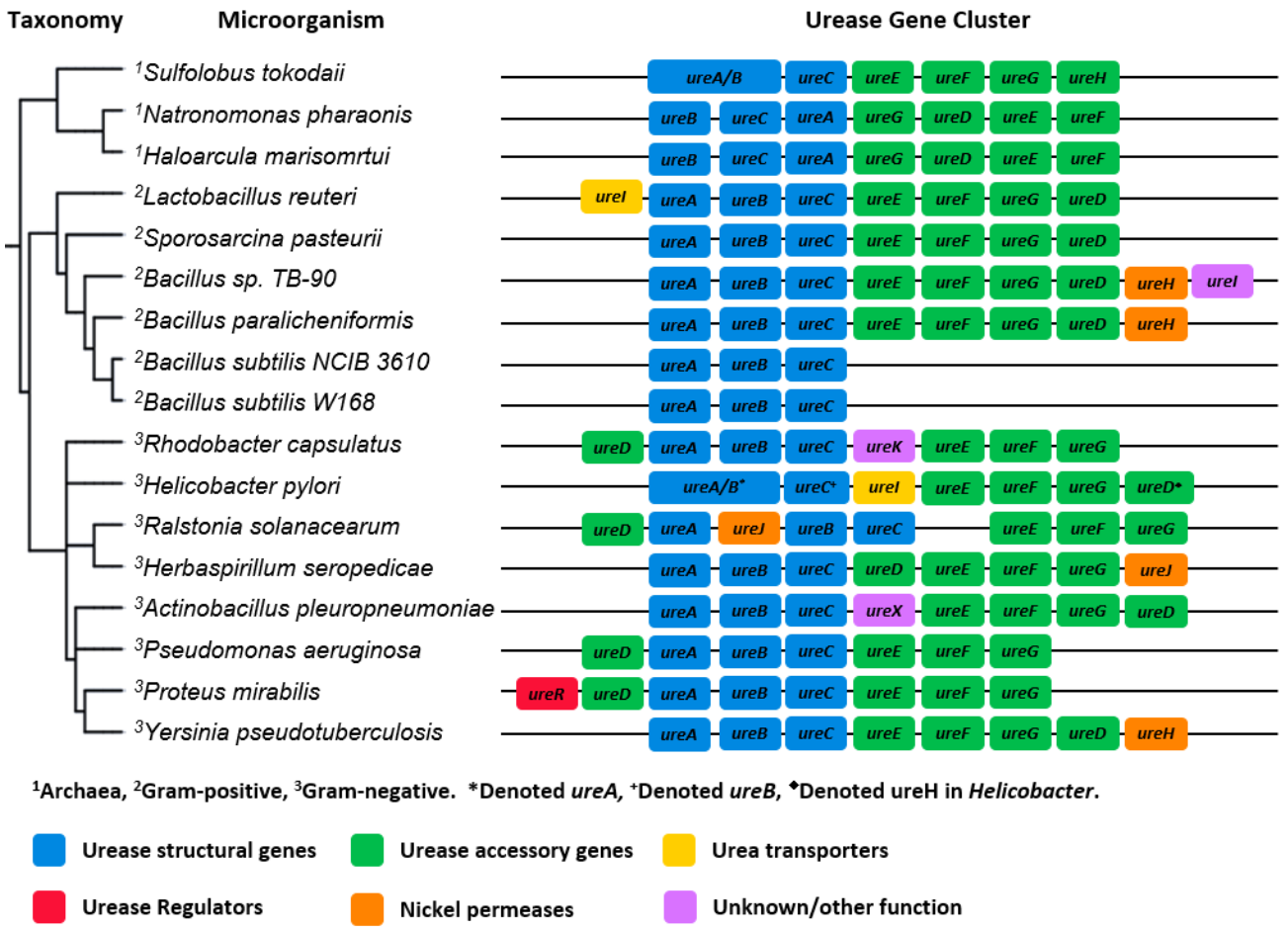

Figure 8. Structure of urease gene clusters in different microorganisms. The phylogram of bacterial species shown on the left was generated using online tools phyloT and iTOL based on NCBI taxonomy data (Sayers *et al.*, 2009; Letunić, 2015; Letunic and Bork, 2016). Urease gene cluster data summarised from gene annotations and homology searches from genomes on NCBI with accession numbers listed in Supplementary 2. Colour scheme indicates gene category as shown above.

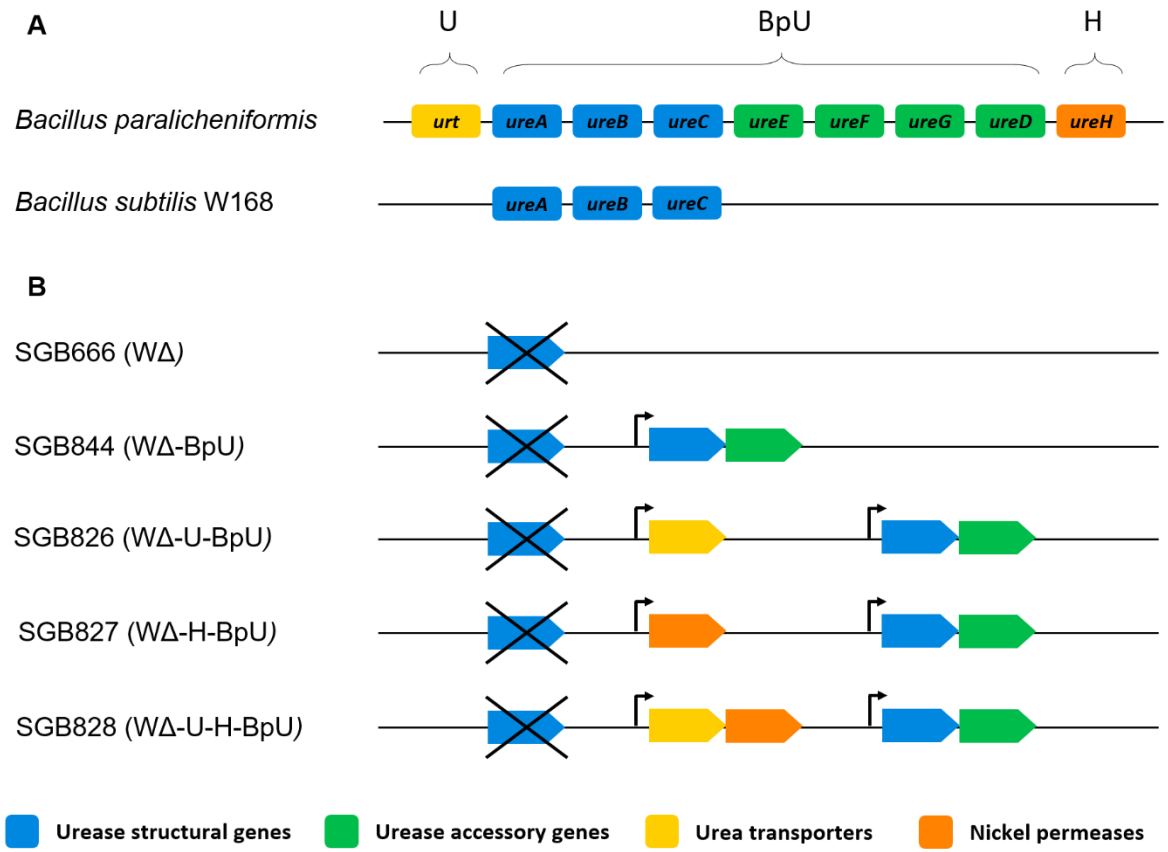

Figure 9. Urease and accessory genes in *Bacillus paralicheniformis*, *Bacillus subtilis* W168 and *Bacillus subtilis* W168 heterologous urease strains. Native urease and accessory genes in *B. paralicheniformis* and *B. subtilis* W168 (A). *B. subtilis* W168 heterologous urease strains (B). Colour scheme indicates gene category as shown above. Cross indicates gene deletion. Promoter represents P_{xylA}.

4.2.1.3 Semi-quantitative urease activity assay.

Measuring urease activity of *B. subtilis* strains carrying the *B. paralicheniformis* genes in RUB using the assay described above showed that strains with the BpU construct displayed urease activity following induction with xylose. However, this assay was purely qualitative and, while it showed that heterologous expression of BpU worked in principle, it did not allow differentiation in activity between different heterologous constructs. Therefore, there was a need for a quantitative assay to gain higher resolution of urease activity. Urease activity is commonly assessed quantitatively through the colourimetric Nessler Reaction or the Berthelot's Reaction (Mobley and Hausinger, 1989). These methods require cell collection, cell lysis, filtration, and calibration against total protein content. However, characterising bacterial strains for the purpose of applied BICP technologies should evaluate activities in whole cells, as the bacterial cells are directly applied in these processes. Characterisation in this manner would take into account substrate import and product export from within the cell where the enzymatic reaction occurs (Fujita *et al.*, 2017). Therefore, a semi-quantitative colourimetric urease assay was chosen based on the RUB and adapted from Okyay and Rodrigues (Okyay and Rodrigues, 2013). The assay was conducted in 96-well plates for high throughput and continued monitoring of activity over time, while incubating at 30°C. The change in RUB test broth colour from yellow to pink was indicative of an increase in pH as a result of the ammonia build up from ureolysis, and was monitored by the emergence of a peak in absorbance at 560 nm over time. The earlier the peak at 560 nm emerges and the more rapidly it rises, the stronger the ureolytic activity is. This is due to the quick and sufficient breakdown of urea to yield a change in pH. RUB does not contain sufficient nutrients to sustain cell division, however absorbance at 600 nm was still monitored to verify that changes in cell numbers had no effect on the absorbance reading at 560 nm. It was concluded that there were no influential OD_{600} changes over time, thus wells containing RUB without cells were used as a blank. Semi-quantitative urease assay results of *S. pasteurii* (Sp), *B. paralicheniformis* (Bp), *B. subtilis* (W), WΔ, WΔ-U-BpU, WΔ-H-BpU, WΔ-U-H-BpU and, WΔ-BpU are depicted in Figure 10.

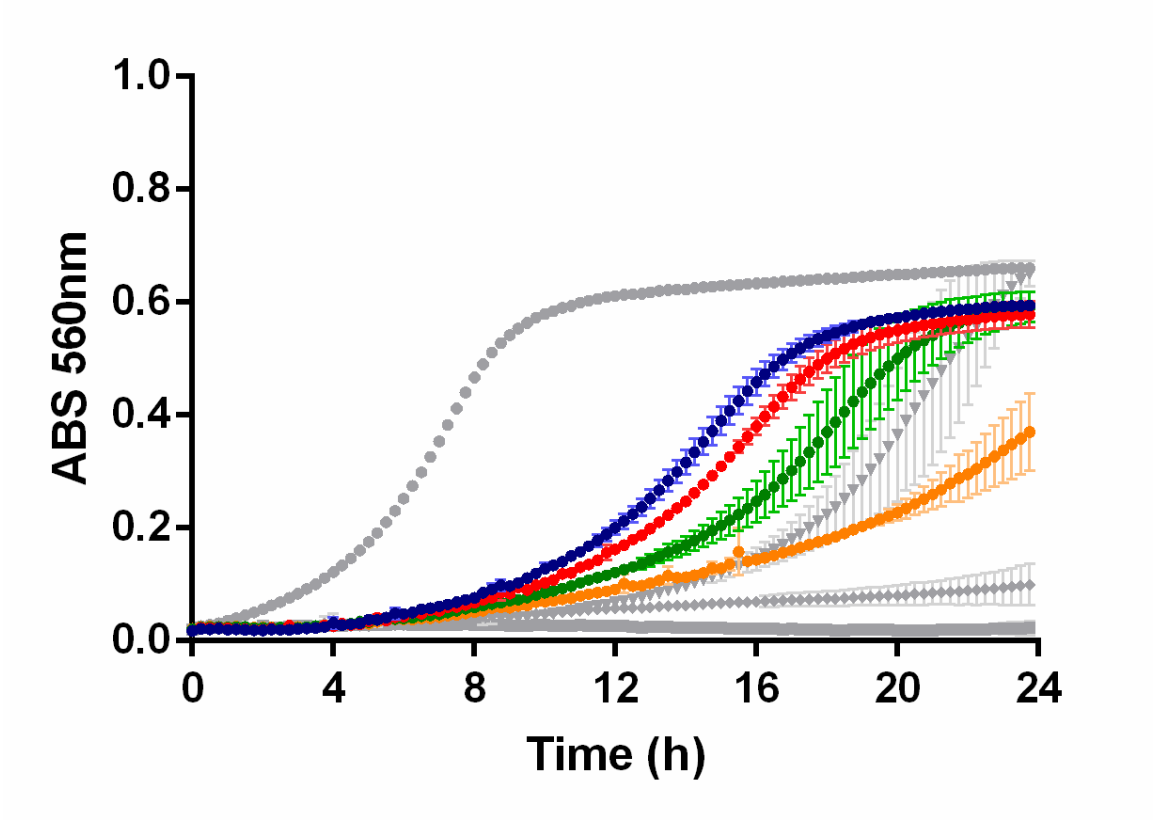

Figure 10. Semi-quantitative urease test broth assay based on changes in pH. An increase in absorbance at 560 nm occurs as a result of colour change from a pH increase due to ureolytic activity. Bacterial strains were inoculate into the test broth with 0.2 % xylose addition to an OD_{600}=0.05 from solid media and incubated at 30°C over 24h with orbital shaking in a TECAN microplate reader. *B. subtilis* strains with heterologous urease genes are displayed in varying coloured circles; WΔ-U-H-BpU in blue circles (●), WΔ-U-BpU in red circles (●), WΔ-H-BpU in green circles (●) and, WΔ-BpU in orange circles (●). Control strains are displayed in grey varying shapes; *S. pasteurii* in grey circles (●), *B. paralicheniformis* in grey triangles (▼), *B. subtilis* in grey diamonds (◆) and WΔ in grey squares (■). The graph is a representative set of three biological repeats; data are shown as average values from two to three technical replicates; error bars represent the standard deviation.

The highest urease activity was seen from the model ureolytic organism *S. pasteuri*, which was to be expected (Figure 10, grey circles). Wildtype *B. subtilis* showed a marginal change in pH (grey diamonds), likely from its low intrinsic urease activity as the native urease deletion strain (WΔ) has no detectable activity (grey squares). The highest urease activity of the *B. subtilis* recombinant strains was always observed from WΔ-U-BpU or WΔ-U-H-BpU (blue and red circles respectively), with marginal differences between the two across repeats. Urease activity was generally higher in the *B. subtilis* strains expressing transporter accessory genes (U or H) (blue, red and green circles) than in the one without (orange circles). This is as expected as the UreH supplies the nickel required to assemble the urease and Urt imports the urea needed to carry out ureolysis. The activity in these

strains was also higher than in their parent *B. paralicheniformis* (grey triangles). The results show that heterologous expression of BpU genes in *B. subtilis* W168 can result in ureolytic activity. This activity can be increased further through the inclusion of accessory transporter genes were the urea transporter (U) seems to have the stronger effect than the nickel transporter (H).

4.2.1.4 Solid media urease and precipitation assay.

To test whether urease activity enables *B. subtilis* W168 to precipitate calcite, an assay on a solid media is better suited to monitoring crystal formation. Therefore the next step was to characterise urease activity of the recombinant strains on solid media to see if the effect of the accessory genes was the same as in liquid RUB and if the strains with a high urease activity could induce the precipitation of calcite. For this, LB precipitation media (LBC) supplemented with phenol red and pH adjusted to 7.2 was chosen. This medium contained the required urea and a pH indicator to visualise urease activity as a change in pH, as well as calcium to be able to from calcite precipitates. Strains were spotted onto LBC phenol red and incubated at 30°C with activity monitored over 7 days.

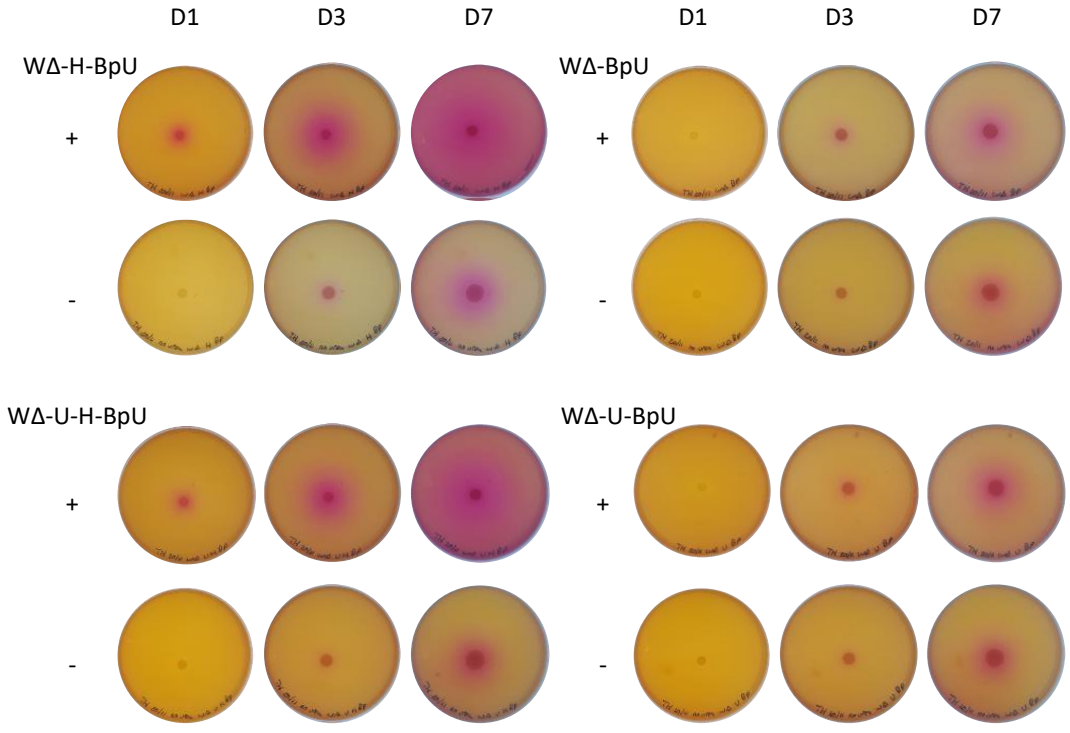

Figure 11. Solid media urease activity and precipitation assay. Urease strains were spotted onto LBC media supplemented with phenol red and pH adjusted to 7.2. Plates with urea (+) and without urea (-) are indicated. Plates were incubated at

30°C and activity monitored over 7 days. Images of activity from day 1 (D1), day 3 (D3) and day 7 (D7) are illustrated. The results are representative of three biological repeats.

In Figure 11 ureolytic activity on solid media can be observed as a spatial gradient that changed over time as the pH increase from ureolysis. The diffusion of ions (which change the pH) into the surrounding media can be seen as a colour change of the pH indicator from yellow to pink. Strains that produced the strongest colour change correspond to the highest ureolytic activity. *B. subtilis* W168 heterologous strains containing BpU with and without accessory genes all showed urease activity, as indicated by the colour change. Some colour change was still observed on plates without urea, which can be attributed to basal metabolic activity, e.g. breakdown of amino acids in the growth media. Urease activity was generally higher in the *B. subtilis* W168 strains expressing transporter accessory genes (U or H) than in the one without. More specifically, on solid media, presence of H yielded a higher activity on its own than U. The strongest ureolytic strains were thus WΔ-H-BpU and WΔ-U-H-BpU. This pH change was different to liquid media were in RUB the strongest pH change from ureolytic activity was observed in strains WΔ-U-BpU and WΔ-U-H-BpU (Figure 10). The main difference between the two assay compositions is the nutrient availability. In RUB (which is nutrient poor) the strains that had the urea transporter U yielded a higher activity. On LBC phenol red plates (which are nutrient rich) the strains that had the nickel transporter H yielded a higher activity. This suggest that the transporters play different roles in ureolysis depending on the growth conditions and surrounding environment. To further test this, RUB was solidified with the addition of 1.5 % agar and strains WΔ-H-BpU, WΔ-U-BpU and WΔ-U-H-BpU were spotted on and incubated overnight at 30°C.

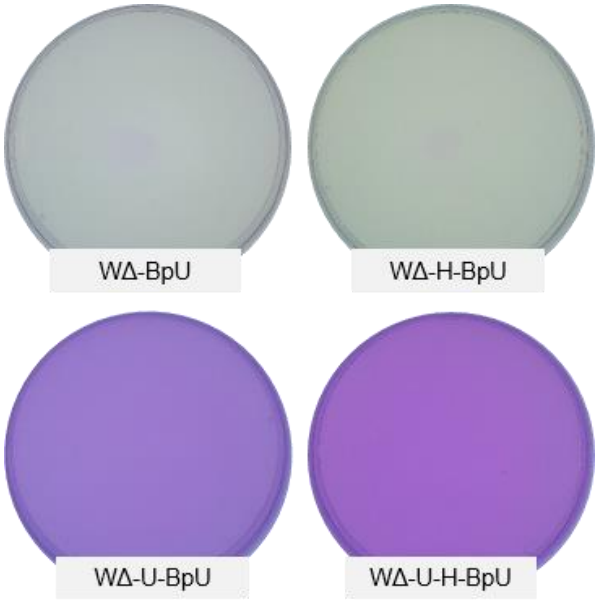

Figure 12. Solid RUB urease assay. A colour change from a pH increase due to ureolytic activity. Strains were spotted onto the middle of the plates and incubated at 30°C overnight. Result are of one experiment.

Urease activity on solidified RUB (Figure 12) yielded similar results as RUB liquid, where strains with the urea transporter U yielded higher activity than those with a nickel transporter H (Figure 10). This indicated that accessory transporter genes will provide advantages in different environments depending on whether the urea/nutrients are rate limiting or the urease enzyme and its activation forms the bottleneck i.e. access to nickel for incorporation into the urease active site. The difference in activity between strains was more drastic on solidified RUB compared to liquid RUB with no colour change observed for WΔ-H-BpU and WΔ-BpU. This could possibly be explained as a product of media viscosity. In liquid media, due to agitation, urea would be more readily distributed than on solid media where it has to diffuse towards the growing cells. For subsequent precipitation assays on LBC phenol red media the strains with the highest urease activity, WΔ-H-BpU and WΔ-U-H-BpU, were therefore expected to mostly like induce calcite precipitation.

To test if the heterologous strains with engineered urease activity had also gained the ability to precipitate calcite, strains spotted onto LBC phenol red media and incubated at 30°C were monitored for crystal formation on their colonies. No crystal precipitates were observed on colonies after 7 days of incubation across all tested strains. Only after a further 7 days were crystal precipitates observable on colonies of WΔ-H-BpU and WΔ-U-H-BpU, with the largest number visible on the former. Colonies were left at room temperature for a further 9 days before imaging at day 23.

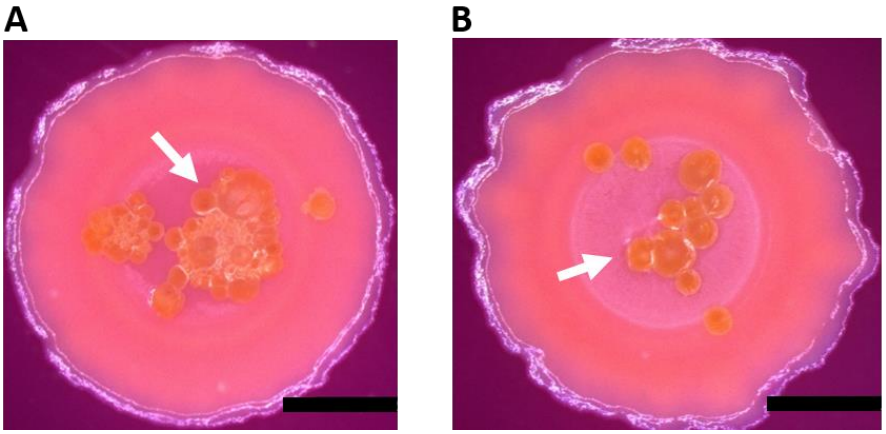

Figure 13. Mineral crystal formation by urease-producing strains of *B. subtilis*. Representative image of mineral precipitate on the surface of a colony of WΔ-H-BpU (A) and WΔ-U-H-BpU (B) spotted onto LBC media supplemented with phenol red and pH adjusted to 7.2. Colonies imaged at day 23 under a stereomicroscope. Scale bars represent 4 mm.

The formation of mineral precipitates (Figure 13) correlated with the strains that showed the strongest pH change from ureolytic activity on solid media, namely WΔ-H-BpU and WΔ-U-H-BpU (Figure 11). The results showed that engineering BICP into *B. subtilis* W168 was possible through the introduction of heterologous urease genes, with calcite precipitates forming on colonies of strains with the strongest urease activity.

4.2.1.5 Calcite precipitation on LB and B4 precipitation media.

To further assess the calcite precipitation ability of *B. subtilis* strains WΔ-H-BpU and WΔ-U-H-BpU, the strains were assayed on LBC and B4 precipitation media. LBC precipitation medium was chosen as this composition was used for the previously shown precipitation assay, but here it was used without pH adjustment and the addition of the pH indicator, to rule out any potentially interfering effects. B4 precipitation medium was chosen as it is an established precipitation media used to assess biomineralisation potential of environmental isolates (Boquet *et al.*, 1973).

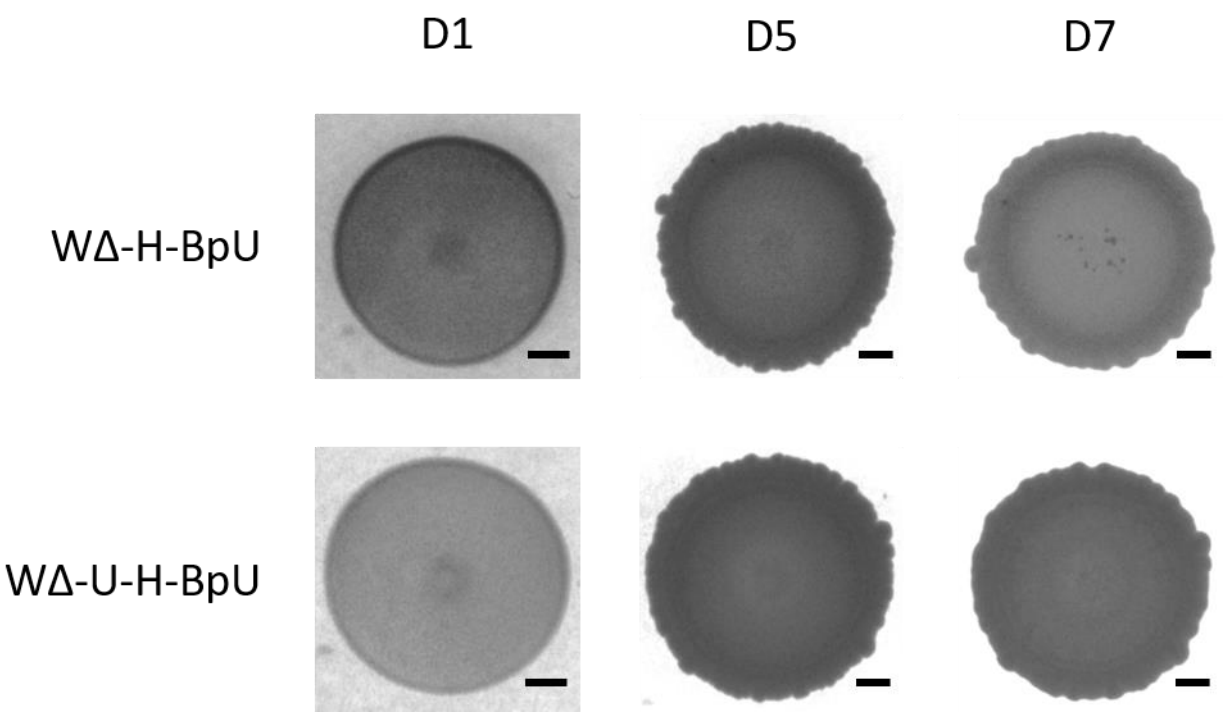

Figure 14. Calcite precipitation on LBC media. Urease-producing strains were spotted on LBC precipitation media and incubated at 30°C. Calcite precipitation and morphology on the colony surface was monitored over seven days. Images were taken under a stereomicroscope at day 1 (D1), day 5 (D5), and, day 7 (D7). Scale bars represent 1 mm in size. The results are a representative series from three biological repeats and show the series with the median amount of crystal formation.

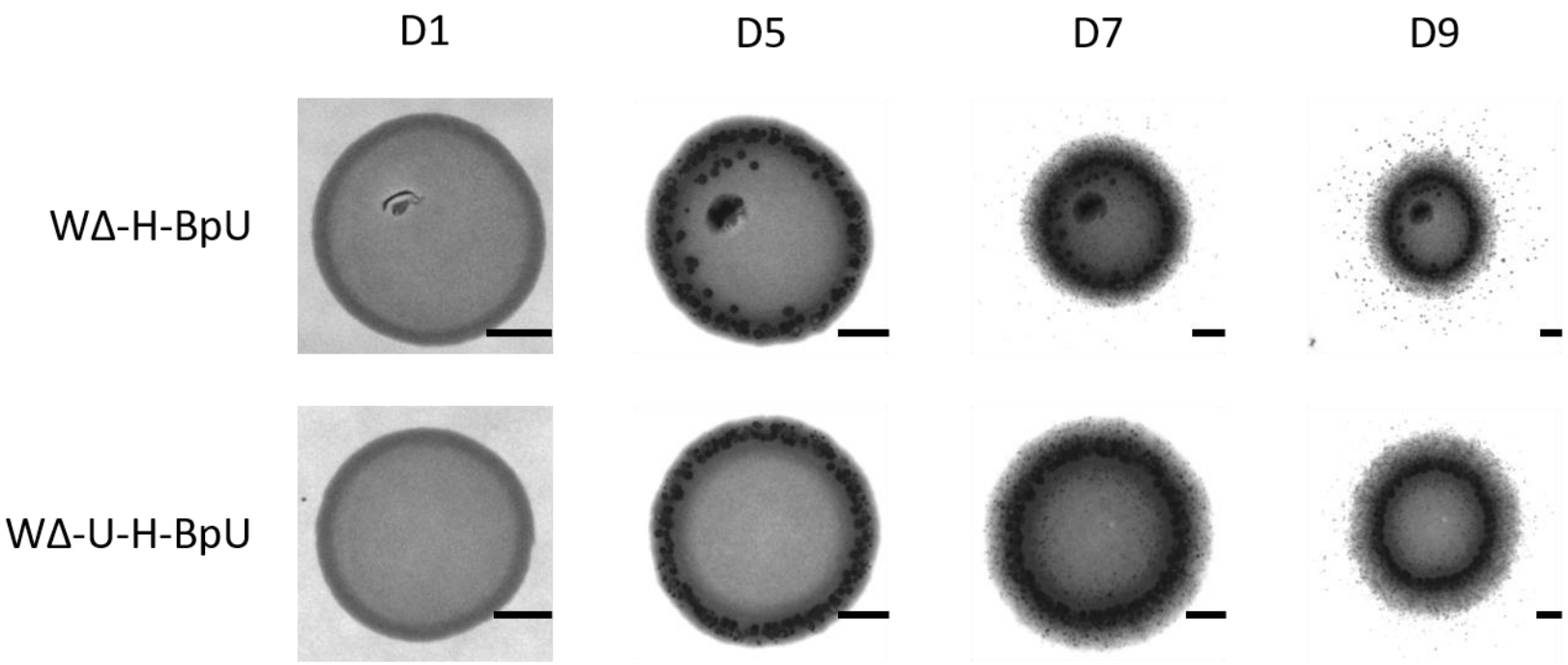

Figure 15. Calcite precipitation on B4 media. Urease strains were spotted on B4 precipitation media and incubated at 30°C. Calcite precipitation and morphology on the colony surface was monitored over nine days. Images taken under a stereomicroscope at day one (D1), day five (D5), day seven (D7) and, day nine (D9) are illustrated. Image area shown in the figure varies between days to allow visualisation of crystals outside the colony area on D7 and D9. Scale bars represent 1 mm in size. The results are representative of two biological repeats.

The observable amount of precipitate and onset of crystal formation varied slightly across repeat trials on LBC (Figure 14) and B4 (Figure 15) media but the trends remained the same. On both LBC and B4, the strongest precipitation was displayed by strain WΔ-H-BpU. On LBC media, precipitation was usually visible after seven days for strain WΔ-H-BpU, but rarely for WΔ-U-H-BpU. Figure 14 shows the presence of precipitate on the colony surface for WΔ-H-BpU, but absent from a colony of WΔ-U-H-BpU. On B4 precipitation media, precipitation onset was visible as early as three days for both WΔ-H-BpU and WΔ-U-H-BpU. This started with crystals localised to the colony surface and later spread to the surrounding media, visible clearly for both WΔ-H-BpU and WΔ-U-H-BpU after nine days (Figure 15). Across the two media, precipitation onset was always earlier on B4 media compared LBC media and much more prominent.

Difference in precipitation across LBC and B4 media, but also to an extent between experimental repeats and batches of media, could be due to inconsistent supersaturation kinetics as a result of variations in metabolites and media composition. This difference in media composition can create a supersaturation gradient over which nucleation varies. The idea that supersaturation is not constant has previously been noted as an overlooked aspect of precipitation in microbial media (González-Muñoz and Chekroun, 2000). From a mechanistic understanding of precipitation, the stronger the urease activity the stronger the pH shift and the more likely supersaturation will favour the precipitation of calcite. A recent study by Reeksting *et al*, has shown that the speed of precipitation will cause differences in spatial distribution of crystals. Slow urease activity was found to induce localised precipitation on or near the bacterial cells, while strong urease activity was found to induce precipitation in the media surrounding the bacteria (Reeksting *et al.*, 2020). In the experiments using the engineered *B. subtilis* W168 strains, we here also observed spatial precipitation differences dependent on media composition and urease activity, with strains causing precipitation into the surrounding media on B4 but not on LBC (Figure 14 and Figure 15). LBC is a richer growth medium with a higher proportion of complex components than B4 with a yeast extract content of 5g/l *vs* 1g/l and a tryptone content of 10g/l *vs* 0g/l, so there is more buffering potential. B4 is also adjusted to pH 8 while LBC is around pH 7, which gives B4 a head start in terms of the pH required to reach favourable precipitation conditions. However, low buffering capacity could also lead to a dilution effect where a pH increase could dissipate into the surround media. This has been noted as a potential reason for observable differences in precipitation in liquid *vs* on solid media (González-Muñoz and Chekroun, 2000). The results showed that the stronger the ureolytic activity of a strain the stronger the BICP, in terms of time of precipitation onset and observable precipitation amount. The spatial distribution and observable quantity of precipitate

was also linked to the strength of ureolytic activity as well as the surrounding media environment, which is thought to further influence precipitation saturation kinetics.

4.2.1.6 SEM imaging of calcite colony precipitates.

The first mineral precipitates produced by *B. subtilis* were observed on the LBC phenol red media for WΔ-H-BpU and WΔ-U-H-BpU as shown in Figure 13. To confirm these were calcite and to examine their morphology, the crystals were scrapped from the colonies, washed and imaged under the Scanning Electron Microscope (SEM) with Energy Dispersive X-Ray (EDX) elemental analysis.

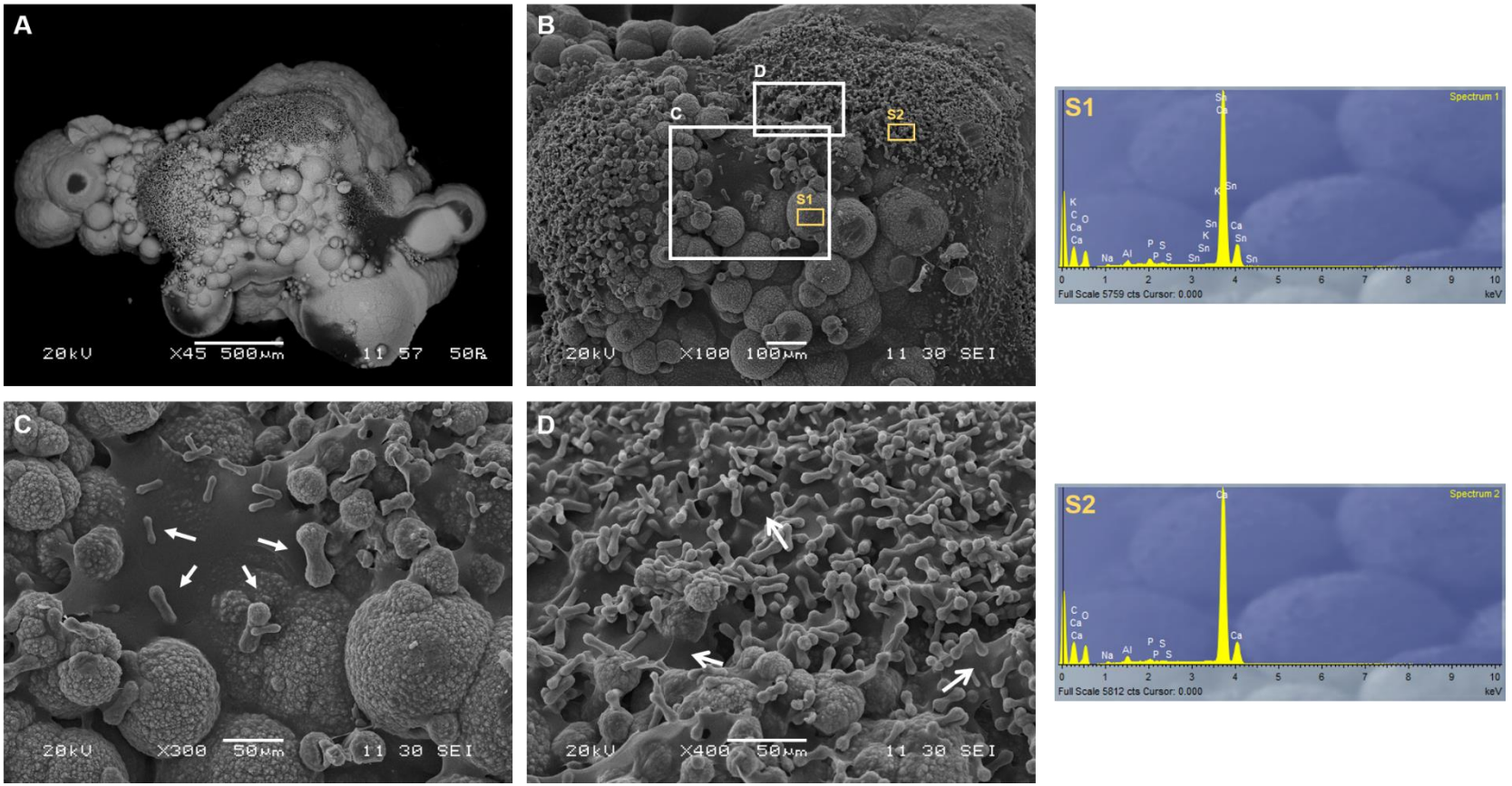

Figure 16. Scanning electron microscopy of calcite crystals produced by WΔ-H-BpU. A-D sequential zoom in on a crystal precipitated onto a WΔ-H-BpU colony, on LBC phenol red media. Calcite crystals on bacterial colonies developed over two weeks at 30°C and one week at room temperature after which they were scraped off. The samples were imaged on a SEM with gold splutter coating. The closed arrows indicate the different sized stages of crystals in the commonly observed 'dumbbell' morphology. The open arrows indicate the web-like material observed between the dumbbell shaped crystals. EDX elemental analysis was performed at two image sites (S1 and S2) indicated in panel C to verify the precipitate composition to be predominated by calcium.

EDX analysis is a technique used for the elemental analysis of a sample and was therefore used to analyse the bacterial precipitates. EDX analysis revealed the precipitates to be calcium carbonate as indicated by a high calcium (Ca) peak (Figure 16-S1&2). It is further inferred that the calcium carbonate is calcite as it is the most stable and abundant polymorph (Ni and Ratner, 2008). Scanning electron microscopy generally revealed the larger crystals to be made up of aggregated crystals (Figure 16-A) with varying surface texture under higher magnifications. In a number of imaged precipitates, further smaller structures of round shapes were visible (Figure 16-A&B) and at higher resolutions these were revealed as having a 'dumbbell' shaped morphology (Figure 16-C&D). More of these structures were seen on WΔ-H-BpU than on WΔ-UH-BpU. The morphology was often seen in subsequent rounds of assays and imaging but not always reproducible and not always to the same extent. We therefore believe the dumbbell morphology to be sensitive to conditions and timing of collection for imaging. Dumbbell morphologies have been previously observed to be precipitated in association with microbial activity (González-Muñoz and Chekroun, 2000; Warthmann *et al.*, 2000). It is possible that encased bacteria lie at the centre around which layers of calcite are deposited overtime until they turn from a dumbbell morphology into larger spherical morphologies (Figure 16-C). Sulphate-reducing bacteria precipitating dolomite have been observed to form dumbbell morphologies, with initial stages of crystal growth thought to occur at the polar ends of the bacterial cell and in association with organic material (Warthmann *et al.*, 2000). The presence of possible organic material can also be observed as the web-like material between dumbbells in Figure 16-D. Dumbbell crystal morphologies can occur without the presence of cells but have been shown to be promoted in the presence of organic additives and magnesium ions (Meldrum and Hyde, 2001; Xiang *et al.*, 2008). Furthermore, dumbbell formation has also been shown to occur as a result of transformation between the calcium carbonate polymorphs aragonite and calcite and has been explained as a result of crystallisation kinetic behaviours over temperature changes (Koga *et al.*, 2013). Elucidating the precise reasons for formation of these observed morphologies and the role of bacteria in dumbbell formation are outside of the scope and aim of this investigation. Of observational interest was that possible bacterial surface characteristics and/or biofilm production could play a role in precipitation and morphology. This led to the next stage of investigation which was to characterise biofilm production and surface charge modulation on the precipitation potential of *B. subtilis* heterologous urease expressing strains. Taken together, the experiments revealed that heterologous expression of urease genes in *B. subtilis* W168 is an approach by which bacteria-induced calcite precipitation can be engineered into an intrinsic low precipitator. It was found that the stronger the ureolytic activity, the stronger the precipitation phenotype was in terms of the time of precipitation onset and observable quantity of precipitate.

Ureolytic activity was able to be modulated through the presence and absence of accessory genes where nickel transporters were advantageous on nutrient rich media and urea transporters on nutrient poor media. The results also showed that the strains environment, in terms of media, influenced precipitation spatial distribution, time of onset and observable quantity as the environment likely further influences precipitation saturation states and kinetics.

4.2.2 The role of biofilm on calcite precipitation in *Bacillus subtilis* W168.

4.2.2.1 Establishing a biofilm precipitation model in *Bacillus subtilis*.

The second objective was to evaluate the role of biofilm formation in *Bacillus subtilis* on its ability to precipitate calcite. Robust biofilm formation in *Bacillus subtilis* is suggested to be deficient in the laboratory strain W168. Instead, the model strain for *Bacillus subtilis* biofilm study is the undomesticated strain NCIB 3610 (Branda *et al.*, 2001). Therefore, strain NCIB 3610 was chosen initially to assess the role of biofilm production on calcite precipitation. Furthermore, a urease positive background was also selected to help speed up calcite precipitation. This required moving the urease constructs from *B. subtilis* W168 into *B. subtilis* NCIB 3610 using phage transduction. Using the same nomenclature as previously, the resulting strains constructed were NΔ (SGB905), NΔ-U-BpU (SGB921), NΔ-H-BpU (SGB922), NΔ-U-H-BpU (SGB923), and NΔ-BpU (SGB915).

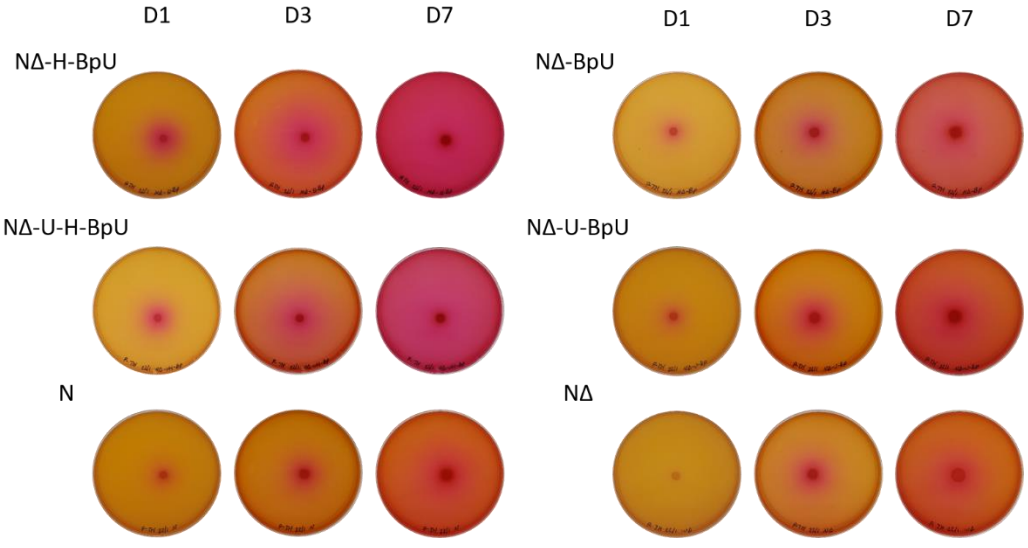

Figure 17. *B. subtilis* NCIB 3610 solid media urease activity and precipitation assay. Urease strains were spotted on LBC media supplemented with phenol red and pH adjusted to 7.2. Plates were incubated at 30°C and activity monitored over 7 days. Images of activity from day one (D1), day three (D3) and day seven (D7) are illustrated. Results are of one experiment.

The first step was to verify the urease activity of the *B. subtilis* NC1B 3610 recombinant strains. Testing the NCIB 3160 urease recombinant strains on LBC supplemented with phenol red and pH adjusted to 7.2, showed that urease was heterologous produced (Figure 17). There was a stronger colour change as a result of ureolytic activity from plates with heterologous urease constructs compared to the control strains N and NΔ. The colour change in the controls can be attributed to basal metabolic activity such as amino acid degradation. Urease activity was the strongest for strains NΔ-H-BpU, NΔ-U-H-BpU as was the case with W168 (Figure 11). This also illustrates that the genes required to drive the strongest ureolytic phenotype are likely the same across different strains of the same species. Thus it can be said that in *B. subtilis*, accessory urease genes are required to bring out the strongest urease phenotype.

To test if the heterologous strains with engineered urease activity had also gained the ability to precipitate calcite, strains in Figure 17 were monitored for crystal formation on their colonies. Results showed no precipitates formed on plates over the seven day period, as was the case with *B. subtilis* W168 on LBC with phenol red. To better assess calcite precipitation without potential interference from the adjusted pH and phenol red indicator, the NCIB 3610 ureolytic strains were spotted onto normal LBC plates (Figure 18-A) and B4 (Figure 18-B) with crystal growth monitored over 9 days at 30°C. No crystal formation was visible on LBC, and therefore strains had an even lower biomineralisation activity than the equivalent strains in W168 (Figure 14). Contrarily, crystal formation was visible on B4 media from both NΔ-H-BpU and NΔ-U-H-BpU, with precipitates forming in the surrounding media as well as on the colony surface. Similarly to W168, this was strongest in NΔ-H-BpU compared to NΔ-U-H-BpU. Unlike with WΔ-H-BpU and WΔ-U-H-BpU, onset of precipitation in the surrounding media in the NCIB 3610 equivalent strains occurred earlier. Crystal formation also covered the entire colony surface and was not just localised to the colony edges. Overall, the urease activity and calcite precipitation ability of NΔ-H-BpU and NΔ-U-H-BpU, compared to its W168 equivalent were still very similar across LBC and B4. This supports the role that these urease genes can bring out similar precipitation phenotypes across *B. subtilis* strains. To be noted is that the *B. subtilis* strains W168 and NCIB 3610 are very similar in their genome sequences, with one of their larger differences in the *trpC* region. The origins and similarities of different *B. subtilis* strains has been best described by Zeigler and colleagues (Zeigler *et al.*, 2008). Our data also showed that simply choosing a biofilm competent strain by itself did not lead to a difference in precipitation.

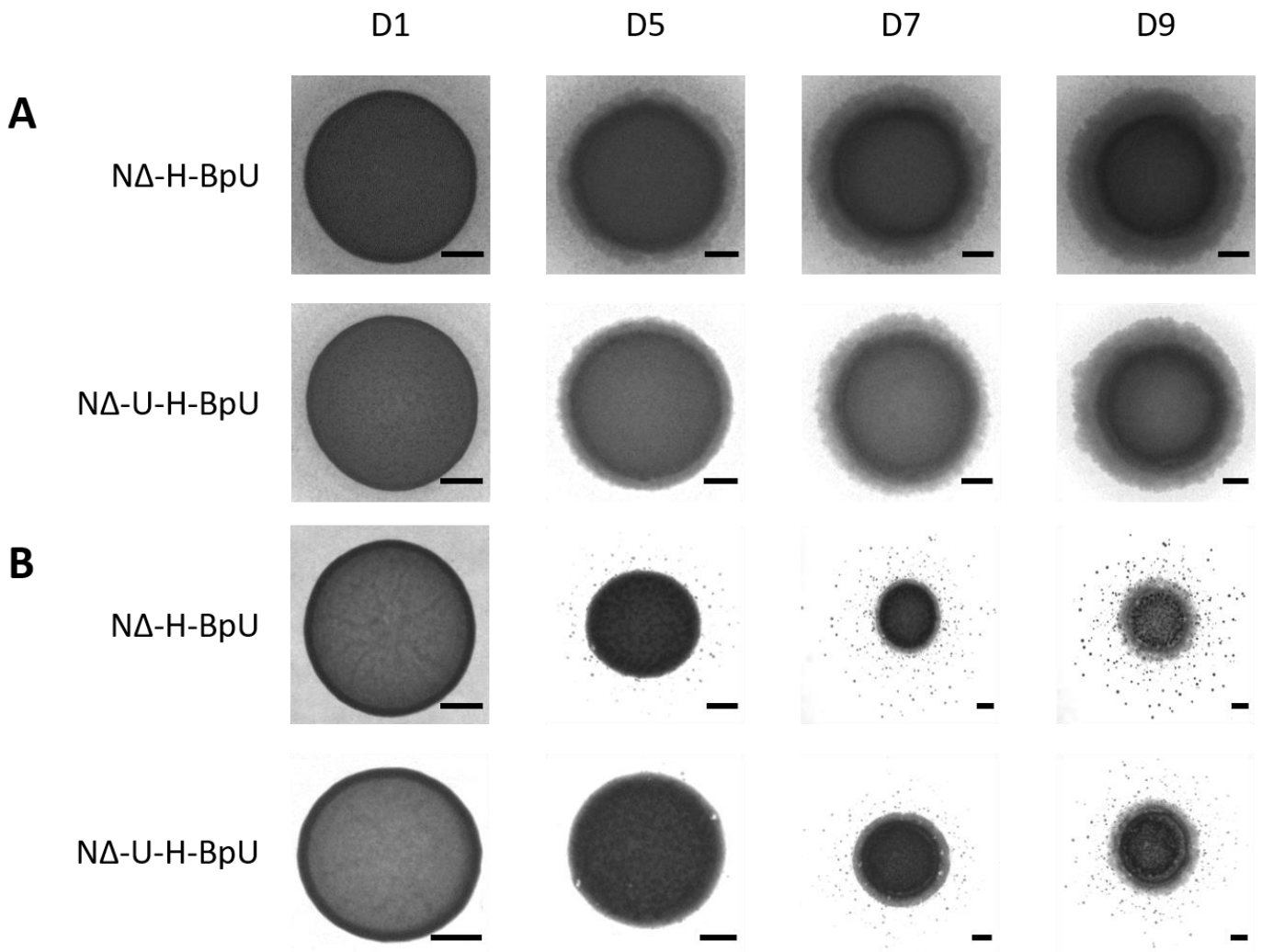

Figure 18

Figure 18. *B. subtilis* NCIB 3610 calcite precipitation on LBC and B4. Urease strains were plated on LBC precipitation media (A) and B4 precipitation media (B) and incubated at 30°C. Calcite precipitation and morphology on the colony surface was monitored over nine days. Images taken under a stereomicroscope at day one (D1), day five (D5), day seven (D7) and, day nine (D9) are illustrated. Image area shown in the figure varies between days to allow visualisation of crystals outside the colony area on D7 and D9. Scale bars represent 1 mm in size. The results are representative of two biological repeats.

To test the influence of biofilm formation on calcite precipitation in more detail, a different media was required. Biofilm formation likely needed to be actively induced, something that needs to be considered in respect to application. LBC and B4 media does not promote biofilm formation in *B. subtilis* as observed by a lack of rugose colony structures, therefore the next step was to prepare a precipitation media that also encourages biofilm formation. A very commonly used biofilm promoting medium for the study of *B. subtilis* is MSgg (Branda *et al.*, 2001). MSgg is, however, a minimal medium and with the addition of the excess urea and calcium (required for precipitation driven by ureolytic pathway) did not support robust growth of the *B. subtilis* strains used here. An alternative medium is LBGM which in contrast to MSgg, is a rich medium (Shemesh and Chaia, 2013). LBGM is made of LB as a base with the sole extra addition of glycerol and manganese. The glycerol in the LBGM is thought to be recognised by KinD, which is part of the histidine kinase signalling system that activates Spo0A, which in turn removes SinR and AbrB repression of the *eps* and *tap* operons to promote biofilm formation (Shemesh and Chaia, 2013). The manganese is thought the play a role as a cofactor within this signalling cascade (Shemesh and Chaia, 2013). Using this medium, with the addition of urea and calcium (LBGMC), further provided an ideal comparison to the LBC precipitation media used above.

To assess their calcite precipitation ability in conjunction with biofilm formation, the NCIB 3610-derived urease producing strains were spotted onto LBGMC. Results showed a clear biofilm morphology with colony growth over a larger surface area and with a smooth surface for strains NΔ-H-BpU and NΔ-U-H-BpU (Figure 19). Contrarily, strains N, NΔ, NΔ-BpU, and NΔ-U-BpU were much smaller in size with rougher colony edge and surface architecture (Figure 20). These were also darker, making their surfaces overall harder to visualise under a light microscope and so calcite precipitation was not clearly observable. The dark colouration was likely from the production of a brown pigment called pulcherrimin previously noted to form alongside biofilm production on LBGM (Shemesh and Chaia, 2013; Arnaouteli *et al.*, 2019). The masking of potential calcite precipitation by biofilm formation on strains N, NΔ, NΔ-BpU, and NΔ-U-BpU meant that these were not further analysed. When colonies of NΔ-H-BpU and NΔ-U-H-BpU were inspected for crystal formation, a notable increase in crystal number was observed, and these also appeared earlier, with the first

visible after 4-5 days (Figure 19). Precipitation was not only observed on the surface but also on the underside of the colonies indicating at enhanced precipitation potential. The results clearly showed that LBGMC did induce calcite precipitation and much more strongly than on LBC. Thus, biofilm formation, triggered by the addition of glycerol and manganese in the medium, did have an enhancing effect on biomineralisation induced by heterologous production of urease.

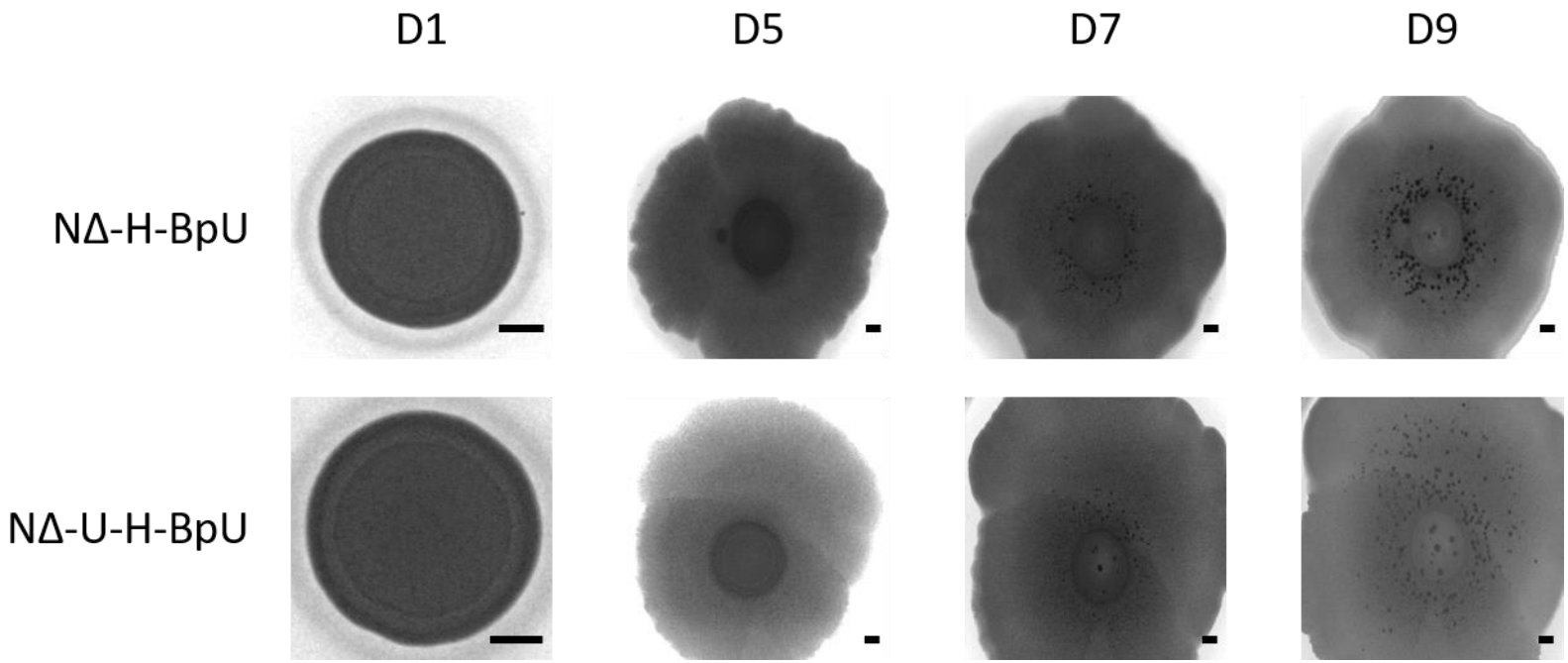

Figure 19. *B. subtilis* NCIB 3610 calcite precipitation on LBGMC. Urease strains were plated on LBGMC precipitation media and incubated at 30°C. Calcite precipitation and morphology on the colony surface was monitored over nine days. Images taken under stereomicroscope at day one (D1), day five (D5), day seven (D7) and, day nine (D9) are illustrated. Scale bars represent 1 mm in size. The results are representative of two biological repeats.

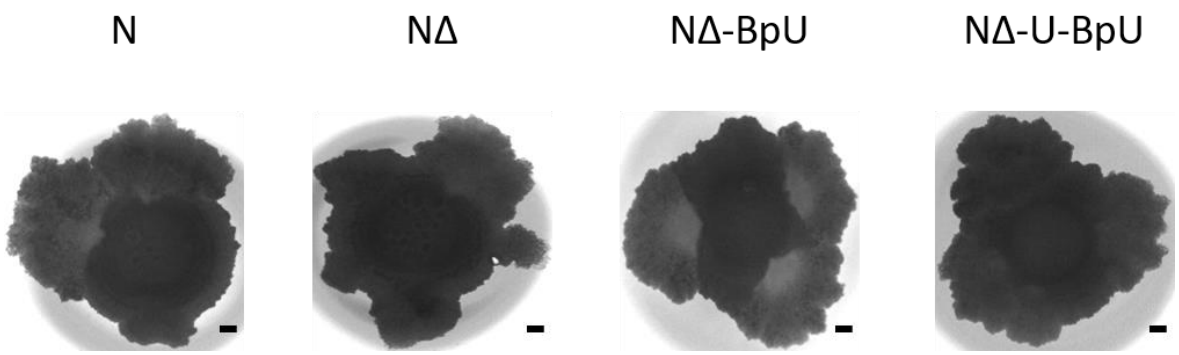

Figure 20. *B. subtilis* NCIB 3610 Complex Colony Morphologies on LBGMC. Urease strains were plated on LBGM precipitation media and incubated at 30°C. Images taken at day nine under a stereomicroscope are illustrated. Scale bars represent 1 mm in size. The results are representative of two biological repeats.

4.2.3 The effect of modulating biofilm on calcite precipitation in *B. subtilis* W168.

While the results establish that biofilm formation sped up the onset and quantity of crystal formation, changes in colony morphology of the NCIB 3610-derived strains made it difficult to accurately quantify the differences. As the surface area increases there are more potential sites for precipitation. It was therefore unclear whether increase in precipitation was the result of increased colony area or of biofilm formation *per se*. Further, the more complex, compact and dark appearance of the some of the strains made it difficult to visually observe and quantify precipitation. To more precisely define which aspects of biofilm formation contributed to precipitation, further testing was required in a strain that does not undergo major morphological changes on LBGMC medium. It was therefore hypothesised that using *B. subtilis* W168 which has low intrinsic ability of biofilm formation, might be better to detect links between precipitation and biofilm components.

Initial experiments found colony morphology of W168-derived strains to be similar between LBC and LBGMC. Monitoring colony surfaces importantly found that, as with NCIB 3610-derived strains, crystal formation on LBGMC occurred earlier and much more strongly than on LBC (Figure 21). The results showed that while W168 is not traditionally the strain of choice to study biofilm formation, the biofilm promoting conditions did enhance biomineralisation. In contrast to NCIB 3610-derived strains, the W168 derivatives produced reduced pigmented and uniform colonies that facilitated accurate enumeration of the crystals formed on the colony. This provided a suitable experimental system to elucidate the contribution of individual elements of biofilm formation on calcite precipitation.

For the testing of individual contribution of biofilm components on biomineralisation, the strain W-H-BpU background was chosen, as this gave the strongest calcite production. The first approach was to eliminate biofilm formation completely. It has been shown that a deletion of the regulatory protein Spo0A abolished biofilm formation on LBGM in *B. subtilis* NCIB 3610 (Shemesh and Chaia, 2013). We therefore deleted Spo0A in the urease producing background, resulting in strain WΔ-Δs-H-BpU (SGB994).

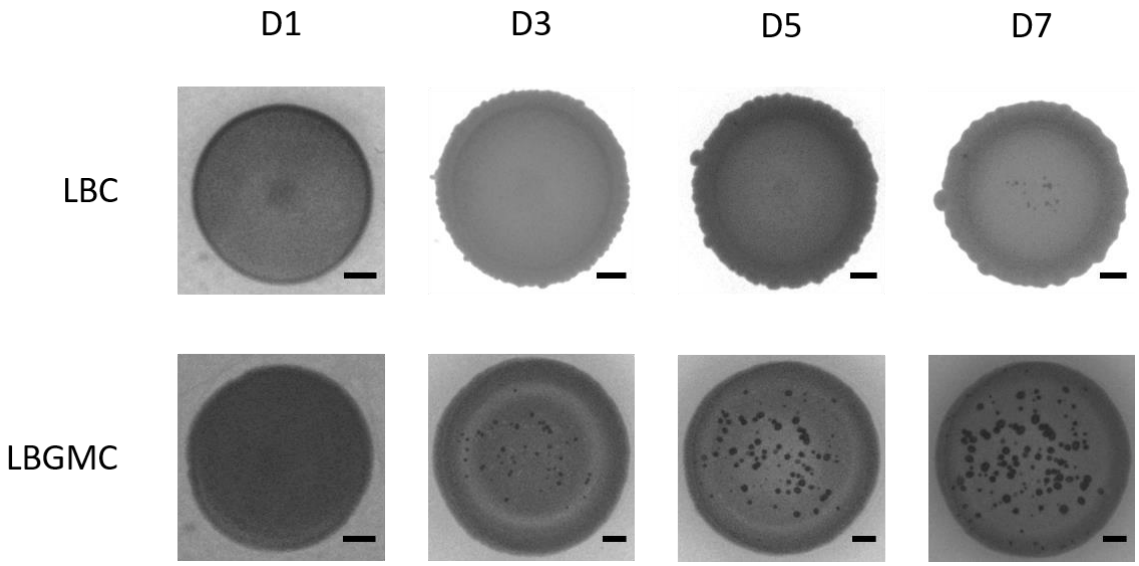

Figure 21. *B. subtilis* WΔ-H-BpU calcite precipitation on LBC and LBGMC. The strain was plated on LBC and LBGMC ad incubated at 30°C. Calcite precipitation and morphology on the colony surface was monitored over seven days. Images taken under a stereomicroscope at day one (D1), day three (D3), day five (D5) and day seven (D7). Scale bars represent 1 mm in size. The images are a representative series from three to four biological repeats and show the series with the median amount of crystal formation.

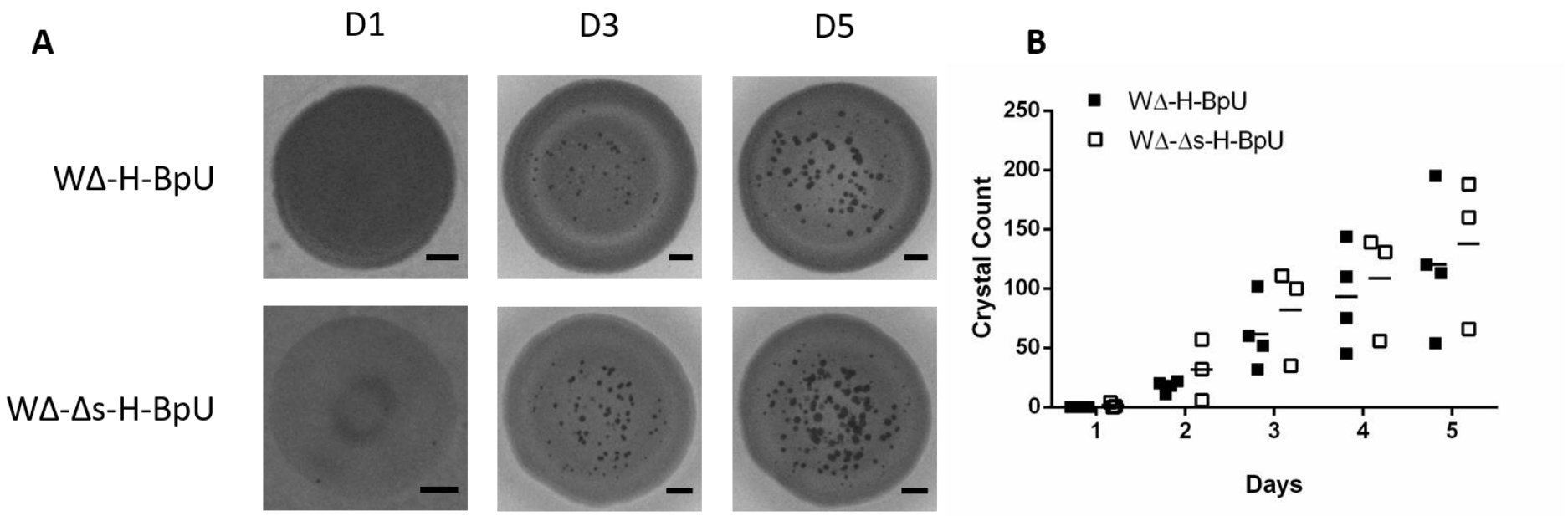

Figure 22. Effect of *spo0A* deletion on biomineralisation. WΔ-Δs-H-BpU (□) and its parent strain WΔ-H-BpU (■) were spotted onto LBGMC precipitation media and grown at 30°C over a period of five days. Individual calcite crystals on the colony surface were counted daily under a stereomicroscope. The results are from three to four biological repeats. Colony surface images of a representative series are depicted (A), where the scale bar represents 1 mm in size. The number of crystals counted on colony surfaces each day across repeats are depicted (B), where bars represent the average.

To test if deletion of Spo0A (and thus biofilm formation) did reduce biomineralisation activity, strain WΔ-Δs-H-BpU and its parent strain WΔ-H-BpU were assayed on LBGMC for their calcite precipitation ability over five days at 30°C. The number of calcite crystals formed on the colony were counted and depicted in Figure 22-B with the images of the precipitates on the colonies depicted in Figure 22-A. Surprisingly, examination of the strains revealed that the Spo0A deletion strain did not in fact display reduced biomineralisation (Figure 22). This was supported by statistical analysis using a standard two-way ANOVA test, which showed a significant effect of time ($p<0.0001$), but not of strain background ($p=0.2940$). The unchanged biomineralisation activity was unexpected as a *spo0A* deletion has been shown in literature to remove the biofilm phenotype in *B. subtilis* NCIB 3610 (Shemesh and Chaia, 2013) and therefore, one would have hypothesised less precipitation if the precipitation was a result of the biofilm. Spo0A deletion has pleiotropic effects, because the protein controls additional important factors such as sporulation, DNA replication and competence (Schultz *et al.*, 2009). It is therefore possible that unintended side-effects of the deletion, e.g. compensatory changes in the cell masked a direct effect of biofilm formation on biomineralisation.

To determine how biofilm formation contributes to biomineralisation, we therefore decided to target specific genes, instead of the previous broad approach by deleting a regulatory gene. The genes chosen were *epsH* and *tasA*, encoding a glycosyltransferase for exopolysaccharide synthesis and an extracellular fibre forming protein, respectively. Both operons have been shown to be upregulated on LBGM media (Shemesh and Chaia, 2013). The *eps* operon was reported to be upregulated 9-fold and the *tap* operon 20-fold on LBGM compared to LB in *B. subtilis* NCIB 3610, while *epsH* deletion was also shown to abolish the typical colony morphology associated with biofilm formation, as well as the biofilm colony morphology lost on an *epsH* deletion (Shemesh and Chaia, 2013). To test their role in calcite precipitation, the *epsH* deletion and a *tasA* deletion were introduced into the strong precipitator WΔ-H-BpU. This led to the construction of strain WΔ-Δe-H-BpU (SGB992) and strain WΔ-Δt-H-BpU (SGB993), respectively.

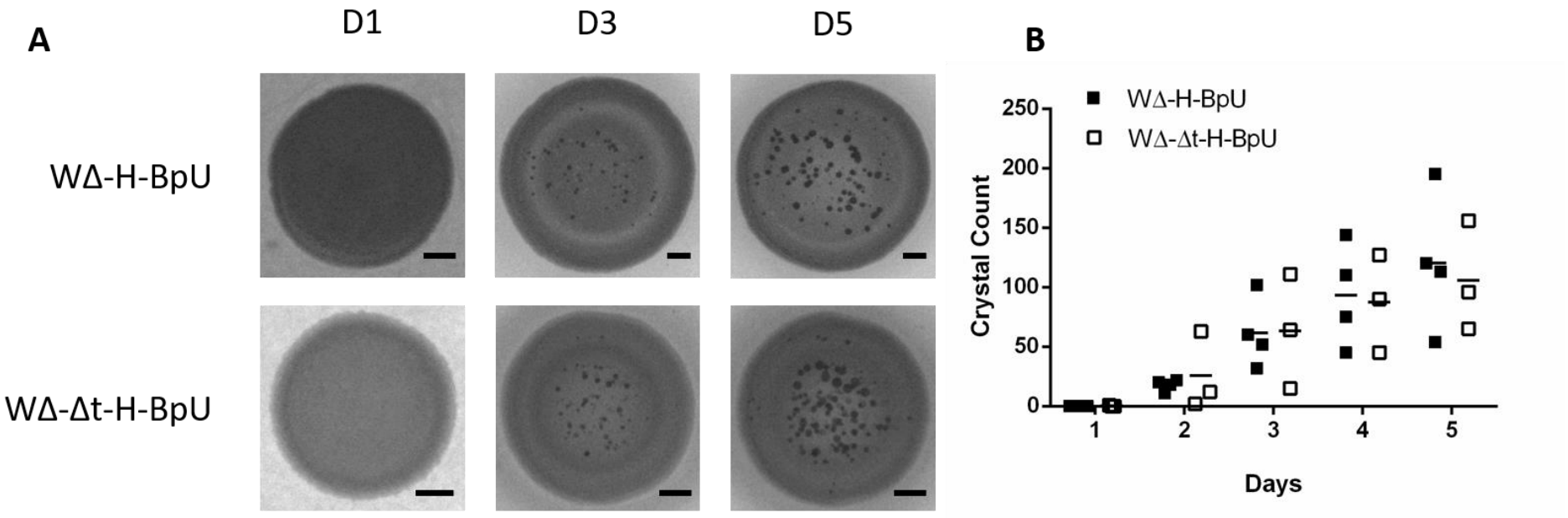

Figure 23. Effect of *tasA* deletion on biomineralisation. WΔ-Δt-H-BpU (□) and its parent strain WΔ-H-BpU (■) were spotted onto LBGMC precipitation media and grown at 30°C over a period of five days. Individual calcite crystals on the colony surface were counted daily under a stereomicroscope. The results are from three to four biological repeats. Colony surface images of a representative series are depicted (A), where the scale bar represents 1 mm in size. The number of crystals counted on colony surfaces each day across repeats are depicted (B), where bars represent the average. Results depicted for the parent strain WΔ-H-BpU (the control) are the same as in Figure 22.

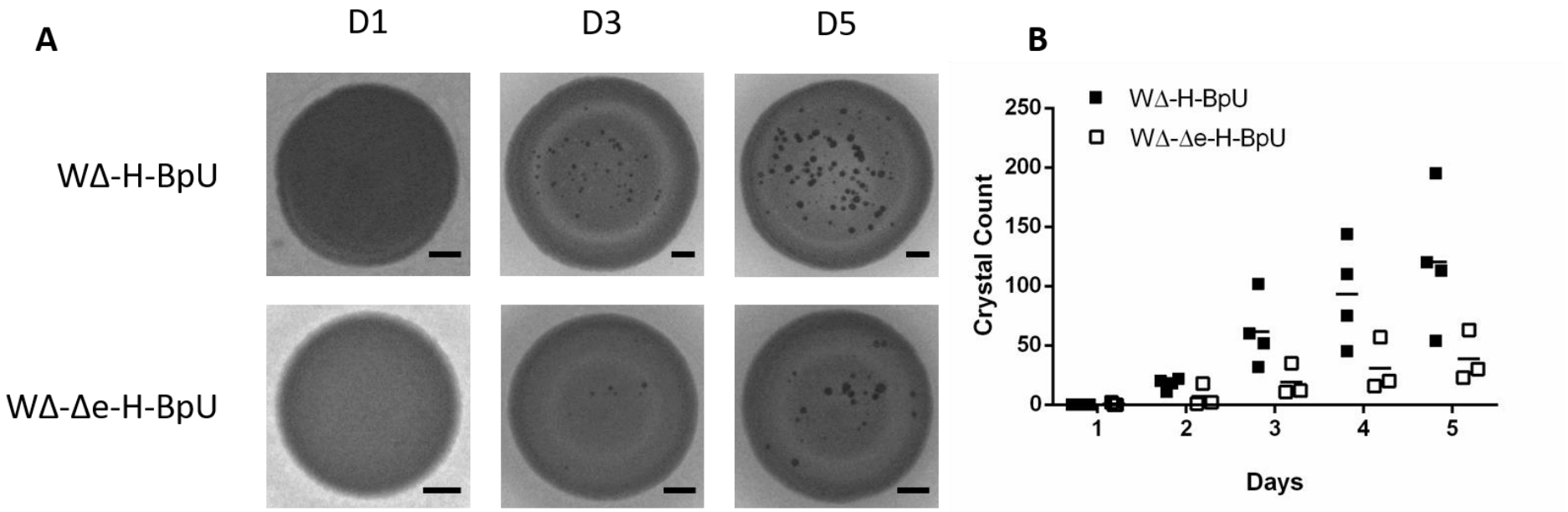

Figure 24. Effect of *epsH* deletion on biomineralisation. WΔ-Δe -H-BpU (□) and its parent strain WΔ-H-BpU (■) were spotted onto LBGMC precipitation media and grown at 30°C over a period of five days. Individual calcite crystals on the colony surface were counted daily under a stereomicroscope. The results are from three to four biological repeats. Colony surface images of a representative series are depicted (A), where the scale bar represents 1 mm in size. The number of crystals counted on colony surfaces each day across repeats are depicted (B), where bars represent the average. Results depicted for the parent strain WΔ-H-BpU (the control) are the same as in Figure 22.

Strains WΔ-Δt-H-BpU and WΔ-Δe-H-BpU were assayed on LBGMC for their calcite precipitation ability over five days at 30°C. The results for calcite precipitation on WΔ-Δt-H-BpU are depicted in Figure 23 and for WΔ-Δe-H-BpU in Figure 24. When examining the biomineralisation of the *tasA* deletion strain alongside its WΔ-H-BpU control no clear difference in precipitation was exhibited (Figure 23). This was supported by statistical analysis using a standard two-way ANOVA test, which showed a significant effect of time ($p<0.0001$), but not of strain background ($p=0.8610$). When examining the biomineralisation of the *epsH* deletion strain alongside its WΔ-H-BpU control, a decrease in the amount of precipitation on the colony was clearly observable (Figure 24). A two-way ANOVA showed a significant effect of time ($p=0.0001$), as well as strain ($P=0.0005$). These sets of experiments showed that biofilm stimulation does increase bacteria-induced calcite precipitation. However, a complex biofilm phenotype masks the precise role of individual components on precipitation. Using the *B. subtilis* W168 as an intrinsically poor biofilm producer, a deletion of Spo0A did not prove informative due to a complex phenotype. Deletion of two genes to disrupt biosynthesis of the polysaccharide and protein components of the biofilm EPS gave clear results on the relative contribution. The *tasA* mutant did not have a significant effect, while the *epsH* mutant showed drastically reduced biomineralisation. This showed that not only does biofilm formation promote calcite precipitation, but it is specifically the polysaccharides in the EPS that are responsible for this beneficial effect.

4.2.4 The role of surface charge on calcite precipitation of *Bacillus subtilis* W168.

4.2.4.1 Establishing surface charge changes in *Bacillus subtilis* W168: Electrophoretic mobility measurements, cytochrome C assay and nisin time dependent kill curves.

The third objective of this investigation was to explore an approach to increase the overall negative surface charge of *B. subtilis* W168 with the hypothesis that it would attract more calcium cations required for calcium carbonate precipitation. Modulation of surface charge was examined through the deletion and upregulation of *dltABCDE* in *B. subtilis* W168. The *dlt* operon is responsible for the D-alanylation of teichoic acids and is depicted in Figure 25. In wildtype cells, teichoic acids contribute to the net negative charge due to a phosphate rich backbone. Cells can control the degree of this charge through D-alanylation, controlled by the *dlt* operon. In the absence of *dlt* the cell surface is expected to bear a greater negative charge due to the decreased masking of phosphate backbone negative charges by positively charged amine groups. The deletion of the *dltABCDE* operon in *B. subtilis* W168 resulted in construction of strain W-Δdlt (SGB926).

To determine if hyper-alanylation of teichoic acids might reduce biomineralisation due to an insufficiently negatively charged cell surface, over-production of the *dlt* system was also explored.

To this end, the *B. subtilis dltABCDE* including its native RBS was cloned into pBS2E under control of the strong constitutive promoter P_{veg} (Radeck *et al.*, 2013). This led to the construction of *B. subtilis* W168 strain W-↑d (SGB984). The construct should have integrated into *lacA* but PCR analysis of the transformants showed that it instead integrated into the native *dlt* locus, likely due to the large insert, which would facilitate homologous recombination in the *dlt* site. This resulted in a single cross-over insertion, which disrupted the native operon but inserted a new copy driven by P_{veg} into its place. This was still expected to lead to the intended effect of high constitutive *dlt* operon expression.

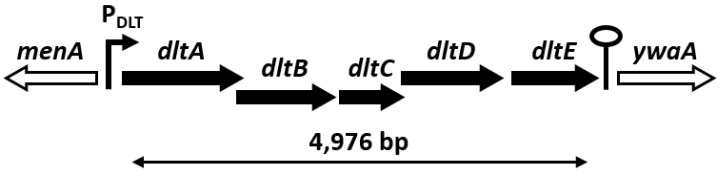

Figure 25. *Bacillus subtilis* W168 dltABCDE operon. Composed of the D-alanyl-D-alanine carrier ligase protein DltA (1,512 bp), the D-alanine transfer protein DltB (1,188 bp), the D-alanine carrier protein DltC (237 bp), the D-alanine transfer protein DltD (1,179 bp) and the D-alanine transfer protein DltE (759 bp). P_{DLT}, putative promoter region; stem-loop structure, putative Rho independent terminator. (Genome NCBI database accession number: NC_000964.3).

To verify that deletion or overproduction of the dlt operon did indeed change the surface charge, the electrical potential of the *dlt* strains were determined via zeta potential measurements (Figure 26). Zeta potential measurements determine the potential differences between two phases, which is the bulk fluid and the fluid attached to a surface. Suspended particles, such as bacterial cells, are surrounded by a double layer the inner of which is the stern layer, a rigid layer of ions/particles surrounding the negatively charged cell. This is surrounded by the diffusion layer which is created as more particles are attracted and repelled to the cell. Both the stern and diffusion layer are referred to together as the double layer. The point where the diffusion layer meets the bulk liquid phase is known as the slipping plane. The zeta potential specifically measures the electrical potential at the location of the slipping plane to infer surface charge (Hunter, 1981).

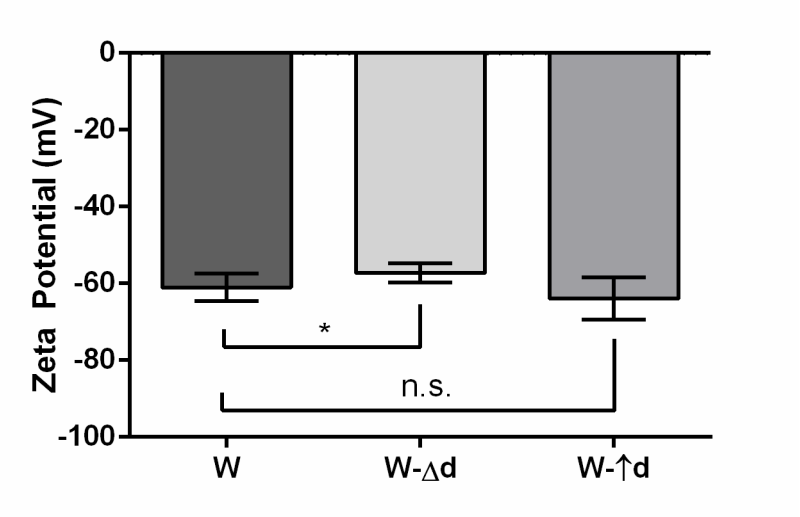

Figure 26. Zeta potential of *B. subtilis* strains with *dlt* operon deletion or overexpression. Zeta potential measurements of exponentially growing cells (OD_{600}= 0.5-1) of *B. subtilis* W168 wildtype (W), *dltABCDE* deletion (W-Δd), and *dltABCDE* overexpression (W-↑d). Cells were harvested, washed and re-suspended in dH_2O to an OD_{600}=0.5 for measurement. The data show the mean and standard deviation of the zeta potential in mV of three biological repeats each with triplicate measurements. Data were analysed with an un-paired t-test where n.s. is a $p>0.05$ and * is a $p\leq0.05$.

As previously stated, deletion of *dlt* was expected to increase the net negative charge of the cell surface. However, the zeta potential measurements unexpectedly showed a slight decrease in negative charge of the *dlt*ABCDE deletion strain (W-Δd) compared to the wildtype *B. subtilis* (W) Figure 26. An unpaired t-test confirmed this to be statistically significant at a value of p=0.0205. This result was the opposite of the predicted higher negative charge due to the lack of D-alanylation in a *dltABCDE* deletion strain. Comparing the charge between wildtype *B. subtilis* (W) and the *dltABCDE* overexpression strain (W-↑d), there was no significant difference. It is possible that zeta potential measurements are too indirect to measure small differences in cell surface charge caused by modulation of *dlt* activity. Alternatively, it may be that *dlt* deletion or overexpression in B*. subtilis* did not have the expected effect on cell surface charge.

To test if the unexpected results were due to limitations of the zeta potential measurements or an accurate reflection of the cell surface charge in the three strains tested, further testing was carried out in the form of a cytochrome C binding assay. This was done on stationary phase cells to more accurately reflect the conditions under which biomineralisation should occur (Figure 27). Measurements of CytC binding are commonly used to characterise surface charge whereby the adsorption of the positively charged cytochrome C protein to bacterial cell surface is used as a proxy for negative surface charge. When the three strains with *dlt* variations were tested for their cytochrome C binding ability the results showed no significant difference in cytochrome c binding

ability between wildtype *B. subtilis* (W) and the deletion (W-Δd) or overexpression (W-↑d) strain (Figure 27). The results were consistent with the zeta potential assay and appeared to suggest that *dlt* deletion and overexpression may not have led to desired changes in cell surface charge.

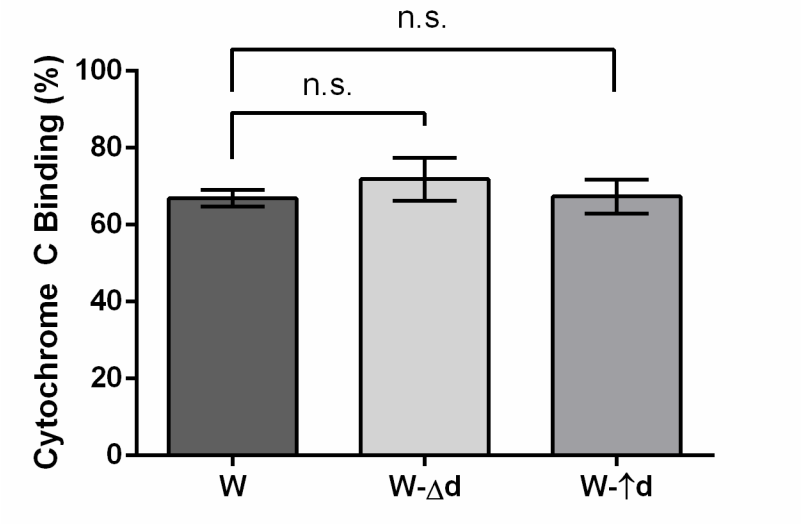

Figure 27. Cytochrome C binding by *B. subtilis* strains with *dlt* operon deletion or overexpression. Overnight cultures of *B. subtilis* W168 wildtype (W), *dltABCDE* deletion (W-Δd), and *dltABCDE* overexpression (W-↑d) re-suspended in MOPS to an OD_{600}=2.5 were incubated with 250 µg/ml cytochrome C for 10 minutes at room temperature. Percentage binding was calculated from the supernatant after centrifugation as the absorbance difference relative to sample without bacteria. Data are shown as the mean and standard deviation of three to four independent biological repeats. Results of unpaired t-tests are shown as n.s. (p>0.05).

It was again unexpected to see such a small effect of the *dlt* deletion, when in other Gram-positives (such as in *Lactobacillus*) this assay gave a measurable difference on a *dlt* deletion strain (Revilla-Guarinos *et al.*, 2013). This could possibly mean that the role of *dlt* is different in *B. subtilis* W168. Much of the information on *Bacillus dlt* comes from the study of antimicrobial peptide resistance, with the theory that *dlt* reduces the net negative charge to reduce attraction of cationic antimicrobials (Kamar *et al.*, 2017; Abi Khattar *et al.*, 2009; Kingston *et al.*, 2013). Therefore the third and final approach to characterise a surface charge effect was through a nisin time dependent kill curve. Testing the susceptibility of strains towards cationic antimicrobial peptides is an established approach to quantifying charge modulations of *dlt* mutants in other bacteria as the *dlt* operon is considered a resistance mechanism to cationic peptides (Revilla-Guarinos *et al.*, 2014). The benefit of the antimicrobial approach is that it amplifies subtle charge differences as when the antibiotic is adsorbed to the surface it is not just simply bound but inflicts an effect that can be measured as the death of cells. Therefore, we tested for their susceptibility to killing by nisin over

time (Figure 28). The results showed an increased susceptibility toward the antibiotic nisin in the *dlt* mutant strain over that of the wildtype. The wildtype strain grew at a nisin concentration of 16 µg/ml while the mutant experienced growth inhibition (Figure 28). The *dlt* overexpression strain susceptibility was more closely aligned with that of the wildtype. From these sets of experiments it was determined that *dlt* expression by P_{veg} did not cause any detectable changes, possibly because of its genome integration location into the wildtype *dlt* operon or because expression level of *dlt* is not a bottleneck to surface charge. It was further determined that the *dlt* deletion did have an effect on the cell surface, but this was only visible in the nisin killing experiments and not by zeta potential or cytochrome C binding. Similar observations have been made in *Lactococcus lactis* where variations in D-Alanylation of teichoic acids alter cationic antimicrobial resistance but did not have a measurable effect on charge by electrophoretic mobility (Giaouris *et al.*, 2008). The rationale was that that the charge modifications are buried inside the cell wall and not exposed at the cell surface, thereby not changing global negative charge (Giaouris *et al.*, 2008). This may suggest that the charge changes caused by the *dlt* deletion here were too subtle to be resolved by the first two assays. Alternatively, the changes are more complex and the *dlt* deletion may have resulted in compensatory changes in other cell envelope components and that this could mask the effect of measurements such as the zeta potential. Difference in bacterial growth and growth rate have been previously noted to ultimately influence zeta potential (Soon *et al.*, 2011). Measuring zeta potential of exponentially growing cells might not have been as representative as there were slight differences in OD_{600} during sub culturing between W-Δd and W during the experiments. Calcite precipitation also occurs much later in the growth stage of the cells, so stationary phase cells might be more representative. However deletion of *dltABCD* in *B. subtilis* has previously been shown to be not to affect cell growth (Perego *et al.*, 1995) and growth in the nisin killing experiments showed closely aligned growth curves. There is another conflicting theory to a pure charge effect of *dlt*, which is that the changes in D-alanylation leads to a structural change of the cell wall altering permeability towards cationic antimicrobial peptides (Saar-Dover *et al.*, 2012; Revilla-Guarinos *et al.*, 2014). In this fashion there is no true global change in surface charge but charge changes instead incur structural changes which interfere with the antimicrobial effect of nisin. It is assumed that the biding assays work on electrostatic attraction between cell surface and ligand however, the contributions of cell wall interactions other than d-anylated teichoic acids also needs be considered (Revilla-Guarinos *et al.*, 2014).

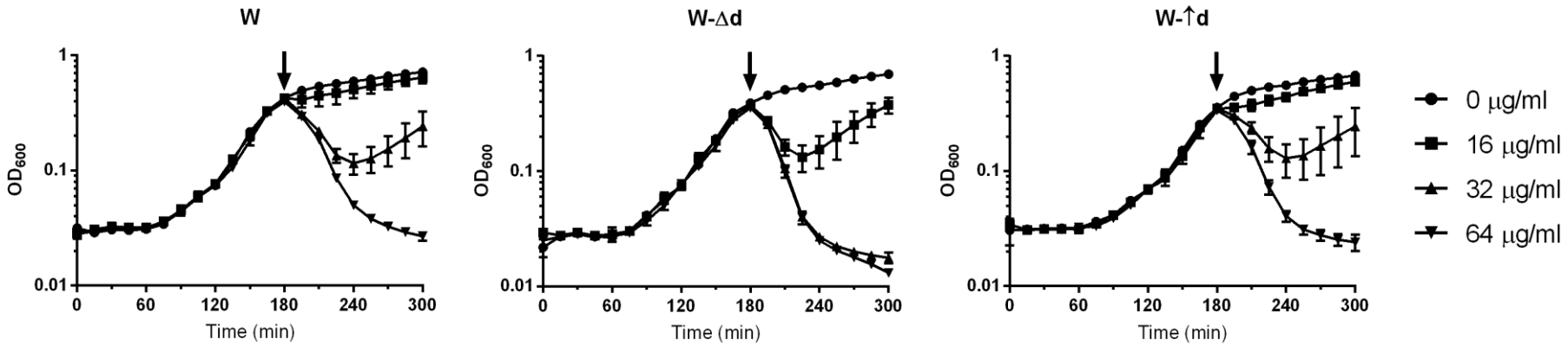

Figure 28. Nisin concentration dependent killing of *Bacillus subtilis* strains. Cells were grown in LB in a Tecan Plate Reader to OD=0.4-0.5, after which nisin was added at concentrations of 0 µg/ml (●), 16 µg/ml (■), 32 µg/ml (▲) and 64 µg/ml (▼). The time of nisin addition is indicated by arrows. Data are shown as mean and standard deviation of three technical repeats. Graphs are representative of three biological repeats.

4.2.4.2 Surface charge: calcite precipitation assays.

After establishing that there was a possible subtle modulation of surface charge in strain W-Δd, the next stage was to examine the effect of this charge change on calcite precipitation. To evaluate the baseline effect of just surface charge on precipitation ability without additional drive from ureolytic activity, the *dltABCDE* deletion introduced into the *B. subtilis ureABC* deletion strain to construct strain WΔ-Δd (SGB985). Calcite precipitation was tested on LBGMC precipitation media, as this was found to enhance crystal formation facilitating the quantification of precipitation on cell colony surfaces. Strains WΔ-Δd and its parent WΔ were spotted onto LBGMC and the crystal formation monitored over seven to ten days at 30°C. Across three biological repeats, no precipitates formed on colonies of either WΔ or WΔ-Δd. This indicated that loss of D-alanylation of teichoic acids was not sufficient to bring about a calcite precipitation phenotype in this model.

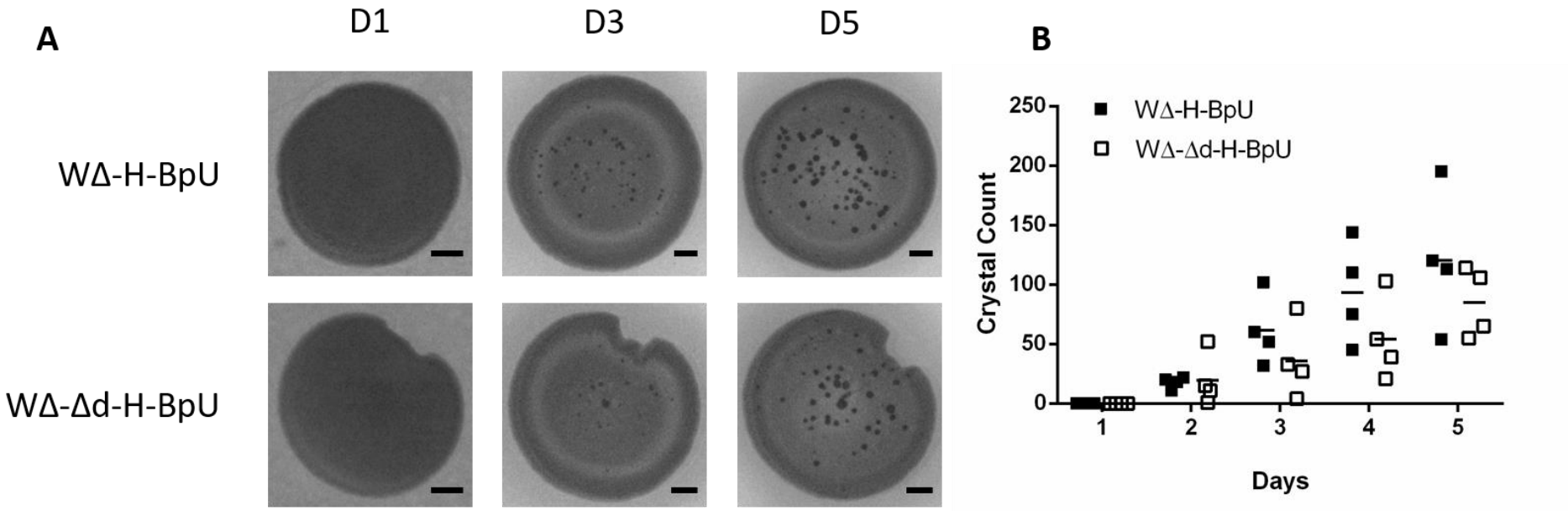

Figure 29. Effect of *dlt* deletion on calcite precipitation in a strong ureolytic background. WΔ-Δd-H-BpU (□) and its parent strain WΔ-H-BpU (■) were spotted onto LBGMC precipitation media and grown at 30°C over a period of five days. Individual calcite crystals on the colony surface were counted daily under a stereomicroscope. The results are from four biological repeats. Colony surface images of a representative series are depicted (A), where the scale bar represents 1 mm in size. The number of crystals counted on colony surfaces each day across repeats are depicted (B), where bars represent the average. Results depicted for the parent strain WΔ-H-BpU (the control) are the same as in Figure 22.

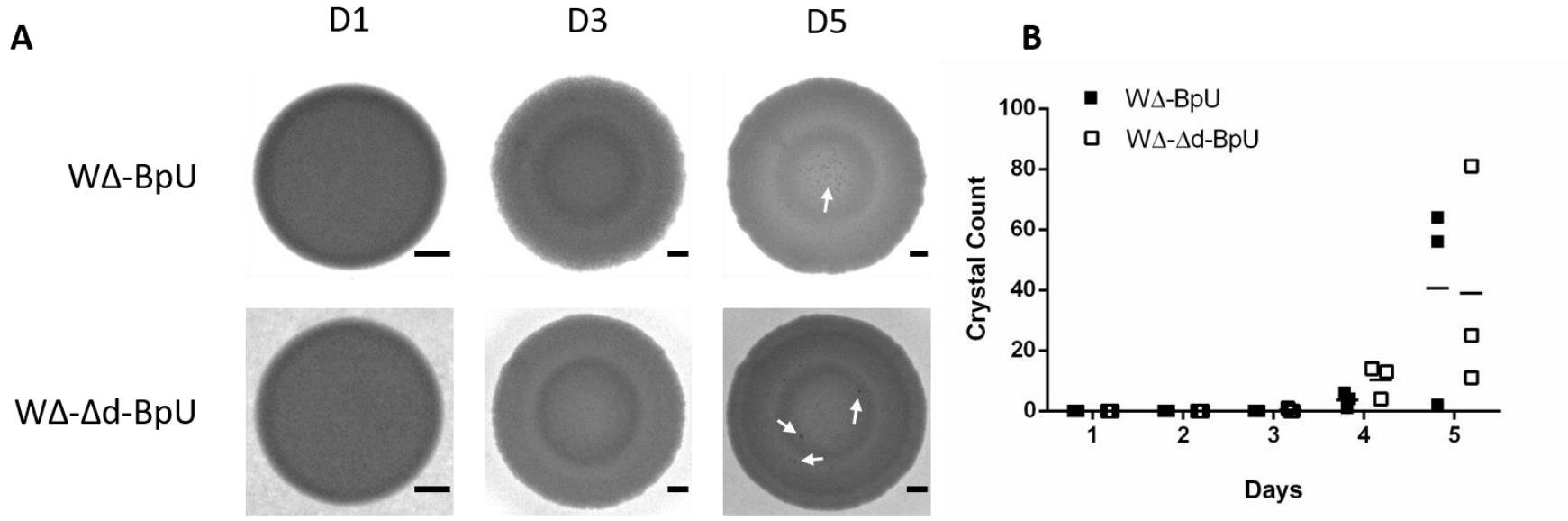

Figure 30. Effect of *dlt* deletion on calcite precipitation in a weak ureolytic background. WΔ-Δd-BpU (□) and its control WΔ-BpU (■) were spotted onto LBGMC precipitation media and grown at 30°C over a period of five days. Individual calcite crystals on the colony surface were counted daily under a stereomicroscope. The results are from three biological repeats. Colony surface images of a representative series are depicted (A), where the scale bar represents 1 mm in size. Arrows indicate at areas of crystal formation. The number of crystals counted on colony surfaces each day across repeats are depicted (B), where bars represent the average.

The lack of precipitation on colonies of WΔ-Δd suggests that the effect of the *dlt* deletion on cell surface chemistry was too subtle to induce calcite precipitation by itself, however it may still have an enhancing effect in a strain that already has a baseline ability for biomineralisation. Therefore, the next step was to introduce the *dltABCDE* deletion into the strong ureolytic strain WΔ-H-BpU and weak ureolytic strain WΔ-BpU, leading to the construction of strains WΔ-Δd-H-BpU (SGB988) and WΔ-Δd-BpU (SGB989). Strains WΔ-Δd-H-BpU and WΔ-Δd-BpU were spotted onto LBGMC and their crystal formation monitored over five days at 30°C.

When the effect of the *dlt* deletion on calcite precipitation was studied in the strong ureolytic background, an apparent decrease in the number of crystals forming on the colony surface compared to the parent strain WΔ-Δd-H-BpU was observed (Figure 29). Results of a two-way ANOVA however, revealed no significant strain affect with a value of $p=0.0550$ and significant time effect with a value of $p<0.0001$. The result was unexpected, as an increase in negative charge was hypothesised to be associated with an increased potential in attracting cations for precipitation. A *dlt* deletion in the weak ureolytic background showed only slight variability in the precipitation ability compared to the parent strain WΔ-BpU (Figure 30). When analysed by comparing grouped individual biological runs, on day four (the first day crystals were visible for both strains) WΔ-Δd-BpU consistently precipitated more crystals than its parent strain WΔ-BpU. The total amount of precipitation on day four, when averaged across all biological repeats, was however not significantly different between the two strains as confirmed by an unpaired t-test. There still may be a subtle phenotype in the speed of crystal formation onset rather than quantity. After longer incubation there is a lot more variability and no apparent difference in precipitation between strains. A two-way ANOVA revealed no significant strain effect with a value of $p=0.8566$ and significant time effect, with a value of $p=0.0011$ when looking at the absolute amount of individual crystals formed. Precipitation quantification in the weak ureolytic background was further complicated by the formation of crystals on the colony underside rather than on the typical surface. This could be possibly the result of different local concentration gradients created by the weak ureolytic strain *vs* those of the stronger ureolytic strain. For this reason, crystals were hardly visible on the surface (Figure 30-A).

4.2.4.3 SEM imaging of calcite colony precipitates from strains grown on LBGMC and LBC.

After establishing that biofilm formation promotes mineral precipitation and surface charge does not have a beneficial impact on precipitation (in an already strongly precipitating strain) we were interested in analysing the calcite crystal morphologies that formed on the colonies. Calcite crystals

on WΔ-H-BpU (the strongest precipitation strain) and WΔ-Δd-H-BpU (the strongest precipitation strain with the *dlt* deletion) were chosen for further analysis. The strains were grown on LBC and LBGMC to reflect a non-biofilm and biofilm promoting condition, and incubated at 30°C. Crystals were allowed to form over a course of 1-2 weeks after which they were scraped off, washed and imaged under an SEM. A selection of different calcite crystal surface morphologies observed are depicted in Figure 31 for growth on LBGMC and Figure 32 for growth in LBC.

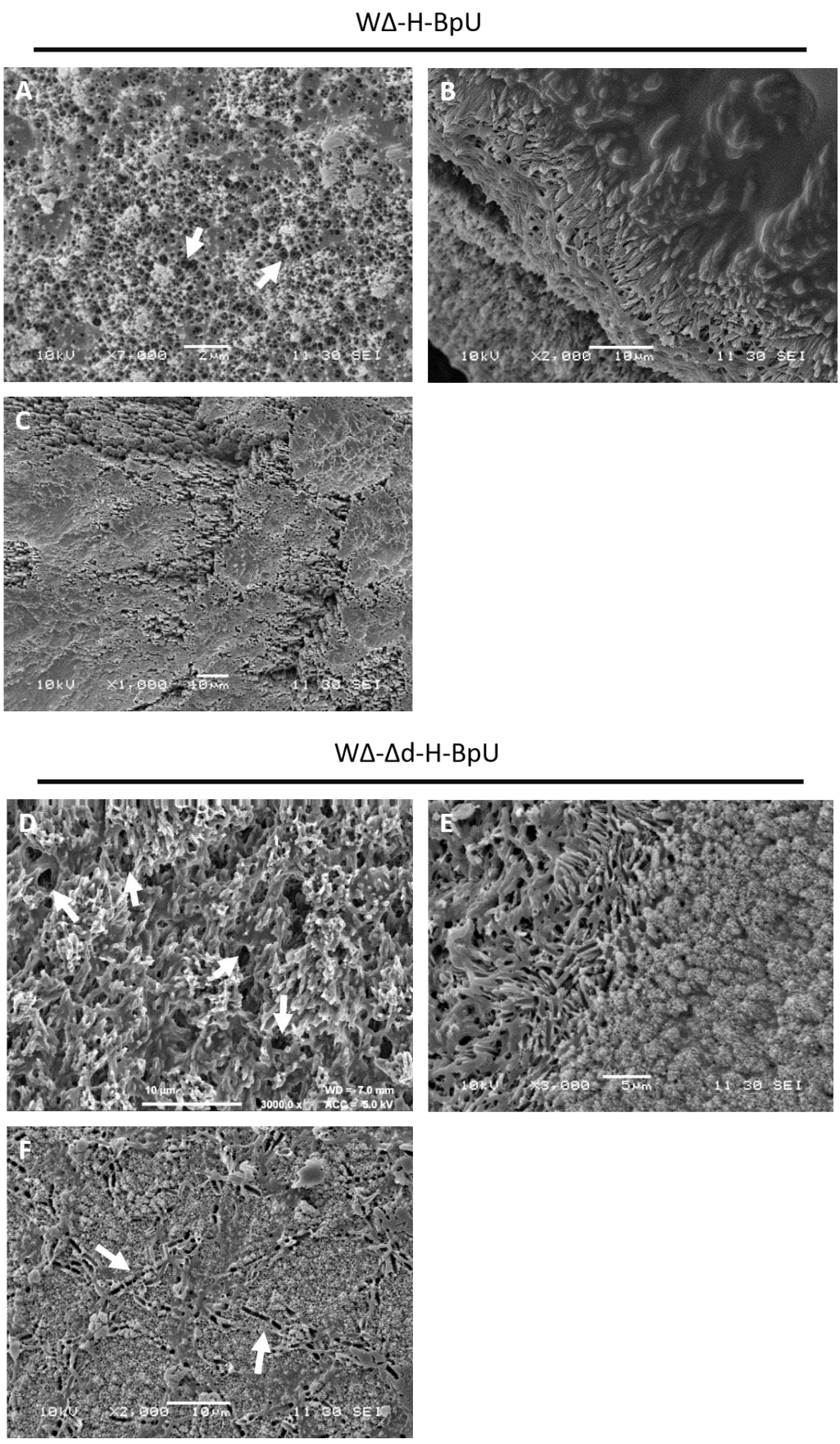
WΔ-H-BpU
A
10kU X7,000 2μm 11 30 SEI
B
10kU X2,000 10μm 11 30 SEI
C
10kU X1,000 10μm 11 30 SEI
WΔ-Δd-H-BpU
D
10 μm WD = 7.0 mm
3000.0 x ACC = 5.0 kV
E
10kU X3,000 5μm 11 30 SEI
F
10kU X2,000 10μm 11 30 SEI

Figure 31

Figure 31. SEM analysis of mineral precipitates from LBGMC plates. Crystals precipitated on colonies of WΔ-H-BpU and WΔ-Δd-H-BpU grown on LBC 30°C for 1-2 weeks. The samples were imaged on a SEM (A, B, C, E & F) with gold splutter coating or an FE-SEM (D) with chromium splutter coating. Arrows indicate at negative spaces within the crystal precipitates from 'holes' (A and D) to bacterial 'footprints' (F).

Interestingly, under biofilm promoting conditions on LBGMC (Figure 31), both WΔ-H-BpU and WΔ-Δd-H-BpU calcite crystals had smooth surfaces as well as rough/porous surfaces. These differences depended on where the calcite crystal is imaged. Figure 31-B and Figure 31-E show cross-section like areas on the crystals where layers of mesh like rough biofilm crystals are covered by a smooth layer. Some regions were very porous with mesh-like structure with many 'holes' or negative spaces (Figure 31-A and Figure 31-D, indicated by arrows). These were likely formed by bacterial cells, around which calcite has deposited. The appearance of these structures under biofilm promoting conditions may suggest that the calcite precipitated on the extracellular biofilm material. This is more clearly evident in Figure 31-F (indicated by arrows) where bacterial 'footprints' can be observed as obvious rod shapes with the septum visible separating individual cells. Together the images show the likely sequential layers of calcite and growth of the crystal over time with bacteria at the centre.

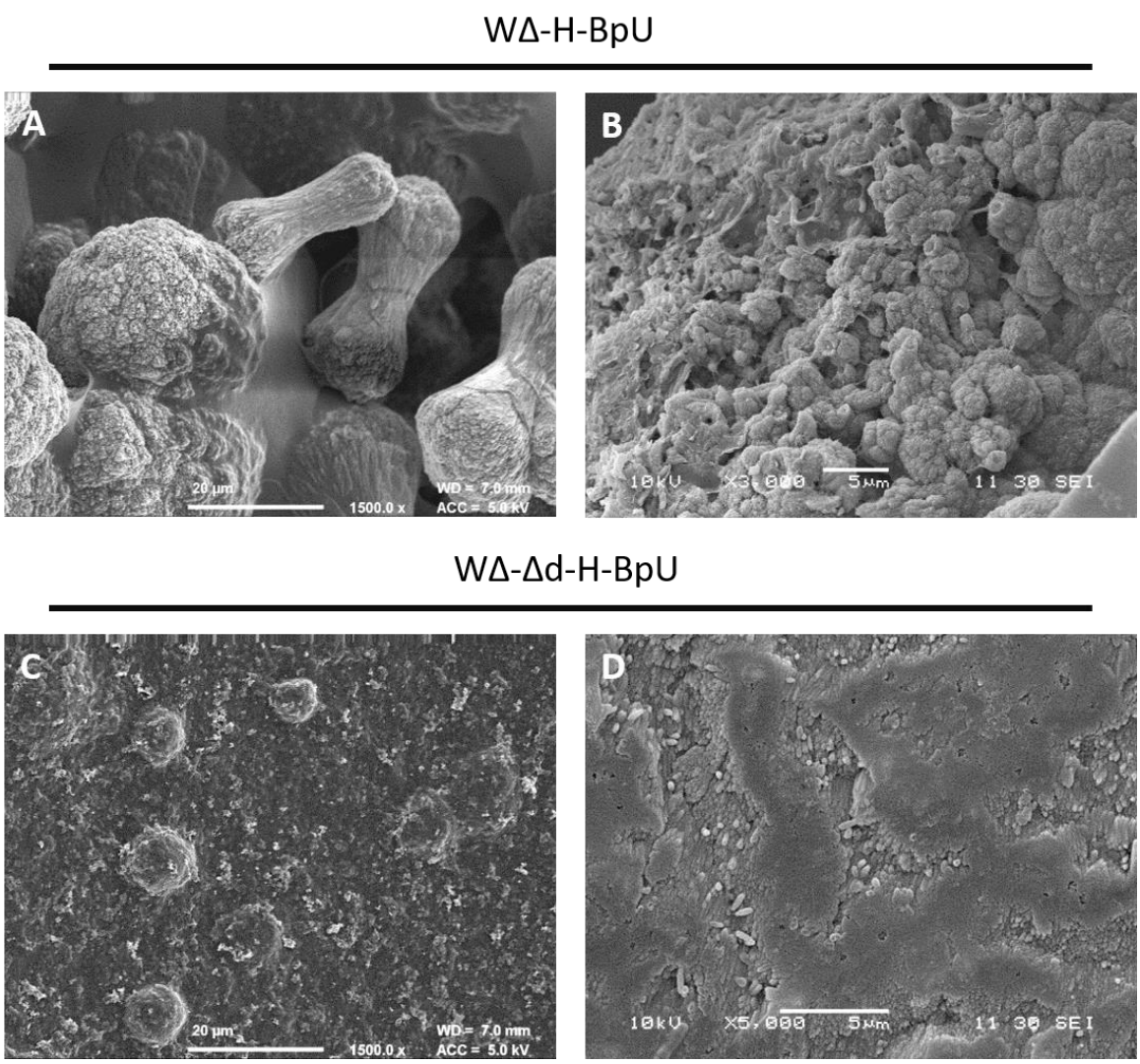

Figure 32. SEM analysis of mineral precipitates from LBC plates. Crystals precipitated on colonies of WΔ-H-BpU and WΔ-Δd-H-BpU grown on LBC 30°C for 1-2 weeks. The samples were imaged on a SEM (B & D) with gold splutter coating or an FE-SEM (A & C) with chromium splutter coating.

In contrast, on LBC under non-biofilm promoting conditions no mesh-like areas were observed, with the majority of the crystal area imaged showing a smooth surface morphology (Figure 32-B and Figure 32-C). There also was more of a difference between crystal morphologies of WΔ-Δd-H-BpU and WΔ-H-BpU, with the former having a much smoother crystal surface (Figure 32-C) than the latter, which showed an on overall rougher terrain (Figure 32-B). This difference on LBC could suggest that the *dlt* deletion did cause slight structural changes of the cell surface, while on LBGMC this might have been masked by the production of biofilm. Dumbbell morphologies as described in section 2.1.6 were observed just for WΔ-H-BpU on LBC, but this was a much rarer occurrence than reported earlier (Figure 32-A), where the same strain was grown on media containing pH indicator

and was pH adjusted at the start. This again highlights the sensitivity of precipitation to environmental conditions as well as timing. Overall, most noteworthy of the SEM imaging is that it shows that biofilm production acts as a good source for calcite deposition as evident by the bacterial footprints within, possibly acting as a scaffold and/or microenvironment to promote precipitation.

4.3 Discussion.

4.3.1 Urease discussion.

The aim of this investigation was to use a bottom-up approach to engineering BICP into the Gram-positive bacterium *B. subtilis* W168 to understand which bacterial and genetic feature or processes drive BICP. This was approached by exploring the role of ureolysis, biofilm formation, and cell surface charge, as well as combinations thereof, on BICP. The first objective was to determine whether heterologous urease expression could drive calcite precipitation and which genes of the urease cluster were important for the process. Conducting a semi-quantitative urease assay showed that heterologous expression of *B. paralicheniformis* urease structural genes *ureABCEFGD* in *B. subtilis* induced ureolytic activity (Figure 10). The speed of precipitation on LBC phenol red precipitation plates correlated with the strength of ureolytic activity in the respective strains WΔ-H-BpU and WΔ-U-H-BpU, which carried the core urease genes plus accessory genes *ureH* and/or *urt* (Figure 13). The results highlight that the stronger the ureolytic activity the faster the critical pH and saturation conditions for precipitation were reached. Testing ureolytic activity in liquid and on solid media revealed that the strength of ureolysis was dependent on the presence or absence of the accessory nickel transporter UreH and the urea transporter Urt. Additionally, the strain exhibiting the strongest urease activity changed depending on the media composition and, by extension, the environment. In rapid urease broth media (where nutrients were limited) the availability of the Urt transporter yielded a higher ureolytic activity (Figure 10 and Figure 12). In contrast, on LBC phenol red media (where nutrients were plenty) the availability of the UreH transporter yielded a higher ureolytic activity (Figure 11). Thus, when incorporation of nickel into the urease enzyme provides a bottleneck to ureolysis, the UreH transporter appears to be of benefit, while when nutrients or urea are limiting, the Urt transporter appears to be of benefit.

Overall, the results showed that heterologous expression of urease genes was suitable for inducing calcite precipitation in Gram-positive bacteria. Urease activity increased with the presence of accessory genes which was in line with previous research on urease gene clusters. It has generally been reported in the literature when characterising bacterial ureases that changes in activity were

dependent on the presence and absence of accessory genes (Lee *et al.*, 1992) and accessory transporters (Sebbane, Mandrand-Berthelot, *et al.*, 2002; Sebbane, Bury-Moné, *et al.*, 2002). This is because accessory genes such as *ureD*, *ureF*, *ureG*, and *ureE* help form the metallocentre, and other accessory transporter genes may provide nickel and urea for the enzyme. Absence of *ureH* from recombinantly expressed *B. paralicheniformis* urease genes in *E. coli* had previously been shown to cause a reduction in activity of the purified urease enzyme (Liu *et al.*, 2017). Urease activity dependent on accessory urease genes has predominantly been studied in bacteria such as *Klebsiella*, *Helicobacter*, *Escherichia* and *Pseudomonas* and mainly using purified proteins or crude enzyme extracts. For example, plasmid expressed *E. coli* urease genes in *E. coli* and *P. aeruginosa* yielded lower ureolytic activity per cell than in the native strain (Connolly *et al.*, 2013). *S. pasteurii* urease genes expressed in *E. coli* yielded lower urease activity and precipitation compared to *S. pasteurii* wildtype. This was only improved upon the addition of nickel into the growth media (Bachmeier *et al.*, 2002). *S. pasteuri* urease genes expressed in *P. aeruginosa* resulted in reduced ureolytic activity but comparable rates of precipitation compared to *S. pasteurii* wildtype (Bergdale *et al.*, 2012). Further, noteworthy is that heterologous expression of urease genes has not always been found to be dependent on the same genes. A set of *H. pylori* genes expressed in *Campylobacter jejuni* gave a positive ureolytic phenotype but not when expressed in *E. coli* (Labigne *et al.*, 1991). Instead, a different set of urease genes were essential while the others were not (Cussac *et al.*, 1992). The difference in which genes are needed depending on the host bacterium highlights the need to study ureolysis on application relevant organisms. All these previous investigations have been done in Gram-negatives which is not reflective of the chassis organisms required for application. Application such as self-healing concrete is usually done with Gram-positive bacteria, ideally spore forming ones to ensure compatibility with application and long term survival. The difference in genes required for optimal urease activity even observed between Gram-negative bacteria, illustrates the importance to study this in a Gram-positive spore former and as a function of whole cell activity, if it is to be applied to biotechnologies.

Further scope for investigation remains such as whether expressing *ureH* or *urt* on their own in the native *B. subtilis* W168 background would increase its low intrinsic ureolytic activity, or whether the accessory genes *ureEFGD* could be added to the native *B. subtilis* W168 *ureABC* structural genes to increase ureolytic activity. Knowing this could reduce the number of urease genes that would need to be introduced into a better suited *Bacillus* chassis for application, instead of introducing a large recombinant gene cluster. This would also minimise potential metabolic burden or genetic disruptions in the new host. Other studies have also identified the importance of genes outside of the urease gene cluster: in *E. coli* expressing *S. pasteuri* urease genes it was found that the presence

or absence of genes directly outside of the urease gene cluster affected urease activity (Liang *et al.*, 2018). These genes encoded for transporter proteins that influenced calcium uptake and putative proteins involved in aromatic amino acid metabolism (Liang *et al.*, 2018). The authors summarise that these surrounding genes can influence urease activity and consequently biomineralisation but did not identify a clear correlation or mechanism (Liang *et al.*, 2018). Thus, ultimately genetic background of the host is likely to have an effect on ureolytic driven BICP.

Media composition further influenced the precipitation quantity and precipitation spatial distribution of the strongest ureolytic strains, WΔ-H-BpU and WΔ-U-H-BpU. Precipitation on LBC was slow and only occurred on the colony surface, while on B4 media precipitation was much faster with crystals forming on colonies as well as in the surrounding media (Figure 14 and Figure 15). This was likely due to the buffering capacity and starting pH of the media. B4 has a higher initial pH and a lower buffering capacity than LBC, allowing the optimal pH and saturation conditions for calcite precipitation to be reached faster. Difference in media composition has only been sparsely noted in BICP (González-Muñoz and Chekroun, 2000) and more understanding can be drawn upon from material science. In the field of material science, the study of crystallisation in gels reports that media composition will affect solute movement and thereby supersaturation (Asenath-Smith *et al.*, 2012). Media composition such as agarose concentrations influences diffusion by varying density/porosity, which in turn affects supersaturation and thus precipitation (Asenath-Smith *et al.*, 2012; Lopez-Berganza *et al.*, 2019). While both LBC and B4 had the same agar concentrations, their composition likely still varied enough to influence supersaturation conditions. Media can further influence precipitation beyond a function of simple saturation kinetics if components have chemical functionality that for example act as heterogeneous nuclei to promote precipitation (Asenath-Smith *et al.*, 2012). When it comes to studying BICP biotechnologies it may therefore be important to tailor media compositions closer to application. Laboratory experimentation was limited to agar based matrices, while application environments differ and thus may lead to further different spatial distributions.

Difference in spatial distribution of precipitates has also been shown to be dependent on ureolytic strength. Environmental strains with differing levels of ureolytic activity showed that slow ureolysis formed precipitates on the colony, while fast ureolysis formed precipitation in the surrounding media (Reeksting *et al.*, 2020). As with our observations of precipitation spatial distribution variation across media, this can be explained by the speed at which saturations conditions for calcite precipitation are reached. The stronger the ureolytic activity, the quicker supersaturation of

the microenvironment occurs increasing the potential for precipitates to form in the surrounding media to create different spatial distribution of calcite. This shows that both the precipitation potential and spatial distribution of precipitates are a factor of the bacteria modulating supersaturation conditions through ureolytic activity. The strength of urease activity has recently been modulated using gene copy number and RBS optimisation, and it was shown that ureolytic strength had a negative relationship with calcite crystal size (Liang *et al.*, 2018; Heveran *et al.*, 2019). Simply increasing ureolytic activity may thus not be favourable for application such as self-healing concrete, and a more delicate fine-tuning of BICP for may be an advantage.

To use the knowledge gained here under laboratory conditions for optimising application of BICP, it is important to consider the likely conditions encountered during application. In practice concrete is mixed with tap water and not distilled water, which should supply some trace amounts of nickel, at a upper limit of 20 µg/L nickel (Drinking Water Inspectorate, 2017). Therefore, generally, nickel may be more available in application than under the experimental conditions used here. This also does not take into account additional nickel leaching from pipes between the point of quality control at a municipality level and the end user. Further trace elements are introduced from the cement itself which can contain up to 825 ppm nickel (Schubert *et al.*, 1989). This however may be bio-unavailable for the bacteria as nickel becomes water insoluble due to the alkalinity of the cement (Schubert *et al.*, 1989). Only nutrients and ions in the direct environment of the bacteria are likely available as the rest is trapped in the cement matrix. Ultimately, nutrients added to the concrete are much more likely to be the limiting factor to BICP. Addition of nutrients is restricted by the balance that needs to be struck between bacterial benefit and concerns over cement setting and hardening (Alazhari *et al.*, 2018). It has however been observed in self-healing concrete systems that the quantity of available nutrients (such as yeast extract) correlates with the speed of calcium carbonate formed by bacteria, likely due to an increase in bacterial biomass (Tan *et al.*, 2020). In terms of strain selection this means the ureolytic strains with the accessory urea transporter Urt should fare better than ureolytic strains without Urt or with just UreH. Optimising access to the limited nutrients should accelerate ureolysis and provide energy to maintain cell function. A strain harbouring both Urt and UreH transporters to cover both limitations may fare equally well. However, experiments here showed WΔ-U-H-BpU to produce less calcite than WΔ-H-BpU, possibly due to more demand on the cell by production of an additional heterologous protein. If genetic engineered bacteria are to be applied to self-healing concrete, genetic compatibility needs to be optimised and genetic changes minimised to reduce the burden on the bacterium. Alternatively, due to regulatory limitations on the use of genetically modified bacteria, the understanding gained

from this work can be used to sample the environment for bacteria that contain these genetic elements. This could involve screening bacteria for ureolytic activity, to maximise precipitation potential, while also selecting under nutrient and pH pressures encountered in concrete to identify candidates better suited to BICP in application. The final step would be testing the strains in concrete application. It has to be kept in mind that there will be variability in conditions, as concrete composition differs across brands, types, raw materials and application purpose. This variability highlights the need for specific validations of strains directly in the final application. Concrete formulations will need to be developed alongside the bacteria as each depends on the other. The difference in precipitation speed and spatial distribution across B4 and LBC media of the same strain highlight the complexity of precipitation dependent on environmental factors. The more suited a bacterium is to the concrete environment and *vice versa*, as well as the more genetic elements the bacterium harbours for BICP, the higher the chance for faster and stronger self-healing. The characterisation for genetic elements that drive BICP to identify or mobilise them to application suited bacteria is therefore key to improving BICP technologies.

BICP is not just restricted to ureolytic bacteria and there are other non-ureolytic pathways that may also drive the process. Recent research has shown that that non-ureolytic pathways ultimately precipitate the same amount as ureolytic pathways, just slower (Reeksting *et al.*, 2020). This raises the importance of further dissecting apart the genetic factors that influence precipitation and how they interplay such as with biofilm and surface charge.

4.3.2 Biofilm discussion.

The second objective of this investigation was to explore the modulation of biofilm production on the ability of *B. subtilis* to precipitate calcite. Initial attempts at studying biofilm formation in *B. subtilis* NCIB 3610-derived ureolytic strains showed an increase in calcite precipitation on biofilm promoting media LBGMC but not on LBC (Figure 18 and Figure 19). There were however, colony morphology changes as a result of biofilm production, which masked some finer detail in the role of biofilm components contribution towards precipitation (Figure 19 and Figure 20). Increased surface area as a result of biofilm formation increases the potential sites at which precipitation can occur. This makes it difficult to say whether increased precipitation was a direct result of nucleation on a specific biofilm component or the result of increased surface sites for nucleation or both. Testing precipitation of *B. subtilis* W168 heterologous urease-producing strains (intrinsically low in ability to form biofilm) on LBGMC revealed an increased precipitation phenotype compared to that on LBC, and allowed for a quantification of the calcite formed. This showed that testing the role of

proteinaceous and exopolysaccharide biofilm components on precipitation may be more informative in a low-biofilm strain background. The strongly ureolytic strain harbouring the *spo0A* deletion, WΔ-Δs-H-BpU, which should be deficient in biofilm formation, surprisingly showed an increase in calcite precipitation compared to WΔ-H-BpU (Figure 22). This was likely a result of Spo0A pleiotropic role in the cell as a master regulator. The strongly ureolytic strain harbouring the *epsH* deletion, WΔ-Δe-H-BpU, showed a large decrease in calcite precipitation compared to WΔ-H-BpU (Figure 24). This suggested that the exopolysaccharide component of biofilm played a strong role in calcite precipitation ability. How the polysaccharide component precisely influences precipitation remains to be elucidated. This could be due to the formation of a microenvironment or interactions with specific residues that favours precipitation. The effect may possibly even be secondary, as the deletion of *eps* disrupts the formation of the BslA coat (Epstein *et al.*, 2011; Kobayashi and Iwano, 2012). BslA is a small protein secreted into the biofilm that assembles into a lattice that confers a hydrophobic protective barrier towards the colony (Arnaouteli *et al.*, 2016). Future work could explore the role of BslA deletion on colonies ability to precipitation calcite. Previous investigations have used purified EPS from *Pseudomonas putida* (Yin *et al.*, 2020), *Schizothrix* sp. (Kawaguchi and Decho, 2002), and *Bacillus firmus* and *Bacillus spahericus* (Ercole *et al.*, 2007) to show the role of EPS in biomineralisation in cell-free set ups. Our results support the precipitation promoting effect of EPS using live bacteria. However, not all studies have concluded that EPS plays a major role in BICP. A study showed that *Bacillus* JH7 grown in glycerol-supplemented conditions increased EPS production but not calcite precipitation compared to conditions lacking glycerol (Kim *et al.*, 2017). EPS was shown to bind more calcium ions, but precipitation conditions were not reached likely due to an acidification of the local environmental by glycerol metabolism (Kim *et al.*, 2017). The results led the authors to highlight the importance of media and the cell environment on precipitation and not just the cell physiology itself (Kim *et al.*, 2017). This discrepancy between precipitation dependence or not on surface groups has been reviewed in more detail in Chapter 1 and is ultimately a result of experimental conditions and strains used. A further challenge remains that characteristics vary between bacterial species and even strains of the same species. For example EPS production has been found to vary among strains of *Streptococcus thermophilus* (Vaningelgem *et al.*, 2004). This highlights the further complexity each strain potentially brings with it to the overall BICP potential. Multiple factors influencing BICP illustrate the complexity of precipitation and the need to study it under application relevant conditions and in application-relevant organisms for improved biotechnologies. Importantly, the study of biofilm formation also showed the interplay between surface chemistry and pH. In our experimental system, pH conditions were influenced by ureolytic activity. Our results showed that wildtype *Bacillus* strains grown on LBGMC

did not display increased precipitation over the time period tested; only in ureolytic strains did biofilm formation have a positive effect. This shows that different bacterial process and structures likely complement or synergise with each other to create improved conditions for calcite precipitation. When considering application in self-healing concrete, the pH of the concrete is already very alkaline and so a strong metabolic drive for further pH increase might not be required and instead EPS may exert the predominant effect on BICP.

In contrast to the EPS results, the strongly ureolytic strain harbouring a *tasA* deletion WΔ-Δt-H-BpU, showed no difference in its calcite precipitation compared to WΔ-H-BpU (Figure 23). This revealed that the proteinaceous component likely does not contribute to precipitation in the strain. On LBGM media *tasA* is more strongly upregulated than *epsH* in *B. subtilis* NCIB 3610 (Shemesh and Chaia, 2013). TasA is also more strongly upregulated on LB and MSgg as shown by expression level data on SubtiWiki for *B. subtilis* (Nicolas *et al.*, 2012). If expression levels correspond to absolute quantity of biofilm then these data show that it is not just the mass and surface area, but specific elements of the biofilm that help promote precipitation. In literature it has been noted that the specific compositions of EPS will influence the specific minerology of the precipitate formed, further highlighting the finely grained differences each component likely contributes (Kawaguchi and Decho, 2002). Both *epsH* and *tasA* deletions have been previously shown to reduce calcite precipitation in *B. subtilis* NCIB 3610, affecting spatial distribution and complex colony architecture (Oppenheimer-Shaanana *et al.*, 2016). While that study saw an effect of *epsH* and *tasA* on calcite precipitation, they also saw colony morphology differences which makes it difficult to preclude any conclusion on cause *vs* effect. As was shown in our initial trials with *B. subtilis* NCIB 3610, changes in colony morphology mask the finer detail in precipitation because colony surface area can have by itself an effect on calcite precipitation. Here we expanded on this notion to show a quantifiable contribution of *epsH* but not *tasA* on calcite precipitation that was not the result of colony morphological changes.

Building on this understanding, questions arise as to whether exopolysaccharides as a component of biofilms may be modulated to increase calcite precipitation in an applied setting. For an overall increased production of biofilm, future investigations could explore deleting the repressors of the *epsA-O* operon SinR and AbrB, the loss of which was shown to increase biofilm production and cause a biofilm colony phenotype (Chu *et al.*, 2008; Chu *et al.*, 2006). With the loss of these repressors one would hypothesise an increase in biofilm formation and thus biomineralisation on non-biofilm promoting media such as LBC. The practicality of this for application still remains questionable as AbrB is also involved in the sporulation signalling pathway and has a wider global transcriptional regulation role (Shafikhani and Leighton, 2004; Chumsakul *et al.*, 2011). Sporulation

is an important characteristic for bacteria used in making self-healing concrete as it is the form in which they are added to the concrete mix allowing them to remain dormant until a crack forms. It also potentially allows them to re-enter spore state after healing for repeated self-healing cycles. SinR may be a better target for fine tuning biofilm production even though it is also involved in sporulation regulation. Point mutations in SinR were identified to increase biofilm phenotype while not affecting spore formation (Mandic-Mulec *et al.*, 1995; Chu *et al.*, 2006; Leiman *et al.*, 2014). In practicality, depending on application (self-healing concrete, surface repair or soil consolidation) and encapsulation it may be better to avoid genetic engineering and add nutrients along with the bacteria that stimulate biofilm production, for example with the addition of manganese and/or glycerol. These have been shown to increase biofilm formation in *Bacillus* strains to varying degrees, depending on strain used (Hussain *et al.*, 2018; Morikawa *et al.*, 2006; Shemesh and Chaia, 2013). Concrete environments with their low nutrient availability could lend themselves to biofilm formation naturally. A recent study observed a gel-like biofilm substance forming in cracks of bacterial based self-healing mortars (Tan *et al.*, 2020). Over time this by-product disappeared to leave behind large calcite precipitates (Tan *et al.*, 2020). This shows that biofilm promoting conditions can be reached in concrete applications. Nutrient depletion and particularly starvation lead *B. subtilis* vegetative cells to either sporulate or form biofilm (Hamon and Lazazzera, 2001). Biofilm formation is supported as long as sufficient nutrients are available for basal metabolic activity (Hamon and Lazazzera, 2001; Gingichashvili *et al.*, 2020; Zhang *et al.*, 2014). The choice of biofilm formation *vs* spore formation under nutrient limitation has also been found to vary among different species of *Bacillus* (Lindsay *et al.*, 2006). Therefore, careful consideration have to be taken when selecting the approach to maximise biofilm formation in terms of choice of *Bacillus* species, nutrients and application environment. In natural environments, *Bacillus subtilis* is a soil organism that forms biofilms in association with plants, with signals such as manganese, glucose, and L-malate promoting biofilm production (Mielich-Süss and Lopez, 2015). Soil clay minerals and iron oxides have also been investigated in their ability to stimulate biofilm formation (Ma *et al.*, 2017). Goethite (an iron hydroxide mineral) was found to induce a biofilm response, probably as the result of a stress response as it was shown to be toxic to the cells before biofilm formation was established, and killed cells were likely used as nutrients by the survivors (Ma *et al.*, 2017). Goethite has been used for concrete compositions (Ouda, 2015; El-Samrah *et al.*, 2018). Exploring mineral compositions better suited to concrete that may induce a biofilm phenotype in bacteria could be an avenue worth taking. The environment could also be further sampled for bacteria isolated under biofilm forming conditions and media with compositions that are closer to application-relevant conditions. Overall the results on biofilm formation and BICP identified exopolysaccharide

production as a potentially suitable target for modulating calcite precipitation in *B. subtilis*. With this understanding future investigations can make more informed decisions of which surface characteristics to potentially genetically engineer or select for in environmental isolates for BICP biotechnologies.

4.3.3 Surface charge discussion.

The third objective of this investigation was to explore the modulation of surface charge through the *dlt* operon on the ability of *B. subtilis* to precipitate calcite. The strain over-expressing the *dlt* operon (W_d↑) showed no difference in surface charge compared to the wildtype, as established *via* zeta potential measurements, cytochrome C binding, and a nisin-dependent killing curve. This demonstrated that *dlt* expression was likely not a bottleneck for controlling positive/negative charge. Zeta potential measurements of the *B. subtilis* W168 *dlt* deletion strain WΔd showed a reduction in negative charge from -61 mV to -57 mV compared to wildtype (counter to what was expected (Figure 26)), while testing with the cytochrome C binding assay showed no significant charge changes (Figure 27). These two results suggested that Dlt may only play a minor role on the surface charge of *B. subtilis*. In contrast, testing using time-dependent killing by nisin revealed that the strain WΔd was more sensitive to the positively charge antibiotic than the wildtype (Figure 28). This in turn suggested that there was a slight surface charge modification, but possibly masked by other components of the cell envelope and as such the Dlt system did not exert a strong global surface charge effect. Testing the strain WΔd for its calcite precipitation ability, no biomineralisation was observed. This supported the subtle charge change observed for this strain, which was apparently not sufficient to induce calcite precipitation on its own. Introduction of the *dlt* deletion into the weakly ureolytic background of WΔ-BpU did not show a significant difference in overall precipitation when data from repeat experiments were averaged. However, when directly comparing the strain to its parent within a single repeat experiment, the WΔ-BpU strain consistently showed a greater speed of precipitation. Due to the variability of the data between repeats, this difference was no longer observed when data were averaged (Figure 30). The lack of an overall change in precipitation quantity suggested that the charge difference was too subtle to affect precipitation in a detectable way, or that the role of surface charge on precipitation has been oversimplified in the literature (Zhang *et al.*, 2018). An alternative theory to the idea of a change in net surface charge being the repelling force that protects from cationic antimicrobial peptides (CAMPS), is the theory that a change in D-alanylation causes a difference in the packing of teichoic acids due to changes in electrostatic interactions in the cell wall, which alters the permeability towards CAMPS (Saar-Dover *et al.*, 2012; Revilla-Guarinos *et al.*, 2014). As such, our observed

sensitivity of the *dlt* deletion strain to nisin may not be a simple effect of global surface charge. Steric, rather than charge effects of Dlt activity might explain the lack of precipitation difference between WΔd and WΔ-Δd-BpU and their respective parent strains. To investigate surface structural changes would require transmission scanning electron and atomic force microscopy approaches (Saar-Dover *et al.*, 2012). If there was an observable difference in the density and rigidity of the cell wall compared to the control, this would suggest a structural change accrued and that Dlt in *Bacillus* would not be a suitable target for modulating global surface charge.

Contrary to these observations, introduction of the *dlt* deletion into the strongly ureolytic background of WΔ-H-BpU showed an apparent decrease in the quantity of precipitation compared to the parent strain (Figure 29). This could have occurred due a decrease in ureolytic activity by the WΔ-Δd-H-BpU strain compared to the WΔ-H-BpU strain. UreH is a membrane protein, specifically a nickel and iron transporter; if the cell surface is more negatively charged, it may chelate some of the free nickel or iron from the environment, making it inaccessible to the transporter. Reduced import would reduce the availability of nickel/iron needed for the urease enzyme and in turn decrease urease activity and subsequently mineral precipitation. To investigate if such an effect may have occurred here, future experiments could run WΔ-Δd-H-BpU and WΔ-Δd-H-BpU in the semi-quantitate urease assay to measure their activity and see if supplementing nickel or iron affects this activity. If this was indeed the case, it would suggest that *dlt* deletion did in fact cause a subtle change in surface charge. Teichoic acids on bacterial surfaces are known to have a function in ion homeostasis (Brown *et al.*, 2013). Thereby, there is a balance between the ability for a bacterium to attract ions and the need for these to diffuse to the membrane (Thomas and Rice, 2015). Excessive strength in ion binding by the cell surface may therefore be counterproductive to the cell and may impair ion transport ability. If increased binding of cations does impair ion transport ability and consequently metabolism and other cellular processes, then the role of surface charge in BICP is more delicate than previously thought. As such the idea that an increase in negative charge increases the precipitation ability of a bacterium would be an oversimplification or at best an over-generalisation. Suggestions that the role of surface charge is an oversimplification/generalisation in BICP aligns with observations by other work. Real-time single cell level monitoring of calcite precipitation by *Sporosarcina pasteurii* showed that, on soft agar, precipitates mostly formed independently of the bacterial cells and were not associated with their surface, while in liquid media, some micron-sized precipitates were associated with cell surfaces (Zhang *et al.*, 2018). The authors continued to show that cells and functional groups on artificial polymers did not by themselves provide a nucleation site, but that cellular metabolism was required, concluding that the role of surface charge attracting ions is an oversimplification (Zhang

et al., 2018). However, one has to note that *S. pasteurii* is a strongly ureolytic strain and, as has been shown in our work, strong ureolytic activity is sufficient by itself to drive precipitation. This means that in a strongly ureolytic strain, cell surface charge probably plays a minor role in precipitation, which is instead predominantly driven by ureolysis. In our results we observed that surface changes may even possibly negatively affect precipitation if they interfere with pathways of metabolically driven precipitation. However, it cannot be excluded that in another bacterium with a weak metabolic drive for precipitation a stronger surface charge modulation (that does not interfere with other cellular functions) may be beneficial. This was noticeable when precipitation onset was consistently faster in paired repeats of WΔ-Δd-BpU compared to WΔ-BpU, but a lack in difference in overall precipitation quantity could be explained by the overall subtle charge modulation.

Whether or not the *dlt* deletion caused a charge and/or structural change, there were some small observable differences in calcite crystal morphologies between those precipitated by WΔ-H-BpU and those by WΔ-Δd-H-BpU (Figure 32). Precipitates on LBC by WΔ-Δd-H-BpU were much smoother than those of WΔ-H-BpU possibly due to surface changes induced by the *dlt* deletion. No such differences were obvious on LBGMC where both WΔ-Δd-H-BpU and WΔ-H-BpU produced calcite in the surrounding biofilm matrix, leaving behind negative spaces were the bacteria used to be (Figure 32). The absence of a distinguishable calcite surface morphology difference between WΔ-Δd-H-BpU and WΔ-H-Bp on LBGMC (unlike in LBC) could be a result of the biofilm promoting media masking any subtle *dlt* deletion phenotype in *B. subtilis* by changing the biofilm production. This further highlights the complexity of calcite precipitation by bacteria, with a delicate balance of multiple components that facilitate the process. Ultimately, the variability in bacterial strain surface conformation and composition will have different influences on precipitation. Our results showed that modulating surface charge through the *dlt* operon in *B. subtilis* W168 likely has too subtle an effect to affect precipitation through a genetic engineering approach. An alternative approach to modulating surface charge could be explored through the lysinylation of lipids by the protein MprF. MprF adds L-lysine to phospholipids of the cell membrane, thereby increasing positive surface charge and decreasing the affinity towards cationic antimicrobial peptides (Ernst *et al.*, 2009; Ernst *et al.*, 2018). Over-expression of *mprF* in *B. subtilis* leads to a decrease in daptomycin susceptibility while deletion mutants of *mprF* increased daptomycin susceptibility (Hachmann *et al.*, 2009). In future investigations this could be considered as a potential genetic engineering target. However, the fact remains that the relationship between surface charge and precipitation is a very complex and delicate system and still likely to be very condition and strain dependent. Differences in surface

charge across strains may still have an effect on precipitation but modulating these within a strain is more likely to lead to detrimental effects, such as structural or homeostatic imbalances.

4.3.4 General summary.

In conclusion, under conditions assessed in this work, our results showed that heterologous urease expression was sufficient to bring about a precipitation phenotype in a bacterial strain of low intrinsic ability for BICP. This precipitation was dependent on the strength of ureolytic activity that could be enhanced by the supply of accessory nickel (*ureH)* and urease (*urt)* transporter genes. Thus, bacterial metabolic activity can be a driver of bacteria-induced precipitation if the required pH and ion concentrations for supersaturation and subsequent precipitation are reached. The more strongly this metabolic activity modulates supersaturation conditions, the more likely precipitation will occur. The findings reveal the first analysis of variations in urease gene composition on whole cell urease activity and calcite precipitation of a Gram-positive model and industrial relevant organism. Furthermore, the results showed that biofilm production synergises with ureolytic activity to increase the calcite precipitation, but was not on its own sufficient to drive biomineralisation. Of the biofilm components, exopolysaccharides were found to be the largest contributors to precipitation. Lastly, the results here also showed that modulation of surface charge was insufficient to promote precipitation in *B. subtilis* W168. From this comprehensive investigation of molecular features that drive BICP, the genetic targets *ureABCEFGD*, *ureH*, *urt* and *epsH* showed the best potential to control precipitation in *Bacillus*. Heterologous expression and changes in regulation of these genes in synergy will provide optimal targets to help engineer chassis organisms that are better suited to conditions in applied settings into strong precipitators for bacteria-induced calcite precipitation biotechnologies.

Chapter 5

Genetic Modification of the *Bacillus* Genus: A Conjugational Toolkit

ABSTRACT *Environmental strains of Bacillus species and close relatives prove to be promising in applications of microbe-induced calcite precipitation biotechnologies, but rational strain development is impeded by genetic inaccessibility. Here we report the development of a conjugational toolkit to expand the genetic accessibility of a range of undomesticated Bacillus species.*

5.1 Introduction.

Bacillus species and their close relatives are of particular interest for bacteria-induced calcite precipitation biotechnologies, particularly self-healing concrete, due to their ability to sporulate, as well as their potential for biofilm formation and alkali-tolerance (Chapter 2). Application of these bacteria in self-healing concrete to date has focused majorly on the identification and use of environmental isolates. Environmental bacteria well-suited to survive and grow under application conditions could however benefit from the introduction of foreign DNA to impart favourable metabolic and surface traits that improve overall biomineralisation properties and thus performance in application. While there has been recent work on genetic engineering of bacteria-induced calcite precipitation (Chapter 4), the development of well-suited chassis organisms as optimal calcite precipitates for application are often impeded by genetic inaccessibility (Hertel *et al.*, 2015; Heveran *et al.*, 2019). Improvements and expansion of genetic engineering techniques to include environmental *Bacillus* species that show promise in BICP technologies will help the development towards sustainable biotechnologies.

The first step in genetic manipulation of undomesticated strains relies on the ability to introduce recombinant DNA into the host. Methods for recombinant DNA uptake can be split into three separate categories; i) transformation, ii) transduction and iii) conjugation (Mazodier and Davies, 1991; Nazarian *et al.*, 2018). The first approach, transformation, involves the acquisition of DNA from the environment and can be achieved, amongst others, *via* i) chemical competence, ii) electrochemical competence or, iii) natural competence. Transformations involve a preparation step, whereby the recipient is prepared for DNA uptake, a 'shock' step, whereby the bacteria are exposed to a non-lethal shock which allows the DNA to permeate the cell, and a final recovery step, whereby the cell restores any damage (Aune and Aachmann, 2010). Chemical competence or chemo-transformation approaches disrupt cell surfaces by modifying cell membranes and weakening the cell wall, allowing for the easier uptake of DNA and this can further involve protoplast/spheroplast transformation (Aune and Aachmann, 2010). Electrochemical competence or electroporation builds on chemical competence and uses an electrical pulse alongside chemical surface disruption to facilitate DNA uptake by inducing temporary breakdown of the cell membrane for permeation. This method is also considered more efficient than chemo-transformation (Aune and Aachmann, 2010). The applicability and success of these two methods is dependent on membrane and cell wall structures, as well as restriction modification systems and nucleases of the recipients, which ultimately differ across strains (Aune and Aachmann, 2010). Furthermore, protoplast/spheroplast preparation is particularly time consuming and delicate (Heinze *et al.*, 2018; Aune and Aachmann, 2010). Therefore, transformation protocols cannot be readily transferred to

other strains (even of the same species) due to differential media requirements, chemical treatment and restriction/modification system differences (Heinze *et al.*, 2018). Similarly, electroporation also needs to be optimised for each cell in terms of media composition and electric field strength (Heinze *et al.*, 2018; Aune and Aachmann, 2010). In contrast, natural competence is reliant on intrinsic DNA-uptake machinery but is found only amongst limited species (Johnston *et al.*, 2014). It also requires induction of a regulated physiological state often achieved by growth in specific conditions and there is no generalised approach to achieve this state (Thomas and Nielsen, 2005). Thereby transformation protocols are generally limited by their specificity to each applied strain.

The second approach, transduction, relies on the ability of a bacteriophage to package bacterial chromosomal DNA or plasmid DNA (generalised-transduction) and transfer it to another strain (Deichelbohrer *et al.*, 1985). However, a major limitation to this approach is the typically narrow host range of bacteriophages (Yosef *et al.*, 2017). Limitations arise from factors such as restriction-modification systems in the host, as well as barriers to initial binding of the phage to the host (Bertozzi Silva *et al.*, 2016; Moller *et al.*, 2019).

The third approach, conjugation, is considered to have the broadest host range (Brophy *et al.*, 2018; Mazodier and Davies, 1991; Klümper *et al.*, 2015). Conjugation involves the transfer of mobile genetic elements from a donor cell to a recipient cell through direct contact, the transfer of plasmids being the most studied and characterised (Norman *et al.*, 2009). The process is dependent on the presence of transfer (*tra*) and mobilization (*mob*) genes (Raleigh, 2001; Ramsay and Firth, 2017). These encode for four components the origin of transfer (*oriT*), relaxase, type IV secretion system (T4SS) and type IV coupling protein (T4CP) (Smillie *et al.*, 2010). Plasmids transferred by conjugation are either classed as conjugative or mobilisable. Conjugative plasmids are self-transmissible, that is they carry the *oriT*, relaxase, T4SS and T4CP needed for transfer (Smillie *et al.*, 2010; Trokter and Waksman, 2018). Due to the self-transmissible nature, conjugative plasmids spread diverse phenotypes across populations and as such are considered a contributor to the spread of antibiotic resistance (Carattoli, 2013; Huddleston, 2014; Sultan *et al.*, 2018; Partridge *et al.*, 2018). Mobilisable plasmids can be transferred by co-resident conjugative plasmids or co-resident chromosomal conjugative elements (Strand *et al.*, 2014; Miyano *et al.*, 2018). As such mobilisable plasmids lack T4SS and typically contain only the *oriT*, relaxase, and T4CP (Smillie *et al.*, 2010), although plasmids with just an *oriT* have also been shown to be sufficiently mobilised (Ramsay and Firth, 2017; Miyano *et al.*, 2018). The conjugation process involves the relaxase recognising a phosphodiester bond at the *oriT,* producing a nick to which it binds at the 5' end to form a relaxosome complex. The T4CP interacts with the relaxosome to target the single stranded

plasmid DNA for transfer through the T4SS. In the recipient cell the plasmid then re-circularises and replicates to mature to a double stranded form (Miyano *et al.*, 2018; Prozorov, 2003; Smillie *et al.*, 2010; Grohmann *et al.*, 2003). Mobilisable plasmids can be transferred to a recipient to introduce genetic elements *via* triparental or biparental transfer, depending on the transfer function localisation (Schweizer, 2008). A schematic of the two methods is depicted in Figure 33.

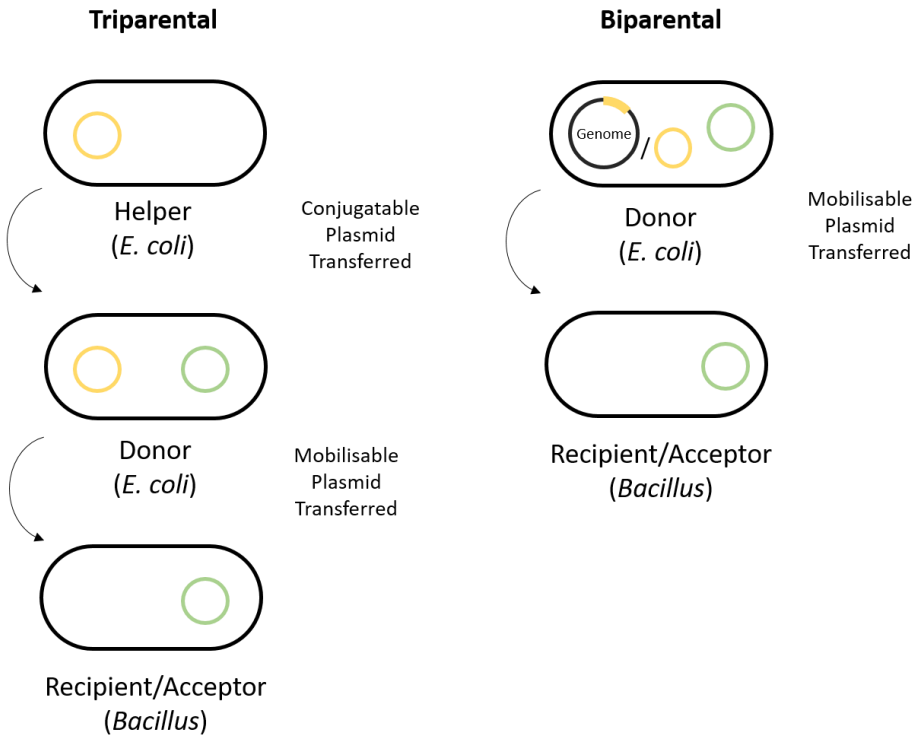

Figure 33. Triparental and biparental conjugation schematic. Triparental conjugation involves the transfer of a conjugative plasmid (yellow circle) from the helper strain to the donor strain. In the donor strain the conjugative plasmid transfers the mobilisable plasmid (green circle) to the target recipient/acceptor strain. Biparental conjugation involves the transfer of a mobilisable plasmid by conjugative elements present on the genome or on a co-resident conjugative plasmid in the donor strain to the target recipient/acceptor strain.

In triparental mating, a conjugative plasmid present in a helper strain is transferred to the donor strain containing the mobilisable plasmid. Once in the donor strain, the conjugative plasmid assists the transfer of the mobilisable plasmid to a recipient/acceptor strain (Heinze *et al.*, 2018). In biparental mating common donor strains like *E.coli* SM10/S17 and its derivatives (such as ST18/RH03) contain the conjugative IncP type plasmid RP4 integrated into their chromosome and can thus facilitate the mobilisation of plasmids bearing an RK2/RP4 *oriT* (Thoma and Schobert, 2009; Simon *et al.*, 1983; López *et al.*, 2009; Strand *et al.*, 2014). If biparental mating is to progress *via* a

co-resident conjugative plasmid it needs to be of a different incompatibility group compared to the mobilisable plasmid. In triparental mating if the conjugative plasmid and the mobilisable plasmid belong to the same Inc group, they do not need to be stably maintained in the donor strain for transfer to occur. Plasmids are divided into Inc groups depending on their replication and partitioning system. Plasmids of the same Inc group cannot exist stably over generations in a cell (Novick, 1987; Kittell and Helinski, 1993; Thomas, 2014). A disadvantage to conjugation is the length of the procedure (Zeaiter *et al.*, 2018). While conjugation offers a broad host range, some barriers still exist such as general establishment of foreign DNA (discussed in the following paragraph). Ultimately the efficiency of successful transfer of DNA is dependent on donor strain conjugation initiation, mating conditions, and establishment in recipient (Dimitriu *et al.*, 2019; De Gelder *et al.*, 2005).

Barriers to establishment of the acquired DNA in the recipient are due to genetic compatibility and apply to all methods for recombinant DNA transfer. The genes of a plasmids origin of replication will determine host range and stable maintenance. Similarity of the plasmid DNA with the recipient genome could further facilitate wanted or unwanted chromosomal integration through recombination (Thomas and Nielsen, 2005). Host defence systems may recognise the DNA as foreign and may target it for degradation. This can be through restriction modification systems recognising methylation patterns or other specific sites (Thomas and Nielsen, 2005; Aune and Aachmann, 2010). Conjugation is thought to offer some protection to intrinsic restriction systems as a result of the transfer of single stranded DNA compared to double stranded DNA (Thomas and Nielsen, 2005; Lacks and Springhorn, 1984). Once a plasmid has established, recipient-compatible selection markers are required to select for plasmid-bearing strains such as antibiotics, other antimicrobials or metabolic markers (Schweizer, 2008). In conjugation, further counter-selection is required to separate donor, recipients, and transconjugants. Counter-selection can take advantage of intrinsic bacterial properties and physiology such as antimicrobial resistances, metabolic properties or plasmid properties such as temperature sensitive replicons (Schweizer, 2008). Lastly, it is required that promoters, gene products and other genetic elements are compatible with the host's cellular machinery (Schweizer, 2008).

Bacillus species are a major workhorse for biotechnology, particularly in the production of enzymes, vitamins and surfactants, amongst others (Sansinenea, 2011; Schallmey *et al.*, 2004; Preiss *et al.*, 2015). This has led to the development of an array of genetic engineering approaches as most wildtype and industrial strains have low natural genetic competence (Hertel *et al.*, 2015; Duitman *et al.*, 2007). Non-exhaustive examples of existing strategies include phage transduction (Yasbin and Young, 1974), protoplast transformation (Romero *et al.*, 2006; Chang and Cohen, 1979;

Akamatsu and Sekiguchi, 1982), electroporation (Xiao *et al.*, 2014; Xue *et al.*, 1999), and conjugation (Prozorov, 2003; Heinze *et al.*, 2018; Poyart and Trieu-Cuot, 2006; Trieu-Cuot *et al.*, 1987; Tominaga *et al.*, 2016; Kostner *et al.*, 2017; Charpentier *et al.*, 1999; Miyano *et al.*, 2018; Brophy *et al.*, 2018; Hertel *et al.*, 2015; Rachinger *et al.*, 2013; Richhardt *et al.*, 2010).

While a range of techniques have been developed over the years for the transfer of foreign DNA into *Bacillus* species, each with their advantages and limitations, there is still scope to expand host range. In the field of self-healing concrete alkaliphilic bacteria are of particular interest. These have seen limited gene transfer techniques in literature, encompassing, to our knowledge, only electroporation (Ito and Nagane, 2001) and protoplast transformation (Ito *et al.*, 1997; Kudo *et al.*, 1990; Gao *et al.*, 2011). The downside to these methods is that they require the adjustment of conditions for different strains that have to be determined experimentally for each new recipient (Tominaga *et al.*, 2016). In contrast, conjugation offers an approach whereby large plasmids can be transferred to a broad host range (Schweizer, 2008; Thomas and Nielsen, 2005). Therefore, we strived to develop a biparental conjugational method for the transfer of a mobilisable plasmid that has a wide host range to include *Bacillus* species favourable for self-healing concrete applications, such as alkaliphilic *Bacillus pseudofirmus*. Expanding genetic engineering tools will allow for the future development of improved bacteria-induced calcite precipitating strains for application in self-healing concrete using rational strain development.

5.2 Results.

5.2.1 Construction of the mobilisable reporter plasmid pAT28-P_{veg}-GFPmut1.

The aim of this investigation was to construct a broad host range mobilisable vector for Gram-positive bacteria with a GFP reporter to explore the range of *Bacillus* species in which such a recombinant plasmid can be introduced through conjugation. A similar approach, but through transformation, was previously explored whereby a green fluorescent variant of vector pAT28 was electroporated into a range of *Streptococcus*, *Enterococcus* and *Staphylococcus* strains (Aymanns *et al.*, 2011). Therefore we chose the plasmid backbone to be derived from vector pAT28, which is mobilisable from *E. coli* to Gram-positives using co-resident IncP transposable elements (Trieu-Cuot *et al.*, 1990). The plasmid pAT28 contains the *oriT* from the IncP plasmid RK2, *E. coli* origin of replication from the pUC plasmids (specifically pBM1), origin of replication in Gram-positives from the *Enterococcus* plasmid pAMß1 (*repE*) and a *Staphylococcus* spectinomycin resistance marker expressed in both Gram-positives and Gram-negatives (Murphy, 1985; Yanisch-Perron *et al.*, 1985; Trieu-Cuot *et al.*, 1990; Leblanc and Lee, 1984). It had also been previously shown that pAMß1 replicates in *Bacillus subtilis* (Bruand and Ehrlich, 1998), suggesting that with this specific replication

origin pAT28 could be promising as a mobilisable plasmid for bacilli. To construct pAT28-P_{veg}-GFPmut1, the GFPmut1 gene encoding a green fluorescent protein codon-optimised for *Bacillus subtilis* (Thorsten Mascher Lab) under the control of the *B. subtilis* constitutive promoter P_{veg} (Lam *et al.*, 1998) was inserted into the pAT28 multiple cloning site. A fluorescent reporter gene was chosen to act as an additional marker to verify plasmid uptake and to determine whether the promotor would drive gene expression in the chosen host. A plasmid map of pAT28-P_{veg}-GFPmut1 is depicted in Figure 34.

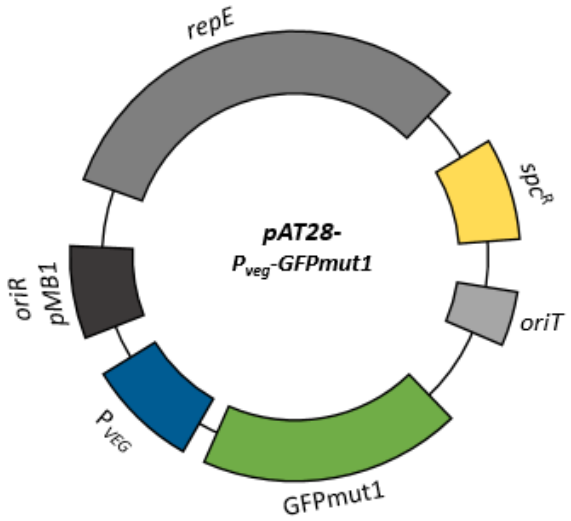

Figure 34. Plasmid pAT28-P_{veg}-GFPmut1, used for the mobilisation to and fluorescent labelling of a broad host range of Gram-positives. Plasmid derived from pAT28 with origin of replication (for Gram-positive hosts, *repE*, and Gram-negative hosts, ori pMB1), origin of transfer (*oriT*), as well as spectinomycin resistance gene (spc^R) indicated. *Bacillus subtilis* constitutive promoter P_{veg} controls expression of a *B. subtilis* codon optimised GFPmut1 green fluorescent protein.

5.2.2 Establishment of selection and counter-selection conditions for all recipient species tested.

The object was to test the introduction of the plasmid pAT28-P_{veg}-GFPmut1 carrying a spectinomycin resistance marker *via* conjugation into the *Bacillus* species *B. subtilis* ATCC 6633, *B. licheniformis* DSM 13, *B. paralicheniformis* ATCC 9945a and *B. cohnii* DSM 6307 and *B. pseudofirmus* DSM 8715. Minimal inhibitory concentrations of spectinomycin for the *Bacillus* species were established prior so as to enable selection of colonies harbouring the plasmid pAT28-P_{veg}-GFPmut1 after conjugation. Table 5 shows the spectinomycin resistance to four of the *Bacillus* species. The results showed that some strains could grow at a spectinomycin concentration of 50 µg/ml but none at 75 µg/ml of 100 µg/ml, and thus 100 µg/ml spectinomycin was used for selection. Donor *E. coli* SM10 was chosen over S17 as, unlike its counterpart, it is not resistant to spectinomycin/streptomycin (Simon *et al.*, 1983). Further, sufficient resistance of the *Bacillus*

species against polymixin B had to be demonstrated in order to ensure counter-selection against the donor *E. coli* from the conjugation mixture. For alkaliphilic *Bacillus* strains growth on LB Alk was used as the counter-selection against the donor *E. coli*. Table 6 shows the susceptibility of polymixin B to the donor *E. coli* and the three non-alkaliphilic *Bacillus* strains. The results showed that *E. coli* SM10 was susceptible to polymixin B at a concentration over 2.5 µg/ml, while the *Bacillus* species were all resistant up to a concentration of 20 µg/ml, and thus 20 µg/ml polymixin B was used as counter-selection.

Table 5. Establishing spectinomycin resistance for plasmid selection.

Strain	Spectinomycin Concentration µg/ml			
	25	50	75	100
B. subtilis ATCC 6633	✓	✗	✗	✗
B. licheniformis DSM 13	✓	✓	✗	✗
B. paralicheniformis ATCC 9945a	✓	✓	✗	✗
B. cohnii DSM 6307	✓	✗	✗	✗

Strains were grown in overnight cultures at 30°C with varying spectinomycin concentrations. Growth (✓) / no growth (✗) indicated.

Table 6. Establishing polymixin resistance for donor counter-selection.

Strain	Polymixin Concentration µg/ml			
	2.5	10	20	40
E. coli SM10	✓	✗	✗	✗
B. subtilis ATCC 6633	✓	✓	✓	✗
B. licheniformis DSM13	✓	✓	✓	✓
B. paralicheniformis ATCC 9945a	✓	✓	✓	✓

The bacteria were streaked in small patches onto LB plates with varying polymixin concentrations, incubated overnight at 30°C for bacilli and 37°C for *E. coli*. Growth (✓) / no growth (✗) indicated.

5.2.3 Transfer of pAT28-P_{veg}-GFPmut1 to different Gram-positive bacteria.

Biparental conjugative transfer of pAT28-P_{Veg}-GFPmut1 from *E. coli* SM10 to various *Bacillus* species was carried out as described in the methods section (Chapter 3). A range of different ratios of donor *E. coli* to recipient bacilli were tested. Generally, for slow-growing bacilli strains the donor to

acceptor ratio of 1:10 was chosen as to avoid outcompeting by the faster growing *E. coli*. Where the bacilli strains grew faster than the *E. coli*, a donor to acceptor ratio of 10:1 or 3:1 was used. Puddle mating was conducted at 37°C on LB agar across all combinations tested, as it is the preferred environment of the donor. Puddle mating was left for approximately 24h hours to increase the chance of successful transfer. Selection for recipients, transconjugants and donors occurred on selection plates, as explained in the previous section, at 30°C. After selection, colonies were transferred to fresh plates to confirm antibiotic resistance. Subsequently, colonies were analysed with a colony PCR using primers SG1053/SG1054 to amplify a fragment of the GFPmut1 gene to determine plasmid uptake.

Table 7. Transfer of pAT28-P_{veg}-GFPmut1 to different Gram-positive bacteria.

Strain	Conjugation/Transformation (Donor:Acceptor)	Resistance	PCR
B. subtilis W168	Transformation	✓	✗
B. subtilis ATCC 6633	Conjugation (3:1)	✗	✗
B. cohnii DSM 6307	Conjugation (1:10)	✓	✗
B. pseudofirmus DSM 8715	Conjugation (1:10)	✓	✗
B. licheniformis DSM13	Conjugation (3:1)	✗	✗
B. paralicheniformis ATCC 9945a	Conjugation (1:10)	✓	✗
	Conjugation (3:1)	✓	✗
	Conjugation (10:1)	✓	✗
E. faecalis	Electroporation	✓	✓

Successful establishment of plasmid was determined through growth with antibiotics, where growth (✓) indicated plasmid derived resistance and thus uptake, and no growth (✗) indicated no plasmid uptake. Additionally colony PCR was carried out, where (✓) indicates successful amplification of plasmid DNA and thus uptake, and (✗) indicates unsuccessful amplification of plasmid.

The results for the transfer of pAT28-P_{Veg}-GFPmut1 to different Gram-positive bacteria are tabulated in Table 7. Unexpectedly, the plasmid did not successfully establish in any of the *Bacillus* strains tested. Mobilisation of the plasmid into *B. licheniformis* and *B. subtilis* ATCC 6633 yielded no observable colonies on the transconjugants selection plates and thus, conjugation was regarded unsuccessful. For *B. paralicheniformis* colonies formed and grew on selection and patch plates, however transconjugants yielded no positive colony PCR (data not shown). The retrieved colonies

were possibly spontaneous mutants or the strong biofilm phenotype of *B. paralicheniformis* may have allowed them to grow despite the antibiotic, consequently the conjugation was considered unsuccessful. The alkaliphilic bacilli *B. cohnii* and *B. pseudofirmus* formed colonies on the selection and replicated plates, but subsequent colony PCR failed to yield a positive result (Figure 35, Panel A). Further attempts to improve colony PCR through modification of lysis protocols or to retrieve the whole plasmid did not yield results (data not shown). This was also evident when the colonies that grew on selective LB Alk solid media did not grow in liquid culture under the same selection. The antibiotic concentration in liquid media had to be reduced to 5 µg/ml to allow growth, which is not selective and thus, like with *B. paralicheniformis* the obtained colonies were considered false-positives. As a control to check the functionality of the plasmid without relying on the conjugation machinery, *B. subtilis* W168 was transformed with plasmid pAT28-P_{Veg}-GFPmut1. The colony morphology of the resultant transformants was not typical for strain W168, growing much more slowly and forming smaller colonies. Testing these colonies did not yield a positive colony PCR (Figure 35, Panel B), and it was therefore concluded that the plasmid was not successfully established. As a further control the plasmid was electroporated into *Enterococcus faecalis*; this yielded positive transformants as determined by antibiotic resistance and colony PCR (Figure 35, Panel C).

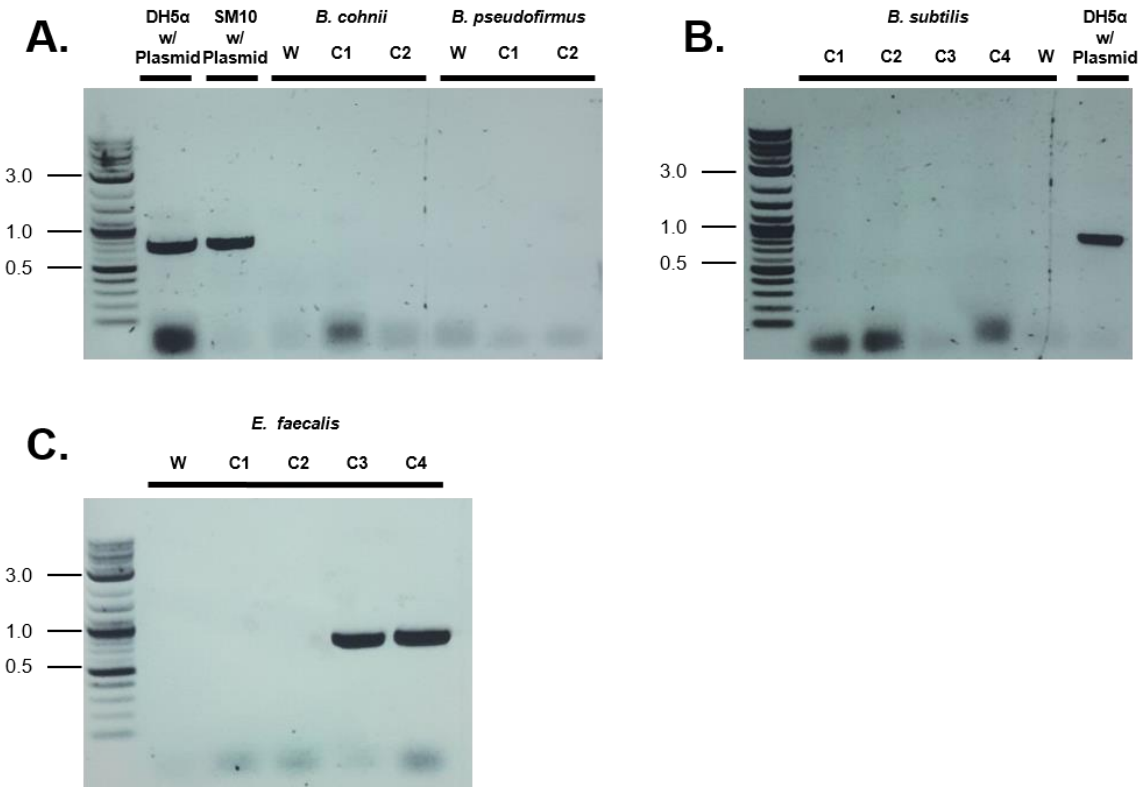

Figure 35. Colony PCR of transformants / transconjugants for the presence pAT28-Pveg-GFPmut1. To confirm the presence of pAT28-P_{veg}-GFPmut1, colony PCR was conducted with primers SG1053/SG1054 to target a 743 bp fragment of the GFPmut1 gene. (A) Colony PCR of alkaliphilic *B. cohnii* and *B. pseudofirmus* transconjugants, (B) *B. subtilis* W168 transformants and *E. faecalis* transformants. Sizes of key bands in the DNA ladder are shown in kb.

The lack of plasmid establishment in *B. subtilis* was surprising as the replication of origin of pAT28 (*repE* from pAMß1) had been previously shown to drive the successful replication of the plasmid pAMß1 in *B. subtilis* (Bruand and Ehrlich, 1998). The *repE* origin of replication was also present on pAT187 which was previously shown to be mobilisable to *B. thuringiensis* (Trieu-Cuot *et al.,* 1987). The lack of establishment of the plasmid both *via* conjugation and transformation suggested that the problem was likely not a result of conjugation itself. Establishment of the plasmid in *E. faecalis* showed that the plasmid was functional, and more likely just better-suited to its primary intended hosts *Enterococcus*/*Streptococcus* (Trieu-Cuot *et al*., 1990; Aymanns *et al.,* 2011). This is in line with other research where a pAT28 plasmid was constructed carrying the green fluorescent protein gene *egfp* and subsequently successfully electroporated into a range of *Enterococcus*, *Streptococcus* and *Staphylococcus* species (Aymanns *et al*., 2011). Elucidating the precise reason for a lack of establishment of pAT28-P_{veg}-GFPmut1 in the bacilli strains tested in this study was not the scope of this investigation, and as such the focus was shifted to finding an alternative plasmid.

5.2.4 Construction of the mobilisable reporter plasmid pDG148-P_{veg}-GFPmut1-oriT and establishment of selection and counter-selection conditions.

After the pAT28 derived plasmid was found to be unsuccessful for conjugation into the tested *Bacillus* species the next step was to use a plasmid that was well established for use in *Bacillus* species. Consequently a mobilisable plasmid based on the *Bacillus subtilis* replicative vector pDG148-stu (Joseph *et al.,* 2001) was constructed. Plasmid pDG148 contains the broad host range replication origin *repB* from pUB110 that uses rolling-circle replication (McKenzie *et al.*, 1986; Allignet *et al.*, 1998); the replicon was previously denoted *repH*/*repU* (Khan, 1997; Müller *et al.*, 1995; Alonso *et al.*, 1988). In contrast, pAT28 with its *repE* replicon, replicates by the theta mechanism (del Solar *et al.*, 1998; Lilly and Camps, 2015; Bruand and Ehrlich, 1998). Plasmid pUB110 was originally isolated from *Staphylococcus* but was found to be transferable to *B. subtilis* (Gryczan *et al.*, 1978; Boe *et al.*, 1989). Plasmid pUB110 was also previously electroporated into *B. pseudofirmus* OF4, and transferred by conjugative transposon Tn925 into *B. pseudofirmus* (Guffanti *et al.*, 1991; Ito and Nagane, 2001). Therefore, pDG148-stu posed to be a promising backbone for construction of a mobilisable plasmid for *Bacillus* species. The first step was to engineer the mobility

function into pDG148-stu by introducing an *oriT* that had been shown to work for conjugative transfer of a plasmid from *E. coli* to *Geobacillus* (David Leak, personal communication). The IncP type *oriT* was amplified from pDG2k-oriT-GFP-GG_ready (David Leak Lab) and cloned into the BamHI restriction site of pDG148-stu. In initial preliminary tests, the plasmid pDG148-oriT was transferred from the *E. coli* donor strain S17 to *B. subtilis* W168 using 10 µg/ml kanamycin as selection and 20 µg/ml polymixin as counter-selection. This was done to establish plasmid functionality before the addition of the fluorescent marker and testing to further bacilli. In this instance, donor *E. coli* S17 was chosen over SM10 as, unlike its counterpart, it is not resistant to kanamycin which allows kanamycin to be used as an additional antibiotic marker alongside zeocin on pDG148-P_{Veg}-GFPmut1-oriT (Simon *et al.*, 1983). The test was successful as determined by a colony PCR using primers SG1073/SG1074 and showed that *oriT* was functional for transfer of a pDG148-stu from an *E. coli* to a *Bacillus*. To test gene expression the next step was to introduce the P_{veg}-GFP reporter (as described previously) into the Stu1 restriction site of pDG148-stu-oriT to construct pDG148-P_{veg}-GFPmut1-oriT. A plasmid map of pDG148-P_{veg}-GFPmut1-oriT is depicted in Figure 36.

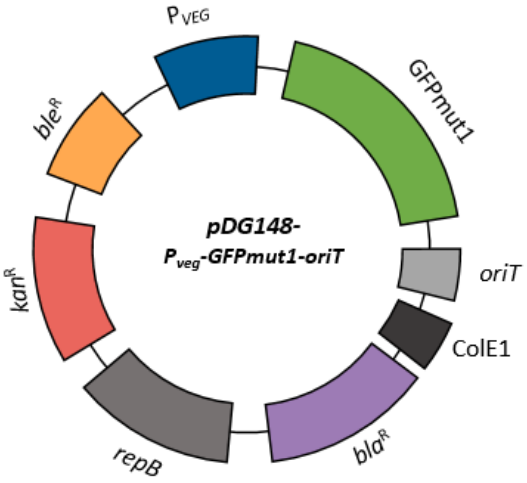

Figure 36. Plasmid pDG148-Pveg-GFPmut1-oriT, used for the mobilisation to and fluorescent labelling of a broad host range of Gram-positives. Plasmid derived from pDG148-stu with origin of replication (for Gram-positive hosts, *repB*, and Gram-negative hosts, ColE1), origin of transfer (*oriT*), as well as kanamycin (*kan*^{R}), ampicillin (*bla*^{R}) and bleomycin/phleomycin (ble^R) resistance genes indicated. The constitutive *B. subtilis* promoter P_{veg} controls expression of a *B. subtilis* codon optimised GFPmut1 green fluorescent protein.

For introduction of the plasmid pDG148-P_{veg}-GFPmut1-oriT via conjugation into the *Bacillus* species *B. subtilis* W168, *B. pseudofirmus* DSM 8715 and *B. cohnii* DSM 6307, the selection marker had to be changed from kanamycin (as used in the initial trial). This was because strains *B. pseudofirmus*

and *B. cohnii* were resistant to kanamycin when grown in overnight cultures up to the tested maximum of 1000 µg/ml (Table 8). Therefore minimal inhibitory concentrations of zeocin for the *Bacillus* species were established prior so as to enable selection of colonies harbouring the plasmid pDG148- P_{veg}-GFPmut1-oriT after conjugation. Counter-selection against the *E. coli* was done as previously described for the respective bacilli. Table 9 shows the zeocin resistance of the three *Bacillus* species. The results showed that all wildtype strains were susceptible to a Zeocin concentration of 10 µg/ml and thus 20 µg/ml zeocin was used for selection.

Table 8. Establishing kanamycin resistance of alkaliphiles.

Strain	Kanamycin Concentration µg/ml						
	0	10	50	100	250	500	1000
B. pseudofirmus DSM 8715	✓	✓	✓	✓	✓	✓	✓
B. cohnii DSM 6307	✓	✓	✓	✓	✓	✓	✓

Strains were grown in overnight cultures at 30°C with varying kanamycin concentrations. Growth (✓) / no growth (✗) indicated.

Table 9. Establishing zeocin resistance for plasmid selection.

Strain	Zeocin Concentration µg/ml					
	0	10	20	40	80	100
B. subtilis W168	✓	✗	✗	✗	✗	✗
B. subtilis W168 + pDG148-oriT	✓	✓	✓	✓	✓	✓
B. pseudofirmus DSM 8715	✓	✗	✗	✗	✗	✗
B. cohnii DSM 6307	✓	✗	✗	✗	✗	✗

Strains were grown in overnight cultures at 30°C for alkaliphiles and 37°C for *B. subtilis* with varying zeocin concentrations. Growth (✓) / no growth (✗) indicated.

5.2.5 Transfer of pDG148-P_{veg}-GFPmut1-oriT to Gram-positive bacteria.

Biparental conjugative transfer of pDG148-P_{Veg}-GFPmut1-oriT from *E. coli* S17 to bacilli species was carried out as described in the methods section (Chapter 3). The work-flow for establishing transfer of the plasmid to the Gram-positive bacteria followed that described in section 5.2.3. Plasmid pDG148-P_{Veg}-GFPmut1-oriT was successfully established in *B. subtilis* W168 and *B. pseudofirmus*

DSM 8715, as confirmed by zeocin resistance (Table 10) and colony PCR amplifying the P_{veg}-GFPmut1 insert (Figure 37). Due to the global situation regarding SARS-CoV-2 some of the following conjugations and fluoresce measurement experimental work had to be postponed and could not be completed in the scheduled timeframe of this project and therefore lack some substantiation. Results so far for conjugation into *B. pseudofirmus* found a conjugation ratio of 10:1 (Donor to Acceptor ratio) yielded an average of forty times more transconjugants colonies than a ratio of 1:10 (Table 10). Preliminary conjugation efficiencies were calculated to be 1.18 for *B. subtilis* W168 (ratio 10:1), 5.91×10^{-4} for *B. pseudofirmus* (ratio 10:1) and 1.25×10^{-5} for *B. pseudofirmus* (ratio 1:10).

Table 10. Transfer of pDG148-P_{veg}-GFPmut1-oriT to Gram-positive bacteria.

Strain	Conjugation (Donor:Acceptor)	Resistance (CFU/ml transconjugants)	PCR
B. subtilis W168	Conjugation (10:1)	✓ (1.97×10^{3})	✓
B. pseudofirmus DSM 8715	Conjugation (10:1)	✓ (2.60×10^{6})	✓
	Conjugation (1:10)	✓ (6.42×10^{4})	✓

The CFU/ml of transconjugants was calculated from the number of colonies present in three separate 20 µl spots on the respective selection plates. CFU/ml results are of one biological repeat for *B. subtilis* W168, the average of two biological repeats for *B. pseudofirmus* (1:10) and the average of three biological repeats for *B. pseudofirmus* (10:1).

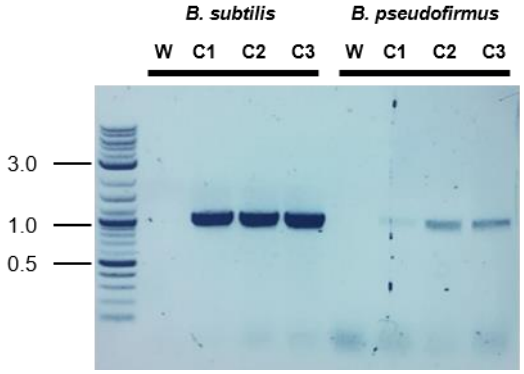

Figure 37. Colony PCR of transconjugants for the presence pDG148-Pveg-GFPmut1-oriT. To confirm the presence of pDG148-P_{veg}-GFPmut1-oriT colony PCR was conducted with primers SG1075/SG1077 to target the 1029 bp P_{veg}-GFPmut1 insert. Sizes of key bands in the DNA ladder are shown in kb.

5.2.6 Measurement of GFPmut1 fluorescence.

After successfully establishing the transfer of pDG148-P_{Veg}-GFPmut1-oriT from *E. coli* S17 to *B. subtilis* W168 and *B. pseudofirmus* DSM 8715 the objective was to test the expression of the gfp gene on the plasmid in the new hosts to determine promotor and gene functionality. Therefore relative fluorescence of the wildtype and respective transconjugants was measured. Transconjugants with a greater fluorescence than the wildtype would be evidence of successfully expressing GFPmut1. Fluorescence was measured in overnight cultures and in exponentially growing cells and the results are summarised in Table 11. Results identified fluorescence to be strongest in strains form overnight cultures with an average increase in transconjugants fluorescence relative to the respective wildtype at 5.4-fold for *B. subtilis* and 2.2-fold for *B. pseudofirmus*. This showed that gene expression was possible from pDG148-stu-oriT using the promoter P_{veg} not just in *B. subtilis* W168 but also in the alkaliphile *B. pseudofirmus* DSM 8715. The result is a plasmid system that can be mobilised from *E. coli* to not only neutrophilic lab strain, but also an alkaliphilic *Bacillus* species for which introduction of foreign DNA to date has only been achieved via protoplast transformation and electroporation. Furthermore the constitutive promoter P_{veg} from *B. subtilis* can be used to drive expression of genes inserted into the MCS of this plasmid, allowing for heterologous gene expression in the host.

Table 11. GFPmut1 fluorescens of bacilli carrying the pDG148-P_{Veg}-GFPmut1-oriT.

Strain	Relative fluorescence/OD_{600}	
	Transconjugants (A / B)	Wildtype
B. subtilis (overnight)	107,624 / 69,741	16,266
B. pseudofirmus (overnight)	64,743±2,274**** / 73,808±11,824**	31,459±2,173
B. subtilis (sub culture)	78,383 / 92,143	28,726
B. pseudofirmus (sub culture)	62,378±4,804** / 60,743±4,410**	43,604±3,872

For overnight growth strains were grown overnight in LB at 37°C for *B. subtilis* and LB Alk at 30°C, for *B. pseudofirmus*. For subcultures strains were inoculated to an OD_{600}=0.1 and grown in LB at 37°C for *B. subtilis* and LB Alk at 30°C, for *B. pseudofirmus* until and OD_{600}=0.5. End-point fluorescence (excitation at 479 nm and emission monitored at 520 nm) and OD_{600} were measured in a SYNERGY H1 microplate reader. Results are from one biological repeat for *B. subtilis* and the average of three biological repeats for *B. pseudofirmus*. Two independent clones A and B for transconjugants and one independent clone for the wildtype were used. Results for *B. pseudofirmus* include the standard deviation and un-paired t-tests between the transconjugant and wildtype where ** is p≤0.01 and **** is p≤0.0001.

5.3 Discussion.

The objective of this investigation was to develop a mobilisable plasmid for conjugation into a range of *Bacillus* species for use as an expression vector. Initial trials with the broad host range mobilisable plasmid pAT28-P_{VEG}-GFPmut1 for Gram-positive bacteria surprisingly did not show any establishment in *B. subtilis*, *B. licheniformis*, *B. paralicheniformis*, *B. cohnii or B. pseudofirmus* (Table 10 and Figure 35). Subsequently, an established *Bacillus subtilis* replicative vector, pDG148-stu, was chosen and an *oriT* was successfully introduced to make it mobilisable for conjugation as well as a selection regime determined that works for a range of *Bacillus* species. With the addition of a promoter driven GFP gene the final constructed plasmid pDG148-P_{VEG}-GFPmut1-oriT, successfully transferred and established *via* biparental mating to *B. pseudofirmus* DSM 8715 and *B. subtilis* W168 as demonstrated by antibiotic resistance of transconjugants and a positive colony PCR (Table 10 and Figure 37). While there have been some studies on conjugation in *B. subtilis* strains (Prozorov, 2003; Miyano *et al.*, 2018) the ability of this plasmid to conjugate through biparental inheritance from *E. coli* to *B. subtilis* W168 further opens the possibility of conjugation into other strains of *B. subtilis* that are not naturally competent, such as the model biofilm producer *B. subtilis* NCIB 3610 or the industrial relevant *B. subtilis* var. natto. Expanding their respective genetic engineering toolkits with such a system is desirable from both a biotechnological point of view as well as a laboratory research perspective. Most notable however was that establishment of the plasmid in *B. pseudofirmus* where the transconjugants showed an average 2-2-fold higher GFP fluorescence compared to the wild type (Table 11). This confirmed that the strong *Bacillus* constitutive promoter P_{veg} functioned in an alkaliphilic *Bacillus* species and was able to drive the expression of the *B. subtilis* codon optimised green fluorescent protein GFPmut1. The results show, to our knowledge, the successful construction of the first mobilisable plasmid for transfer from *E. coli* to alkaliphilic bacilli. To date, one conjugative plasmid from an alkaliphilic and halotolerant Bacillaceae strain has been identified and was suggested by the authors to offer the potential to function as a cloning vector to shuttle between alkaliphilic Bacillaceae and *E. coli*, *Bacillus* spp. and *Staphylococcus* spp., but this was not developed further (Guo and Mahillon, 2013). This plasmid contains a different replication of origin shown to be functional in *B. thuringiensis*, *B. subtilis* and *S. aureus* (Guo and Mahillon, 2013). Establishment of pDG148- P_{veg}-GFPmut1-oriT but not pAT28-P_{veg}-GFPmut1 in *Bacillus* suggested that possibly *repB* was better suited for bacilli than *repE*. This is in line with previous investigations where plasmids used for genetic engineering of alkaliphilic *Bacillus pseudofirmus* OF4 contained *repB* (specifically plasmids pUB110 and pYH56) (Ito *et al.*, 1997; Ito and Nagane, 2001).

Further work needs to be conducted to determine the precise host range and efficiencies of conjugational transfer of pDG148- P_{veg}-GFPmut1-oriT to encompass potential hosts for self-healing concrete such as *B. licheniformis*, *B. paralicheniformis* and *B. cohnii* among others. Additional species of interest would include the many bacilli used in biotech such as *B. thuringiensis*, *B. clausii* and *B. halodurans* but also medically important bacilli like *B. cereus* and *B. anthracis* which have few genetic tools. The plasmid pDG148-oriT may offer to be a versatile vector for the transfer of various genetic traits into a host and could be very useful for fundamental lab research as well as biotechnology. Gene expression could be driven from P_{veg} but further promoters could also be tested. The GFP could be used as a reporter for transcription/translation events with uncharacterised promoters. Systems could also be created whereby a regulator/promoter pair in conjunction with a reporter like GFP could be used to make biosensors. In context of this PhD project investigation it would be interesting to explore transfer of genetic traits that help promoter calcite precipitation into a range of environmental isolates better suited to concrete application. For example, urease genes could be shuttled to the Gram-positive environmental isolate MM1_1, a non-ureolytic biofilm producer shown to have potential in self-healing mortars (Reeksting *et al.*, 2020) or non-ureolytic alkaliphilic *B. cohnii* and *B. pseudofirmus* (Sharma *et al.*, 2017). This would be the next step towards the rational design of better precipitators suited to application, once target genes are identified.

To increase the potential for such genetic engineered strains to be suitable for biotechnologies, a few further considerations need to be taken. Replicating plasmids require selective pressures usually from antibiotics to be maintained within the cell or can otherwise be lost (Oliveira and Mairhofer, 2013; Kachroo *et al.*, 2009). However, addition of antibiotics to self-healing concrete would not be practical for a number of different reasons including costs, stability and efficacy. Additionally, such plasmids may disseminate among environmental communities possibly contributing to the spread of antibiotic resistance. To avoid this, the genetic information could be stably integrated into the chromosome without the need of an antibiotic marker. This can be achieved among others *via* site-specific recombinases such as tyrosine recombinases or serine integrases (Olorunniji *et al.*, 2017; Gaj *et al.*, 2014; Yan *et al.*, 2008). Chromosomal integration techniques are often strain specific and therefore better-suited to development once an ideal strain is found. For alkaliphiles, to our knowledge, there is a lack of chromosomal integration techniques. A solution could be the use of bacteriophage site specific recombinases. The genome of BCJA1 alkaliphilic bacteriophage active against *Bacillus clarkii* contains a tyrosine recombinase (Kropinski *et al.*, 2005); these facilitate the integration between a phage sequence site *attP* and bacterial sequence site *attB*. Phage isolated from haloalkaline environments may harbour further

recombinase/integrases that could be capitalised on (Van Zyl *et al.*, 2016). These potentially offer the parts to engineer more complex systems that allow for chromosomal cassette exchange whereby multiple *attP*/*attB* sites allow for a targeted region (or expression module) of a plasmid to be integrated onto the chromosome (Stark, 2017). This would lead to the loss of selection markers like antibiotic resistance genes and other plasmid replicative genes during strain construction. Another approach to circumvent the use of antibiotics is through toxin-antitoxin systems also known as plasmid addiction systems. These consist of a protein toxin that in the absence of the antitoxin can inhibit cellular processes, as well as a protein or RNA antitoxin which under normal growth inhibits the toxin (Page and Peti, 2016). In biotechnology this can be capitalised on by expressing a toxin gene on a bacterial chromosome or plasmid to ensure prevalence of a plasmid containing the antitoxin. Thereby the system stabilises plasmid presence within cells without the need for antibiotic markers and antibiotic use (Unterholzner *et al.*, 2013).

Overall, this work has been a first step towards expanding the genetic engineering toolbox of *Bacillus* to encompass strains suited for self-healing concrete application. The plasmid pDG148-oriT and promoter P_{veg} can be used as the basis to drive gene expression in application relevant bacilli with the aim to facilitate their rational strain improvement.

Chapter 6

Final Discussion

ABSTRACT *This Chapter Discusses how the results presented in this thesis fit into the bigger picture of BICP and self-healing concrete development. Future prospects, challenges and next steps for the field of BICP, self-healing concrete and other related technologies are addressed.*

6.1 Final discussion.

6.1.1 Conclusion of findings: a new picture of BICP.

The aim of this project was to explore the genetic optimisation of bacteria-induced calcite precipitation to be able to develop improved precipitators better suited for self-healing concrete application. As part of the first objective, we identified that engineering of ureolytic activity was sufficient to drive precipitation in the intrinsically low calcite precipitator *Bacillus subtilis* W168 (Chapter 4). Characterisation of the urease genes revealed that accessory urea and nickel transporter genes can increase urease activity and precipitation by overcoming urea or nickel bottlenecks. The second objective was to characterise the role of surface charge and biofilm on calcite precipitation. It was found that surface charge by itself, and in conjugation with ureolysis, did not improve calcite precipitation (Chapter 4). On the other hand, biofilm production, particularly the exopolysaccharide component of EPS, synergised with ureolytic activity to increase calcite precipitation ability of *B. subtilis* W168 (Chapter 4). Together, these investigations identified genetic 'modules' that bring about favourable calcite precipitation. Currently, legislation would limit the use of genetically modified organisms in application, but with the knowledge gained on which genetic elements contribute to precipitation, better screens for environmental strains could be carried out. Targeted selection for ureolytic and biofilm bacteria from the environment should reveal ones that have a strong calcite precipitation phenotype. As part of the final objective, a mobilisable plasmid was developed that was able to be shuttled to alkaliphilic bacilli already used in self-healing concrete (Chapter 5). This provides the tool whereby the previously identified favourable genetic 'modules' can be transferred to a better suited organism for application. These results provide the first systematic approach to identifying genetic components of calcite precipitation in a Gram-positive model and industrially relevant organism *Bacillus subtilis* W168 as well as potentially mobilising these to various Gram-positives. The findings pave the way to select for or rationally design better suited precipitators for application.

The findings of this project also expand our fundamental understanding of BICP, particularly how multiple factors can synergistically influence the calcite precipitation ability of a bacterium. Modulating ureolytic activity on its own was found to contribute more strongly to calcite precipitation than modulating biofilm formation (Chapter 4). This is because ureolysis increases the pH which pushes the carbonate equilibrium towards CO_3^{2-}, thus increasing the saturation index to thermodynamically favour precipitation (Phillips *et al.*, 2013; Dupraz *et al.*, 2009). Contrarily, organic materials such as biofilm components, are thought to both have the potential to inhibit precipitation and enhance precipitation (Rodriguez-Navarro *et al.*, 2007). In our work, the presence of *epsH*, and thus the ability to produce the exopolysaccharide component of EPS helped calcite

formation either by acting as a nucleation template and/or by creating a microenvironment that favours supersaturation conditions (Chapter 5). Supersaturation only leads to precipitation once the nucleation activation energy barrier is overcome, and this can occur at different levels of supersaturation dependent on the system (Phillips *et al.*, 2013). Bacteria-induced calcite precipitation may well be initiated by bacterial nucleation surface sites like EPS allowing it to occur at lower supersaturation conditions.

The study of precipitation in an intrinsically low calcite preceptor has shown that multiple bacterial characteristics and processes drive precipitation, and the mechanism of BICP is not simply dividable into ureolytic driven and non-ureolytic driven. Figure 38 summarise the cellular processes and features in *B. subtilis* W168 that drive precipitation in the native strain and the heterologous urease expressing strain. The ureolytic *B. subtilis* W168, while increasing precipitation relative to the wild type did not behave like the benchmark ureolytic organism *Sporsarcina pasteureii*, where precipitates form much faster and also dominantly in the surrounding media as a result of the strong pH shift. Instead precipitation occurred localised to the cell surface and was composed of a mineral-organic precipitate when examined under the SEM. Changing the media to a less buffered variety did induce some crystal formation in the surrounding environment indicating that the ureolytic activity was not strong enough under all media conditions to give rise to a precipitation phenotype like *S. pasteurii*. The localisation of precipitation to the cell surface of ureolytic *B. subtilis* W168 was similarly observed on non-ureolytic environmental isolates grown on solid media (Reeksting *et al.*, 2020). The precipitates of these environmental isolates where equally composed of a mineral-organic phase, however it has to be noted that they were collected from growth in liquid media compared to growth on solid media in this study (Reeksting *et al.*, 2020). These observations show that bacteria-induced precipitation is not linear but a continuum of different processes. In the ureolytic *B. subtilis* W168 precipitation happens as a result of both surface and metabolic features. The cell surface and EPS provides templates for reducing the nucleation activation energy barrier while the increase in pH deprotonates surface functional groups and pushes the carbonate equilibrium increasing saturation index to favour precipitation. Thus in the engineered ureolytic *B. subtilis* W168 precipitation is not solely driven, but instead assisted by ureolysis, counter to what is found by the strong ureolytic bacterium *S. pasteurii*, which likely does not require surface features due to the strong and fast chemical pH shift. Native *B. subtilis* W168 likely had/has the capacity for low levels of precipitation that were un-detected by the method and

conditions used in this investigation. Instead engineering of urease activity was required to amplify and synergise with the precipitation mediated by native surface structures. As such the engineered ureolytic *B. subtilis* W168 strain combines traits of both ureolytic/non-ureolytic strains and this combination gives a deeper understanding of the different processes and how they can interplay. To date studies have typically focused on the extremes, i.e. strong ureolytic due to their obvious advantageous at precipitation or non-ureolytic due to other cellular or metabolic advantageous, but the environment is more likely to yield bacteria that have hybrid properties. It could even be advantageous not to have a ureolytic activity as strong as *S. pasteurii* as it has been shown to be kill off its own culture (Reeksting *et al.*, 2020). This is possibly a result of both high pH production and entombment by calcite. Having the ability of biofilm production may even help such a strain if it provides some protection. For example *Proteus mirabilis* forms efficient crystalline biofilms as a result of ureolytic and biofilm properties (Holling *et al.*, 2014). The understanding provided by the presented data will facilitate the fine-tuning of BICP for various applications beyond that of self-healing concrete. For example, in soil consolidation technologies fast precipitators can cause unwanted premature clogging at injection sites, reducing the depth at which the cementation occurs (Cheng and Cord-Ruwisch, 2014). Having a toolbox of characterised genetic elements that contribute to varying levels of precipitation can help design or select for a more optimally suited strain. This helps us move away from focusing just on precipitation level but also consider the finer mechanisms by which BICP occurs.

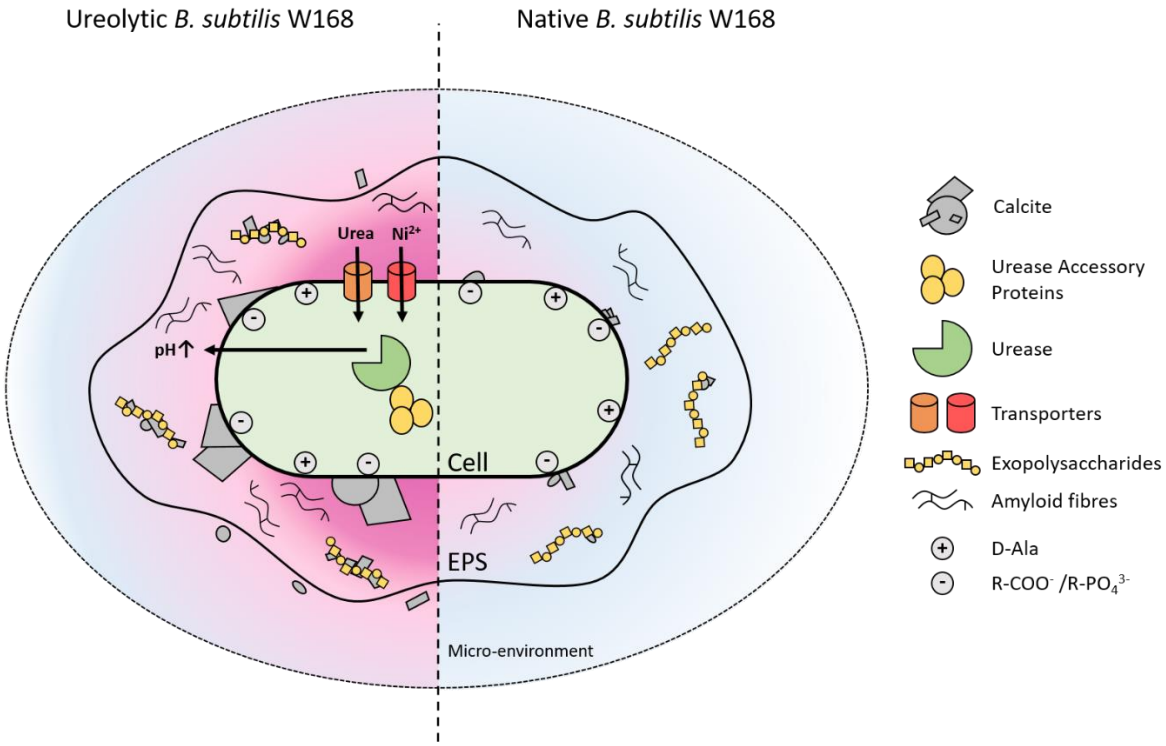

Figure 38. Model for calcite precipitation in *Bacillus subtilis* W168. Schematic representation of the cellular process and features that drive calcite precipitation in ureolytic *B. subtilis* W168 (left) and native *B. subtilis* W168 (right). In the Ureolytic *B. subtilis* W168 the urease enzyme catalyses the breakdown of urea leading to an increased pH of the microenvironment (pink gradient) such that supersaturation favours calcite precipitation. The presence of accessory protein UreE, UreF, UreG, and UreD as well as urea and nickel transporters contribute to increased ureolysis. The rise in pH amplifies precipitation promoted by exopolysaccharides of EPS and negatively charged sites on the cell surface which likely act as nucleation templates. Amyloid fibres were not found to promote precipitation. Under strong enough pH conditions, precipitates may even form in the micro-environment away from the cell. Native *B. subtilis* W168 increases the localised pH only slightly from metabolic activities (such as amino acid degradation) which is not sufficient reach supersaturation conditions required for precipitation. Low levels of undetected precipitates are still likely to form on the cell surface and EPS.

6.1.2 Future Directions: continued characterisation and fine-tuning.

The continued need for characterisation of bacteria-induced calcite precipitation however remains. An understanding of the range of pathways that can contribute to precipitation will be important in determining the ideal pairing of bacterial strains with application, environments and compositions. For example in self-healing concrete, cracks can run into anoxic conditions in crack depths where diffusion is limited; this also occurs as the cracks begin to close from BICP. Consequently, the oxygen limitation slows down the BICP-dependent healing process by aerobic bacteria. To overcome oxygen limitations, a material science approach to the problem has been the investigation of adding oxygen-releasing compounds to the concrete mix to increase oxygen availability for the bacteria (Seifan *et al.*, 2017). Alternatively, BICP-capable bacteria with anaerobic metabolism, such as nitrate reducers, might offer an advantage over aerobic bacteria (Nielsen *et al.*, 2020). Such facultative anaerobes could be selected to also have the ability for biofilm production or engineered to produce it, so as to further increase calcite precipitation. Different speeds and mechanisms of precipitation will also lead to different precipitate morphologies, ranging from fine crystals to larger organic-mineral compositions, which will inevitably affect application performance (Liang *et al.*, 2018; Reeksting *et al.*, 2020). Apart from specific environments, concrete compositions can also be delicate such that nutrients needed for the bacteria, which are added to the concrete directly or accidently released from capsules during mixing, may affect the setting and hardening (Chen *et al.*, 2019). Common nutrients such as sugars, calcium acetate, peptone, and yeast extract (depending on how much is released into the cement mix) can negatively affect cement setting, hydration kinetics, and compressive strength (Jonkers *et al.*, 2010; Paine, 2016; Chen *et al.*, 2019). This can be overcome by changing nutrient source, e.g. corn-steep liquor instead of yeast extract (Amiri and Bundur, 2018) or calcium nitrate as a setting accelerator (Aggoun *et al.*, 2008) instead of calcium acetate. The versatility in bacterial metabolic pathways may also pose a solution to this problem. Selecting bacteria on concrete-compatible nutrients and then testing for calcite precipitation could identify bacteria with different metabolic pathways that can perform effective BICP. Nutrient choice is critical as it will ultimately dictate technology price, thus influencing up-scaling and market feasibility (Phillips *et al.*, 2013). Investigating the addition of cheap and/or recycled feedstocks therefore aims to address these factors (Achal, Mukherjee, Basu and Reddy, 2009) but bacterial metabolic pathway diversity might be a key to the solution.

Another genetic target to improve calcite precipitation could be carbonic anhydrases. Carbonic anhydrases are metalloenzymes that catalyse the reversible hydration of carbon dioxide, with the carbonate produced being able to react with free calcium ions to precipitate as calcite (Li *et al.*,

2011). Only a few genetic approaches have explored the whole cell role of carbonic anhydrase on calcite precipitation (Oppenheimer-Shaanana *et al.*, 2016; Jo *et al.*, 2013). The small size of the genes encoding carbonic anhydrase offers potentially easier manipulation that could be explored in synergy with biofilm and urease-driven calcite precipitation. Further genetic improvements to the pathways that contribute to calcite precipitation will be needed to design precipitators that withstand application. Preliminary experiments as part of this project (data not shown) were unsuccessful in changing BICP of *B. subtilis* W168 when deleting/overexpressing native intracellular β-carbonic anhydrase genes *yvdA* and *ytiB*. Heterologous expression of an extracellular α-carbonic anhydrase from *Bacillus halodurans* also yielded no changes in precipitation in *B. subtilis* W168. This could have been the result of a lack of expression as a colourimetric assay was founded to be invalid for detection and, flag tagging of the proteins for western blotting still needed to be carried out. Provided there was successful gene expression, a lack of precipitation could have been the result of a subtle influence on precipitation that was not detectable in *B. subtilis* W168. Possibly in the ureolytic *B. subtilis* W168 background, engineering of carbonic anhydrase would amplify any effects it has on precipitation. Along with verifying expression through western blot this would be the next step in characterisation of these genes. Furthermore in bacteria carbonic anhydrases comprise α-, β-, and γ- families, offering a range of targets for characterisation.

Future characterisation could also be approached through random mutagenesis to identify further pathway or genetic traits of a bacterium that are not obviously associated with calcite precipitation. Examples of unexpected associations include one in *B. subtilis* 168 where it has been shown that the gene *etfA* putatively involved in fatty acid metabolism is essential for precipitation as its inactivation causes a decrease in pH and thus acidification of the microenvironment (Barabesi *et al.*, 2007; Marvasi, Visscher, Perito, *et al.*, 2010). Gene deletion and heterologous expression experiments have also identified that genes outside the urease gene cluster in *E. coli* affected ureolytic activity and thus precipitation (Liang *et al.*, 2018). These examples highlight that multiple genetic traits ultimately play a role in the precipitation ability of a bacterium and the scope for characterisation that still remains.

Currently, the heterologous ureolytic pathway in *B. subtilis* was shown to have limited strength and stability, and improvements would have to be made to ensure reliable urease activity. This can be addressed though techniques such as codon optimisation; different promoters and RBS binding sites could also be screened to further fine-tune expression (Guiziou *et al.*, 2016). The effects could be monitored as end stage activity assays, expression levels through qPCR or protein content through Western blot analyses. Rational mutagenesis approaches targeting the urease enzyme have been used to increase solubility and consequently activity (Whitaker, 2016), and this approach

could also be considered. Directed evolution and random mutagenesis approaches could be used to further improve ureolytic activity or calcite precipitation in general, something that has not been explored much (Achal, Mukherjee, Basu and Sudhakara Reddy, 2009). Generally, as genetic optimisation approaches are time and resource consuming, they are best carried out once a strain has been found which already suits application and only requires final optimisation. In this work the approach has been to identify the genetic factors behind BICP to facilitate their future optimisation and potentially move the corresponding genes to strains better suited for application. For example ureolytic bacteria could be sampled from environments more closely suited to harsh application environments such as alkaline salt lakes (Arias *et al.*, 2019). Alternatively, attempts could be made to take strains that are strong precipitators (such as *Sporosarcina pasteuri*) and adapt them to be more alkalitolerant and/or halotolerant through directed evolutionary approaches, for example using continuous culture or serial subcultures. If a strain cannot be found or engineered to have all favourable characteristics the next move would be to investigating mixed communities, deviating away from the typical pure cultures. Concrete structures are naturally colonised by bacteria over time, often leading to undesired biofouling. Initial colonisation occurs with autotrophic bacteria before heterotrophic bacteria can occupy the niche (Gaylarde and Morton, 1999). The formation of natural communities leads to the idea that exploiting such communities may be a better solution to sustain bacteria in concrete with desired BICP properties. Establishing a mixed community of biofilm and ureolytic strains could overcome genetic engineering challenges of burdening a single strain to accomplish all functions. This is only slowly starting to be investigated, with approaches including co-culturing of ureolytic and non-ureolytic strains, selection for microbial consortia and isolation of natural communities (Son *et al.*, 2018; Zhang *et al.*, 2017; Jroundi *et al.*, 2017; Gat *et al.*, 2014; Van Mullem *et al.*, 2020). Based on our findings biofilm can promote precipitation by a weak ureolytic strain. Too rapid precipitation by ureolytic organisms can also be unhelpful in application and a mineral-organic phase could be better. Therefore, mixing a strain with low ureolytic activity for gradual precipitation, combined with a biofilm producer to enhance the precipitation could therefore be a promising combination for application.

6.1.3 Remaining challenges: bringing to market and public perception.

In taking the fundamental understanding gained here towards developing better precipitators the next critical step is the need to tests strains in application. This moves the understanding from a laboratory setting to the actual application. Extensive validation is necessary if barriers towards technological adaptation are to be overcome. While BICP can find use in a range of applications,

the following discussion will focus on self-healing concrete as an example to illustrate the challenges faced in bringing novel-based technologies to market. As with any development of new technologies, for self-healing concrete to be adopted there needs to be: (i) extensive experimental validation and optimisation, (ii) certification to national and international standards, (iii) assessments for commercial viability, particularly up-scalability and (iv) design procedures and testing methodologies for safety (Al-Tabbaa *et al.*, 2018). Industries are risk-adverse and so adaptation of new technologies may need to be approached carefully. In the construction sector this could be done through the repair market to demonstrate performance before moving to larger applications (Al-Tabbaa *et al.*, 2018). This could likely be followed by application in, hard-to-access and costly to repair structures such as tunnels and piping systems. These structures are more likely to benefit from an initial higher investment using bacteria based self-healing concrete as it can be offset by considerable financial savings in repairs over the service life of the structure. There is however also a potential risk because if the self-healing concrete does not perform as expected the structure becomes more expensive. The more bacteria based self-healing concrete is proven to work in utility structures and then general infrastructure the more likely it will adopted to ever more applications. Trials by researches and companies developing bacteria based self-healing concrete and liquid/mortar repair technologies have encompassed concrete roof slabs of inspection pits (Van Mullem *et al.*, 2020), concrete test panels (Davies *et al.*, 2018), concrete irrigation canals (Wiktor and Jonkers, 2016; Sierra-Beltran *et al.*, 2015; Wiktor and Jonkers, 2015), sealing/repair of underground parking garages (Sierra Beltran and Jonkers, 2015; Hernandez, 2016), a concrete water basin as well as sealing/repair of underground basement constructions of the Het Loo Palace museum and Groninger Forum (Peplow, 2020). In addition to satisfactory performance from an industry standpoint as well as a cost-benefit balances that allow wide-spread use, a second major challenge to overcome is acceptance by the public particularly if the technology is to become mainstream and is applied to the construction of buildings for housing and commercial purposes.

The public's perception and acceptance of new technologies that are considered a large shift from current norms inevitably influences their implementation into everyday society, posing both as an opportunity and a barrier. The public's perception of the risks associated with new emerging technologies is often dictated by the attitude towards previous technologies, such as GMO foods (Akin *et al.*, 2019). This is thought to be the result of how scientific information is conveyed and a lack of time spent to self-inform, so individuals may resort to cues from preceding technologies and issues to inform on new ones (Akin *et al.*, 2019; Brossard, 2013). For example, for GMOs the lack of public support is thought to be a result of scientific illiteracy and a lack of knowledge on its benefits (Rommens, 2010; Wunderlich and Gatto, 2015). Furthermore, an individual's cultural experience

and worldviews influence the perceived risk of a technology (Akin *et al.*, 2019). Collectively, multiple factors influence the risk and benefit perception of a new technology such as information (scientific and general knowledge), attitude and intention (preconception), beliefs, and normative compliance (morality/ethics) (Kumar *et al.*, 2017; Scott *et al.*, 2018). Therefore there is a need to increase public awareness and understanding by conducting public engagement and outreach. For effective communication with the public on the advantageous of bacteria based self-healing technologies to be implemented successfully, understanding the current media landscape is important as individuals increasingly turn online to find information about science on social media platforms where not only scientists but also lay audiences participate in production of science communication content (Brossard, 2013). Further understanding of the target audience in terms of their beliefs and values is important in correctly addressing concerns (National Academies of Sciences and Medicine, 2017; Kumar *et al.*, 2017). The earlier, public engagement is carried out, the more impactful it is and the more effective the scientific background behind bacteria based self-healing technologies can be communicated. Effective communication itself builds on a large collection of communication frameworks and knowledge (National Academies of Sciences and Medicine, 2017). The perception of bacteria in the public is often considered to be negative in respect to health; similarly, in the built environment bacteria are mainly associated with decay (Gadd, 2017). Future work would therefore benefit from engaging with the public alongside the development of BICP applications to proactively engage with the public on the advantageous of possibly new disruptive technologies that involve bacteria.

The use of genetically modified organisms that are better precipitators for self-healing will have greater legislative and regulatory challenges and are also more likely to become a contentious technology in the public sphere than the use of natural environmental strains. Technology safety using genetically modified bacteria will likely need to be approached like it is in the food industry, where marker-free and all-native DNA manipulation methods can be applied (Rommens, 2010). Construction of such food-grade mutants (strains with no traces of foreign DNA) becomes viable once a specific strain suitable to application is found that could benefit from additional improvements. Genetic engineering approaches need to be in line with legislation, as mutagenesis techniques have recently been placed under EU GMO legislation unless they have been previously shown to have a long standing safety record (Bruetschy, 2019). BICP technologies based on environmental isolates are likely to be associate with fewer regulatory restrictions and possibly more consumer acceptance with regard to safety concerns. As such, fundamental understanding of BICP gained through genetic modification approaches can illuminate which genes and traits need to be sampled for. The results presented in this thesis may offer the fundamental knowledge

required to pursue both a GM and a natural route to finding the best bacteria which will allow for a flexible approach to technology development in a changing landscape of public perception of science and legislation around the use of GM organisms.

6.1.4 Summary: key findings.

Overall this project brought about insight into bacteria-induced calcite precipitation through genetic engineering of *Bacillus subtilis*. Specifically, the results from this study showed that (i) ureolysis can be sufficient to drive BICP in an intrinsically low precipitator, (ii) parts of biofilm production can synergise with ureolysis to increase precipitation, (iii) surface charge modulation did not significantly influence precipitation. Furthermore, a mobilisable plasmid for conjugation into Gram-positives was constructed to allow for the shuttling of genes into undomesticated bacteria suited for BICP application. As such, the results presented in this work provide both fundamental knowledge and genetic engineering approaches whereby bacteria for BICP-based application can be genetically improved or better strains selected. This study presents the first comprehensive investigation into genetic optimisation of BICP as a bottom-up approach towards understanding the process and will help drive forward the development of the field and new technologies, which will have to go hand-in-hand with engaging industrial and public stakeholders to ensure uptake and acceptance of this novel technology.

Supplementary

Supplementary 1: cDNA codon usage frequencies.

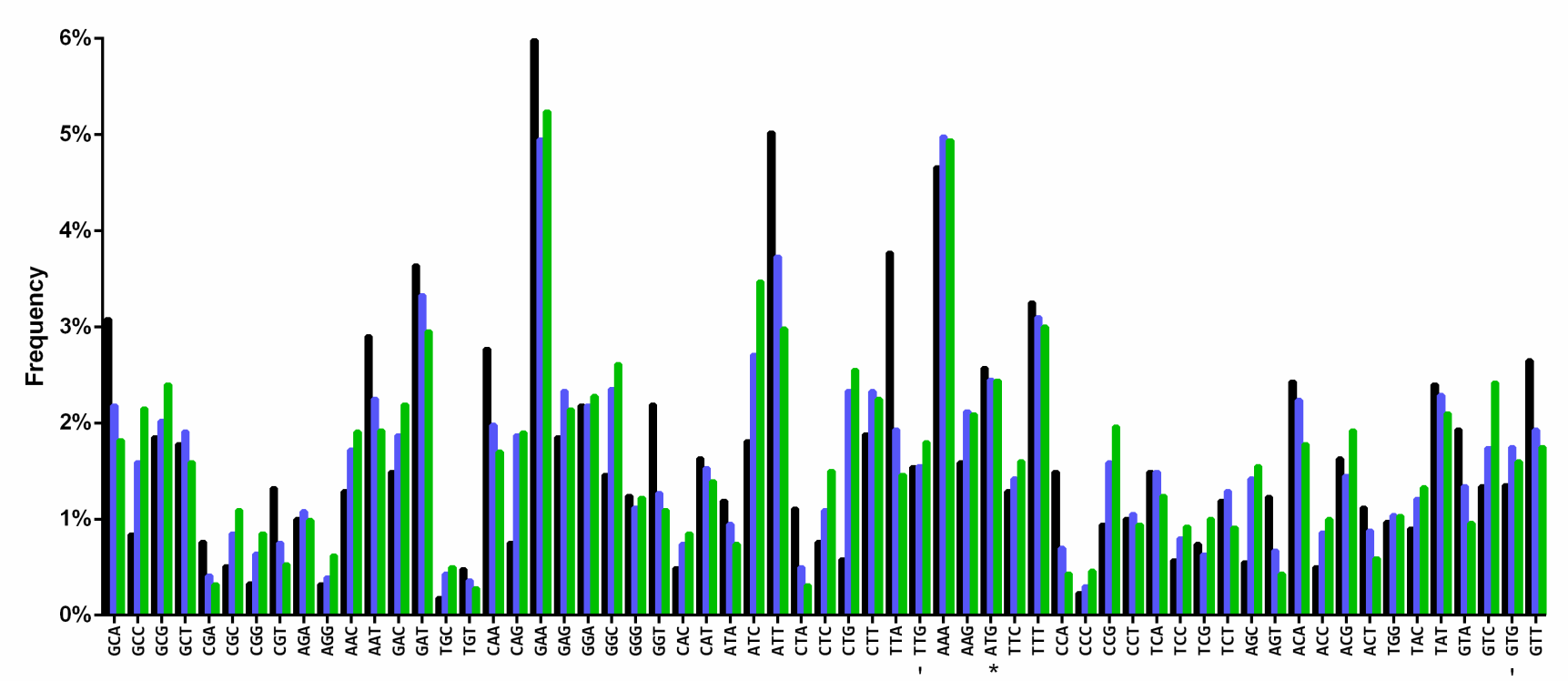

Codon usage frequencies of cDNA from the complete genomes of *Sporosarcina pasteurii* DSM33 (Black, NCBI: NZ_UGYZ01000002.1), *Bacillus subtilis* 168 (Blue, NCBI: NC_000964.3) and *Bacillus paralicheniformis* ATCC 9945a (Green, Genbank: CP005965.1) were extracted using the Amino Acid and Codon Usage Statistics web tool (Mrázek and Xie, 2019). Start codon denoted (*), alternative start codons denoted (‘). Stop codon frequencies were not calculated as part of the analysis.

Supplementary 2: Urease gene cluster accession numbers.

Microorganism	Accession Number
Sulfolobus tokodaii	NC_003106.2
Natronomonas pharaonis	NC_007426.1
Haloarcula marisomrtui	AB119092.1
Lactobacillus reuteri	AAPZ02000001.1
Sporosarcina pasteurii	KR133628.1
Bacillus sp. TB-90	D14439.1
Bacillus paralicheniformis	NC_021362.1
Bacillus subtilis NCIB 3610	CP020102.1
Bacillus subtilis W168	NZ_CP010052.1
Rhodobacter capsulatus	AB006984.1
Helicobacter pylori	FM991728.1
Ralstonia solanacearum	NC_020799.1
Herbaspirillum seropedicae	CP002039.1
Actinobacillus pleuropneumoniae	U89957.1
Pseudomonas aeruginosa	NC_002516.2
Proteus mirabilis	AM942759.1
Yersinia pseudotuberculosis	CP000720.1

List of NCBI/Genbank genome accession numbers used to extract urease gene information for the construction of Figure 8.

References

Abi Khattar, Z., Rejasse, A., Destoumieux-Garzón, D., Escoubas, J.M., Sanchis, V., Lereclus, D., Givaudan, A., Kallassy, M., Nielsen-Leroux, C., and Gaudriault, S., 2009. The dlt operon of Bacillus cereus is required for resistance to cationic antimicrobial peptides and for virulence in insects. *Journal of Bacteriology*, 191(22), pp.7063–7073.

Achal, V., Mukherjee, A., Basu, P.C., and Reddy, M.S., 2009. Lactose mother liquor as an alternative nutrient source for microbial concrete production by Sporosarcina pasteurii. *Journal of Industrial Microbiology and Biotechnology*, 36(3), pp.433–438.

Achal, V., Mukherjee, A., Basu, P.C., and Sudhakara Reddy, M., 2009. Strain improvement of Sporosarcina pasteurii for enhanced urease and calcite production. *Journal of Industrial Microbiology and Biotechnology*, 36(7), pp.981–988.

Achal, V., Pan, X., Fu, Q., and Zhang, D., 2012. Biomineralization based remediation of As(III) contaminated soil by Sporosarcina ginsengisoli. *Journal of Hazardous Materials*, 201–202, pp.178–184.

Adolphe, J.P., Loubière, J.F., Paradas, J., and Soleilhavoup, F., 1990. Procédé de traitement biologique d'une surface artificielle. *European patent 90400G97. 0 (after French patent 8903517, 1989)*.

Aggoun, S., Cheikh-Zouaoui, M., Chikh, N., and Duval, R., 2008. Effect of some admixtures on the setting time and strength evolution of cement pastes at early ages. *Construction and Building Materials*, 22(2), pp.106–110.

Akamatsu, T. and Sekiguchi, J., 1982. Transformation of bacillus protoplasts by plasmid pTP4 dna. *Agricultural and Biological Chemistry*, 46(6), pp.1617–1621.

Akin, H., Yeo, S.K., Wirz, C.D., Scheufele, D.A., Brossard, D., Xenos, M.A., and Corley, E.A., 2019. Are attitudes toward labeling nano products linked to attitudes toward GMO? Exploring a potential 'spillover' effect for attitudes toward controversial technologies. *Journal of Responsible Innovation*, 6(1), pp.50–74.

Al-Tabbaa, A., Lark, B., Paine, K., Jefferson, T., Litina, C., Gardner, D., and Embley, T., 2018. Biomimetic cementitious construction materials for next-generation infrastructure. *Proceedings of the Institution of Civil Engineers - Smart Infrastructure and Construction*, 171(2), pp.67–76.

Alazhari, M., Sharma, T., Heath, A., Cooper, R., and Paine, K., 2018. Application of expanded perlite encapsulated bacteria and growth media for self-healing concrete. *Construction and Building Materials*, 160, pp.610–619.

Allignet, J., Liassine, N., and El Solh, N., 1998. Characterization of a staphylococcal plasmid related to pUB110 and carrying two novel genes, vatC and vgbB, encoding resistance to streptogramins A and B and similar antibiotics. *Antimicrobial Agents and Chemotherapy*, 42(7), pp.1794–1798.

Aloisi, G., Gloter, A., Krüger, M., Wallmann, K., Guyot, F., and Zuddas, P., 2006. Nucleation

of calcium carbonate on bacterial nanoglobules. *Geology*, 34(12), p.1017.

Alonso, J.C., Leonhardt, H., and Stiege, C.A., 1988. Functional analysis of the leading strand replication origin of plasmid pUB110 in Bacillus subtilis. *Nucleic Acids Research*, 16(19), pp.9127–9145.

Amiri, A. and Bundur, Z.B., 2018. Use of corn-steep liquor as an alternative carbon source for biomineralization in cement-based materials and its impact on performance. *Construction and Building Materials*, 165, pp.655–662.

Anbu, P., Kang, C.-H., Shin, Y.-J., and So, J.-S., 2016. Formations of calcium carbonate minerals by bacteria and its multiple applications. *SpringerPlus*, 5(1), p.250.

Anderson, S., Appanna, V.D., Huang, J., and Viswanatha, T., 1992. A novel role for calcite in calcium homeostasis. *FEBS Letters*, 308(1), pp.94–96.

Andrew, R.M., 2019. Global CO2 emissions from cement production, 1928–2018. *Earth System Science Data*, 11(4), pp.1675–1710.

Arias, D., Cisternas, L., and Rivas, M., 2017. Biomineralization Mediated by Ureolytic Bacteria Applied to Water Treatment: A Review. *Crystals*, 7(11), p.345.

Arias, D., Cisternas, L.A., Miranda, C., and Rivas, M., 2019. Bioprospecting of ureolytic bacteria from laguna salada for biomineralization applications. *Frontiers in Bioengineering and Biotechnology*, 6, p.209.

Arnaouteli, S., MacPhee, C.E., and Stanley-Wall, N.R., 2016. Just in case it rains: building a hydrophobic biofilm the Bacillus subtilis way. *Current Opinion in Microbiology*, 34, pp.7–12.

Arnaouteli, S., Matoz-Fernandez, D.A., Porter, M., Kalamara, M., Abbott, J., MacPhee, C.E., Davidson, F.A., and Stanley-Wall, N.R., 2019. Pulcherrimin formation controls growth arrest of the Bacillus subtilis biofilm. *Proceedings of the National Academy of Sciences of the United States of America*, 116(27), pp.13553–13562.

Asada, R. and Tazaki, K., 2001. Silica biomineralization of unicellular microbes under strongly acidic conditions. *The Canadian Mineralogist*, 39(1), pp.1–16.

Asenath-Smith, E., Li, H., Keene, E.C., Seh, Z.W., and Estroff, L.A., 2012. Crystal growth of calcium carbonate in hydrogels as a model of biomineralization. *Advanced Functional Materials*, 22(14), pp.2891–2914.

Aune, T.E.V. and Aachmann, F.L., 2010. Methodologies to increase the transformation efficiencies and the range of bacteria that can be transformed. *Applied Microbiology and Biotechnology*, 85(5), pp.1301–1313.

Aymanns, S., Mauerer, S., van Zandbergen, G., Wolz, C., and Spellerberg, B., 2011. High-level fluorescence labeling of Gram-positive pathogens. *PLoS ONE*, 6(6), p.e19822.

Baas Becking, L.G.M. and Moore, D., 1961. Biogenic sulfides. *Economic Geology*, 56(2), pp.259–272.

Bachmeier, K.L., Williams, A.E., Warmington, J.R., and Bang, S.S., 2002. Urease activity in microbiologically-induced calcite precipitation. *Journal of Biotechnology*, 93(2),

pp.171–181.

Banik, V., 2019. *Self-healing Concrete Market by Type (Intrinsic Healing, Capsule based Healing, Vascular Healing) by End User (Residential & Commercial, Industrial, and Civil Infrastructure): Global Opportunity Analysis and Industry Forecast, 2018 - 2025*.

Banks, E.D., Taylor, N.M., Gulley, J., Lubbers, B.R., Giarrizo, J.G., Bullen, H.A., Hoehler, T.M., and Barton, H.A., 2010. Bacterial Calcium Carbonate Precipitation in Cave Environments: A function of Calcium Homeostasis. *Geomicrobiology Journal*, 27(5), pp.444–454.

Bansal, R., Dhami, N.K., Mukherjee, A., and Reddy, M.S., 2016. Biocalcification by halophilic bacteria for remediation of concrete structures in marine environment. *Journal of Industrial Microbiology & Biotechnology*, 43(11), pp.1497–1505.

Barabesi, C., Galizzi, A., Mastromei, G., Rossi, M., Tamburini, E., and Perito, B., 2007. Bacillus subtilis gene cluster involved in calcium carbonate biomineralization. *Journal of Bacteriology*, 189(1), pp.228–235.

Basnakova, G., Stephens, E.R., Thaller, M.C., Rossolini, G.M., and Macaskie, L.E., 1998. The use of Escherichia coli bearing a phoN gene for the removal of uranium and nickel from aqueous flows. *Applied Microbiology and Biotechnology*, 50(2), pp.266–272.

Bäuerlein, E., 2003. Biomineralization of Unicellular Organisms: An Unusual Membrane Biochemistry for the Production of Inorganic Nano- and Microstructures. *Angewandte Chemie - International Edition*, 42(6), pp.614–641.

Beckers, G., Bendt, A.K., Krämer, R., and Burkovski, A., 2004. Molecular identification of the urea uptake system and transcriptional analysis of urea transporter and urease encoding genes in *Corynebacterium glutamicum*. *Journal of Bacteriology*, 186(22), pp.7645–7652.

De Belie, N., Gruyaert, E., Al-Tabbaa, A., Antonaci, P., Baera, C., Bajare, D., Darquennes, A., Davies, R., Ferrara, L., Jefferson, T., Litina, C., Miljevic, B., Otlewska, A., Ranogajec, J., Roig-Flores, M., Paine, K., Lukowski, P., Serna, P., Tulliani, J.M., Vucetic, S., Wang, J., and Jonkers, H.M., 2018. A Review of Self-Healing Concrete for Damage Management of Structures. *Advanced Materials Interfaces*, 1800074, pp.1–28.

Benning, L.G. and Waychunas, G.A., 2008. Nucleation, Growth, and Aggregation of Mineral Phases: Mechanisms and Kinetic Controls. In: S. L. Brantley, J. D. Kubicki, & A. F. White, eds. *Kinetics of Water-Rock Interaction*. New York, NY: Springer New York, pp.259–333.

Benzerara, K., Menguy, N., Guyot, F., Skouri, F., de Luca, G., Barakat, M., and Heulin, T., 2004. Biologically controlled precipitation of calcium phosphate by Ramlibacter tataouinensis. *Earth and Planetary Science Letters*, 228(3–4), pp.439–449.

Bergdale, T.E., Pinkelman, R.J., Hughes, S.R., Zambelli, B., Ciurli, S., and Bang, S.S., 2012. Engineered biosealant strains producing inorganic and organic biopolymers. *Journal of Biotechnology*, 161(3), pp.181–189.

Bertozzi Silva, J., Storms, Z., and Sauvageau, D., 2016. Host receptors for bacteriophage adsorption. *FEMS Microbiology Letters*, 363(4), pp.1–11.

Beveridge, T.J. and Fyfe, W.S., 1985. Metal fixation by bacterial cell walls. *Canadian Journal of Earth Sciences*, 22(12), pp.1893–1898.

Beveridge, T.J. and Koval, S.F., 1981. Binding of metals to cell envelopes of Escherichia coli K-12. *Applied and Environmental Microbiology*, 42(2), pp.325–335.

Beveridge, T.J. and Murray, R.G.E., 1976. Uptake and Retention of Metals by cell Walls of Bacillus subtilis. *Journal of Bacteriology*, 127(3), pp.1–17.

Beveridge, T.J. and Murray, R.G.E., 1980. Sites of metal deposition in the cell wall of Bαcillus subtilis. *Journal of Bacteriology*, 141(2), pp.876–887.

Biswas, M., Majumdar, S., Chowdhury, T., Chattopadhyay, B., Mandal, S., Halder, U., and Yamasaki, S., 2010. Bioremediase a unique protein from a novel bacterium BKH1, ushering a new hope in concrete technology. *Enzyme and Microbial Technology*, 46(7), pp.581–587.

Boe, L., Gros, M.F., Te Riele, H., Ehrlich, S.D., and Gruss, A., 1989. Replications origins of single-stranded-DNA plasmid pUB110. *Journal of Bacteriology*, 171(6), pp.3366–3372.

Bontognali, T.R.R., Vasconcelos, C., Warthmann, R.J., Dupraz, C., Bernasconi, S.M., and McKenzie, J.A., 2008. Microbes produce nanobacteria-like structures, avoiding cell entombment. *Geology*, 36(8), pp.663–666.

Boquet, E., Boronat, A., and Ramos-Cormenzana, A., 1973. Production of Calcite (Calcium Carbonate) Crystals by Soil Bacteria is a General Phenomenon. *Nature*, 246(5434), pp.527–529.

Borukhin, S., Bloch, L., Radlauer, T., Hill, A.H., Fitch, A.N., and Pokroy, B., 2012. Screening the incorporation of amino acids into an inorganic crystalline host: The case of calcite. *Advanced Functional Materials*, 22(20), pp.4216–4224.

Bossé, J.T., Gilmour, H.D., Macinnes, J.I., and Innes, J.I.M. a C., 2001. Novel Genes Affecting Urease Activity in Actinobacillus pleuropneumoniae Novel Genes Affecting Urease Activity in Actinobacillus pleuropneumoniae. *Journal of Bacteriology*, 183(4), pp.1242–1247.

Bossé, J.T. and MacInnes, J.I., 1997. Genetic and biochemical analyses of Actinobacillus pleuropneumoniae urease. *Infection and immunity*, 65(11), pp.4389–94.

Braissant, O., Cailleau, G., Dupraz, C., and Verrecchia, E.P., 2003. Bacterially Induced Mineralization of Calcium Carbonate in Terrestrial Environments: The Role of Exopolysaccharides and Amino Acids. *Journal of Sedimentary Research*, 73(3), pp.485–490.

Braissant, O., Decho, A.W., Dupraz, C., Glunk, C., Przekop, K.M., and Visscher, P.T., 2007. Exopolymeric substances of sulfate-reducing bacteria: Interactions with calcium at alkaline pH and implication for formation of carbonate minerals. *Geobiology*, 5(4), pp.401–411.

Branda, S.S., Chu, F., Kearns, D.B., Losick, R., and Kolter, R., 2006. A major protein component of the Bacillus subtilis biofilm matrix. *Molecular Microbiology*, 59(4), pp.1229–1238.

Branda, S.S., González-Pastor, J.E., Ben-Yehuda, S., Losick, R., and Kolter, R., 2001. Fruiting body formation by Bacillus subtilis. *Proceedings of the National Academy of Sciences of the United States of America*, 98(20), pp.11621–6.

Branda, S.S., González-Pastor, J.E., Dervyn, E., Ehrlich, S.D., Losick, R., and Kolter, R., 2004. Genes involved in formation of structured multicellular communities by Bacillus subtilis. *Journal of Bacteriology*, 186(12), pp.3970–3979.

Breugel, K. Van, 2012. Self-healing material concepts as solution for aging infrastructure. *37th Conference on Our World in Concrete & Structures*, pp.1–17.

Brophy, J.A.N., Triassi, A.J., Adams, B.L., Renberg, R.L., Stratis-Cullum, D.N., Grossman, A.D., and Voigt, C.A., 2018. Engineered integrative and conjugative elements for efficient and inducible DNA transfer to undomesticated bacteria. *Nature Microbiology*, 3(9), pp.1043–1053.

Brossard, D., 2013. New media landscapes and the science information consumer. *Proceedings of the National Academy of Sciences of the United States of America*, 110(SUPPL. 3), pp.14096–14101.

Brouwers, G.J., De Vrind, J.P.M., Corstjens, P.L.A.M., Cornelis, P., Baysse, C., and De Vrind-De Jong, E.W., 1999. cumA, a Gene Encoding a Multicopper Oxidase, Is Involved in Mn2+ Oxidation in Pseudomonas putida GB-1. *Applied and Environmental Microbiology*, 65(4), pp.1762–1768.

Brown, S., Santa Maria, J.P., and Walker, S., 2013. Wall Teichoic Acids of Gram-Positive Bacteria. *Annual Review of Microbiology*, 67(1), pp.313–336.

Bruand, C. and Ehrlich, S.D., 1998. Transcription-driven DNA replication of plasmid pAMβ1 in Bacillus subtilis. *Molecular Microbiology*, 30(1), pp.135–145.

Bruetschy, C., 2019. The EU regulatory framework on genetically modified organisms (GMOs). *Transgenic Research*, 28(s2), pp.169–174.

Buczynski, C. and Chafetz, H.S., 1991. Habit of bacterially induced precipitates of calcium carbonate and the influence of medium viscosity on mineralogy. *Journal of Sedimentary Research*, 61(2), pp.226–233.

Bury-Moné, S., Skouloubris, S., Labigne, A., and De Reuse, H., 2001. The Helicobacter pylori UreI protein: Role in adaptation to acidity and identification of residues essential for its activity and for acid activation. *Molecular Microbiology*, 42(4), pp.1021–1034.

Carattoli, A., 2013. Plasmids and the spread of resistance. *International Journal of Medical Microbiology*, 303(6–7), pp.298–304.

Castanier, S., Le Métayer-Levrel, G., and Perthuisot, J.P., 1999. Ca-carbonates precipitation and limestone genesis - the microbiogeologist point of view. *Sedimentary Geology*, 126(1–4), pp.9–23.

Castro-Alonso, M.J., Montañez-Hernandez, L.E., Sanchez-Muñoz, M.A., Macias Franco, M.R., Narayanasamy, R., and Balagurusamy, N., 2019. Microbially Induced Calcium Carbonate Precipitation (MICP) and Its Potential in Bioconcrete: Microbiological and Molecular Concepts. *Frontiers in Materials*, 6(126), pp.1–15.

Chang, S. and Cohen, S.N., 1979. High frequency transformation of Bacillus subtilis protoplasts by plasmid DNA. *MGG Molecular & General Genetics*, 168(1), pp.111–115.

Charpentier, E., Gerbaud, G., and Courvalin, P., 1999. Conjugative mobilization of the rolling-circle plasmid pIP823 from Listeria monocytogenes BM4293 among gram-positive and gram-negative bacteria. *Journal of Bacteriology*, 181(11), pp.3368–3374.

Chen, P.-H., Liu, H.-L., Chen, Y.-J., Cheng, Y.-H., Lin, W.-L., Yeh, C.-H., and Chang, C.-H., 2012. Enhancing CO2 bio-mitigation by genetic engineering of cyanobacteria. *Energy & Environmental Science*, 5(8), p.8318.

Chen, X., Yuan, J., and Alazhari, M., 2019. Effect of microbiological growth components for bacteria-based self-healing on the properties of cement mortar. *Materials*, 12(8), p.1303.

Chen, Z., Pan, X., Chen, H., Guan, X., and Lin, Z., 2016. Biomineralization of Pb(II) into Pb-hydroxyapatite induced by Bacillus cereus 12-2 isolated from Lead-Zinc mine tailings. *Journal of Hazardous Materials*, 301, pp.531–537.

Cheng, L. and Cord-Ruwisch, R., 2014. Upscaling Effects of Soil Improvement by Microbially Induced Calcite Precipitation by Surface Percolation. *Geomicrobiology Journal*, 31(5), pp.396–406.

Chu, F., Kearns, D.B., Branda, S.S., Kolter, R., and Losick, R., 2006. Targets of the master regulator of biofilm formation in Bacillus subtilis. *Molecular Microbiology*, 59(4), pp.1216–1228.

Chu, F., Kearns, D.B., McLoon, A., Chai, Y., Kolter, R., and Losick, R., 2008. A novel regulatory protein governing biofilm formation in Bacillus subtilis. *Molecular Microbiology*, 68(5), pp.1117–1127.

Chumsakul, O., Takahashi, H., Oshima, T., Hishimoto, T., Kanaya, S., Ogasawara, N., and Ishikawa, S., 2011. Genome-wide binding profiles of the Bacillus subtilis transition state regulator AbrB and its homolog Abh reveals their interactive role in transcriptional regulation. *Nucleic Acids Research*, 39(2), pp.414–428.

Connolly, J., Kaufman, M., Rothman, A., Gupta, R., Redden, G., Schuster, M., Colwell, F., and Gerlach, R., 2013. Construction of two ureolytic model organisms for the study of microbially induced calcium carbonate precipitation. *Journal of Microbiological Methods*, 94(3), pp.290–299.

CORDIS, 2013. *HEALCON: Self-healing concrete to create durable and sustainable concrete structures - 309451*. Community Research and Development Information Service.

COST, 2016. *Self-healing As prevention Repair of Concrete Structures - CA15202*. European Cooperation in Sience & Technology.

Crosby, C.H. and Bailey, J. V., 2012. The role of microbes in the formation of modern and ancient phosphatic mineral deposits. *Frontiers in Microbiology*, 3(241), pp.1–7.

Cruz-Ramos, H., Glaser, P., Wray, L. V, and Fisher, S.H., 1997. The Bacillus subtilis ureABC operon. *Journal of Bacteriology*, 179(10), pp.3371–3373.

Cubillas, P. and Anderson, M.W., 2010. Synthesis Mechanism: Crystal Growth and Nucleation. In: J. Čejka, A. Corma, & S. Zones, eds. *Zeolites and Catalysis: Synthesis, Reactions and Applications*. Weinheim, Germany: Wiley-VCH Verlag GmbH & Co. KGaA, pp.1–55.

Cussac, V., Ferrero, R.L., and Labigne, A., 1992. Expression of Helicobacter pylori urease genes in Escherichia coli grown under nitrogen-limiting conditions. *Journal of Bacteriology*, 174(8), pp.2466–2473.

Dattelbaum, J.D., Lockatell, C.V., Johnson, D.E., and Mobley, H.L.T., 2003. UreR, the transcriptional activator of the Proteus mirabilis urease gene cluster, is required for urease activity and virulence in experimental urinary tract infections. *Infection and Immunity*, 71(2), pp.1026–1030.

Davies, R., Teall, O., Pilegis, M., Kanellopoulos, A., Sharma, T., Jefferson, A., Gardner, D., Al-Tabbaa, A., Paine, K., and Lark, R., 2018. Large Scale Application of Self-Healing Concrete: Design, Construction, and Testing. *Frontiers in Materials*, 5(51), pp.1–12.

Deichelbohrer, I., Alonso, J.C., Luder, G., and Trautner, T.A., 1985. Plasmid transduction by Bacillus subtilis bacteriophage SPP1: Effects of DNA homology between plasmid and bacteriophage. *Journal of Bacteriology*, 162(3), pp.1238–1243.

Deng, H., Shen, X.C., Wang, X.M., and Du, C., 2013. Calcium carbonate crystallization controlled by functional groups: A mini-review. *Frontiers of Materials Science*, 7(1), pp.62–68.

Deng, H., Wang, S., Wang, X., Du, C., Shen, X., Wang, Y., and Cui, F., 2015. Two competitive nucleation mechanisms of calcium carbonate biomineralization in response to surface functionality in low calcium ion concentration solution. *Regenerative Biomaterials*, 2(3), pp.187–195.

Deng, S., Dong, H., Lv, G., Jiang, H., Yu, B., and Bishop, M.E., 2010. Microbial dolomite precipitation using sulfate reducing and halophilic bacteria: Results from Qinghai Lake, Tibetan Plateau, NW China. *Chemical Geology*, 278(3–4), pp.151–159.

Derre, I., Rapoport, G., and Msadek, T., 2000. The CtsR regulator of stress response is active as a dimer and specifically degraded in vivo at 37°C. *Molecular Microbiology*, 38(2), pp.335–347.

Dhami, N.K., Reddy, M.S., and Mukherjee, M.S., 2013. Biomineralization of calcium carbonates and their engineered applications: A review. *Frontiers in Microbiology*, 4, pp.1–13.

Dimitriu, T., Marchant, L., Buckling, A., and Raymond, B., 2019. Bacteria from natural populations transfer plasmids mostly towards their kin. *Proceedings of the Royal Society B: Biological Sciences*, 286(1905), p.20191110.

Douglas, S. and Beveridge, T.J., 1998. Mineral formation by bacteria in natural microbial communities. *FEMS Microbiology Ecology*, 26(2), pp.79–88.

Doyle, R.J., Matthews, T.H., and Streips, U.N., 1980. Chemical basis for selectivity of metal ions by the Bacillus subtilis cell wall. *Journal of Bacteriology*, 143(1), pp.471–480.

Drinking Water Inspectorate, 2017. What are the Drinking Water Standards? *DWI Advice Leaflets*, p.5.

Duitman, E.H., Wyczawski, D., Boven, L.G., Venema, G., Kuipers, O.P., and Hamoen, L.W., 2007. Novel methods for genetic transformation of natural Bacillus subtilis isolates used to study the regulation of the mycosubtilin and surfactin synthetases. *Applied and Environmental Microbiology*, 73(11), pp.3490–3496.

Dupraz, C., Reid, R.P., Braissant, O., Decho, A.W., Norman, R.S., and Visscher, P.T., 2009. Processes of carbonate precipitation in modern microbial mats. *Earth-Science Reviews*, 96(3), pp.141–162.

Dupraz, C. and Visscher, P.T., 2005. Microbial lithification in marine stromatolites and hypersaline mats. *Trends in Microbiology*, 13(9), pp.429–438.

Ehrlich, H.L., 1999. Microbes as geologic agents: Their role in mineral formation. *Geomicrobiology Journal*, 16(2), pp.135–153.

Eitinger, T., Suhr, J., Moore, L., and Smith, J.A.C., 2005. Secondary transporters for nickel and cobalt ions: Theme and variations. *BioMetals*, 18(4), pp.399–405.

El-Samrah, M.G., Abdel-Rahman, M.A.E., and Kany, A.M.I., 2018. Study Characteristics of New Concrete Mixes and their Mechanical, Physical, and Gamma Radiation Attenuation Features. *Zeitschrift fur Anorganische und Allgemeine Chemie*, 644(2), pp.92–99.

EPSRC, 2012. Materials for Life (M4L) - EP/K026631/1.

EPSRC, 2017. Resilient Materials for Life (RM4L) - EP/P02081X/1.

Epstein, A.K., Pokroy, B., Seminara, A., and Aizenberg, J., 2011. Bacterial biofilm shows persistent resistance to liquid wetting and gas penetration. *Proceedings of the National Academy of Sciences of the United States of America*, 108(3), pp.995–1000.

Ercole, C., Cacchio, P., Botta, A.L., Centi, V., and Lepidi, A., 2007. Bacterially induced mineralization of calcium carbonate: The role of exopolysaccharides and capsular polysaccharides. *Microscopy and Microanalysis*, 13(1), pp.42–50.

Ernst, C.M., Slavetinsky, C.J., Kuhn, S., Hauser, J.N., Nega, M., Mishra, N.N., Gekeler, C., Bayer, A.S., and Peschel, A., 2018. Gain-of-Function Mutations in the Phospholipid Flippase MprF Confer Specific Daptomycin Resistance. *mBio*, 9(6), pp.e01659-18.

Ernst, C.M., Staubitz, P., Mishra, N.N., Yang, S.J., Hornig, G., Kalbacher, H., Bayer, A.S., Kraus, D., and Peschel, A., 2009. The bacterial defensin resistance protein MprF consists of separable domains for lipid lysinylation and antimicrobial peptide repulsion. *PLoS Pathogens*, 5(11), pp.1–9.

Ersan, Y., Gruyaert, E., Louis, G., Lors, C., De Belie, N., and Boon, N., 2015. Self-protected nitrate reducing culture for intrinsic repair of concrete cracks. *Frontiers in Microbiology*, 6(1228), pp.1–15.

Erşan, Y.Ç., Verbruggen, H., De Graeve, I., Verstraete, W., De Belie, N., and Boon, N., 2016. Nitrate reducing CaCO3 precipitating bacteria survive in mortar and inhibit steel

corrosion. *Cement and Concrete Research*, 83, pp.19–30.

Fan, L.-H., Liu, N., Yu, M.-R., Yang, S.-T., and Chen, H.-L., 2011. Cell surface display of carbonic anhydrase on Escherichia coli using ice nucleation protein for CO2 sequestration. *Biotechnology and Bioengineering*, 108(12), pp.2853–2864.

Farrugia, M.A., Macomber, L., and Hausinger, R.P., 2013. Biosynthesis of the urease metallocenter. *Journal of Biological Chemistry*, 288(19), pp.13178–13185.

Fernández-Remolar, D.C., Preston, L.J., Sánchez-Román, M., Izawa, M.R.M., Huang, L., Southam, G., Banerjee, N.R., Osinski, G.R., Flemming, R., Gómez-Ortíz, D., Prieto Ballesteros, O., Rodríguez, N., Amils, R., and Darby Dyar, M., 2012. Carbonate precipitation under bulk acidic conditions as a potential biosignature for searching life on Mars. *Earth and Planetary Science Letters*, 351–352, pp.13–26.

Fishman, M.R., Giglio, K., Fay, D., and Filiatrault, M.J., 2018. Physiological and genetic characterization of calcium phosphate precipitation by Pseudomonas species. *Scientific Reports*, 8(1), pp.1–14.

Fong, Y.H., Wong, H.C., Yuen, M.H., Lau, P.H., Chen, Y.W., and Wong, K.B., 2013. Structure of UreG/UreF/UreH Complex Reveals How Urease Accessory Proteins Facilitate Maturation of Helicobacter pylori Urease. *PLoS Biology*, 11(10).

Fortin, D., Ferris, F.G., and Beveridge, T.J., 1997. Surface-mediated mineral development by bacteria. *Reviews in Mineralogy and Geochemistry*, 35(1), pp.161–180.

Frankel, R.B. and Bazylinski, D.A., 2003. Biologically Induced Mineralization by Bacteria. *Reviews in Mineralogy and Geochemistry*, 54(1), pp.95–114.

Frankel, R.B., Papaefthymiou, G.C., Blakemore, R.P., and O'Brien, W., 1983. Fe3O4 precipitation in magnetotactic bacteria. *Biochimica et Biophysica Acta (BBA) - Molecular Cell Research*, 763(2), pp.147–159.

Fujita, M., Nakashima, K., Achal, V., and Kawasaki, S., 2017. Whole-cell evaluation of urease activity of Pararhodobacter sp. isolated from peripheral beachrock. *Biochemical Engineering Journal*, 124, pp.1–5.

Gadd, G.M., 2017. Geomicrobiology of the built environment. *Nature Microbiology*, 2(4), p.16275.

Gaj, T., Sirk, S.J., and Barbas, C.F., 2014. Expanding the scope of site-specific recombinases for genetic and metabolic engineering. *Biotechnology and Bioengineering*, 111(1), pp.1–15.

Gao, C., Xue, Y., and Ma, Y., 2011. Protoplast transformation of recalcitrant alkaliphilic bacillus sp. with methylated plasmid DNA and a developed hard agar regeneration medium. *PLoS ONE*, 6(11), p.e28148.

Gat, D., Tsesarsky, M., Shamir, D., and Ronen, Z., 2014. Accelerated microbial-induced CaCO3precipitation in a defined coculture of ureolytic and non-ureolytic bacteria. *Biogeosciences*, 11(10), pp.2561–2569.

Gaylarde, C.C. and Morton, L.H.G., 1999. Deteriogenic biofilms on buildings and their

control: A review. *Biofouling*, 14(1), pp.59–74.

De Gelder, L., Vandecasteele, F.P.J., Brown, C.J., Forney, L.J., and Top, E.M., 2005. Plasmid donor affects host range of promiscuous IncP-1β plasmid pB10 in an activated-sludge microbial community. *Applied and Environmental Microbiology*, 71(9), pp.5309–5317.

Giaouris, E., Briandet, R., Meyrand, M., Courtin, P., and Chapot-Chartier, M.P., 2008. Variations in the degree of D-alanylation of teichoic acids in Lactococcus lactis alter resistance to cationic antimicrobials but have no effect on bacterial surface hydrophobicity and charge. *Applied and Environmental Microbiology*, 74(15), pp.4764–4767.

Gilbert, P.U.P.A., Albrecht, M., and Frazer, B.H., 2005. The Organic-Mineral Interface in Biominerals. *Reviews in Mineralogy and Geochemistry*, 59(1), pp.157–185.

Gingichashvili, S., Duanis-Assaf, D., Shemesh, M., Featherstone, J.D.B., Feuerstein, O., and Steinberg, D., 2020. The adaptive morphology of Bacillus subtilis biofilms: A defense mechanism against bacterial starvation. *Microorganisms*, 8(1), p.62.

González-Muñoz, M. and Chekroun, K., 2000. Bacterially induced Mg-calcite formation: role of Mg2+ in development of crystal morphology. *Journal of Sedimentary Research*, 70(3), pp.559–564.

González-Muñoz, M.T., De Linares, C., Martínez-Ruiz, F., Morcillo, F., Martín-Ramos, D., and Arias, J.M., 2008. Ca-Mg kutnahorite and struvite production by Idiomarina strains at modern seawater salinities. *Chemosphere*, 72(3), pp.465–472.

Greene, A.C. and Madgwick, J.C., 1991. Microbial formation of manganese oxides. *Applied and Environmental Microbiology*, 57(4), pp.1114–1120.

Grohmann, E., Muth, G., and Espinosa, M., 2003. Conjugative Plasmid Transfer in Gram-Positive Bacteria. *Microbiology and Molecular Biology Reviews*, 67(2), pp.277–301.

Gryczan, T.J., Contente, S., and Dubnau, D., 1978. Characterization of Staphylococcus aureus plasmids introduced by transformation into Bacillus subtilis. *Journal of Bacteriology*, 134(1), pp.318–329.

Guérout-Fluery, A.-M., Shazand, K., Frandsen, N., and Stragier, P., 1995. Antibiotic-resistance casettes for Bacillus subtilis. *Gene*, 167, pp.335–336.

Guffanti, A.A., Quirk, P.G., and Krulwich, T.A., 1991. Transfer of Tn925 and plasmids between Bacillus subtilis and alkaliphilic Bacillus firmus OF4 during Tn925-mediated conjugation. *Journal of Bacteriology*, 173(5), pp.1686–1689.

Guiziou, S., Sauveplane, V., Chang, H.-J., Clerté, C., Declerck, N., Jules, M., and Bonnet, J., 2016. A part toolbox to tune genetic expression in Bacillus subtilis. *Nucleic Acids Research*, 44(15), pp.7495–7508.

Guo, S. and Mahillon, J., 2013. pGIAK1, a Heavy Metal Resistant Plasmid from an Obligate Alkaliphilic and Halotolerant Bacterium Isolated from the Antarctic Concordia Station Confined Environment. *PLoS ONE*, 8(8), pp.1–8.

Hachmann, A.B., Angert, E.R., and Helmann, J.D., 2009. Genetic analysis of factors affecting

susceptibility of bacillus subtilis to daptomycinvt. *Antimicrobial Agents and Chemotherapy*, 53(4), pp.1598–1609.

Hammes, F., Boon, N., De Villiers, J., Verstraete, W., Siciliano, S.D., and Villiers, J. De, 2003. Strain-Specific Ureolytic Microbial Calcium Carbonate Precipitation Strain-Specific Ureolytic Microbial Calcium Carbonate Precipitation. *Applied and Environmental Microbiology*, 69(8), pp.4901–4909.

Hammes, F. and Verstraete, W., 2002. Key roles of pH and calcium metabolism in microbial carbonate precipitation. *Reviews in Environmental Science and Biotechnology*, 1(1), pp.3–7.

Hamon, M.A. and Lazazzera, B.A., 2001. The sporulation transcription factor Spo0A is required for biofilm development in Bacillus subtilis. *Molecular Microbiology*, 42(5), pp.1199–1209.

Harwood, C.R. and Cutting, S.M., 1990. *Molecular Biological Methods for Bacillus*. Chichester, United Kingdom: John Wiley and Sons Ltd.

Heinze, S., Kornberger, P., Grätz, C., Schwarz, W.H., Zverlov, V. V., and Liebl, W., 2018. Transmating: Conjugative transfer of a new broad host range expression vector to various Bacillus species using a single protocol. *BMC Microbiology*, 18(1), pp.1–10.

Hernandez, M., 2016. *Using Self-Healing Concrete for Concrete Repairs on Aging Concrete Structures*.

Hertel, R., Volland, S., and Liesegang, H., 2015. Conjugative reporter system for the use in Bacillus licheniformis and closely related Bacilli. *Letters in Applied Microbiology*, 60(2), pp.162–167.

Heveran, C.M., Liang, L., Nagarajan, A., Hubler, M.H., Gill, R., Cameron, J.C., Cook, S.M., and Srubar, W. V., 2019. Engineered Ureolytic Microorganisms Can Tailor the Morphology and Nanomechanical Properties of Microbial-Precipitated Calcium Carbonate. *Scientific reports*, 9(1), p.14721.

Holling, N., Lednor, D., Tsang, S., Bissell, A., Campbell, L., Nzakizwanayo, J., Dedi, C., Hawthorne, J.A., Hanlon, G., Ogilvie, L.A., Salvage, J.P., Patel, B.A., Barnes, L.M., and Jones, B. V., 2014. Elucidating the genetic basis of crystalline biofilm formation in Proteus mirabilis. *Infection and Immunity*, 82(4), pp.1616–1626.

Huddleston, J.R., 2014. Horizontal gene transfer in the human gastrointestinal tract: Potential spread of antibiotic resistance genes. *Infection and Drug Resistance*, 7, pp.167–176.

Hunter, R.J., 1981. *Zeta Potential in Colloid Science-Principles and Applications*. R. H. Ottewill, ed. London, UK: Academic Press.

Hussain, M.S., Kwon, M., and Oh, D.H., 2018. Impact of manganese and heme on biofilm formation of Bacillus cereus food isolates. *PLoS ONE*, 13(7), pp.1–20.

IEA, 2017. *Energy Technology Perspectives 2017*. Paris.

Inoue, H., Nojima, H., and Okayama, H., 1990. High efficiency transformation of Escherichia

coli with plasmids. *Gene*, 96(1), pp.23–28.

Ito, M., Guffanti, A.A., Zemsky, J., Ivey, D.M., and Krulwich, T.A., 1997. Role of the nhaC-encoded Na+/H+ antiporter of alkaliphilic Bacillus firmus OF4. *Journal of Bacteriology*, 179(12), pp.3851–3857.

Ito, M. and Nagane, M., 2001. Improvement of the electro-transformation efficiency of facultatively alkaliphilic Bacillus pseudofirmus OF4 by high osmolarity and glycine treatment. *Bioscience, Biotechnology and Biochemistry*, 65(12), pp.2773–2775.

Jo, B.H., Kim, I.G., Seo, J.H., Kang, D.G., and Cha, H.J., 2013. Engineered Escherichia coli with periplasmic carbonic anhydrase as a biocatalyst for CO2 sequestration. *Applied and environmental microbiology*, 79(21), pp.6697–6705.

Johnston, C., Martin, B., Fichant, G., Polard, P., and Claverys, J.P., 2014. Bacterial transformation: Distribution, shared mechanisms and divergent control. *Nature Reviews Microbiology*, 12(3), pp.181–196.

Jonkers, H.M., 2007. Self Healing Concrete: A Biological Approach. In: S. van der Zwaag, ed. *Self Healing Materials: An Alternative Approach to 20 Centuries of Materials Science*. Dordrecht: Springer Netherlands, pp.195–204.

Jonkers, H.M., 2011. Bacteria-Infused Self-Healing Concrete. *Heron*, 56(1/2), pp.1–12.

Jonkers, H.M. and Schlangen, E., 2007. Crack repair by concrete-immobilized bacteria. *Proceedings of the First International Conference on Self Healing Materials*.

Jonkers, H.M., Thijssen, A., Muyzer, G., Copuroglu, O., and Schlangen, E., 2010. Application of bacteria as self-healing agent for the development of sustainable concrete. *Ecological Engineering*, 36(2), pp.230–235.

Joseph, P., Fantino, J.R., Herbaud, M.L., and Denizot, F., 2001. Rapid orientated cloning in a shuttle vector allowing modulated gene expression in Bacillus subtilis. *FEMS Microbiology Letters*, 205(1), pp.91–97.

Joshi, S., Goyal, S., Mukherjee, A., and Reddy, M.S., 2017. Microbial healing of cracks in concrete: a review. *Journal of Industrial Microbiology and Biotechnology*, 44(11), pp.1511–1525.

Jroundi, F., Schiro, M., Ruiz-Agudo, E., Elert, K., Martín-Sánchez, I., González-Muñoz, M.T., and Rodriguez-Navarro, C., 2017. Protection and consolidation of stone heritage by self-inoculation with indigenous carbonatogenic bacterial communities. *Nature Communications*, 8(1), pp.1–12.

Jürgensen, A., Widmeyer, J.R., Gordon, R.A., Bendell-Young, L.I., Moore, M.M., and Crozier, E.D., 2004. The structure of the manganese oxide on the sheath of the bacterium Leptothrix discophora: An XAFS study. *American Mineralogist*, 89(7), pp.1110–1118.

Kachroo, A.H., Jayaram, M., and Rowley, P.A., 2009. Metabolic engineering without plasmids. *Nature Biotechnology*, 27(8), pp.729–731.

Kamar, R., Réjasse, A., Jéhanno, I., Attieh, Z., Courtin, P., Chapot-Chartier, M.P., Nielsen-Leroux, C., Lereclus, D., el Chamy, L., Kallassy, M., and Sanchis-Borja, V., 2017. DltX of

bacillus thuringiensis is essential for D-Alanylation of teichoic acids and resistance to antimicrobial response in insects. *Frontiers in Microbiology*, 8(1437), pp.1–13.

Kang, C.-H., Oh, S.J., Shin, Y., Han, S.-H., Nam, I.-H., and So, J.-S., 2015. Bioremediation of lead by ureolytic bacteria isolated from soil at abandoned metal mines in South Korea. *Ecological Engineering*, 74, pp.402–407.

Katz, A.K., Glusker, J.P., Markham, G.D., and Bock, C.W., 1998. Deprotonation of water in the presence of carboxylate and magnesium ions. *Journal of Physical Chemistry B*, 102(33), pp.6342–6350.

Kawaguchi, T. and Decho, A.W., 2002. A laboratory investigation of cyanobacterial extracellular polymeric secretions (EPS) in influencing CaCO3 polymorphism. *Journal of Crystal Growth*, 240(1–2), pp.230–235.

Kaźmierczak, J., Fenchel, T., Kühl, M., Kempe, S., Kremer, B., Łącka, B., and Małkowski, K., 2015. Caco3 precipitation in multilayered cyanobacterial mats: Clues to explain the alternation of micrite and sparite layers in calcareous stromatolites. *Life*, 5(1), pp.744–769.

Kearns, D.B., Chu, F., Branda, S.S., Kolter, R., and Losick, R., 2005. A master regulator for biofilm formation by Bacillus subtilis. *Molecular Microbiology*, 55(3), pp.739–749.

Kearns, D.B. and Losick, R., 2003. Swarming motility in undomesticated Bacillus subtilis. *Molecular Microbiology*, 49(3), pp.581–590.

Keren, R., Mayzel, B., Lavy, A., Polishchuk, I., Levy, D., Fakra, S.C., Pokroy, B., and Ilan, M., 2017. Sponge-associated bacteria mineralize arsenic and barium on intracellular vesicles. *Nature Communications*, 8, pp.1–12.

Khan, S.A., 1997. Rolling-circle replication of bacterial plasmids. *Microbiology and molecular biology reviews : MMBR*, 61(4), pp.442–455.

Kibbe, W.A., 2007. OligoCalc: An online oligonucleotide properties calculator. *Nucleic Acids Research*, 35(SUPPL.2).

Kim, H.J., Shin, B., Lee, Y.S., and Park, W., 2017. Modulation of calcium carbonate precipitation by exopolysaccharide in Bacillus sp. JH7. *Applied Microbiology and Biotechnology*, 101(16), pp.6551–6561.

Kim, J.K., Mulrooney, S.B., and Hausinger, R.P., 2005. Biosynthesis of Active Bacillus subtilis Urease in the Absence of Known Urease Accessory Proteins. , 187(20), pp.7150–7154.

Kingston, A.W., Liao, X., and Helmann, J.D., 2013. Contributions of the σW, σM and σX regulons to the lantibiotic resistome of Bacillus subtilis. *Molecular Microbiology*, 90(3), pp.502–518.

Kingston, A.W., Zhao, H., Cook, G.M., and Helmann, J.D., 2014. Accumulation of heptaprenyl diphosphate sensitizes Bacillus subtilis to bacitracin: Implications for the mechanism of resistance mediated by the BceAB transporter. *Molecular Microbiology*, 93(1), pp.37–49.

Kittell, B.L. and Helinski, D.R., 1993. Plasmid Incompatibility and Replication Control. In: C.

D.B, ed. *Bacterial Conjugation*. Boston, MA: Springer, pp.223–242.

Kluge, S. and Weston, J., 2005. Can a hydroxide ligand trigger a change in the coordination number of magnesium ions in biological systems? *Biochemistry*, 44(12), pp.4877–4885.

Klümper, U., Riber, L., Dechesne, A., Sannazzarro, A., Hansen, L.H., Sørensen, S.J., and Smets, B.F., 2015. Broad host range plasmids can invade an unexpectedly diverse fraction of a soil bacterial community. *ISME Journal*, 9, pp.934–945.

Kobayashi, K. and Iwano, M., 2012. BslA(YuaB) forms a hydrophobic layer on the surface of Bacillus subtilis biofilms. *Molecular Microbiology*, 85(1), pp.51–66.

Koga, N., Kasahara, D., and Kimura, T., 2013. Aragonite crystal growth and solid-state aragonite-calcite transformation: A physico-geometrical relationship via thermal dehydration of included water. *Crystal Growth and Design*, 13(5), pp.2238–2246.

Konhauser, K., 2007. Cell surface reactivity and metal sorption. In: *Introduction to Geomicrobiology*. Oxford: Blackwell.

Konhauser, K.O., 1997. Bacterial iron biomineralization in nature. *FEMS Microbiology Reviews*, 20(August), pp.315–126.

Konhauser, K.O., Fyfe, W.S., Schultze-Lam, S., Ferris, F.G., and Beveridge, T.J., 1994. Iron phosphate precipitation by epilithic microbial biofilms in Arctic Canada. *Canadian Journal of Earth Sciences*, 31(8), pp.1320–1324.

Kooli, W.M., Comensoli, L., Maillard, J., Albini, M., Gelb, A., Junier, P., and Joseph, E., 2018. Bacterial iron reduction and biogenic mineral formation for the stabilisation of corroded iron objects. *Scientific Reports*, 8(1), pp.1–11.

Kostner, D., Rachinger, M., Liebl, W., and Ehrenreich, A., 2017. Markerless deletion of putative alanine dehydrogenase genes in bacillus licheniformis using a codBA-Based counterselection technique. *Microbiology (United Kingdom)*, 163(11), pp.1532–1539.

Krajewska, B., 2017. Urease-aided calcium carbonate mineralization for engineering applications: A review. *Journal of Advanced Research*.

Krause, S., Liebetrau, V., Löscher, C.R., Böhm, F., Gorb, S., Eisenhauer, A., and Treude, T., 2018. Marine ammonification and carbonic anhydrase activity induce rapid calcium carbonate precipitation. *Geochimica et Cosmochimica Acta*, 243, pp.116–132.

Kremer, B., Kazmierczak, J., and Stal, L.J., 2008. Calcium carbonate precipitation in cyanobacterial mats from sandy tidal flats of the North Sea. *Geobiology*, 6(1), pp.46–56.

Kropinski, A.M., Hayward, M., Agnew, M.D., and Jarrell, K.F., 2005. The genome of BCJA1c: A bacteriophage active against the alkaliphilic bacterium, Bacillus clarkii. *Extremophiles*, 9(2), pp.99–109.

Kudo, T., Hino, M., Kitada, M., and Horikoshi, K., 1990. DNA sequences required for the alkalophily of Bacillus sp. strain C-125 are located close together on its chromosomal DNA. *Journal of Bacteriology*, 172(12), pp.7282–7283.

Kumar, A., D'Souza, R., and Asthana, M., 2017. Genetic engineering and public perception. In: *Biotechnology for Sustainable Agriculture: Emerging Approaches and Strategies*. Woodhead Publishing, pp.335–373.

Kunal, Rajor, A., and Siddique, R., 2016. Bacterial treatment of alkaline cement kiln dust using Bacillus halodurans strain KG1. *Brazilian Journal of Microbiology*, 47(1), pp.1–9.

Labigne, A., Cussac, V., and Courcoux, P., 1991. Shuttle cloning and nucleotide sequences of Helicobacter pylori genes responsible for urease activity. *Journal of Bacteriology*, 173(6), pp.1920–1931.

Lacks, S.A. and Springhorn, S.S., 1984. Transfer of recombinant plasmids containing the gene for DpnII DNA methylase into strains of Streptococcus pneumoniae that produce DpnI or DpnII restriction endonucleases. *Journal of Bacteriology*, 158(3), pp.905–909.

Lam, K.H.E., Chow, K.C., and Wong, W.K.R., 1998. Construction of an efficient Bacillus subtilis system for extracellular production of heterologous proteins. *Journal of Biotechnology*, 63(3), pp.167–177.

Lauchnor, E.G., Schultz, L.N., Bugni, S., Mitchell, A.C., Cunningham, A.B., and Gerlach, R., 2013. Bacterially induced calcium carbonate precipitation and strontium coprecipitation in a porous media flow system. *Environmental Science and Technology*, 47(3), pp.1557–1564.

Leblanc, D.J. and Lee, L.N., 1984. Physical and genetic analyses of streptococcal plasmid pAM beta 1 and cloning of its replication region. *Journal of Bacteriology*, 157(2), pp.445–453.

Lee, M.H., Mulrooney, S.B., Renner, M.J., Markowicz, Y., and Hausinger, R.P., 1992. Klebsiella aerogenes urease gene cluster: sequence of ureD and demonstration that four accessory genes (ureD, ureE, ureF, and ureG) are involved in nickel metallocenter biosynthesis. *Journal of Bacteriology*, 174(13), pp.4324–4330.

Lee, Y.S. and Park, W., 2018. Current challenges and future directions for bacterial self-healing concrete. *Applied Microbiology and Biotechnology*, 102(7), pp.3059–3070.

Lefèvre, C.T., Menguy, N., Abreu, F., Lins, U., Pósfai, M., Prozorov, T., Pignol, D., Frankel, R.B., and Bazylinski, D.A., 2011. A cultured greigite-producing magnetotactic bacterium in a novel group of sulfate-reducing bacteria. *Science*, 334(6063), pp.1720–1723.

Leiman, S.A., Arboleda, L.C., Spina, J.S., and McLoon, A.L., 2014. SinR is a mutational target for fine-tuning biofilm formation in laboratory-evolved strains of Bacillus subtilis. *BMC Microbiology*, 14(1), pp.1–10.

Letunić, I., 2015. *phyloT: a tree generator* [Online]. Available from: https://phylot.biobyte.de/

Letunic, I. and Bork, P., 2016. Interactive tree of life (iTOL) v3: an online tool for the display and annotation of phylogenetic and other trees. *Nucleic acids research*, 44(W1), pp.W242–W245.

Li, L., Qian, C., Cheng, L., and Wang, R., 2010. A laboratory investigation of microbe-inducing

CdCO3 precipitate treatment in Cd2+ contaminated soil. *Journal of Soils and Sediments*, 10(2), pp.248–254.

Li, W., Liu, L.P., Zhou, P.P., Cao, L., Yu, L.J., and Jiang, S.Y., 2011. Calcite precipitation induced by bacteria and bacterially produced carbonic anhydrase. *Current Science*, 100(4), pp.502–508.

Liang, L., Heveran, C., Liu, R., Gill, R.T., Nagarajan, A., Cameron, J., Hubler, M., Srubar, W. V., and Cook, S.M., 2018. Rational Control of Calcium Carbonate Precipitation by Engineered Escherichia coli. *ACS Synthetic Biology*, 7(11), pp.2497–2506.

Lilly, J. and Camps, M., 2015. Mechanisms of Theta Plasmid Replication. *Microbiology spectrum*, 3(1), pp.139–148.

Lindsay, D., Brözel, V.S., and Von Holy, A., 2006. Biofilm-spore response in Bacillus cereus and Bacillus subtilis during nutrient limitation. *Journal of Food Protection*, 69(5), pp.1168–1172.

Liu, B., Deng, X., Han, N., Xing, F., and Zhang, J., 2016. Investigation of Self-healing by Using Ethyl Cellulose Encapsulated Bacterium in Cementitious Materials. In: *Proceedings of the 9th International Conference on Fracture Mechanics of Concrete and Concrete Structures*. IA-FraMCoS, pp.84–87.

Liu, Q., Chen, Y., Yuan, M., Du, G., Chen, J., and Kang, Z., 2017. A Bacillus paralicheniformis iron-containing urease reduces urea concentrations in rice wine. *Applied and Environmental Microbiology*, 83(17), pp.19–21.

Lopez-Berganza, J.A., Chen, S., and Espinosa-Marzal, R.M., 2019. Tailoring Calcite Growth through an Amorphous Precursor in a Hydrogel Environment. *Crystal Growth and Design*, 19(6), pp.3192–3205.

López, C.M., Rholl, D.A., Trunck, L.A., and Schweizer, H.P., 2009. Versatile dual-technology system for markerless allele replacement in Burkholderia pseudomallei. *Applied and Environmental Microbiology*, 75(20), pp.6496–6503.

Lovley, D.R., 1991. Dissimilatory Fe (III) and Mn (IV) reduction. *Microbiology Reviews*, 55(2), pp.259–287.

Lovley, D.R. and Phillips, E.J.P., 1992. Reduction of uranium by Desulfovibrio desulfuricans. *Applied and Environmental Microbiology*, 58(3), pp.850–856.

Ma, W., Peng, D., Walker, S.L., Cao, B., Gao, C.H., Huang, Q., and Cai, P., 2017. Bacillus subtilis biofilm development in the presence of soil clay minerals and iron oxides. *npj Biofilms and Microbiomes*, 3(1), pp.0–1.

Macaskie, L., Empson, R., Cheetham, A., Grey, C., and Skarnulis, A., 1992. Uranium bioaccumulation by a Citrobacter sp. as a result of enzymically mediated growth of polycrystalline HUO2PO4. *Science*, 257(5071), pp.782–784.

Macaskie, L.E., Bonthrone, K.M., and Rouch, D.A., 1994. Phosphatase-mediated heavy metal accumulation by a Citrobacter sp. and related enterobacteria. *FEMS Microbiology Letters*, 121(2), pp.141–146.

Madigan, M.T., Bender, K.S., Buckley, D.H., Sattley, M.W., and Stahl, D.A., 2018. *Brock Biology of Microorganisms*. 15th ed. New York, USA: Pearson Higher Education.

Mandic-Mulec, I., Doukhan, L., and Smith, I., 1995. The Bacillus subtilis SinR protein is a repressor of the key sporulation gene spo0A. *Journal of Bacteriology*, 177(16), pp.4619–4627.

Mann, S., Sparks, N.H., Scott, G.H., and de Vrind-de Jong, E.W., 1988. Oxidation of Manganese and Formation of Mn3O4 (Hausmannite) by Spore Coats of a Marine Bacillus sp. *Applied and Environmental Microbiology*, 54(8), pp.2140–2143.

Martinez, R.E., Gardés, E., Pokrovsky, O.S., Schott, J., and Oelkers, E.H., 2010. Do photosynthetic bacteria have a protective mechanism against carbonate precipitation at their surfaces? *Geochimica et Cosmochimica Acta*, 74(4), pp.1329–1337.

Martinez, R.E., Pokrovsky, O.S., Schott, J., and Oelkers, E.H., 2008. Surface charge and zeta-potential of metabolically active and dead cyanobacteria. *Journal of Colloid and Interface Science*, 323(2), pp.317–325.

Martinez, R.J., Beazley, M.J., Taillefert, M., Arakaki, A.K., Skolnick, J., and Sobecky, P.A., 2007. Aerobic uranium (VI) bioprecipitation by metal-resistant bacteria isolated from radionuclide- and metal-contaminated subsurface soils. *Environmental Microbiology*, 9(12), pp.3122–3133.

Marvasi, M., Visscher, P.T., and Casillas Martinez, L., 2010. Exopolymeric substances (EPS) from Bacillus subtilis: Polymers and genes encoding their synthesis. *FEMS Microbiology Letters*, 313(1), pp.1–9.

Marvasi, M., Visscher, P.T., Perito, B., Mastromei, G., and Casillas-Martínez, L., 2010. Physiological requirements for carbonate precipitation during biofilm development of Bacillus subtilis etfA mutant. *FEMS Microbiology Ecology*, 71(3), pp.341–350.

Mazodier, P. and Davies, J., 1991. Gene Transfer Between Distantly Related Bacteria. *Annual Review of Genetics*, 25(1), pp.147–171.

McFarland, J., 1907. The nephelometer:an instrument for estimating the number of bacteria in suspensions used for calculating the opsonic index and for vaccines. *JAMA: The Journal of the American Medical Association*, XLIX(14), p.1176.

McKenzie, T., Hoshino, T., Tanaka, T., and Sueoka, N., 1986. The nucleotide sequence of pUB110: Some salient features in relation to replication and its regulation. *Plasmid*, 15(2), pp.93–103.

Meldrum, F.C. and Hyde, S.T., 2001. Morphological influence of magnesium and organic additives on the precipitation of calcite. *Journal of Crystal Growth*, 231(4), pp.544–558.

Merroun, M.L., Nedelkova, M., Ojeda, J.J., Reitz, T., Fernández, M.L., Arias, J.M., Romero-González, M., and Selenska-Pobell, S., 2011. Bio-precipitation of uranium by two bacterial isolates recovered from extreme environments as estimated by potentiometric titration, TEM and X-ray absorption spectroscopic analyses. *Journal of Hazardous Materials*, 197, pp.1–10.

Merroun, M.L., Raff, J., Rossberg, A., Hennig, C., Reich, T., and Selenska-Pobell, S., 2005. Complexation of uranium by cells and S-layer sheets of Bacillus sphaericus JG-A12. *Applied and Environmental Microbiology*, 71(9), pp.5532–5543.

Mielich-Süss, B. and Lopez, D., 2015. Molecular mechanisms involved in Bacillus subtilis biofilm formation. *Environmental Microbiology*, 17(3), pp.555–565.

Miyano, M., Tanaka, K., Ishikawa, S., Takenaka, S., Miguel-Arribas, A., Meijer, W.J.J., and Yoshida, K. ichi, 2018. Rapid conjugative mobilization of a 100kb segment of Bacillus subtilis chromosomal DNA is mediated by a helper plasmid with no ability for self-transfer. *Microbial Cell Factories*, 17(1), pp.1–10.

Mizuki, T., Kamekura, M., Dassarma, S., Fukushima, T., Usami, R., Yoshida, Y., and Horikoshi, K., 2004. Ureases of Extreme Halophiles of the Genus Haloarcula with a Unique Structure of Gene Cluster. *Bioscience, Biotechnology, and Biochemistry*, 68(2), pp.397–406.

Mobley, H.L. and Hausinger, R.P., 1989. Microbial ureases: significance, regulation, and molecular characterization. *Microbiological reviews*, 53(1), pp.85–108.

Mobley, H.L., Island, M.D., and Hausinger, R.P., 1995. Molecular biology of microbial ureases. *Microbiological reviews*, 59(3), pp.451–480.

Moller, A.G., Lindsay, J.A., and Read, T.D., 2019. Determinants of phage host range in Staphylococcus species. *Applied and Environmental Microbiology*, 85(11), pp.1–16.

Morikawa, M., Kagihiro, S., Haruki, M., Takano, K., Branda, S., Kolter, R., and Kanaya, S., 2006. Biofilm formation by a Bacillus subtilis strain that produces γ-polyglutamate. *Microbiology*, 152(9), pp.2801–2807.

Mrázek, J. and Xie, S., 2019. *Amino Acid and Codon Usage Statistics* [Online]. Available from: https://www.cmbl.uga.edu/software/codon_usage.html

Van Mullem, T., Gruyaert, E., Caspeele, R., and De Belie, N., 2020. First Large Scale Application with Self-Healing Concrete in Belgium: Analysis of the Laboratory Control Tests. *Materials*, 13(4), p.997.

Müller, A.K., Rojo, F., and Alonso, J.C., 1995. The level of the pUB110 replication initiator protein is autoregulated, which provides an additional control for plasmid copy number. *Nucleic Acids Research*, 23(11), pp.1894–1900.

Murai, R. and Yoshida, N., 2013. Geobacillus thermoglucosidasius endospores function as nuclei for the formation of single calcite crystals. *Applied and Environmental Microbiology*, 79(9), pp.3085–3090.

Murphy, E., 1985. Nucleotide sequence of a spectinomycin adenyltransferase AAD(9) determinant from Staphylococcus aureus and its relationship to AAD(3") (9). *Molecular and General Genetics MGG*, 200(1), pp.33–39.

De Muynck, W., De Belie, N., and Verstraete, W., 2010. Microbial carbonate precipitation in construction materials: A review. *Ecological Engineering*, 36(2), pp.118–136.

Mykytczuk, N.C.S., Lawrence, J.R., Omelon, C.R., Southam, G., and Whyte, L.G., 2016.

Microscopic characterization of the bacterial cell envelope of Planococcus halocryophilus Or1 during subzero growth at −15 °C. *Polar Biology*, 39(4), pp.701–712.

Naik-Samant, S. and Furtado, I., 2019. Formation of Rhodochrosite by Haloferax alexandrinus GUSF-1. *Journal of Cluster Science*, 30(6), pp.1435–1441.

National Academies of Sciences and Medicine, E., 2017. *Communicating Science Effectively*. Washington, D.C.: National Academies Press.

Nazarian, P., Tran, F., and Boedicker, J.Q., 2018. Modeling multispecies gene flow dynamics reveals the unique roles of different horizontal gene transfer mechanisms. *Frontiers in Microbiology*, 9, p.2978.

Newsome, L., Morris, K., and Lloyd, J.R., 2014. The biogeochemistry and bioremediation of uranium and other priority radionuclides. *Chemical Geology*, 363, pp.164–184.

Ngwenya, B.T., Magennis, M., Podda, F., and Gromov, A., 2014. Self-preservation strategies during bacterial biomineralization with reference to hydrozincite and implications for fossilization of bacteria. *Journal of the Royal Society Interface*, 11(100), p.20140845.

Ni, M. and Ratner, B.D., 2008. Differentiating calcium carbonate polymorphs by surface analysis techniques-an XPS and TOF-SIMS study. *Surface and Interface Analysis*, 40(10), pp.1356–1361.

Nicolas, P., Mader, U., Dervyn, E., Rochat, T., Leduc, A., Pigeonneau, N., Bidnenko, E., Marchadier, E., Hoebeke, M., Aymerich, S., Becher, D., Bisicchia, P., Botella, E., Delumeau, O., Doherty, G., Denham, E.L., Fogg, M.J., Fromion, V., Goelzer, A., Hansen, A., Hartig, E., Harwood, C.R., Homuth, G., Jarmer, H., Jules, M., Klipp, E., Le Chat, L., Lecointe, F., Lewis, P., Liebermeister, W., March, A., Mars, R.A.T., Nannapaneni, P., Noone, D., Pohl, S., Rinn, B., Rugheimer, F., Sappa, P.K., Samson, F., Schaffer, M., Schwikowski, B., Steil, L., Stulke, J., Wiegert, T., Devine, K.M., Wilkinson, A.J., Maarten van Dijl, J., Hecker, M., Volker, U., Bessieres, P., and Noirot, P., 2012. Condition-Dependent Transcriptome Reveals High-Level Regulatory Architecture in Bacillus subtilis. *Science*, 335(6072), pp.1103–1106.

Nielsen, S.D., Koren, K., Löbmann, K., Hinge, M., Scoma, A., Kjeldsen, K.U., and Røy, H., 2020. Constraints on CaCO3 precipitation in superabsorbent polymer by aerobic bacteria. *Applied Microbiology and Biotechnology*, 104(1), pp.365–375.

Norman, A., Hansen, L.H., and Sørensen, S.J., 2009. Conjugative plasmids: Vessels of the communal gene pool. *Philosophical Transactions of the Royal Society B: Biological Sciences*, 364(1527), pp.2275–2289.

Novick, R.P., 1987. Plasmid incompatibility. *Microbiological reviews*, 51(4), pp.381–95.

Okyay, T.O. and Rodrigues, D.F., 2013. High throughput colorimetric assay for rapid urease activity quantification. *Journal of Microbiological Methods*, 95(3), pp.324–326.

Oliveira, P.H. and Mairhofer, J., 2013. Marker-free plasmids for biotechnological applications - implications and perspectives. *Trends in Biotechnology*, 31(9), pp.539–547.

Olorunniji, F.J., McPherson, A.L., Rosser, S.J., Smith, M.C.M., Colloms, S.D., and Marshall

Stark, W., 2017. Control of serine integrase recombination directionality by fusion with the directionality factor. *Nucleic Acids Research*, 45(14), pp.8635–8645.

Omoike, A. and Chorover, J., 2004. Spectroscopic study of extracellular polymeric substances from Bacillus subtilis: Aqueous chemistry and adsorption effects. *Biomacromolecules*, 5(4), pp.1219–1230.

Oppenheimer-Shaanana, Y., Sibony-Nevo, O., Bloom-Ackermann, Z., Suissa, R., Steinberg, N., Kartvelishvily, E., Brumfeld, V., and Kolodkin-Gal, I., 2016. Spatio-temporal assembly of functional mineral scaffolds within microbial biofilms. *npj Biofilms and Microbiomes*, 57(6), pp.10–13.

Ouda, A.S., 2015. Development of high-performance heavy density concrete using different aggregates for gamma-ray shielding. *HBRC Journal*, 11(3), pp.328–338.

Page, R. and Peti, W., 2016. Toxin-antitoxin systems in bacterial growth arrest and persistence. *Nature Chemical Biology*, 12(4), pp.208–214.

Paine, K., 2016. Bacteria-Based Self-Healing of Concrete: Effects of Environment, Exposure and Crack Size. *Proceedings of the RILEM Conference on Microorganisms-Cementitious Materials Interactions*, (1), pp.1–15.

Palin, D., Wiktor, V., and Jonkers, H.M., 2016. A bacteria-based bead for possible self-healing marine concrete applications. *Smart Materials and Structures*, 25(8), p.084008.

Palin, D., Wiktor, V., and Jonkers, H.M., 2017. A Bacteria-Based Self-Healing Cementitious Composite for Application in Low-Temperature Marine Environments. *Biomimetics*, 2(3), p.13.

Partridge, S.R., Kwong, S.M., Firth, N., and Jensen, S.O., 2018. Mobile genetic elements associated with antimicrobial resistance. *Clinical Microbiology Reviews*, 31(4), pp.1–61.

Peplow, M., 2020. Bioconcrete presages new wave in environmentally friendly construction. *Nature Biotechnology*, 38(7), pp.776–778.

Perego, M., Glaser, P., Minutello, A., Strauch, M.A., Leopold, K., and Fischer, W., 1995. Incorporation of D-Alanine into Lipoteichoic Acid and Wall Teichoic Acid in Bacillus subtilis. *Journal of Biological Chemistry*, 270(26), pp.15598–15606.

Phillips, A.J., Gerlach, R., Lauchnor, E., Mitchell, A.C., Cunningham, A.B., and Spangler, L., 2013. Engineered applications of ureolytic biomineralization: A review. *Biofouling*, 29(6), pp.715–733.

Picard, A., Gartman, A., Clarke, D.R., and Girguis, P.R., 2018. Sulfate-reducing bacteria influence the nucleation and growth of mackinawite and greigite. *Geochimica et Cosmochimica Acta*, 220, pp.367–384.

Podda, F., Zuddas, P., Minacci, A., Pepi, M., and Baldi, F., 2000. Heavy Metal Coprecipitation with Hydrozincite [Zn5(CO3)2(OH)6] from Mine Waters Caused by Photosynthetic Microorganisms. *Applied and Environmental Microbiology*, 66(11), pp.5092–5098.

Polgári, M., Gyollai, I., Fintor, K., Horváth, H., Pál-Molnár, E., and Biondi, J.C., 2019. Microbially Mediated Ore-Forming Processes and Cell Mineralization. *Frontiers in Microbiology*, 10.

Power, I.M., Wilson, S.A., Thom, J.M., Dipple, G.M., and Southam, G., 2007. Biologically induced mineralization of dypingite by cyanobacteria from an alkaline wetland near Atlin, British Columbia, Canada. *Geochemical Transactions*, 8, pp.1–16.

Powers, L.G., Mills, H.J., Palumbo, A. V., Zhang, C., Delaney, K., and Sobecky, P.A., 2002. Introduction of a plasmid-encoded phoA gene for constitutive overproduction of alkaline phosphatase in three subsurface Pseudomonas isolates. *FEMS Microbiology Ecology*, 41(2), pp.115–123.

Poyart, C. and Trieu-Cuot, P., 2006. A broad-host-range mobilizable shuttle vector for the construction of transcriptional fusions to β-galactosidase in Gram-positive bacteria. *FEMS Microbiology Letters*, 156(2), pp.193–198.

Preiss, L., Hicks, D.B., Suzuki, S., Meier, T., and Krulwich, T.A., 2015. Alkaliphilic bacteria with impact on industrial applications, concepts of early life forms, and bioenergetics of ATP synthesis. *Frontiers in Bioengineering and Biotechnology*, 3(JUN), pp.1–16.

Del Prete, S., Perfetto, R., Rossi, M., Alasmary, F.A.S., Osman, S.M., AlOthman, Z., Supuran, C.T., and Capasso, C., 2017. A one-step procedure for immobilising the thermostable carbonic anhydrase (SspCA) on the surface membrane of Escherichia coli. *Journal of Enzyme Inhibition and Medicinal Chemistry*, 32(1), pp.1120–1128.

Prozorov, A.A., 2003. Conjugation in bacilli. *Microbiology*, 72(5), pp.517–527.

Pungrasmi, W., Intarasoontron, J., Jongvivatsakul, P., and Likitlersuang, S., 2019. Evaluation of Microencapsulation Techniques for MICP Bacterial Spores Applied in Self-Healing Concrete. *Scientific Reports*, 9(1), pp.1–10.

Purcell, E.M., 1977. Life at low Reynolds number. *American Journal of Physics*, 45(1), pp.3–11.

Rachinger, M., Bauch, M., Strittmatter, A., Bongaerts, J., Evers, S., Maurer, K.H., Daniel, R., Liebl, W., Liesegang, H., and Ehrenreich, A., 2013. Size unlimited markerless deletions by a transconjugative plasmid-system in Bacillus licheniformis. *Journal of Biotechnology*, 167(4), pp.365–369.

Radeck, J., Kraft, K., Bartels, J., Cikovic, T., Dürr, F., Emenegger, J., Kelterborn, S., Sauer, C., Fritz, G., Gebhard, S., and Mascher, T., 2013. The Bacillus BioBrick Box: generation and evaluation of essential genetic building blocks for standardized work with Bacillus subtilis. *Journal of biological engineering*, 7(1), p.29.

Raleigh, E.A., 2001. Conjugation, Bacterial. *Encyclopedia of Genetics*, pp.453–455.

Ramsay, J.P. and Firth, N., 2017. Diverse mobilization strategies facilitate transfer of non-conjugative mobile genetic elements. *Current Opinion in Microbiology*, 38, pp.1–9.

Reeder, R.J., Lamble, G.M., and Northrup, P.A., 1999. XAFS study of the coordination and local relaxation around Co2+, Zn2+, Pb2+, and Ba2+ trace elements in calcite. *American Mineralogist*, 84(7–8), pp.1049–1060.

Reeksting, B.J., Hoffmann, T.D., Tan, L., Paine, K., and Gebhard, S., 2020. In-Depth Profiling of Calcite Precipitation by Environmental Bacteria Reveals Fundamental Mechanistic Differences with Relevance to Application. *Applied and Environmental Microbiology*, 86(7), pp.e02739-19.

Revilla-Guarinos, A., Gebhard, S., Alcántara, C., Staroń, A., Mascher, T., and Zúñiga, M., 2013. Characterization of a regulatory network of peptide antibiotic detoxification modules in lactobacillus casei BL23. *Applied and Environmental Microbiology*, 79(10), pp.3160–3170.

Revilla-Guarinos, A., Gebhard, S., Mascher, T., and Zúñiga, M., 2014. Defence against antimicrobial peptides: Different strategies in Firmicutes. *Environmental Microbiology*, 16(5), pp.1225–1237.

Richhardt, J., Larsen, M., and Meinhardt, F., 2010. An improved transconjugation protocol for Bacillus megaterium facilitating a direct genetic knockout. *Applied Microbiology and Biotechnology*, 86(6), pp.1959–1965.

Riding, R., 2000. Microbial carbonates: the geological record of calcified bacterial algal mats and biofilms. *Sedimentology*, 47, pp.179–214.

Rivadeneyra, A., Gonzalez-Martinez, A., Gonzalez-Lopez, J., Martin-Ramos, D., Martinez-Toledo, M.V., and Rivadeneyra, M.A., 2014. Precipitation of phosphate minerals by microorganisms isolated from a fixed-biofilm reactor used for the treatment of domestic wastewater. *International Journal of Environmental Research and Public Health*, 11(4), pp.3689–3704.

Rivadeneyra, M.A., Ramos-Cormenzana, A., and Garcia-Cervigon, A., 1987. Formation of bobierrite (magnesium phosphate) crystal aggregates by acinetobacter sp. *Mineralogical Journal*, 13(7), pp.443–447.

Roberts, J.A., Kenward, P.A., Fowle, D.A., Goldstein, R.H., González, L.A., and Moore, D.S., 2013. Surface chemistry allows for abiotic precipitation of dolomite at low temperature. *Proceedings of the National Academy of Sciences of the United States of America*, 110(36), pp.14540–14545.

Rodrigue, A., Albareda, M., Mandrand-Berthelot, M.A., and Palacios, J., 2017. Nickel in Microbial Physiology - From Single Proteins to Complex Trafficking Systems: Nickel Import/Export. In: D. Zamble, M. Rowińska-Żyrek, & H. Kozloski, eds. *RSC Metallobiology*. The Royal Society of Chemistry, pp.237–258.

Rodriguez-Navarro, C., Jimenez-Lopez, C., Rodriguez-Navarro, A., Gonzalez-Muñoz, M.T., and Rodriguez-Gallego, M., 2007. Bacterially mediated mineralization of vaterite. *Geochimica et Cosmochimica Acta*, 71(5), pp.1197–1213.

Roh, Y., Liu, S. V, Li, G., Huang, H., Phelps, T.J., and Zhou, J., 2002. Isolation and Characterization of Metal-Reducing Thermoanaerobacter Strains from Deep Subsurface Environments of the Piceance Basin, Colorado. *Applied and Environmental Microbiology*, 68(12), pp.6013–6020.

Romero, D., Pérez-García, A., Veening, J.W., de Vicente, A., and Kuipers, O.P., 2006. Transformation of undomesticated strains of Bacillus subtilis by protoplast

electroporation. *Journal of Microbiological Methods*, 66(3), pp.556–559.

Rommens, C.M., 2010. Barriers and paths to market for genetically engineered crops. *Plant Biotechnology Journal*, 8(2), pp.101–111.

Saar-Dover, R., Bitler, A., Nezer, R., Shmuel-Galia, L., Firon, A., Shimoni, E., Trieu-Cuot, P., and Shai, Y., 2012. D-Alanylation of Lipoteichoic Acids Confers Resistance to Cationic Peptides in Group B Streptococcus by Increasing the Cell Wall Density. *PLoS Pathogens*, 8(9).

Sambrook, J. and W Russell, D., 2001. Molecular Cloning: A Laboratory Manual. *Cold Spring Harbor Laboratory Press, Cold Spring Harbor, NY*.

Sanchez-Moral, S., Luque, L., Cañaveras, J.C., Laiz, L., Jurado, V., Hermosin, B., and Saiz-Jimenez, C., 2004. Bioinduced barium precipitation in St. Callixtus and Domitilla catacombs. *Annals of Microbiology*, 54(1), pp.1–12.

Sansinenea, E., 2011. Bacillus thuringiensis Biotechnology. *Springer, Dordrecht*, 68(70), pp.59–68.

Sayers, E.W., Barrett, T., Benson, D.A., Bryant, S.H., Canese, K., Chetvernin., V., Church, D.M., Dicuccio, M., Edgar, R., Federhen, S., Feolo, M., Geer, L.Y., Helmberg, W., Kapustin, Y., Landsman, D., Lipman, D.J., Madden, T.L., Maglott, D.R., Miller, V., Mizrachi, I., Ostell, J., Pruitt, K.D., Schuler, G.D., Sequeira, E., Sherry, S.T., Shumway, M., Sirotkin, K., Souvorov, A., Starchenko, G., Tatusova, T.A., Wagner, L., Yaschenko, E., and Ye, J., 2009. Database resources of the National Center for Biotechnology Information. *Nucleic Acids Research*, 37(SUPPL. 1), pp.5–15.

Schallmey, M., Singh, A., and Ward, O.P., 2004. Developments in the use of Bacillus species for industrial production. *Canadian Journal of Microbiology*, 50(1), pp.1–17.

Schubert, H.J., Lück, H., and Auermann, E., 1989. Nickel Dermatitis in Construction Workers. In: *Current Topics in Contact Dermatitis*. Berlin, Heidelberg: Springer Berlin Heidelberg, pp.191–194.

Schultz, D., Wolynes, P.G., Jacob, E. Ben, and Onuchic, J.N., 2009. Deciding fate in adverse times: Sporulation and competence in Bacillus subtilis. *Proceedings of the National Academy of Sciences of the United States of America*, 106(50), pp.21027–21034.

Schultze-Lam, S. and Beveridge, T.J., 1994. Nucleation of celestite and strontianite on a cyanobacterial S-layer. *Applied and Environmental Microbiology*, 60(2), pp.447–453.

Schultze-Lam, S., Fortin, D., Davis, B.S., and Beveridge, T.J., 1996. Mineralization of bacterial surfaces. *Chemical Geology*, 132(1–4), pp.171–181.

Schultzelam, S., Harauz, G., and Beveridge, T.J., 1992. Participation of a Cyanobacterial-S Layer in Fine-Grain Mineral Formation. *Journal of Bacteriology*, 174(24), pp.7971–7981.

Schweizer, H.P., 2008. Bacterial genetics: Past achievements, present state of the field, and future challenges. *BioTechniques*, 44(5), pp.633–641.

Scott, S.E., Inbar, Y., Wirz, C.D., Brossard, D., and Rozin, P., 2018. An overview of attitudes

toward genetically engineered food. *Annual Review of Nutrition*, 38, pp.459–479.

Sebbane, F., Bury-Moné, S., Cailliau, K., Browaeys-Poly, E., De Reuse, H., and Simonet, M., 2002. The Yersinia pseudotuberculosis Yut protein, a new type of urea transporter homologous to eukaryotic channels and functionally interchangeable in vitro with the Helicobacter pylori Urel protein. *Molecular Microbiology*, 45(4), pp.1165–1174.

Sebbane, F., Mandrand-Berthelot, M.A., and Simonet, M., 2002. Genes encoding specific nickel transport systems flank the chromosomal urease locus of pathogenic yersiniae. *Journal of Bacteriology*, 184(20), pp.5706–5713.

Seifan, M. and Berenjian, A., 2018. Application of microbially induced calcium carbonate precipitation in designing bio self-healing concrete. *World Journal of Microbiology and Biotechnology*, 34(11), p.168.

Seifan, M. and Berenjian, A., 2019. Microbially induced calcium carbonate precipitation: a widespread phenomenon in the biological world. *Applied Microbiology and Biotechnology*, 103(12), pp.4693–4708.

Seifan, M., Samani, A.K., and Berenjian, A., 2017. A novel approach to accelerate bacterially induced calcium carbonate precipitation using oxygen releasing compounds (ORCs). *Biocatalysis and Agricultural Biotechnology*, 12, pp.299–307.

Sewell, E.W.C. and Brown, E.D., 2014. Taking aim at wall teichoic acid synthesis: New biology and new leads for antibiotics. *Journal of Antibiotics*, 67(1), pp.43–51.

Shafikhani, S.H. and Leighton, T., 2004. AbrB and Spo0E Control the Proper Timing of Sporulation in Bacillus subtilis. *Current Microbiology*, 48(4), pp.262–269.

Sharma, T.K., Alazhari, M., Heath, A., Paine, K., and Cooper, R.M., 2017. Alkaliphilic Bacillus species show potential application in concrete crack repair by virtue of rapid spore production and germination then extracellular calcite formation. *Journal of Applied Microbiology*, 122(5), pp.1233–1244.

Shemesh, M. and Chaia, Y., 2013. A combination of glycerol and manganese promotes biofilm formation in Bacillus subtilis via histidine kinase KinD signaling. *Journal of Bacteriology*, 195(12), pp.2747–2754.

Shepard, B.D. and Gilmore, M.S., 1995. Electroporation and efficient transformation of Enterococcus faecalis grown in high concentrations of glycine. *Methods in molecular biology*, 47, pp.217–226.

Sierra-Beltran, M.G., Jonkers, H.M., and Ortiz, M., 2015. Field application of self--healing concrete with natural fibres as linings for irrigation canals in Ecuador. *Fifth International Conference on Self-Healing Materials*, p.32.

Sierra Beltran, M.G. and Jonkers, H.M., 2015. Crack self-healing technology based on bacteria. *Journal of Ceramic Processing Research*, 16, pp.s33–s39.

Simon, R., Prieffer, U., and Puhler, A., 1983. A broad host range mobilization system for in vivo genetic engineering: Transposon mutagenesis in gram negative bacteria. *Biotechnology*, (1), pp.784–790.

Sleytr, U.B., Schuster, B., Egelseer, E.M., and Pum, D., 2014. S-layers: Principles and applications. *FEMS Microbiology Reviews*, 38(5), pp.823–864.

Smillie, C., Garcillán-Barcia, M.P., Francia, M.V., Rocha, E.P.C., and de la Cruz, F., 2010. Mobility of Plasmids. *Microbiology and Molecular Biology Reviews*, 74(3), pp.434–452.

del Solar, G., Giraldo, R., Ruiz-Echevarría, M.J., Espinosa, M., and Díaz-Orejas, R., 1998. Replication and Control of Circular Bacterial Plasmids. *Microbiology and Molecular Biology Reviews*, 62(2), pp.434–464.

Son, H.M., Kim, H.Y., Park, S.M., and Lee, H.K., 2018. Ureolytic/Non-ureolytic bacteria co-cultured self-healing agent for cementitious materials crack repair. *Materials*, 11(5), p.782.

Soon, R.L., Nation, R.L., Cockram, S., Moffatt, J.H., Harper, M., Adler, B., Boyce, J.D., Larson, I., and Li, J., 2011. Different surface charge of colistin-susceptible and -resistant Acinetobacter baumannii cells measured with zeta potential as a function of growth phase and colistin treatment. *Journal of Antimicrobial Chemotherapy*, 66(1), pp.126–133.

Soriano, A., Colpas, G.J., and Hausinger, R.P., 2000. UreE stimulation of GTP-dependent urease activation in the UreD-UreF-UreG-urease apoprotein complex. *Biochemistry*, 39(40), pp.12435–12440.

Soriano, A. and Hausinger, R.P., 1999. GTP-dependent activation of urease apoprotein in complex with the UreD, UreF, and UreG accessory proteins. *Proceedings of the National Academy of Sciences of the United States of America*, 96(20), pp.11140–11144.

Southam, G., 2000. Bacterial Surface-Mediated Mineral Formation. In: D. R. Lovley, ed. *Environmental Microbe-Metal Interactions*. American Society of Microbiology, pp.257–276.

Stabnikov, V., Jian, C., Ivanov, V., and Li, Y., 2013. Halotolerant, alkaliphilic urease-producing bacteria from different climate zones and their application for biocementation of sand. *World Journal of Microbiology and Biotechnology*, 29(8), pp.1453–1460.

Stark, W.M., 2017. Making serine integrases work for us. *Current Opinion in Microbiology*, 38, pp.130–136.

Staroń, A., Finkeisen, D.E., and Mascher, T., 2011. Peptide antibiotic sensing and detoxification modules of Bacillus subtilis. *Antimicrobial Agents and Chemotherapy*, 55(2), pp.515–525.

Strand, T.A., Lale, R., Degnes, K.F., Lando, M., and Valla, S., 2014. A new and improved host-independent plasmid system for RK2-based conjugal transfer. *PLoS ONE*, 9(3), pp.1–6.

Styles, M.Q., Nesbitt, E.A., Hoffmann, T.D., Queen, J., Ortenzi, M. V, and Leak, D.J., 2020. The heterologous production of terpenes by the thermophile Parageobacillus thermoglucosidasius in a consolidated bioprocess using waste bread. *Metabolic Engineering*, (November).

Sultan, I., Rahman, S., Jan, A.T., Siddiqui, M.T., Mondal, A.H., and Haq, Q.M.R., 2018. Antibiotics, resistome and resistance mechanisms: A bacterial perspective. *Frontiers in Microbiology*, 9(2066), pp.1–16.

Suzuki, Y., Kelly, S.D., Kemner, K.M., and Banfield, J.F., 2003. Microbial populations stimulated for hexavalent uranium reduction in uranium mine sediment. *Applied and Environmental Microbiology*, 69(3), pp.1337–1346.

Ta, K., Peng, X., Chen, S., Xu, H., Li, J., Du, M., Hao, J., and Lin, Y., 2017. Hydrothermal nontronite formation associated with microbes from low-temperature diffuse hydrothermal vents at the South Mid-Atlantic Ridge. *Journal of Geophysical Research: Biogeosciences*, 122(9), pp.2375–2392.

Tan, L., Reeksting, B., Ferrandiz-Mas, V., Heath, A., Gebhard, S., and Paine, K., 2020. Effect of carbonation on bacteria-based self-healing of cementitious composites. *Construction and Building Materials*, 257, p.119501.

Tegethoff, F.W., 2001. *Calcium Carbonate: From the Cretaceous Period into the 21st Century*. Basel: Springer.

Thoma, S. and Schobert, M., 2009. An improved escherichia coli donor strain for diparental mating. *FEMS Microbiology Letters*, 294(2), pp.127–132.

Thomas, C.M., 2014. Plasmid Incompatibility. In: *Molecular Life Sciences*. New York, NY: Springer New York, pp.1–3.

Thomas, C.M. and Nielsen, K.M., 2005. Mechanisms of, and barriers to, horizontal gene transfer between bacteria. *Nature Reviews Microbiology*, 3(9), pp.711–721.

Thomas, K.J. and Rice, C. V., 2014. Revised model of calcium and magnesium binding to the bacterial cell wall. *BioMetals*, 27(6), pp.1361–1370.

Thomas, K.J. and Rice, C. V., 2015. Equilibrium binding behavior of magnesium to wall teichoic acid. *Biochimica et Biophysica Acta - Biomembranes*, 1848(10), pp.1981–1987.

Thompson, J.B. and Ferris, F.G., 1992. Cyanobacterial Precipitation of Gypsum, Calcite and Magnesitre From Natural Lake Water. *Geology*, 18(10), pp.995–998.

Tominaga, Y., Ohshiro, T., and Suzuki, H., 2016. Conjugative plasmid transfer from Escherichia coli is a versatile approach for genetic transformation of thermophilic Bacillus and Geobacillus species. *Extremophiles*, 20(3), pp.375–381.

Trieu-Cuot, P., Carlier, C., Martin, P., Courvalin, P., Qian, H., Fan, W., Wu, J., and Zheng, Z., 1987. Plasmid transfer by conjugation from Escherichia coli to Gram-positive bacteria. *Chin.J.Biotechnol.*, 10(1), pp.289–294.

Trieu-Cuot, P., Carlier, C., Poyart-Salmeron, C., and Courvalin, P., 1990. A pair of mobilizable shuttle vectors conferring resistance to spectinomycin for molecular cloning in Escherichia coli and in gram-positive bacteria. *Nucleic Acids Research*, 18(14), p.4296.

Trokter, M. and Waksman, G., 2018. Translocation through the Conjugative Type IV Secretion System Requires Unfolding of Its Protein Substrate. V. J. DiRita, ed. *Journal*

of Bacteriology, 200(6), pp.e00615-17.

Unterholzner, S.J., Poppenberger, B., and Rozhon, W., 2013. Toxin–antitoxin systems. *Mobile Genetic Elements*, 3(5), p.e26219.

Urrutia Mera, M., Kemper, M., Doyle, R., and Beveridge, T.J., 1992. The membrane-induced proton motive force influences the metal binding ability of Bacillus subtilis cell walls. *Applied and environmental microbiology*, 58(12), pp.3837–44.

Valladares, A., Montesinos, M.L., Herrero, A., and Flores, E., 2002. An ABC-type, high-affinity urea permease identified in cyanobacteria. *Molecular Microbiology*, 43(3), pp.703–715.

Vaningelgem, F., Zamfir, M., Mozzi, F., Adriany, T., Vancanneyt, M., Swings, J., and Vuyst, L. De, 2004. Biodiversity of Exopolysaccharides Produced by Streptococcus thermophilus Strains Is Reflected in Their Production and Their Molecular and Functional Characteristics. *Applied and Environmental Microbiology*, 70(2), pp.900–912.

Velásquez, L. and Dussan, J., 2009. Biosorption and bioaccumulation of heavy metals on dead and living biomass of Bacillus sphaericus. *Journal of Hazardous Materials*, 167(1–3), pp.713–716.

Villalobos, M., Toner, B., Bargar, J., and Sposito, G., 2003. Characterization of the manganese oxide produced by Pseudomonas putida strain MnB1. *Geochimica et Cosmochimica Acta*, 67(14), pp.2649–2662.

Visscher, P.T., Pamela Reid, R., Bebout, B.M., Hoeft, S.E., Macintyre, L.G., and Thompson, J.A., 1998. Formation of lithified micritic laminae in modem marine stromatolites (Bahamas): The role of sulfur cycling. *American Mineralogist*, 83(11–12), pp.1482–1493.

Wach, A., 1995. PCR-Synthesis of Marker Cassettes with Long Flanking Homology Regions for Gene Disruptions in S. cerevisiae. *Yeast Functional Analysis Reports*, 12, pp.259–265.

Wang, J., Mignon, A., Snoeck, D., Wiktor, V., Van Vliergerghe, S., Boon, N., and De Belie, N., 2015. Application of modified-alginate encapsulated carbonate producing bacteria in concrete: A promising strategy for crack self-healing. *Frontiers in Microbiology*, 6, pp.1–14.

Wang, J.Y., Soens, H., Verstraete, W., and De Belie, N., 2014. Self-healing concrete by use of microencapsulated bacterial spores. *Cement and Concrete Research*, 56, pp.139–152.

Warren, L.A. and Haack, E.A., 2001. Biogeochemical controls on metal behaviour in freshwater environments. *Earth-Science Reviews*, 54(4), pp.261–320.

Warthmann, R., Lith, Y. V., Vasconcelos, C., McKenzie, J.A., and Karpoff, A.M., 2000. Bacterially induced dolomite precipitaion in anoxic culture experiments. *Geology*, 28(12), pp.1091–1094.

Webb, S.M., Tebo, B.M., and Bargar, J.R., 2005. Structural characterization of biogenic Mn oxides produced in seawater by the marine bacillus sp. strain SG-1. *American*

Mineralogist, 90(8–9), pp.1342–1357.

Whitaker, J., 2016. Assessing Recombinant Expression of Urease Enzyme From Sporosarcina Ureae As a Carbonatogenic Method for Strength Enhancement of Loose , Sandy Soils. *Msc Thesis*, (June).

Wiktor, V. and Jonkers, H.M., 2015. Field performance of bacteria-based repair system: Pilot study in a parking garage. *Case Studies in Construction Materials*, 2, pp.11–17.

Wiktor, V. and Jonkers, H.M., 2016. Bacteria-based concrete: from concept to market. *Smart Materials and Structures*, 25, p.084006 (8pp).

Wolfram, L., Haas, E., and Bauerfeind, P., 2006. Nickel represses the synthesis of the nickel permease NixA of Helicobacter pylori. *Journal of Bacteriology*, 188(4), pp.1245–1250.

Worrell, E., Price, L., Martin, N., Hendriks, C., and Meida, L.O., 2001. Carbon Dioxide Emissions from the Global Cement Industry. *Carbon*, 26, pp.303–329.

Wright, D.T. and Oren, A., 2005. Nonphotosynthetic bacteria and the formation of carbonates and evaporites through time. *Geomicrobiology Journal*, 22(1–2), pp.27–53.

Wright, D.T. and Wacey, D., 2005. Precipitation of dolomite using sulphate-reducing bacteria from the Coorong Region, South Australia: Significance and implications. *Sedimentology*, 52(5), pp.987–1008.

Wunderlich, S. and Gatto, K.A., 2015. Consumer Perception of Genetically Modified Organisms and Sources of Information. *American Society for Nutrition*, 6(6), pp.842–51.

Xiang, J., Cao, H., Warner, J.H., and Watt, A.A.R., 2008. Crystallization and self-assembly of calcium carbonate architectures. *Crystal Growth and Design*, 8(12), pp.4583–4588.

Xiao, L., Hao, J., Wang, W., Lian, B., Shang, G., Yang, Y., Liu, C., and Wang, S., 2014. The Up-regulation of Carbonic Anhydrase Genes of Bacillus mucilaginosus under Soluble Ca2+Deficiency and the Heterologously Expressed Enzyme Promotes Calcite Dissolution. *Geomicrobiology Journal*, 31(7), pp.632–641.

Xue, G.-P., Johnson, J.S., and Dalrymple, B.P., 1999. High osmolarity improves the electro-transformation efficiency of the gram-positive bacteria Bacillus subtilis and Bacillus licheniformis. *Journal of Microbiological Methods*, 34(3), pp.183–191.

Yan, W., Xiao, X., and Zhang, Y., 2016. Complete genome sequence of the Sporosarcina psychrophila DSM 6497, a psychrophilic Bacillus strain that mediates the calcium carbonate precipitation. *Journal of Biotechnology*, 226, pp.14–15.

Yan, X., Yu, H.J., Hong, Q., and Li, S.P., 2008. Cre/lox system and PCR-based genome engineering in Bacillus subtilis. *Applied and Environmental Microbiology*, 74(17), pp.5556–5562.

Yanisch-Perron, C., Vieira, J., and Messing, J., 1985. Improved M13 phage cloning vectors and host strains: nucleotide sequences of the M13mpl8 and pUC19 vectors. *Gene*, 33(1), pp.103–119.

Yasbin, R.E. and Young, F.E., 1974. Transduction in Bacillus subtilis by Bacteriophage SPP1. *Journal of Virology*, 14(6), pp.1343–1348.

Yates, K.K. and Robbins, L.L., 1998. Production of carbonate sediments by a unicellular green alga. *American Mineralogist*, 83(11–12), pp.1503–1509.

Yates, K.K. and Robbins, L.L., 1999. Radioisotope tracer studies of inorganic carbon and Ca in microbially derived CaCO3. *Geochimica et Cosmochimica Acta*, 63(1), pp.129–136.

Yee, N., Phoenix, V.R., Konhauser, K.O., Benning, L.G., and Ferris, F.G., 2003. The effect of cyanobacteria on silica precipitation at neutral pH: Implications for bacterial silicification in geothermal hot springs. *Chemical Geology*, 199(1–2), pp.83–90.

Yin, X., Weitzel, F., Jiménez-López, C., Griesshaber, E., Fernández-Díaz, L., Rodríguez-Navarro, A., Ziegler, A., and Schmahl, W.W., 2020. Directing Effect of Bacterial Extracellular Polymeric Substances (EPS) on Calcite Organization and EPS-Carbonate Composite Aggregate Formation. *Crystal Growth and Design*, 20(3), pp.1467–1484.

Yoon, J.H., Lee, K.C., Weiss, N., Kho, Y.H., Kang, K.H., and Park, Y.H., 2001. Sporosarcina aquimarina sp. nov., a bacterium isolated from seawater in Korea, and transfer of Bacillus globisporus (larkin and stokes 1967), Bacillus psychrophilus (Nakamura 1984) and Bacillus pasteurii (Chester 1898) to the genus Sporosarcina as Sporosa. *International Journal of Systematic and Evolutionary Microbiology*, 51(3), pp.1079–1086.

Yosef, I., Goren, M.G., Globus, R., Molshanski-Mor, S., and Qimron, U., 2017. Extending the Host Range of Bacteriophage Particles for DNA Transduction. *Molecular Cell*, 66(5), pp.721-728.e3.

Yoshida, N., Higashimura, E., and Saeki, Y., 2010. Catalytic biomineralization of fluorescent calcite by the thermophilic bacterium geobacillus thermoglucosidasius. *Applied and Environmental Microbiology*, 76(21), pp.7322–7327.

Zavarzin, G.A., 2002. Microbial geochemical calcium cycle. *Microbiology*, 71(1), pp.1–17.

Zeaiter, Z., Mapelli, F., Crotti, E., and Borin, S., 2018. Methods for the genetic manipulation of marine bacteria. *Electronic Journal of Biotechnology*, 33, pp.17–28.

Zeebe, R.E. and Wolf-Gladrow, D., 2001. *CO2 in Seawater: Equilibrium, Kinetics, Isotopes*. Amsterdam; New York: Elsevier Science Publishers B.V.

Zeigler, D.R., Prágai, Z., Rodriguez, S., Chevreux, B., Muffler, A., Albert, T., Bai, R., Wyss, M., and Perkins, J.B., 2008. The origins of 168, W23, and other Bacillus subtilis legacy strains. *Journal of Bacteriology*, 190(21), pp.6983–6995.

Zhang, J., Zhou, A., Liu, Y., Zhao, B., Luan, Y., Wang, S., Yue, X., and Li, Z., 2017. Microbial network of the carbonate precipitation process induced by microbial consortia and the potential application to crack healing in concrete. *Scientific Reports*, 7(1), p.14600.

Zhang, W., Ju, Y., Zong, Y., Qi, H., and Zhao, K., 2018. In Situ Real-Time Study on Dynamics of Microbially Induced Calcium Carbonate Precipitation at a Single-Cell Level. *Environmental Science and Technology*, 52(16), pp.9266–9276.

Zhang, W., Seminara, A., Suaris, M., Brenner, M.P., Weitz, D.A., and Angelini, T.E., 2014. Nutrient depletion in Bacillus subtilis biofilms triggers matrix production. *New Journal of Physics*, 16, p.010528.

Zhu, T. and Dittrich, M., 2016. Carbonate Precipitation through Microbial Activities in Natural Environment, and Their Potential in Biotechnology: A Review. *Frontiers in Bioengineering and Biotechnology*, 4, pp.1–21.

van der Zwaag, S. and Brinkman, E., 2015. Self Healing Materials : Pioneering Research in the Netherlands. *Faraday Discuss*, 184, pp.221–235.

Van Zyl, L.J., Nemavhulani, S., Cass, J., Cowan, D.A., and Trindade, M., 2016. Three novel bacteriophages isolated from the East African Rift Valley soda lakes. *Virology Journal*, 13(1), pp.1–14.